Uncertainties in estimates of the oxidative capacity of the urban atmosphere: a modeling and measurement approach

by

Miguel Angel Zavala-Perez

Mechanical Engineer Degree (1998)
Universidad Autónoma de Guanajuato (México)

Master in Environmental Sciences (2000)
Instituto Tecnológico de Estudios Superiores de Monterrey, ITESM (México)

Submitted to the
Department of Earth, Atmospheric and Planetary Sciences
in Partial Fulfillment of the Requirements for the Degree of

Doctor of Philosophy in Atmospheric Sciences

at the

Massachusetts Institute of Technology

September, 2007

Signature of Author.....
Department of Earth, Atmospheric and Planetary Sciences
August 30, 2007

Certified by.....
Mario J. Molina
Institute Professor
Thesis Supervisor

Accepted by.....
Maria Zuber
Head, Department of Earth, Atmospheric and Planetary Sciences

Uncertainties in estimates of the oxidative capacity of the urban atmosphere: a modeling and measurement approach

by

Miguel Angel Zavala-Perez

Submitted to the Department of Earth, Atmospheric and Planetary Sciences on September 5, 2007 in partial fulfillment of the requirements for the Degree of Doctor of Philosophy

ABSTRACT

Mobile emissions represent a significant fraction of the total anthropogenic emissions burden in megacities and have a deleterious effect on air quality at local and regional scales. Due to the significant sources of uncertainties involved during the estimation of mobile emissions, an adequate treatment of emission uncertainties is critical during the design of air quality control strategies using AQMs. This thesis focuses on quantifying the effects of parametric uncertainties of input emission fields on model uncertainties of ozone predictions. We obtained direct measurements of mobile emission sources in the Mexico City Metropolitan Area (MCMA) using a novel measurement technique and quantified the magnitude and variability of key pollutant species. This analysis allowed a direct evaluation of the emissions inventory used in AQMs for the MCMA. Measured selected VOCs and NO_Y showed a strong dependence on traffic mode and indicated a larger than expected burden of emitted NO_X and aldehydes. Our measurements of benzene, toluene, formaldehyde, and acetaldehyde in the MCMA indicate that the emissions of these toxic pollutants are similar or higher than for some US cities. We derived approximate historical trends of the VOC/NO_X emission ratio and quantified the impact of changes of mobile emission sources on the photochemical levels using the Brute Force Method and Direct Decoupled Method sensitivity techniques with the CAMx model. The model reasonably reproduces concentrations of ozone and VOCs and accurately those of CO and NO_X but over predicts OH by about 25% and severely under-predicts HO_2 by a factor of 2 to 3 suggesting that the radical formation pathways in current state of the art AQMs should be revised. The model successfully reproduces the corresponding relative changes in historical observations of ozone peak and diurnal average concentrations and suggests a current moderate VOC-sensitive regime. The analysis of the model's sensitivity coefficients to individual perturbations of VOC group species as described by the SAPRC99 chemical mechanism showed that the model is particularly sensitive to aromatics, higher alkenes, and formaldehyde emissions. We found, however, that NO_X, olefins and aromatic species can potentially contribute significantly to uncertainties in ozone predictions.

Thesis supervisor: Mario J. Molina
Title: Institute Professor

Acknowledgments

I dedicate this thesis to Nancy and Stephanie; they have always been a source of love and support through this amazing journey. Also, this journey would not have been completed without the unconditional support of my parents, Miguel and Isabel, my siblings Edgar and Hanny, and all our family. This work is also a tribute to them.

During these years we have forged strong friendships with many people that have been and will always be very important in our lives; our years at MIT have been unique and wonderful thanks to their friendship. You know who you are and no need to mention names, but sincere thanks for your friendship.

My advisor, Dr. Mario Molina, has always been a source of inspiration and continuous support. His mentorship will remain with me through the rest of my career. Dr. Charles Kolb has contributed to this work in many ways. His positive attitude, kindness and patience have helped me in achieving my goals. My thesis committee members have helped with their suggestions and discussions during the completion of this thesis. I also appreciate having the opportunity to work with Dr. Luisa Molina who has always encouraged and supported me through this work, special thanks to her.

My colleagues in the Molina group and the MCE2 have helped me with feedback, discussions and encouragement through these years and I am fortunate to have their friendship. Many people at Aerodyne Research, Inc., particularly Dr. Scott Herndon, have enormously contributed to this work being always a positive source of ideas, feedbacks, discussions and encouragement. Thanks to all of them.

Finally, I would like to acknowledge the sources of financial support for the different projects involving this work. These include CONACYT, the Department of Energy, The National Science Foundation, the Comision Ambiental Metropolitana and The Molina Fellowship.

Table of Contents

List of figures

List of Tables

Chapter 1. Introduction

1.1. Air pollution in urban areas

Unsustainable growth of urban areas is associated with increased emissions of air pollutants into the atmosphere. A phenomenon with elusive temporal and spatial characteristics, poor air quality in and downwind of urban areas affects millions of people worldwide. Given the accelerated expansion of urban areas in many parts of the world and the driving growing demands for energy primarily provided by fossil fuels, there is an increasing interest in understanding the impacts of urban air pollution on human health, ecosystems viability and climate (Molina and Molina, 2004). Much has been learned in the past decades about reducing urban air pollution levels and significant progress has been made controlling air quality in developed and some developing world megacities. Still, many urban areas continuously experience high pollution levels and their abatement remains elusive, indicating that there is no single successful strategy for improving air quality in megacities.

In urban areas aerosol particles and gases are emitted at significant rates with diurnal patterns characteristic of human activities. Once released, these compounds undergo a series of physical and chemical transformations before they are removed from the atmosphere. Chemical transformation processes can take place on the order of seconds for extremely reactive compounds or decades for the less reactive species, allowing the latter to reach not only all latitudes and longitudes, but also the upper layers of the atmosphere. Physical removal processes occur either via dry or wet deposition phenomena depending on the hygroscopic nature of the emitted pollutants. Given the large range of temporal scales and therefore spatial scales associated with these processes, the exported primary pollutants and their reaction products have the potential to affect ecosystems, atmospheric visibility, weather systems and hydrological cycles. Additionally, the radiative properties of these compounds have the potential to significantly impact the radiative budget of large regions of our planet, affecting climate on all scales. No less importantly, epidemiological and toxicological studies have clearly shown that air pollution from urban areas presents a serious threat to human health.

Ozone, a secondary criteria air pollutant, has been regulated in the U.S. since 1970 through the National Ambient Air Quality Standards (NAAQS) established by the Clean Air Act (CAA). From a recent critical review of the evolution of the NAAQS and its impacts on air quality, it is clear that, by almost any measure, air quality in the US has improved compared to levels in 1970 (Bachmann, 2007). In a peer-reviewed retrospective analysis, the U.S. Environmental Protection Agency (EPA) estimated that the cumulative benefits of reducing air pollution between 1970 and 1990 have been on the order of 6 to 50 trillion dollars compared to compliance costs of $520 billion, (EPA, 1997). Although the estimates are highly uncertain, it is evident that the benefits of controlling and reducing air pollution exceed the costs.

Developed countries can more easily dedicate large financial resources to improve environmental quality, by implementing and enforcing more stringent control measures, as well as developing and using emission control technologies to reduce air pollution. In contrast, in many developing urban areas the design and implementation of air quality control strategies pose greater challenges due to limited financial resources required to fund the research and air quality monitoring needed to understand, evaluate and address the air pollution problems. Because of the large differences in available resources developing areas need more holistic approaches where scientific knowledge is considered along with political, economical, and social factors. Nevertheless, there are tremendous opportunities for developing urban areas to learn from the technological, scientific as well as policy-implementation experiences already gained from successful air pollution abatement examples.

1.1.1 Air pollution in Mexico City

Mainly as a result of the evident deterioration of visibility and concerns of its effects on human health, air pollution in Mexico City started to draw public attention since the early 1980's. At that time, severe thermal inversion episodes producing dense "smog" fogs were very frequent throughout the year and particularly intensive during winter months.

Public awareness grew along with media attention, resulting in massive public demonstrations motivating authorities to get actively involved. Existing environmental legislation was then reviewed, but an ambient ozone standard was not established until 1993 (NOM-020-SSA1-1993). Nevertheless, starting from the early 1990's a number of important and aggressive control measures have been enforced in the city, some more successfully than others. As a result, as will be shown in Chapter 4, over the past two decades in Mexico City the frequency of extremely high pollution episodes has decreased considerably, although high concentrations of ozone, particulate matter (PM) and other pollutants still persist. This has large implications for the design and evaluation of control strategies. The evaluation of a control strategy would be very different if it is based solely on the reduction to acute exposures, as oppose to considering the continuous chronic exposure (years) to high pollutant concentration levels.

The atmosphere of Mexico City, a megacity with about 20 million inhabitants, has been intensively studied in the past two decades. An extensive ambient air quality monitoring network in the city has been in place since 1986 continuously monitoring meteorological parameters, ozone, NO_X NO_2, CO, SO_2, PM10 and, since 2003, PM2.5. Two intensive field campaigns: the MARI project (Mexico City Air Quality Research Initiative) in 1994 and the IMADA-AVER campaign (Investigacion sobre Materia Particulada y Deterioro Atmosferico – Aerosol and Visibility Evaluation Research) in 1997, provided important data for air pollution modeling activities and improved scientific assessments of the causes of air pollution. Several other shorter duration intensive field campaigns, in many cases led by governmental agencies and academic/research institutions, were also conducted in the city in the 1990s.

More recently, intensive major field campaigns during 2002 and 2003, designated MCMA-2002/2003, and in 2006 (MILAGRO-2006), have provided impressively large data sets characterizing the atmosphere of the city and surrounding regions with high temporal, spatial and chemical speciation detail. With the concurrent meteorological and chemical data from these field campaigns, Mexico City has perhaps the world's best characterized urban atmosphere to date. These datasets represent a unique opportunity to

address important unresolved scientific questions regarding the formation, transport and fate of key urban air pollutants. These include the complex chemical processes that characterize the atmospheric oxidation of large hydrocarbons involved in ozone formation as well as the processes that lead to the formation, chemical evolution, growth and removal of fine atmospheric particles. Further, modeling the impacts of air pollution from urban areas on climate and enhancing our ability to predict those effects is an important research activity requiring detailed information on the properties of the gases and particles emitted from large urban areas.

1.2. Role of uncertainty in regional air quality models

A common approach used for the design of emission-based air quality control strategies includes the application of Air Quality Models (AQMs) that, for a relatively short period of time, aim to reproduce the dynamic physicochemical processes that form air pollution at a given location. With assumed emission scenarios as inputs, these models are used to predict ambient concentration profiles of key atmospheric pollutants. These models are typically evaluated using some statistical measure of the comparison between the model results and the available observational data. However, there are many factors that can contribute to the discrepancies between model predictions and the observations. Model predictions are uncertain because of uncertainties in both the input data and the chemical and physical parameters used in their formulation, which are often a reflection of insufficient scientific understanding of the physicochemical processes involved. Therefore, when model predictions are used for the evaluation of control strategies, there may be significant scientific uncertainties about the environmental impacts of such strategies.

Using various numerical schemes, AQMs solve the Advection-Diffusion Equation (ADE) for trace pollutants in the atmosphere:

$$\frac{\partial c_i}{\partial t} + \nabla \cdot (u c_i) = \nabla \cdot (K \nabla c_i) + R_i[c_i, T] \ ,$$

$$\text{Boundary condition: } E_i[x,t] - \left(v_g^i c_i - K \nabla c_i\right) = 0 \ . \qquad (1)$$

In this equation c_i is the concentration of the trace species i, K represents the turbulent diffusion coefficient vector, v_g^i is the deposition velocity of the species i, u is the average horizontal wind speed considered in the advection term, and $E_i[x, t]$ represents the emission input fields (stationary point, area, on- and off-road mobile and biogenic) as a function of space and time. Including photolytic reactions, all chemical reactions are aggregated into the volume term R_i. The result is a set of coupled, nonlinear partial differential equations that satisfy conservation relationships in a turbulent flow. Coupling occurs between pollutant species in the reaction terms and is an important source of non-linearity of the system.

The numerical solution of the ADE requires hundreds of chemical parameters and the knowledge of time-resolved 3-D meteorological and emission fields. In addition, being computationally and data intensive, oftentimes there are insufficient data to support model applications. The large amounts of input data and number of parameters typically required by AQMs pose their own uncertainties and, potentially, contribute to the discrepancies between model predictions and observations.

Because a large number of observations are needed to constrain/evaluate an AQM, there are relatively few case studies of uncertainty analysis of 3D-AQMs in urban areas (Tatang, 1994; Pun, 1998; Fine et al., 2003; Cohan et al., 2005). As formulated by the ADE, the uncertainties in AQM can be described in terms of emissions, meteorology, chemistry, resolution, and observational data (for initial and boundary conditions). In addition, uncertainties can be inherently associated with model formulations such as erroneous or simplified/incomplete representations and numerical solution techniques. As a result, uncertainty studies normally address one or few of the sources of uncertainty and typically base their analysis on the comparisons with photochemical observations, rather than with the (observed) oxidative capacity[1] of the urban atmosphere.

[1]The chemical lifetimes of emitted species and their reaction products are controlled by a series of radicals that act as oxidizing agents. The budget of these radicals is sometimes called the "oxidative capacity" of the atmosphere (Prinn, 2003). Together with photolysis, the radicals OH, HO_2, O, NO_3, and O_3 break down the

Nevertheless, uncertainty studies have shown that besides the emission fields, key parameters in the solution of the ADE include NO_2 photolysis values, mixing height (or its corresponding parameterization in the vertical diffusion coefficients), as well as specific species such as HONO, HNO_3 and H_2CO that actively participate in the overall budget of radicals in the model (Pun, 1998; Fine et al., 2003). Fortunately, as mentioned above these and many other important parameters and input data have been recently measured in the MCMA, allowing the possibility to constrain an AQM with further detail. The first section of Chapter 5 of this thesis is devoted to describing our attempt to use the observational data collected in the MCMA to construct a base case simulation period. The buildup of a base case simulation period using measured local data, and a thorough evaluation of its performance against key observational data (such as hydrocarbon species, photochemical products and radicals) are essential for any attempt to use an AQM for sensitivity and uncertainty propagation studies.

From all the possible sources of uncertainties mentioned above, in this study we will focus on the effects that parametric uncertainties in input emission fields have on model predictions. Emission processes have four characteristics that are necessarily represented in input fields of AQMs: 1) the emission strength (or molar flux emission rate), 2) a temporal distribution, 3) a spatial distribution and 4) a chemical speciation. Together with the construction of a base case emission scenario with observational data, these will be addressed in Chapters 4 and 5. Note, however, that there is another important source of uncertainty in the formulation of emission fields for AQMs not treated here. Despite their anthropogenic or biogenic origin, all but major point emission sources are at the end irremediably treated as area sources emitted at the surface because they are summed at the grid cells and assumed to mix (instantaneously) in the cell's volume at each simulation step. As such, chemistry may be slower than it should in regions near the emission source where concentrations are in reality higher and chemistry may be faster than in regions far the emission source– where actual concentrations are lower. This is a

---

emitted species. OH is believed to be the most important radical contributing to the oxidation of the emitted species.

"formulation" uncertainty so to speak, because is related to the representation of a physical process.

1.3. Thesis objectives

This thesis focuses on quantifying the effects of input parametric uncertainties, particularly from mobile sources, on the photochemical and oxidative capacity predictions of a 3D air quality model (AQM) in an urban area.

A base-case emissions scenario, validated with measurements obtained during a major field campaign, is used to perform sensitivity studies and to study the propagation of uncertainties from mobile emission sources that are inputs to the AQM. The sensitivity studies are carried out using the mathematical Decoupled Direct Method (DDM) and the results are validated using the standard Brute Force Method (BFM).

The specific objectives of this thesis are:

- The quantification of emission rates from mobile sources of a developing urban area using a novel measurement technique. The technique, applied for the first time to obtain systematic fleet-average emission factors by driving mode, revealed higher than expected emission rates of toxic pollutants in the urban area.

- The validation of the mobile emission sources estimations from the official Emissions Inventory for the Mexico City Metropolitan Area (MCMA).

- A unique inter-comparison of emission characteristics from mobile sources in three distinct urban areas (Mexicali, Mexico City and Austin, TX) using the same measurement technique.

- The quantification of the historical perturbations of mobile emission sources in an urban area using both direct emission measurements and a new introduced indirect

approach. Along with the inferred perturbations, we quantify the observed concurrent effects on ozone, CO and NO_X concentration levels.

- Both the magnitude of the perturbations and the corresponding observed effects on air pollutant levels are used to evaluate the results from a modeling sensitivity study. The results from the sensitivity study are in turn used to estimate the propagation of emission uncertainties in model predictions.

1.4. Thesis Structure

This thesis is organized as follows:

- Chapter 2 describes the analysis and results of the on-road measurements of mobile emission sources obtained in Mexico City using the Aerodyne mobile laboratory. The measurements, carried out in April of 2003 during the MCMA-2003 field campaign, have been used to validate the official Emissions Inventory of the city.

- Chapter 3 presents the on-road measurements of mobile sources obtained in Mexicali (2005) and Austin, TX (2003) using the Aerodyne mobile laboratory. We perform an inter-comparison of the results obtained in these two cities with those obtained in the MCMA during the MCMA-2003 field campaign.

- Chapter 4 presents the analysis of the correlations between the historical perturbations of mobile emission sources and air quality trends in the MCMA. The results obtained from this analysis are the basis for the evaluation of the model sensitivity performance and uncertainty analysis results obtained in Chapter 5.

- Chapter 5 first presents the evaluation of the performance of a 3D air quality model (CAMx) during a pollution episode in April 2003 using the comprehensive data sets collected during the MCMA-2003 field campaign. The modeled meteorological/emissions episode constitute the base-case scenario around which

the sensitivity studies are performed. The sensitivity results, evaluated using the historical observations described in Chapter 4, are used to quantify the propagated uncertainty from mobile emissions in the model.

- Chapter 6 presents the conclusions of this thesis and contains suggestions for future research.

1.5. Publications

Four conference papers have been presented on this work at the time of this writing. The contents of Chapter 2 have been published in *Atmospheric Chemistry and Physics* 6, 5129-5242, 2006. Part of Chapter 5 has been published in *Atmospheric Chemistry and Physics* 7, 1347-1366, 2007. Condensed versions of Chapter 3, Chapter 4 and the second part of Chapter 5 will be submitted to *Atmospheric Chemistry and Physics.*

Chapter 2. Characterization of on-road vehicle emissions in the Mexico City Metropolitan Area using a mobile laboratory in chase and fleet average measurement modes during the MCMA-2003 field campaign

2.1. Introduction

Emissions from mobile sources in megacities represent a major contribution to the degradation of air quality at local and regional scales. They contribute to a primary and secondary air pollutant burden that can threaten human health, damage ecosystems and influence climate (Molina and Molina, 2004; Molina et al., 2004).

Mobile emissions are generally quantified in emissions inventories based on activity factors estimated from a vehicle census or traffic counts, and emissions factors obtained from vehicle exhaust measurements, input into individual vehicle or fleet emission models (Mobley, 2005). Despite the significance of mobile emissions in large urban environments, their estimation is highly uncertain for most species, mainly due to the large inter-vehicle variability of the parameters that affect emission rates. Similarly, there are numerous factors that affect the variability in emissions across different vehicles types. These include factors that affect the internal combustion efficiency in the vehicle, and therefore its engine's emission characteristics, such as engine type and size, fuel composition, and combustion temperature and pressure. The character and maintenance of fuel delivering and emission control systems (or lack thereof) significantly affect which engine emissions exit the tailpipe. Traffic modes, road conditions, vehicle maintenance practices, driving behavior and other vehicle operating conditions can significantly affect vehicle emissions (Popp et al., 1999). The influence of all these factors highlights the need for measurement techniques that capture real-world vehicle emissions to validate emission inventories.

Several techniques have been developed to measure vehicle emissions both in laboratory testing and in real world driving conditions. These include measurement techniques using chassis dynamometer studies (Whitfield and Harris, 1998; Yanowitz et al., 1999), traffic tunnel integration studies (Kirchstetter et al., 1999), cross-road remote-sensing studies at tunnels and other fixed sites (Bishop et al., 1989; Jimenez et al., 2000; Schifter et al., 2005), and Portable Emission Measurement System (PEMS) methods (Cadle et al., 2002). Real-world driving emissions measurement techniques may differ from dynamometer based testing techniques in several ways. Carefully controlled, but limited environmental conditions and driving patterns are typically used in chassis dynamometer studies and typically a relatively small number of vehicles are tested.

Real world emission measurement techniques typically sample a much larger number of vehicles, but may do so under a limited range of driving states. Tunnel studies sample hundreds to thousands of vehicles, but are typically limited to fleet average emission values, although some differentiation between light duty and heavy duty vehicle emissions can be obtained when data for tunnel tubes that exclude heavy duty vehicles are compared with comparable mixed traffic tunnel data. Remote sensing measurement techniques typically sample emissions from vehicles with a wide range of ages, models, maintenance and operational histories, but the sampling time is relatively short (~0.1 s) and the range of driving states sampled is usually limited. On-board or trailer mounted PEMS instrumentation can characterize some emissions over a full range of on-road driving states, but are typically deployed on a small number of vehicles in any study. Detailed descriptions of these techniques and a review of their strengths and limitations for determining mobile emission factors are given elsewhere (Wenzel et al., 2000). As mobile emission inventories should accurately represent real world vehicle fleets and driving conditions, on-road measurement techniques that interrogate a wide range of vehicles over a full complement of drive states can make important contributions to this goal.

In recent years, additional techniques for the measurement of vehicle emissions under real-world driving conditions using fast response measurements in on-road mobile

laboratories have been applied in urban areas (Kittelson et al., 2000; Vogt et al., 2003; Kolb et al., 2004; Canagaratna et al., 2004; Herndon et al., 2005a,b; Shorter et al., 2005; Pirjola et al., 2004; Giechaskiel et al., 2005). In the chase technique, a mobile laboratory repeatedly samples the emissions of a target vehicle. Our implementation of this technique makes use of the fast time response and high sensitivity of laser spectroscopic instruments and other fast response trace gas measurement techniques for repeatedly intercepting and measuring the turbulent exhaust plume of the target vehicle. Similar to the traditional remote sensing studies, ratios of a given species to CO_2, used as a tracer of combustion, are obtained during the analysis and the results indicate the number of molecules of the pollutants of interest per CO_2 molecules emitted. In addition to the chase technique, which focuses on a series of selected individual vehicles within a given vehicular class, fleet average on-road emissions can be obtained by processing randomly intercepted vehicle plumes from surrounding traffic (both co-flowing and opposing lanes). In this fleet average mode, even merged plumes from multiple vehicles can be processed and included.

In this study, emission ratios for selected individual vehicles as well as fleet average fuel-use-based vehicle exhaust emissions from mobile laboratory data are deduced from on-road measurements. In the fleet average mode the mobile laboratory measured on-road ambient air mixed with emissions of the surrounding vehicles. Successful application of this method requires a large sample size of these mixed emission periods and a sampling time long enough such that the number of sampled vehicles is large enough to include a representative number of high emitters. Care must also be taken to avoid situations where the intercepted plumes are dominated by a few nearby vehicles for significant portions of the sampling period. On the basis of the central limit theorem, the emission averages should then be normally distributed if the samples are unbiased and sufficiently large.

MCMA-2003 was an extensive field campaign held during the spring of 2003 in the Mexico City Metropolitan Area (MCMA) designed to enhance the understanding of the physico-chemical transformations of emissions at the urban scale and improve air quality modeling validation activities (Molina et al., 2007). The five-week campaign included a

Supersite at the National Center for Environmental Research and Training (Centro Nacional de Investigación y Capacitación ambiental, CENICA), near the center of the city, as well as continuous sampling at other peripheral sites. Measurements were obtained for most important meteorological variables (de Foy et al., 2005; de Foy et al., 2006b; de Foy et al., 2006a), ground level and vertical profiles of several chemical species in gas and aerosol phases and samplings at boundary sites for a better characterization of the background concentration levels (Johnson et al., 2005; Salcedo et al., 2006; Salcedo et al., 2007; Shirley et al., 2006; Volkamer et al., 2005a). A preliminary two week deployment in February 2002 of an older version of the mobile laboratory was used to make initial on-road measurements in Mexico City in order to develop vehicle exhaust measurement techniques and survey the emission levels of selected pollutants as well as their ambient background concentrations.

The MCMA-2003 field campaign featured the use of a new mobile laboratory equipped with fast time response instrumentation to measure the emissions from on-road, in use vehicles in the MCMA. This version of the mobile lab and the measurement modes used during MCMA-2003 have been detailed elsewhere (Kolb et al., 2004). In this work we present the analysis of the emission ratios obtained with chase and fleet average measurement modes during the MCMA-2003 field campaign. We present the analysis of mobile emission ratios for NO_X, NO_Y, NH_3, H_2CO, CH_3CHO, and other selected VOCs for chase sampled vehicles and fleet averaged emissions. The results are compared with the corresponding emissions inventory for the MCMA, other vehicle emissions measurements in the MCMA, and measurements of on-road emissions in US cities.

2.2. Experimental Methods

The mobile laboratory deployed during the MCMA-2003 field campaign was equipped with several high time resolution and high sensitivity instruments (Kolb et al., 2004). As described in Table 2.1, these included Tunable Infrared Laser Differential Absorption Spectrometers (TILDAS) for measuring selected gaseous pollutants, a Proton Transfer Reaction Mass Spectrometry (PTR-MS) for measuring selected volatile organic compounds (VOCs), a commercial NO/NO_Y chemiluminescent detector modified for fast

response measurements, and a Licor Non-Dispersive Infrared (NDIR) instrument for CO_2. Other instruments on board the mobile laboratory included a Global Positioning System (GPS), a sonic anemometer attached close to the laboratory sampling port to detect "tailwind" conditions that might create sampled air volumes contaminated with the mobile lab's engine or onboard generator exhaust and a video camera used to obtain the target vehicle information. The mobile laboratory's velocity and acceleration were measured and recorded continuously during the experiment along with local atmospheric parameters including pressure, temperature, and relative humidity.

Table 2.1. Instrumentation on board the Aerodyne mobile laboratory used during MCMA 2002 and MCMA-2003.

Instrumentation	Measures	Detection Level	Sampling frequency
Proton Transfer Reaction Mass Spectrometer (PTR-MS)[a]	Methanol, acetaldehyde, benzene, toluene, MTBE, etc.	1 - 5 ppb	~ 1 s
Tunable Infrared Laser Differential Absorption Spectroscopy (TILDAS)[b]	NO	1.1 ppb	1 s
	NO_2	700 ppt	1 s
	H_2CO	1.2 ppb	1 s
	NH_3	600 ppt	1 s
Aerosol Mass Spectrometer (AMS)[c]	Nitrate	0.04 $\mu g\ m^{-3}$	4 s
	Sulfate	0.06 $\mu g\ m^{-3}$	4 s
	Ammonium	0.2 $\mu g\ m^{-3}$	4 s
	Organics	0.8 $\mu g\ m^{-3}$	4 s
	Chloride	0.04 $\mu g\ m^{-3}$	4 s
Non-Dispersive Infrared instruments (NDIR) unit (LICOR)[d]	CO_2	0.2 ppm	1 s
Aethalometer (Magee Scientific AE-16)	Black carbon	0.1 $\mu g\ m^{-3}$	1 minute
Photoemission aerosol sensor (EcoChem PAS 2000)	Particulate PAH	10 ng m^{-3}	10 s
Chemiluminescence	NO_X, NO_Y	0.4 ppb	1 to 10 s
Aerosol photometer (TSI DustTrak)	PM2.5	1 $\mu g\ m^{-3}$	1 s
Condensation Particle Counter (CPC)	10 – 100 nm particle number density	0.01 part/cm^3	2 – 3 s

[a] Only those components having proton affinities greater than water are detected using this technique which includes most oxygenated and unsaturated hydrocarbons.

[b] H_2CO was detected using a pair of absorptions lines at 1774.67 and 1774.83 cm^{-1}. Two relatively weak water lines bracket these features, and a very small water line is present in the gap between. The diode used for NO_2 was operated at approximately 1606 cm^{-1} and NO at approximately 1900 cm^{1}. As operated during these measurements, the 1 s rms precisions for H_2CO (diode 1) was normally less than 1.2 ppbv. For NO_2 (diode 2) the 1 s rms precision was 0.8 ppbv. NH_3 was operated with a quantum cascade laser at approximately 960 cm^{-1}.

[c] The detection limits from individual species were determined by analyzing periods in which ambient filtered air was sampled and are reported as three times the standard deviation of the measured mass concentration during those periods.

[d] The Licor-6262 non-dispersive infrared absorption instrument detects CO_2 absorption in the 4.3 μm band. Additional details regarding its performance in this application can be found elsewhere (Herndon et al., 2004). The measured response time of the Licor instrument to flooding the inlet tip with CO_2 free nitrogen gas during these experiments resulted in a 1/e time of 0.9 seconds.

VOCs emissions are of particular interest in this study; all the reported VOCs were measured with the PTR-MS system, except for H_2CO that was measured with the TILDAS instrument. TILDAS instruments have been successfully employed in several field campaigns for measuring trace gas species (Zahniser et al., 1995; Jimenez et al., 1999; Jimenez et al., 2000) and for measuring emissions from passenger buses using the chase technique (Herndon et al., 2005b; Shorter et al., 2005).

H_2CO and NO_2 were measured using a lead salt tunable diode lasers TILDAS instruments and NH_3 measurements were obtained using a quantum cascade laser in the TILDAS system. The PTR-MS system (Ionicon Analytic GMBH) was applied for measuring vehicle emissions during on-road chase events for the first time during this study. It was used to measure selected oxygenated, olefinic, and aromatic VOCs with proton affinities larger than water vapor via ionization through their reaction with H_3O^+. The resulting ions are detected by mass spectrometry at high time resolution and selectivity. Data processing and validation methods for VOCs measured with the PTR-MS system during the MCMA-2003 field campaign are reported elsewhere (Rogers et al., 2006).

NO and NO_Y measurements were obtained with a chemiluminescent instrument using a molybdenum oxide converter modified for high frequency NO_Y sampling (Dunlea et al., 2004). Although in principle the measured NO_Y captures all reactive nitrogen oxides species, the contribution from reservoir and terminal species such as PAN, HNO_3, and organic nitrates, is likely minimal to the overall fresh emitted NO_Y concentration due to the short time (few seconds) between the emissions of NO and NO_2 and their sampling by the mobile laboratory.

High time resolution instrumentation provides invaluable information on the emission exhaust characteristics of individual on-road vehicles. Indeed, this is the property that allows the chase technique to capture the variability from the turbulent exhaust plumes that are quickly diluted in the surrounding air. In the chase technique, the high time response instruments are used to measure the emission exhausts of the targeted vehicle through a sampling port localized at the driver's front side of the mobile lab. The sampled air is then delivered to the various instruments on board. Figure 2.1 shows an example of a sampling period during the chase of a gasoline vehicle. The sampled signals are correlated with CO_2, a combustion tracer, if they are emitted by a target vehicle's exhaust. An emission ratio is obtained by scaling the measured species to the exhaust CO_2 measured immediately behind the chased vehicle. As an example of this procedure, Fig. 2.1 also shows the obtained correlation obtained for the sampled species with CO_2 for the same period.

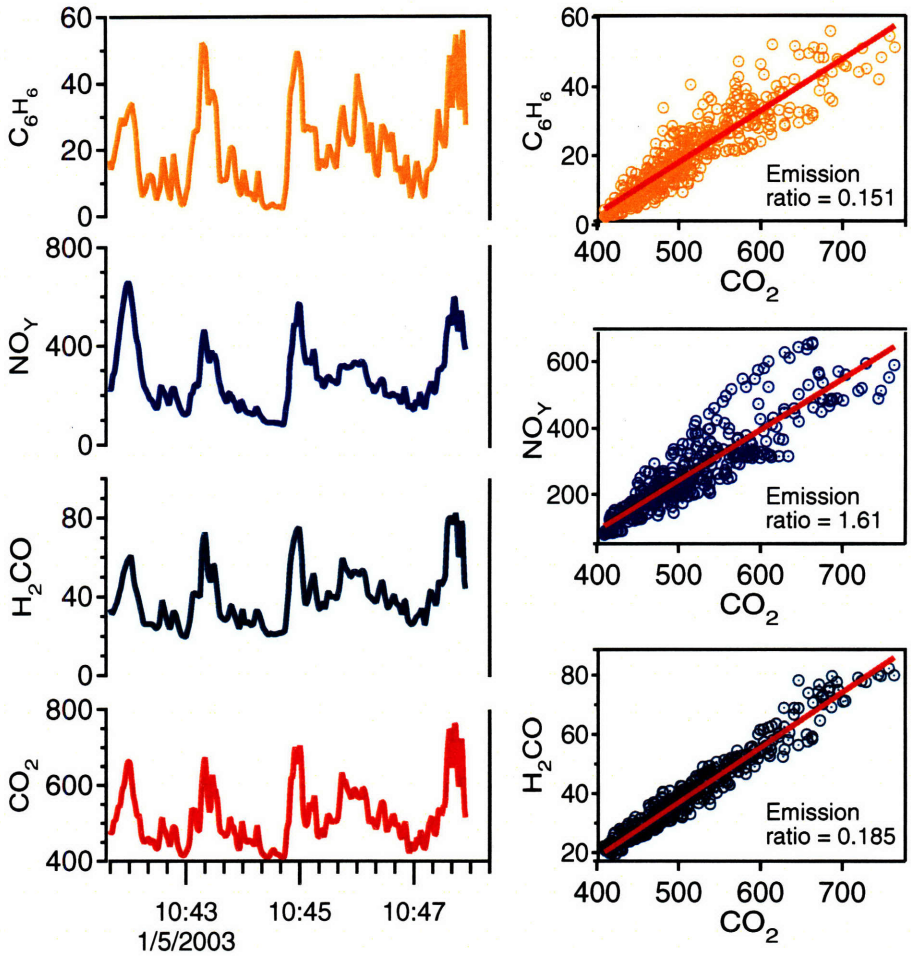

Figure 2.1. Time series of benzene, H_2CO, and NO_Y in ppb units showing correlation with CO_2 in ppm units. Estimated emission ratios in right-hand panels are in ppb/ppm units.

This sampling technique interrogates vehicle exhaust plumes diluted with on-road background air; respective amounts of exhaust plume and background pollutant concentrations are determined by comparing background pollutant concentrations measured just before and after plume encounters with those inside exhaust plumes. In this work, we assume equal dilution for all of the different measured species. Therefore, the dilution experienced by a given emitted species will be equal to the dilution experienced by CO_2, and it cancels in the ratio of excess pollutant (plume - background) divided by excess CO_2 (plume - background). The equal dilution assumption is a very good approximation for the gaseous species in general but may not hold for very short-lived

species (less than ~1 s) due to the potential chemical transformations occurring before sampling.

The challenge then becomes to clearly distinguish between sampled emission exhaust and background concentrations, as well as to distinguish and discount emissions from other non-targeted vehicles. The identification of emission plumes from the data is accomplished by analyzing the multiple, synchronized, instruments on board the mobile laboratory. In addition to the pollutant sensors, these include 1) the readings from the sonic anemometer that allow consideration of the direction and speed of the incoming wind at the sampling port, 2) the images obtained with the video camera for observing the targeted vehicle, and 3) the real-time data log notes written by the researchers on-board the mobile laboratory. The use of these tools together with the analyses of the measured species signals are used to elucidate the presence of background air and emissions related to the targeted vehicle. Similarly, the emissions from the mobile laboratory (vehicle exhaust plus generator exhaust) itself were flagged out in our database using the same discriminants described above, plus the fact that the generator emitted characteristic high levels of methanol. As described in Fig. 2.1, the signals are correlated as long as they are part of the combustion products. When chasing a target vehicle, the instruments on board measure background and in-plume pollutant concentrations and their correlation is obtained using CO_2 as the combustion plume tracer. This technique is made possible by the high time resolution and sensitivity of the instrumentation that is capable of capturing and quantifying the rapidly changing emission concentrations.

In our analysis, we considered a chase event useful when the duration of the chase was at least 5 minutes, in order to characterize the emissions with a sufficient number of plume intercept measurements. After quality assurance procedures, a dataset of about 110 hours containing valid 1-second data points for various species was obtained covering a wide area of the city. A total of 345 events with valid emission ratios were obtained with the procedure described above. Table 2.2 specifies the sample size and types of vehicles measured during the experiment.

Table 2.2. Chase and Fleet Average Vehicle Emissions Experiments.

Event or Chase Type	Sample size	MCMA fleet size[c]	Description
LDV	119	2,700,000	Fleet averaged emissions of Light Duty Vehicles[a]
HDT	61	75,000	Heavy Duty Trucks (e.g. heavy trucks, tractor trailers)
COL	71	32,000	Colectivos[b]
URB	37	30,000	Urban buses[b]
CHR	34	22,000	Inter-city buses or charters
Others[d]	23	620,000	Includes combis, motorcycles, pickups, and non LDV vehicles $\leq$ 3 tons

[a] Includes events classified as SAG, "Stop and Go" (sampling size 12), TRA "Traffic state" (sampling size 19), and CRU, "cruising at high speed" (sampling size 21), see text for details.

[b] Colectivos are medium-size very popular public transport vehicles in the MCMA (for transporting about 25 people) powered by gasoline fuel. Colectivos powered by CNG or LPG are denominated here as COLg (sampling size 26). Urban buses are intra-city diesel buses. See text for details.

[c] Rounded values from the 2002 MCMA Emissions Inventory (CAM, 2004). Number of charters obtained from "Pasaje del Servicio Publico Federal de Autotransporte" in GDF, (2000).

[d] For our measurements, "Others" mean isolated emission plumes, fixed sampling or in specific places.

We estimated fleet average emission ratios for light duty vehicles using the sampling periods when the mobile lab was surrounded by light duty gasoline vehicles under three different traffic conditions. We considered "Stop and Go" (SAG) situations when the mobile lab was in very heavy traffic conditions, with vehicle speeds lower than 16 (±8) km/hr for 5 minutes or more. TRA events represent heavy traffic conditions with prevailing moderate speed, less than 40 (±16) km/hr, for 5 or more minutes, this is the most prevalent traffic mode in the MCMA. Finally, CRU conditions represent sampling periods with prevailing cruising at moderate and high speed in the city, higher than 56 km/hr, for 5 minutes or more. These traffic conditions accounted for 52 classified fleet averaged traffic mode events. As shown in Table 2.2, 67 other measurements of light duty gasoline vehicle emissions were considered but they were not classified within these categories. In those cases, the classification was not possible either because the vehicle speed was not within a given vehicle speed category for more than 5 minutes (changing from one category to another, producing a combination of emission traffic modes) or

because there was a strong influence from the emissions of an individual vehicle nearby (therefore biasing the fleet averaged sample).

Similar to the procedure used in Stedman et al., (1997), on the basis of the central limit theorem, the averaged emission ratios obtained should be approximately normally distributed if the samples were unbiased and sufficiently large. Therefore, the estimation of fleet average emission ratios with this method relies on the collection of average values representing large, unbiased samples of fleet emission measurements of light duty vehicles surrounding the mobile lab. Heavy duty trucks and the other public transport vehicles that were individually sampled, as reported in Table 2.2, are intrinsically easier to measure with the chasing technique due to the strength of their emission signal and to the ease of following them while driving (Herndon et al., 2005b). The mobile laboratory also obtained information from other two types of events: 1) stationary periods when the mobile laboratory was located along a busy road or near a specific emission source, and 2) well-identified individual exhaust plumes for target vehicles but for shorter periods of time (less than 5 minutes). We do not include the analysis of such periods here.

2.3. Data Processing Procedure

The procedure for processing the data is described in the following paragraphs. Consider the general case of a target vehicle whose concentration at the emission exhaust location is given by C_i^e for a given species i while C_i^a represents the ambient or background concentration for the same species i. In this way, the vehicle's emission and background concentrations for CO_2 would be given by C_{CO2}^e and C_{CO2}^a, respectively. Let the dilution f be defined as the volume fraction of the exhaust plume for a given sampled volume in the measurement period (~1 sec). If the superscript m refers to the measured concentration:

$$f = \frac{C_i^m - C_i^a}{C_i^e - C_i^a}. \qquad (1)$$

We can solve for C_i^m as:

$$C_i^m = (1-f)C_i^a + f\,C_i^e\,. \tag{2}$$

If $f = 1$, this implies that a pure exhaust is being measured and when $f = 0$, strictly ambient levels are being sampled. Now we make use of the equal dilution assumption for the species i and for our tracer species CO_2, from Eq. (1):

$$\frac{C_i^m - C_i^a}{C_i^e - C_i^a} = \frac{C_{CO2}^m - C_{CO2}^a}{C_{CO2}^e - C_{CO2}^a}\,. \tag{3}$$

We are interested measuring the emission ratio for the species i defined in this context as:

$$ER_i = \frac{C_i^e}{C_{CO2}^e}\,. \tag{4}$$

We can obtain this quantity from Eq. (3) after a series of simplifications. For example, with a typical concentration of CO_2 in an engine exit plume in excess of 2% and ambient levels generally below 400 ppm, the following approximation is good to better than 2%.

$$C_{CO2}^e - C_{CO2}^a \cong C_{CO2}^e\,. \tag{5}$$

Similarly, for other species it is common to observe C_i^a / C_i^e values smaller than 0.05. Equation (4) simplifies to the intuitive expression,

$$ER_i = \frac{C_i^e}{C_{CO2}^e} \cong \frac{C_i^m - C_i^a}{C_{CO2}^m - C_{CO2}^a}\,. \tag{6}$$

If the concentration C_i^m is plotted against C_{CO2}^m a very simple diagnostic arises, which resembles a locus of points around the ambient concentrations of i and CO_2 with rays extending toward higher concentrations of CO_2 when a plume is sampled. The slope of the correlation plot is indicative of the Emission Ratio for species i under the conditions in which the partially sampled plume was emitted.

2.4. Results

The measured emission ratios for the event types described above are shown in Table 2.3. Except for the fleet averaged light duty gasoline vehicles (SAG, TRA and CRU), the reported emission ratios correspond to the averaged values of the emissions from individual vehicle classes. Since the basis of the analytical procedure uses the covariance of the emitted species concentration to the emitted CO_2 concentration under an equal dilution assumption, and therefore avoiding having to resolve the highly transient plume dilution behavior, we have excluded emission ratios for species measured with the relatively lower sampling frequency instruments described in Table 2.1. In that way, we avoid the uncertainties resulting from correlating a low frequency signal with high frequency signals. An alternative approach to estimating fleet average emissions of pollutants measured with the slower response instrument instruments on-board the Aerodyne Mobile Laboratory during MCMA-2003, is presented by Jiang et al., (2005).

The video camera images were used during the analysis process to discriminate target vehicle plumes from other potential sources. During the chase experiments, the target vehicle's license plate was recorded so registration data could be accessed for additional information. The number of vehicles for which valid history information was available was too small to further classify the results by vehicle age and model.

Due to their large size, high exhaust volume, and relatively slow average speeds, public transport vehicles were sampled through individual chase events and were classified in this work as "colectivos" (COL), urban buses (URB), and charter buses (CHA). Colectivos are medium-size buses, with capacity for transporting about 25 people, and are very popular and intensively used throughout the MCMA. Colectivos are mainly gasoline-powered, although a small but growing fraction of them (~5%) are powered by CNG or LPG (CAM, 2004). By choosing a route used by colectivos fueled with CNG, we were able to sample 26 of this colectivo sub-class, classifying them as COLg. The URB category refers to intra-city urban buses with capacity for transporting about 50 people; these buses were randomly selected as the mobile lab encountered them during on-road operations and a variety of transportation routes (and bus companies) were sampled.

Charter buses, inter-city buses with a larger transport capacity than colectivos or urban buses, were sampled near the major bus terminal in the city. Here, the mobile lab chased the charter buses on a looped circuit as they were entering or leaving the facility. Sampled heavy-duty trucks (HDT) refer to large trucks such as tractor trailers, food supply and construction vehicles.

Table 2.3. Measured emission ratios in [ppb/ppm] during MCMA-2003.

	Medium Vehicles		Light Duty Vehicles				Heavy Duty Vehicles		
Pollutant	**COL[d] (SD)[c]**	**COLg (SD)**	**LDV (SD)**	**SAG (SD)**	**TRA (SD)**	**CRU (SD)**	**URB (SD)**	**CHR (SD)**	**HDT (SD)**
NO_Y	7.8 (3.0)	10.6 (4.1)	4.7 (2.4)	3.2 (1.0)	5.1 (2.0)	5.1 (1.6)	6.0 (1.5)	6.5 (1.9)	7.2 (3.0)
NO_2	0.62 (0.4)	0.66 (0.32)	0.53 (0.45)	0.45 (0.42)	0.43 (0.33)	0.71 (0.30)	0.60 (0.26)	0.78 (0.33)	0.70 (0.35)
NO	6.88 (3.4)	9.40 (3.8)	4.14 (2.4)	2.92 (0.9)	4.58 (2.2)	4.33 (1.7)	5.33 (1.6)	6.22 (1.9)	6.67 (3.2)
H_2CO	0.33 (0.12)	0.34 (0.13)	0.25 (0.11)	0.23 (0.06)	0.23 (0.07)	0.20 (0.07)	0.11 (0.07)	0.07 (0.05)	0.12 (0.08)
CH_3CHO	0.04 (0.02)	0.06 (0.01)	0.04 (0.02)	0.04 (0.02)	0.04 (0.02)	0.04 (0.01)	0.02 (0.02)	0.02 (0.02)	0.03 (0.02)
H_2CO/CH_3CHO[a]	8.1 (2.3)	6.4 (1.1)	6.7 (2.9)	6.2 (1.3)	6.2 (2.0)	6.4 (1.8)	7.2 (2.4)	4.9 (3.2)	5.1 (2.3)
Benzene	0.08 (0.04)	0.03 (0.01)	0.13 (0.08)	0.14 (0.04)	0.10 (0.03)	0.10 (0.04)	0.04 (0.05)	0.02 (0.02)	0.03 (0.03)
Toluene	0.14 (0.07)	0.04 (0.02)	0.25 (0.12)	0.28 (0.07)	0.18 (0.06)	0.18 (0.08)	0.05 (0.05)	0.02 (0.02)	0.04 (0.04)
C2-Benzene	0.19 (0.09)	0.05 (0.04)	0.32 (0.16)	0.32 (0.11)	0.22 (0.09)	0.19 (0.09)	0.06 (0.06)	0.03 (0.04)	0.05 (0.05)
C3-Benzene	0.16 (0.08)	0.03 (0.02)	0.24 (0.15)	0.24 (0.09)	0.15 (0.05)	0.15 (0.08)	0.05 (0.06)	0.03 (0.05)	0.05 (0.06)
m/z 57[e]	0.26 (0.21)	0.03 (0.07)	0.38 (0.23)	0.39 (0.10)	0.29 (0.12)	0.28 (0.10)	0.09 (0.07)	0.04 (0.04)	0.09 (0.08)
NH_3	ND[c]	ND	0.12 (0.07)	0.09 (0.05)	0.09 (0.06)	0.11 (0.07)	0.04 (0.03)	ND	0.06 (0.04)
Aromatics/NO_Y[a,b]	0.09 (0.08)	0.02 (0.01)	0.30 (0.27)	0.31 (0.10)	0.14 (0.07)	0.11 (0.05)	0.03 (0.03)	0.02 (0.02)	0.03 (0.03)

[a] Obtained from individual emission ratios, see text for details, units in ppb/ppb.

[b] For "aromatic VOCs" we considered the sum of Benzene, Toluene, C2-Benzene (sum of xylene isomers, ethylbenzene, and benzaldehyde) and C3-Benzene (sum of C_9H_{12} isomers and C_8H_8O isomers). [c] SD: 1-standard deviation; ND: Non determined.

[d] See Table 2.2 and text for definition of vehicle chasses.

[c] m/z 57 represents the sum of MTBE and butenes for gasoline vehicles. Neutral components have not been assigned to this mass for CNG and diesel vehicles.

Ratios of emitted species reported in Table 2.3, such as aromatic VOCs/NO_Y and H_2CO/CH_3CHO, for each vehicle or fleet type classification were obtained from the ratios of one-second measurements primary data as opposed to using averaged ratios. In Fig. 2.2 we present the frequency distributions of measured emission ratios for various species and ratios of emitted species. The frequency distributions were obtained using all valid emission measurements for all the sampled species and vehicle categories. Similarly, frequency distributions for ratios of emitted species were also obtained from the ratios of individual, one-second, measurements.

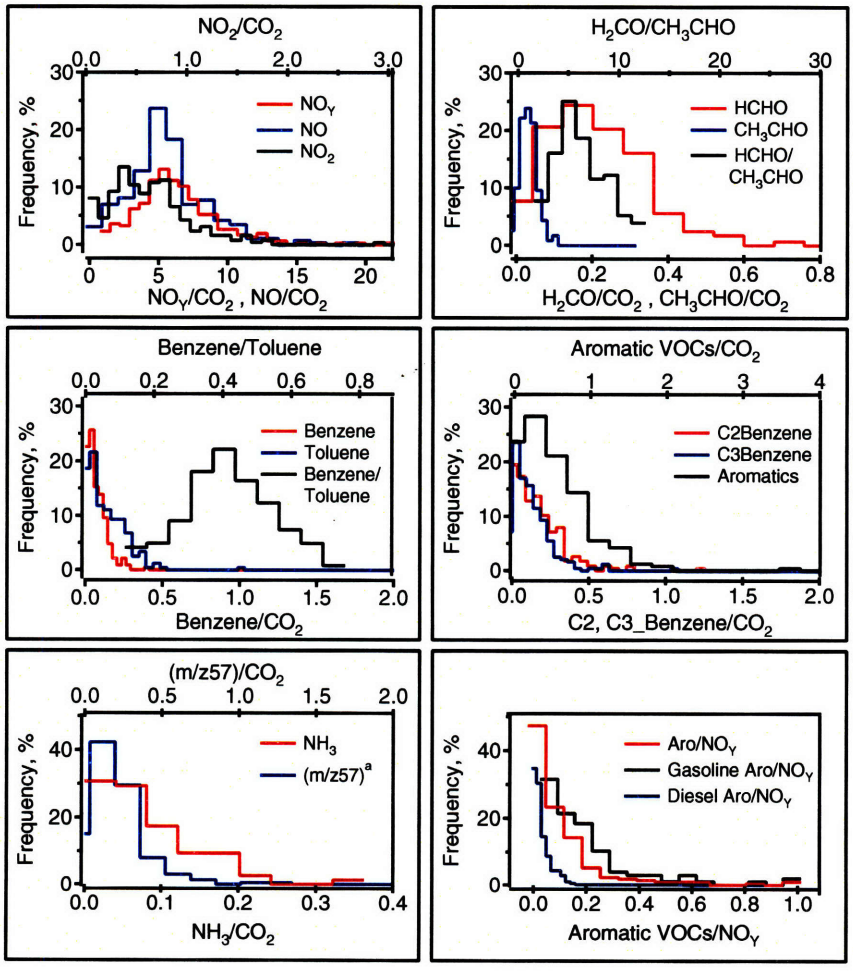

Figure 2.2. Frequency distributions of measured emission ratios [ppb/ppm] during the MCMA.[a] (m/z 57)/CO_2 represents MTBE + butenes for gasoline vehicles.

2.5. Discussion

An important aspect of the analysis of the data collected is to determine how representative it is of the vehicle fleet emissions in the MCMA. Given the large population of the vehicle fleet, the presence of various driving modes and the variability of all other parameters that play a role in the emission process in real world driving conditions, this is certainly an important issue to consider for any emission measurement technique. As shown in Table 2.2, the large size of the vehicle fleet in the MCMA for all vehicle categories predisposes a large sample size for any estimate attempt for a sample to be representative with traditional sampling techniques. Nevertheless, current estimations of emission factors for LDVs in the Emissions Inventory for the MCMA are based on a very small number of measurements performed in 1999 under laboratory-controlled conditions for individual vehicles (CAM, 2004). Furthermore, current estimates of emission factors for HDTs in the same inventory are entirely based on modeling estimates using a modified version of Mobile5, the US Environmental Protection Agency's motor vehicle emission inventory model.

In this work, we have extended the analysis procedure for the chase technique by considering measurements for both fleet averaged and individual in-class vehicle emissions. As described above, we estimated fleet LDV average emissions by analyzing the sampling periods when the mobile laboratory is measuring the mixed background air with the emissions of the surrounding vehicles for sustained periods of time. The assumption in this procedure is that the sampled emissions from a multitude of sources are sufficiently well mixed before arriving at the mobile lab sampling port. Since this condition is not totally controlled *a priori* for the experiment, it has to be determined from the analysis of the emission signals, the anemometer readings and the video camera. We have further classified such periods by driving state as SAG, TRA and CRU with the velocity criteria previously described. On the basis of the central limit theorem, the obtained fleet averages for each driving state should also be approximately normally distributed if the samples are unbiased and sufficiently large. In this case, symmetric

confidence intervals around the average could be established for fleet emissions estimates.

The variability in the emission estimates can be observed in the form of standard deviations reported in Table 2.3. Except for NO_2, the results for fleet vehicle estimates show standard deviations that are significantly smaller than the observed averaged emission values. This is expected for fleet average estimates using the central limit theorem. NO_2 is a difficult species to measure with this technique due to its high reactivity and to potential ambient production via the reaction of NO with oxidizing species, such as ozone, that can be significant in a highly polluted atmosphere. In some cases, the sum of the NO and NO_2 emission ratios is greater than the NO_Y emission ratio. Although this is not physically possible for an individual vehicle, it may occur for the average values of groups of vehicles.

Due to the relatively small sample size and the lack of vehicle model year information, in the case of the individual chase mode emission measurements of HDT and public transport vehicles, the observed variability may not represent the true variability of the population of emissions for these vehicle categories. The larger observed variability in these cases is likely the result of the large range of vehicles models, the variety of engine, fuel delivery, and emission control technologies, distribution of vehicle age and maintenance quality, and the variability of other parameters affecting emissions in real world driving conditions. As such, the averages and confidence intervals for these categories may not be representative of the entire fleet. Unless there is a significant increase of the sampling size, however, at this point the question of how much the obtained frequency distributions would change by increasing the sampling size is unsolved.

In order to further reduce any systematic bias in the measured emission ratios from individual chase events reported in Table 2.3, during the experiment we intentionally did not follow a given vehicle class on the basis of the visible strength and blackness of its exhaust. That procedure helped to avoid over sampling of high emitting vehicles in the

sampling population. Similarly, since the mobile laboratory followed different driving routes each day during the campaign throughout the city, the sampled emissions are most likely not biased by spatial differences in vehicle populations.

The emission frequency distributions shown in Fig. 2.2 provide us with some interesting insights into the mobile emission characteristics in the MCMA. A pronounced cityscape type of graph, as opposed to a smoothed distribution, may indicate the need for a larger sampling size population in our measurements. This is especially evident in the NH_3 emission distribution, which was constructed from about 25% of the sample size for the other species. The smaller sample size for NH_3 was due to the need to divert a LiCOR CO_2 instrument periodically to a shorter sampling inlet designed to avoid surface losses of NH_3 as well as some instrumental problems characteristic of a first field deployment. To our knowledge, this represents the first field deployment of a quantum cascade TILDAS on-board any mobile laboratory.

We define aromatic VOCs as the sum of benzene, toluene, C2-benzene (sum of xylene isomers, ethylbenzene, and benzaldehyde) and C3-benzene (sum of C_9H_{12} isomers and C_8H_8O isomers) as described in Rogers et al., (2006). Figure 2.2 shows that these aromatic VOC/CO_2 emission ratios tend to have higher frequency around a mean value but are also severely skewed towards high values of emission ratios. Although this behavior is often seen with VOC emission distributions, we observe that the reported distributions of the ratios benzene/toluene and H_2CO/CH_3CHO tend to be normally distributed, indicating the co-emission nature of these species in real world driving conditions.

The measured aromatic VOCs/NO_Y ratio presented in Fig. 2.2 shows a highly skewed but smoothly continuous hyperbola type distribution. Since the detected aromatic VOC content of the emissions from the CNG colectivos are very low and close to the instrumental and analytical uncertainty, we have excluded them from the plotted aromatic species distributions. Therefore, an explanation for the behavior of the aromatic VOCs/NO_Y distribution may rely on the emission characteristics of the vehicle fleet

sampled (populations of vehicles with low versus high aromatic VOCs/NO_Y emissions) and on the fact that the two major fuel types, gasoline and diesel, are included in the sample. To investigate which of these two aspects has a greater impact on the aromatic VOCs/NO_Y distribution we included in Fig. 2.2 the corresponding frequency distributions of gasoline and diesel vehicles that were sampled. The comparison of these distributions reveals that within the gasoline vehicle fleet low and high emitting aromatic VOCs/NO_Y vehicles can be distinguished. As long as the frequency distribution is representative of the aromatic VOCs/NO_Y ratio in the vehicle fleet, this result has important implications for the design of air quality control strategies by allowing the possibility of air quality emission reduction strategies to control the aromatic VOCs/NO_Y ratio in different parts of the vehicle fleet and/or ranges of driving modes.

Public transport colectivos and buses are a very important part of the transport system in the MCMA (Gakenheimer et al., 2002). As an example, colectivos represent only about 1% of the vehicle fleet in the MCMA but, together with the other small popular public transport vehicle called "combis", they account for almost 60% of the trips per person per day (CAM, 2004). Results presented in Table 2.3 indicate that, on a mole per mole basis, colectivos showed the highest NO_X emissions ratios among the sampled vehicles, especially for colectivos fueled with CNG. The higher NO_X emissions ratios for CNG colectivos is in accordance with their corresponding higher CH_3CHO/H_2CO ratio compared to gasoline fueled colectivos. The higher aldehyde emission ratios found in this work are consistent with dynamometer studies for CNG heavy duty vehicles performed by Huai et al., (2003) and Kado et al., (2005).

The quantification of high aldehyde emissions from MCMA vehicles may have important impacts on the photochemistry in urban areas (Garcia et al., 2006) and the generally high emissions of aromatic and aldehyde air toxics may have important health implications. H_2CO/CH_3CHO ratios showed a value of 6.2 ± 1.8 [ppb/ppb] averaged over all gasoline vehicle fleet emission measurements and the driving mode did not significantly affect this ratio. Measured emissions indicate that the emitted species that are most influenced by driving mode are NO_X, aromatic VOCs and their aromatic VOCs/NO_Y ratio. That effect

was only investigated in the fleet average gasoline vehicle fleet and not in the individual chase emission measurements. As such, the observed variability within individual vehicle categories may be due to internal variability of the specific power of the vehicles, vehicle age and model, and emission control technology, among others. Nevertheless, the observed variability within driving modes for averaged vehicle fleet emissions indicates that this type of analysis for ratios of selected VOC to NO_X species should be considered during the design of air quality control strategies that are based on the modification of the driving patterns, or modes, within the city.

An important aspect of this work lies in the comparison of these on-road results with the estimates for emission factors used in the official emissions inventory as well as with other measurements performed in the MCMA and other cities. The emissions inventory in the MCMA has been revised or updated every two years since 1994 and with homogenous methodologies since 1998. For comparisons with our results, we use the 2002 official Emissions Inventory (EI) for the MCMA considering the categories of light duty vehicles, colectivos and heavy duty trucks for NO_X emission factors. We present the comparison of our results with other estimations of emission factors in Fig. 2.3. The box plots represent the 10^{th} percentile, 1^{st} quartile, mean, 3^{rd} quartile, and 90^{th} percentile of our measurements for each category whereas the thinner adjacent colored bars represent the range of emission factors used in the emissions inventory. Light bars represent the estimations of emission factors using other techniques. In order to compare the obtained emission ratios in ppb/ppm units with other measurements performed with different sampling techniques it is necessary to make use of fuel properties and stoichiometric combustion assumptions. Data considered for this purpose are presented in the notes for Fig. 2.3.

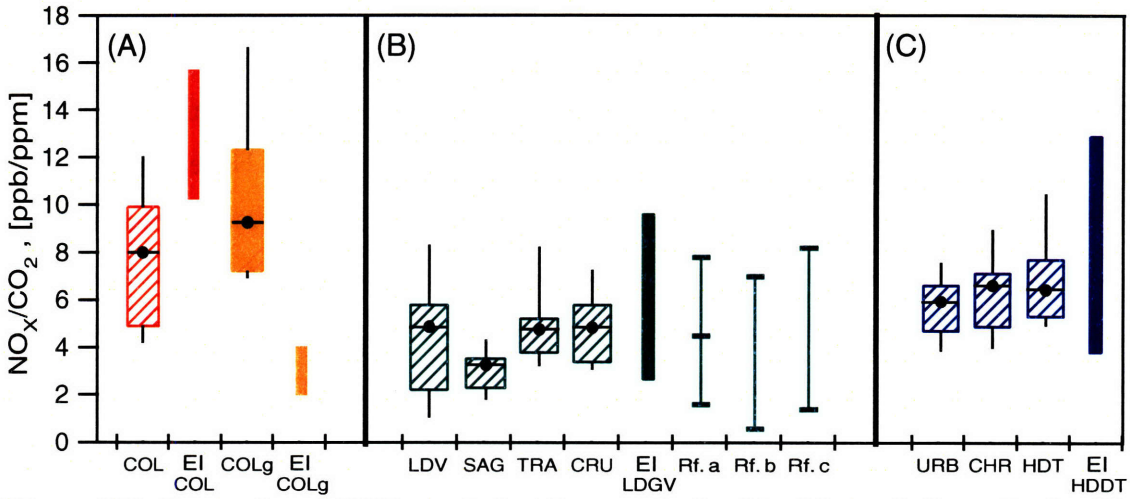

Figure 2.3. Comparison of NO_X emission factors obtained in this work (box plots) with estimates from the official 2002 MCMA Emissions Inventory (EI) (solid bars) and other studies (light lines) for panels: (A) colectivo buses, (B) Ligth duty Gasoline Vehicle (LDGV), and (C) Heavy Duty Diesel Trucks (HDDT). Box plots represent the 10, 25, 75, and 90 percentiles along with the mean of our measurements. Filled bars represent the minimum and the maximum EI estimates for the corresponding vehicle category. Rf. a: Schifter et al., (2005); Rf. b: Schifter et al., (2004); Rf. c: Schifter et al., (2000).

[a] For this comparison, we used fuel densities of 0.75, 0.85 and 0.41 kg/l for gasoline, diesel ad CNG fuels, respectively. Similarly, we considered 70.3, 72.5 and 62.5 moles of C per kg of fuel for gasoline, diesel ad CNG, respectively. Fuel economies were assumed as follows: 10, 2.1 and 1.6 km/l for gasoline, diesel and CNG fleets, respectively.

Figure 2.3 shows that NO_X emissions factors used in the emissions inventory for light duty vehicles are within the range of our measurement results and that a similar range of values are obtained with other techniques for this category. Note however that in Fig. 2.3 the range for the emission factors used in the emissions inventory considers the minimum and the maximum values, which are related to newest and oldest vehicle model years, and does not represent vehicle fleet estimates. However, Schifter et al. (2005) represents values taken from the minimum and maximum averaged emission factors for light duty vehicles from a remote sensing study performed in 2000 in the MCMA. The other two references shown for comparison of LDV emission factors in Fig. 2.3, Schifter et al. (2004) and Schifter et al. (2000), represent laboratory dynamometer studies with prescribed driving cycles. Interestingly, the reported emission factors among the different

techniques are similar. Nevertheless, the reported values are not weighted by the number of vehicles or any other activity parameter that may indicate their relative importance on the estimation of NO_X emissions.

A similar comparison of our results with the NO_X emission factors used in the MCMA emissions inventory for public transport vehicles indicates a possible overestimation in the gasoline-powered colectivos category. Similarly, our results indicate a possibly severe underestimation of NO_X emission factors for CNG-powered colectivos. The emissions inventory uses the same NO_X emission factors for our classified vehicle categories of URB, CHR and HDT, and their range falls within our results. However, in contrast to the comparison with the light duty vehicle fleet, these results correspond to individual vehicle measurements and therefore the observed variability may or may not be representative of a given vehicle category. Note, however, that in the case of the CNG colectivos, the range estimated in the emissions inventory is too small compared to the range of the observed variability. Therefore, assuming that the observed variability is real, this may be indicative of a real underestimation of NO_X emission factors used in the emissions inventory for this category.

The analysis of a possible under/over estimation of emission factors is only a part of the validation of an emissions inventory. Since the emissions inventory is based on assumed values for activity parameters (e.g. distances traveled) that may introduce further uncertainty in the estimation of mobile emissions, the final estimation of emissions is not trivial. A possible way to circumvent this difficulty is to consider the use of fuel based emission factors together with estimates of fuel consumption in a given region (Singer and Harley, 2000). We have followed this approach transforming our measured emission ratios to units of grams per unit of fuel consumed using the previously described assumptions of fuel properties and vehicle fuel efficiency. In the transformation of the emission factors we only considered the gasoline vehicle fleet averaged estimates.

Table 2.4 shows the comparison of our emission estimates for the MCMA with other studies. The results indicate that NO_X emissions estimated for LDVs in the emissions

inventory are within the range estimated using the fuel based emission factors in this work of 100,600 ± 29,200 metric tons per year. The upper and lower limits correspond to 1 standard deviation obtained from the observed emission factor for the LDV category. Although Table 2.4 shows that the comparisons for the total NO_X emissions for light duty vehicles between the emission inventory and this work may be within the confidence intervals, the possible under/over estimation of emission factors for individual vehicles ages and models may still be present in the emissions inventory. The application of the chase technique for systematically comparing emission factors by vehicle age and model would then be desirable to address this question.

Table 2.4. Comparison of mobile emissions (in tons/year) estimated in this work with emissions estimated in other studies for the MCMA and other US cities.

	This work[f]	2002 EI[a]	Jiang et al., 2005[d]	Schifter et al., 2000[b]	Schifter et al., 2005[c]	Los Angeles[e]
NO_X	100,600 +- 29,200	92,500	120,000 +- 3,000	ND	100,200 +- 23,500	280,000
Benzene	4,090 +- 850	ND[h]	3,800 +- 100	1,590	ND	2,290
Toluene	10,100 +- 2,200	ND	ND	ND	ND	ND
H_2CO	3,020 +- 720	ND	ND	397	ND	1,900
CH_3CHO	770 +- 230	ND	ND	167	ND	605
NH_3	900 +- 500	3,120	ND	ND	ND	8,800 – 10,600[g]

[a] Considers the emissions from the gasoline vehicle fleet: private vehicles, taxis, combis, colectivos and pickups.

[b] Based on a laboratory study of around 50 vehicles (ages from 1984 to 1999) tested under a FTP cycle.

[c] Based on a remote sensing study in 2000 for the MCMA.

[d] Considers the total vehicle fleet, LDVs and HDVs.

[e] Total on-road gasoline mobile emissions estimates for 2004 in the South Coast Air Basin. Source: CARB, 2005.

[f] Uses gasoline fuel consumption by the transport sector alone estimated for 2002 in the MCMA Emissions Inventory and the fuel properties reported in Fig. 2.3 of this document.

[g] Data includes all NH_3 on-road mobile emissions taken from Fraser and Cass, (1998).

[h] ND: A value Non Determined in the study.

Our results indicate larger emission estimates for benzene, toluene, formaldehyde and acetaldehyde than Schifter et al. (2000), which was based on a limited sample of vehicles

tested in controlled laboratory conditions. The emissions inventory does not provide estimates of speciated hydrocarbon emissions and therefore, no comparison is possible for these species. In Table 2.4 we also show the comparison of estimated toxic VOC emissions between Los Angeles and the MCMA. The results indicate that the annual estimates of benzene, acetaldehyde and formaldehyde LDV emissions in the MCMA are similar or higher than the corresponding estimated toxic VOC emissions in Los Angeles. For the year of comparison (2003), the vehicle fleet in the Los Angeles area was 3.2 times higher than the entire fleet in the MCMA and the annual gasoline consumption was 3.3 times higher (Molina and Molina, 2004). Besides the larger size of the vehicle fleet and the corresponding higher fuel consumption in the Los Angeles area, two other important aspects of the comparison are the older vehicle fleet composition and the smaller fraction of vehicles with emission control technologies in the MCMA. For example, only about 30% of the vehicle fleet count with Tier (0 and 1) control emission technologies in the MCMA as compared to 91% in Los Angeles (Molina and Molina, 2002). This indicates that an aged vehicle fleet and a smaller fraction of vehicles with efficient emission control technologies may have a significant impact on the overall burden of toxic VOC emissions in the MCMA. (Bishop et al., 2001) has reported a slight but statistically significant increase of NO with increased altitude for heavy duty trucks. Nevertheless, reasons for the altitude relationship are unclear and may be subject to particular characteristics and composition of the sampled vehicle fleet.

As noted above, the sampling size of the measured on-road NH_3 emissions was significantly smaller than the rest of the reported species due to the lack of a dedicated fast response CO_2 monitor on the short, fast flow inlet necessary for NH_3 measurements and some QC-TILDAS instrument problems characteristic of a first field deployment. As such, the NH_3 emission estimate in Table 2.4 has large confidence intervals and may not be fully representative of the LDV vehicle fleet. Nevertheless, the entire range estimate is significantly smaller than the vehicle NH_3 emissions estimated in the current model based emissions inventory for the MCMA and than the on-road NH_3 emission estimate in Los Angeles. Given the median age of the MCMA vehicle fleet, this is not surprising since NH_3 emissions are dominated by newer gasoline powered vehicles equipped with NO_X

reduction catalysts. In our measurements, NH_3 emissions for MCMA LDVs seem to be much higher for newer vehicles, which are presumably equipped with reduction catalysts for NO_X and appear to be relatively independent of driving state. NH_3 emitted from on-road vehicles may react rapidly with acid vapors to form high burdens of secondary particulate matter near heavily traveled roadways, impacting fine particle exposure levels for travelers and near by residents. The level of NH_3 emissions from newer LDV vehicles in the MCMA do appear to be significantly higher than the emissions of similar vehicles in the US (Herndon et al., 2005a). The impact of vehicular NH_3 emissions on the MCMA NH_3 emission inventory will be addressed more thoroughly in a separate publication (Shorter et al., 2007[2]).

2.6. Conclusions

In this work, we have extended the analysis procedure for the on-road mobile laboratory measurements by considering measurements of both fleet averaged emission measurements and individual vehicle emissions. The measured emission ratios represent a sample of emissions of in–use vehicles under real world driving conditions for the MCMA. From the relative amounts of NO_X and selected VOC's sampled, the results indicate that the technique is capable of differentiating among vehicle categories and fuel type in real world driving conditions. We have further classified our results by vehicle categories and driving mode using pre-established velocity criteria in our analysis. Our measurements of emission ratios for both CNG and gasoline powered "colectivos" indicate that -in a mole per mole basis- have significantly larger NO_X and aldehydes emissions ratios as compared to other sampled vehicles in the MCMA. Similarly, ratios of selected VOCs and NO_Y showed a strong dependence on traffic mode. The potential implications of these results are important for the design of air quality control strategies based on the modification of the driving modes and the retrofitting of public transport vehicles.

[2] Shorter, J. H., Herndon, S. C., Zahniser, M. S., et al.: Atmospheric Ammonia in Mexico City during MCMA-2003, Atmos. Chem. Phys., to be submitted, 2007.

By using a fuel consumption based approach together with the measured emission factors in this work, we estimate NO_X emissions as 100,600 ± 29,200 metric tons per year for LDGVs in the MCMA for 2003. According to these results, annual NO_X emissions estimated in the emissions inventory for this category are within the range of our estimated NO_X annual emissions. However, we did not explore the classification of emissions by vehicle age and under/over estimations of NO_X emissions for individual vehicle age categories can still exist in the emissions inventory. We also have estimated annual emissions for benzene, toluene, formaldehyde and acetaldehyde in the MCMA for the first time following a fuel-based procedure. The results indicate that the annual estimates of benzene, acetaldehyde and formaldehyde LDV emissions in the MCMA may be greater than previously reported and that their magnitudes are similar or higher than the corresponding estimated toxic VOC emissions in Los Angeles and other US cities. Vehicle age fleet composition and the relatively small fraction of vehicles with emission control technologies in the MCMA may significantly contribute for these large toxic emissions. Finally, ammonia emitted from newer reductive catalyst equipped LDVs may react rapidly with air vapors to form high burdens of secondary particulate matter near heavily traveled roadways.

Chapter 3. On-road mobile emission ratios measured in Mexicali 2005, Austin, Tx 2003, and MCMA-2003 using the ARI mobile laboratory

3.1. Introduction

In an urban area the chemical composition of the air is influenced by a wide variety of different emission sources. The emissions from transportation sources, primarily on-road motor vehicles, are generally the largest contributors to criteria pollutants such as CO, NO_X and selected VOCs in urban areas; On-road vehicles are also major sources of fine primary particle emissions and specific air toxics. However, despite their importance on determining air quality levels, the estimation of mobile emission sources is highly uncertain in most urban areas. As described in Chapter 2, multiple parameters affect the variability of mobile emissions within and across vehicles types and, as a result, their measurement in real world on-road conditions is a challenge (Cadle et al., 2002). Factors such as engine size and type, fuel composition, temperature and pressure are directly linked to the combustion efficiency (and therefore the emission rates) of in-use vehicles; other external factors such as the character and maintenance of fuel delivering and emission control systems also decisively affect the variability and composition of mobile emissions.

All the aforementioned factors affect the observed variability during the sampling of on-road emissions for a given vehicle type. Similarly, the observed variability during the sampling of on-road emissions in "fleet-average"[3] conditions constitutes the sum of the individual emission variability from a wide range of vehicles. As a result, inter-comparisons of mobile emission measurements using different emission measurement techniques (such as remote sensing, dynamometer and tunnel studies), are intrinsically difficult to perform due to differences in necessary assumptions, sampling times and frequencies as well as the sampling size of measurements.

[3] In here, we use the term "fleet-average" to describe conditions in which the individual plume emissions from a large number of vehicles are captured during the sampling. The larger the sampling size, the more probability that the overall emission characteristics of the fleet are captured.

From April 14 to 23 of 2005 the Aerodyne Research Inc. mobile laboratory (ARI) was deployed in Mexicali, Baja California as part of a field campaign denominated Border Ozone Reduction and Air Quality Improvement Program for the Mexicali-Imperial Valley. This chapter focuses on describing the measurements of on-road mobile emissions obtained during the Mexicali field campaign under different driving modes using the chasing technique described in the previous chapter. We also present a comparison of the obtained on-road emission measurements with corresponding measurements obtained during the MCMA-2003 field campaign. This constitutes a unique opportunity to compare the (gasoline) vehicle fleet emission characteristics of a megacity and a smaller urban area in a developing country. As the measurements were obtained using the same technique, assumptions and instrumentation, the observed differences during the comparison are more likely to be the result of actual differences in fleet emission characteristics. This "clean" comparison could be useful for understanding the fast-evolving characteristics of the vehicle fleet in a US-Mexican border city.

In addition to the measurements obtained in Mexicali, during May 8 to 9 of 2003 the ARI mobile laboratory obtained on-road measurements of heavy duty diesel trucks (HDDT) in and near Austin, TX. The measurements of HDDT on-road emissions were obtained for individual trucks rather than for diesel fleet average emission conditions. Nevertheless, we perform a comparison of the obtained results with measurements obtained from individual HDDTs in Mexico City and Mexicali.

Mexicali on-road emissions data will be presented in four sections. First, we will present and compare the observed emission ratios between the described sampling modes for emitted NO_X, CO, specific VOCs, NH_3, and some primary fine particle components and properties. The clear detection of high emitter on-road vehicles and their comparison with the fleet average emission measurements will be highlighted. Second, specific emitted VOC species measured with the PTR-MS and the TILDAS instruments on board the mobile laboratory are ratioed and inter-compared between the operational sampling modes. In the third section of this document the observed on-road emission indices for particular species are transformed to appropriate units and compared with cataloged

mobile Emissions Inventories. Finally, the observed emission ratio measurements will be compared with other on-road emission ratios similarly obtained in Mexico City for the gasoline vehicle fleet (Zavala et al., 2006) and in Austin, TX for individual HDDTs.

3.2. On-road emission ratios of gasoline and diesel vehicles

Three types of ARI mobile laboratory measurements led to on-road vehicle emission data during the 2005 field campaign in Mexicali: 1) individual identified vehicle emission plumes measured by the roadside sited stationary mobile laboratory; 2) chase experiments, where the mobile laboratory followed a specific vehicle, repeatedly sampling its exhaust plume; and 3) on-road or roadside fleet average sampling modes where no attempt is made to distinguish plumes from individual vehicles and all intercepted vehicle emissions plumes are counted and weighted equally. All identified exhaust pollutant species are correlated with the excess (above background) CO_2 concentration, allowing molar emission ratios to be computed for each measured exhaust pollutant. Fuel based emission indices (g of pollutant to liter of fuel consumed) can readily be computed using the fuel properties from the observed molar emission ratios.

A total of 98 valid mobile emission ratio experiments were obtained during the analysis of 14.5 hours of on-road and roadside data. The samples comprised a variety of engine operational modes (e.g. idling, acceleration, cruising, etc), fuel types (gasoline and diesel), vehicle types (heavy duty diesel trucks and buses, light duty gasoline vehicles) and vehicle model years. Emission ratios from individual emission plumes were obtained during periods of stationary sampling along the road whenever the wind was favorable for transporting the vehicle's emissions to the mobile laboratory sampling port. Chase emission samplings were obtained during the periods in which the mobile laboratory distinguishable captured the emissions from target vehicles (primarily heavy duty diesel trucks and buses) for several minutes. Emission ratios in fleet average sampling mode were obtained by analyzing the periods in which the emission signatures from surrounding vehicles were sufficiently mixed by the time they were sampled by the mobile lab. The particular analytical procedures for obtaining the emission ratios in these

operational sampling modes is described in more detail elsewhere (Zavala et al., 2006). Approximately 55 individual vehicles were characterized by roadside sampling, 19 by dedicated on-road chase, and 24 fleet average experiments sampled between a few tens to several hundred vehicles.

3.2.1 Roadside stationary sampling plumes

The mobile laboratory obtained on-road measurements of emission ratios in stationary sampling mode by situating on the side of a one way road with moderately intense traffic and no visible grade during the 2005 Mexicali campaign. For approximately 1.5 hrs on April 22 the mobile laboratory sampled dozens of individual plumes from passing vehicles. Sampled vehicles included both Light Duty Gasoline Vehicles (LDGV) and HDDT traveling from moderate to high speed. Other measurements of individual vehicle emission plumes were obtained during shorter periods of stationary road-side sampling during the campaign. These will not be specifically discussed in this section but will be included in section 3.2.4 for the inter-comparison with other sampling operational modes.

The mobile laboratory was situated in the prevailing downwind direction from the emitting vehicles as consistently as possible because, in this type of operational sampling mode, a successful measurement of an emission exhaust signature from a passing vehicle is highly dependant on the predominant wind direction and speed at the time of the exhaust event. Once a plume exhaust is emitted from the passing vehicle, the aerosol and gaseous exhaust components are rapidly decelerated by the surrounding ambient air. The initial exhaust also has a significantly higher temperature than the background air. The presence of advection and induced turbulence produces rapid dilution and cooling of the emitted exhaust, dominated by small eddies generated by the inertial wake left by the vehicle. As the temperature gradient between the plume and the surrounding air decreases, further dilution is controlled by the local wind advection and turbulence, and the emissions slowly approach to background on-road concentrations. Given the relatively small mass flux exhaust intensity for some vehicles and the short distance between the vehicle's emission exhaust location and the laboratory's sampling port, the

signatures of the exhausts plumes recorded by the instruments last typically only a few seconds before they are highly diluted by the background air. Therefore, a characteristic time window of only a few seconds exists for high signal to background exhaust emission measurements.

Fortunately, the real-time trace gas and fine PM instruments aboard the mobile laboratory can resolve these short duration plumes allowing successful measurements of individual vehicle emission plumes as long as the selected road was not too heavily traveled. In the cases analyzed, unequivocal distinction of emission signatures for individual passing vehicles was possible due to the relatively large elapsed time in between passing vehicles. Additionally, analysis of recorded wind direction and speed in conjunction with the video camera helped to identify specific vehicles that produced the detected plumes. Highly sensitive and high time-response instruments are clearly critical for obtaining emission ratios for this type of sampling.

Figure 3.1 shows an example of stationary sampling emission plumes of a LDGV and a HDDT. As shown in Figure 3.1, the sampled plumes lasted from 10 to 20 seconds before the emission signature is indistinguishable from the background on-road air. The combustion signature of the plume is observed by the high correlation of the emitted pollutants to above background CO_2 concentrations.

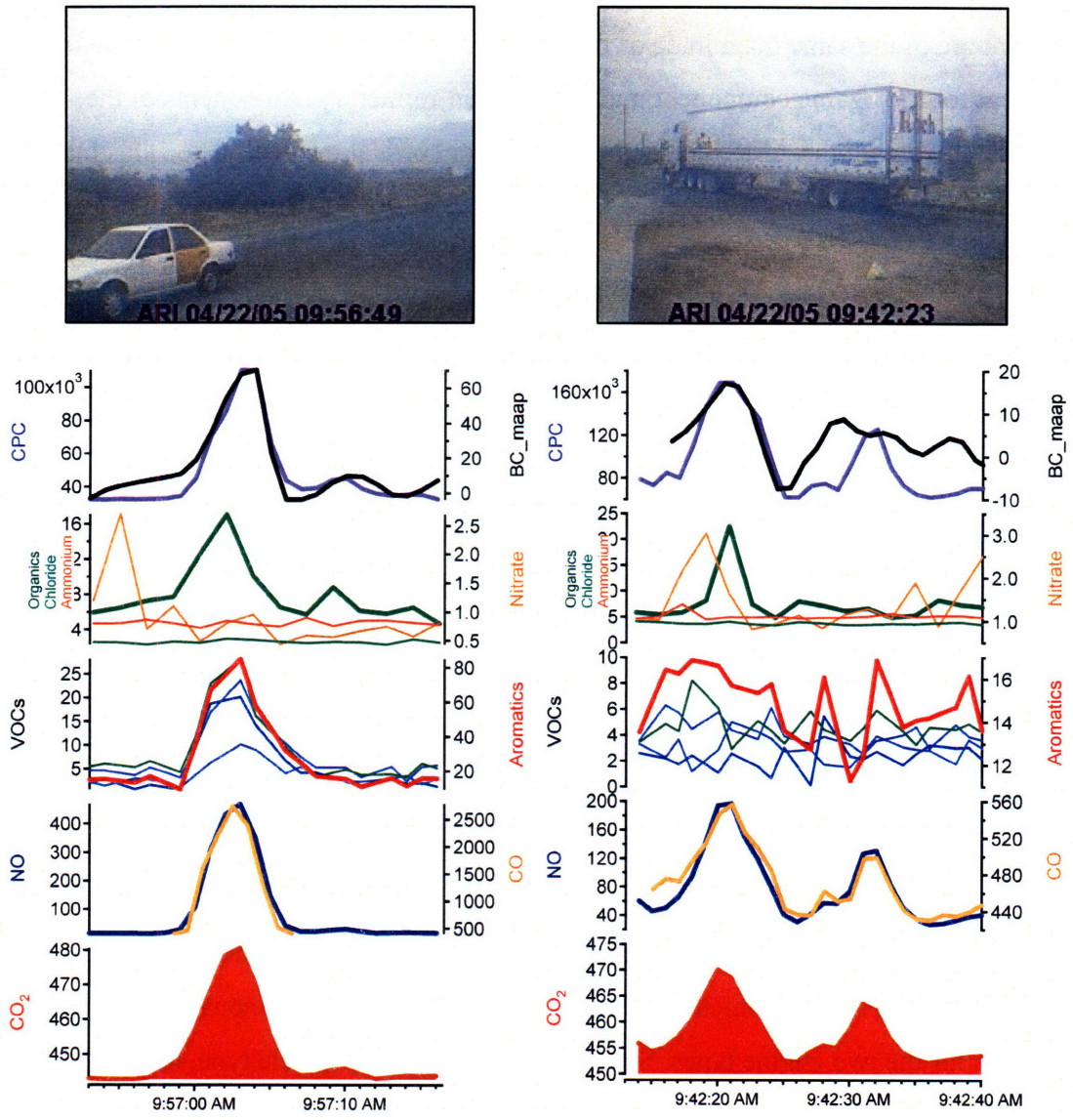

Figure 3.1. Roadside stationary exhaust emission measurements of on-road light duty gasoline (left panels) and heavy duty diesel (right panels) vehicles. All pollutant concentration units are ppbv, except for CO_2 [ppmv], AMS fine PM nonrefractory composition [ug/m3], light absorption [1/m] and fine particle number [pp/cc].

In the particular case of the LDGV shown in Figure 3.1, the vehicle had notoriously high concentrations of most emitted pollutants and consequent high emission ratios. There is however a clear distinction between the emission ratios of the two types of vehicles sampled. The CO and VOCs sampled in the case of the HDDT are significantly lower than the LDGV whereas the emitted NO, particle number density and the organic PM

component are of the same magnitude or higher. Also noticeable in Figure 3.1 is the fact that, except for its organic component, most of the non-refractory components of the aerosols sampled with the AMS had negligible or poor correlations with CO_2. This may be explained by the secondary formation of the chloride, nitrate and ammonium aerosol components, the short time between the emission and the sampling, and the short duration of the sampling time for the plume. The difference of the peak minus the background for the organic component is higher for the HDDT but is clearly significant in the LDGV as well, an indication of a high emitter vehicle.

Figure 3.2 shows a comparison of observed emission ratios of CO, NO, aromatic VOCs (considered here as the sum of benzene, toluene, c3-benzenes and c2-benzenes) and fine particle (10-1000 nm diameter) number density (CPC), of emission plumes from individual gasoline and diesel vehicles sampled in the stationary road-side mode. Each marker in the figure represents an individual measurement of an emission ratio for a given vehicle. Figure 3.2 demonstrates the co-emitting nature of various pollutants for a given vehicle type and the variability between vehicle types.

Figure 3.2 also indicates that the sampled LDGVs showed higher aromatic and CO emissions than the HDDTs, which is a direct result of the different combustion efficiencies for the two engine types. Similarly, within a given vehicle type, high CO and aromatic content in a vehicle's exhaust is an indication of poor combustion efficiency, probably due to a fuel rich Air-to-Fuel (A/F) condition in the engine. Both sampled vehicles present a linear (log) correlation between its aromatic and CO emission ratios whereas more scatter is observed for other species correlations. Typically, diesel engines tend to work on leaner A/F conditions than LDGV engines, producing considerably less CO and unburned hydrocarbons.

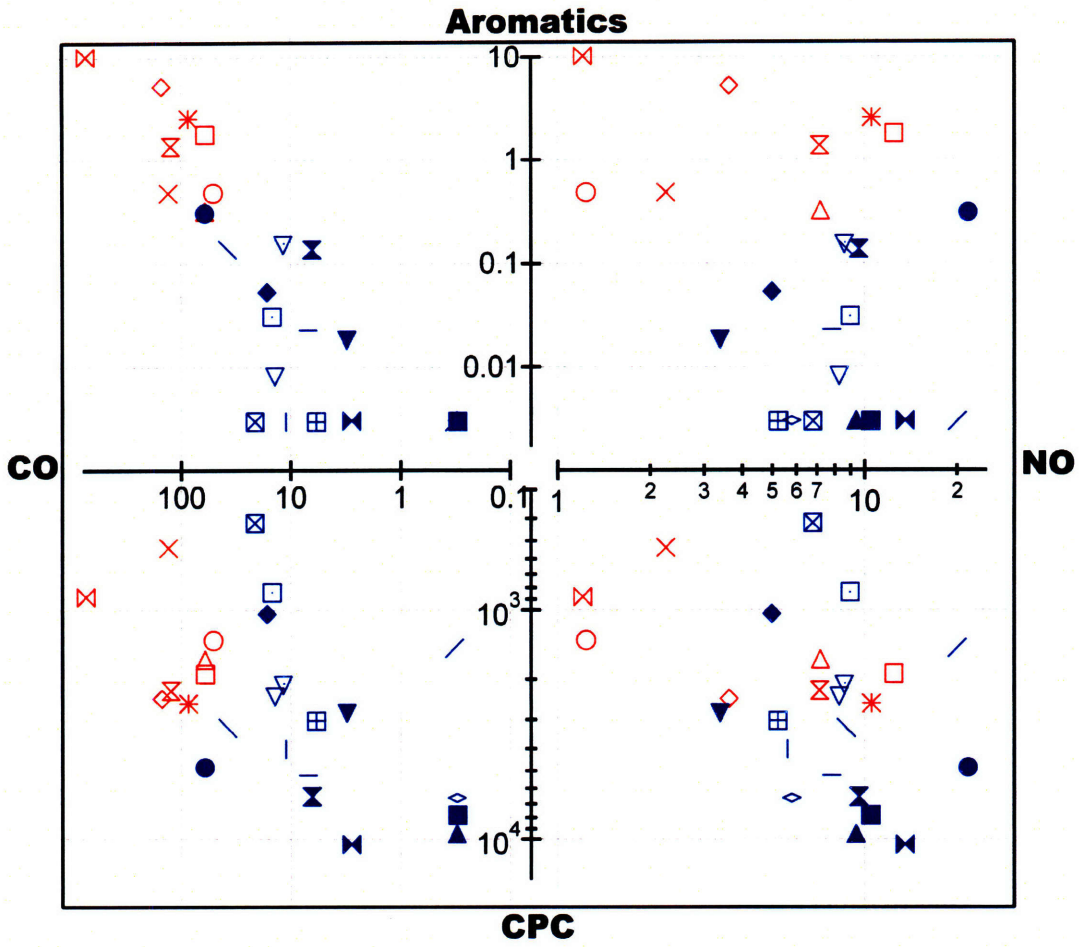

Figure 3.2. Comparison of emission ratios for CO [ppb/ppm], NO [ppb/ppm], aromatics [ppb/ppm] (sum of benzene, toluene, C3-benzenes and c2-benzenes) and particle counting [part/cc/ppm] (CPC), of individual vehicles sampled in stationary mode for gasoline (red) and diesel (blue) vehicles.

Quantification of emitted fine particles and specific gaseous pollutants often reveals large variability even within a given vehicle type. Particle number density and NO emission ratios for HDDTs were, in general, higher than those for LDGVs, as expected, but a larger variability is observed for NO emission ratios from LDGVs. The particularly large variability of NO emission ratios for LDGV may be the result of the different engine combustion temperatures regimes of the sampled vehicles. Higher combustion temperatures are related to higher thermally-formed NO_X species whereas fuel-formed NO_X tends to vary with the type of fuel. As mentioned, there are a large number of

factors that affect the emission characteristics of a given vehicle, all of which affect the observed variability during the sampling of on-road emissions. As such, it is of particular interest to compare the observed variability of the sampled plumes in stationary mode with fleet average emission ratios measurements. In section 3.2.4 we present comparisons of emission ratios obtained during stationary sampling of vehicle's plumes and other operational sampling modes.

As a result of the incomplete combustion process, gases and aerosols are formed at high temperatures and are directed towards the emission exhaust. Before leaving the exhaust system, the gases and aerosols are traveling relatively rapidly due to the vehicle speed and to the flow in the exhaust pipe. However, at this stage they are experiencing negligible dilution. Other sources of particle matter in the exhaust can include metal-based lubricating oil additives and engine wear particles that are entrained in the exhaust products. Whether a direct product of the incomplete combustion process or formed from the additives and/or wear of metallic surfaces, the particles can deposit and accumulate on the surfaces of the exhaust system –including the emission control system- and be removed by later exhaust cycles.

3.2.2 Vehicle chase experiments

The vehicle chase technique was used during the 2005 Mexicali campaign to obtain on-road vehicle emission ratios for specific vehicle types under real-world driving conditions. The analytical procedures used for the data obtained with the chase technique can be found in more detail elsewhere (Herndon et al., 2005a). Briefly, in this technique the on-road emissions plume from a target vehicle are monitored by following it, repeatedly intercepting its exhaust emission plume over a period of several minutes. Similar to the roadside stationary plume sampling, the signals from the emitted plume species are scaled to the above background exhaust carbon dioxide column concentration signal. The scaling of the above background emitted species to carbon dioxide provides an emission ratio quantifying the ratio of concentrations of the emitted species to the plume excess CO_2 concentrations. For gaseous pollutant species these are generally

presented as plume excess concentrations of the target pollutant in ppbv to plume excess CO_2 measured in ppmv.

In the chase technique the identification of emission plumes from the data is done with the analysis of the multiple synchronized instrumental measurements on board the mobile laboratory. These include the readings from the sonic anemometer (to indicate the source of the advected target vehicle plumes), on-road images obtained with the front mounted video camera and notes written into the data control program by the researchers on board the mobile laboratory, as well as each trace gas or fine PM instrument measurement. The species signals are self consistent and correlated if they are all contained in the target combustion exhaust plume. When intercepting a target vehicle's plume, the instruments on board the mobile laboratory quantify these signals and their inherent emission ratios are obtained from their correlation to plume excess CO_2 as the combustion tracer, automatically adjusting for the degree of dilution of the intercepted plume. This technique is only possible due to the high time resolution and sensitivity of the instrumentation that are capable of capturing the rapidly changing emission plume parameters.

Figure 3.3 presents the measured on-road mobile emission ratios in the chase sampling mode for both gasoline and diesel vehicles. HDDTs and other large vehicles are intrinsically easier to measure with the chase technique due to the strength of their fresh plume signals and to the ease of intercepting them while directly following the target vehicle. Few LDGVs, which typically emit smaller and cleaner plumes, were targeted with the chase technique. Nevertheless, a number of visibly high emission gasoline powered vehicles were measured in chase mode, mostly pick-ups and vans, and the results are included in Figure 3.3 for its comparison with measurements from HDDT vehicles.

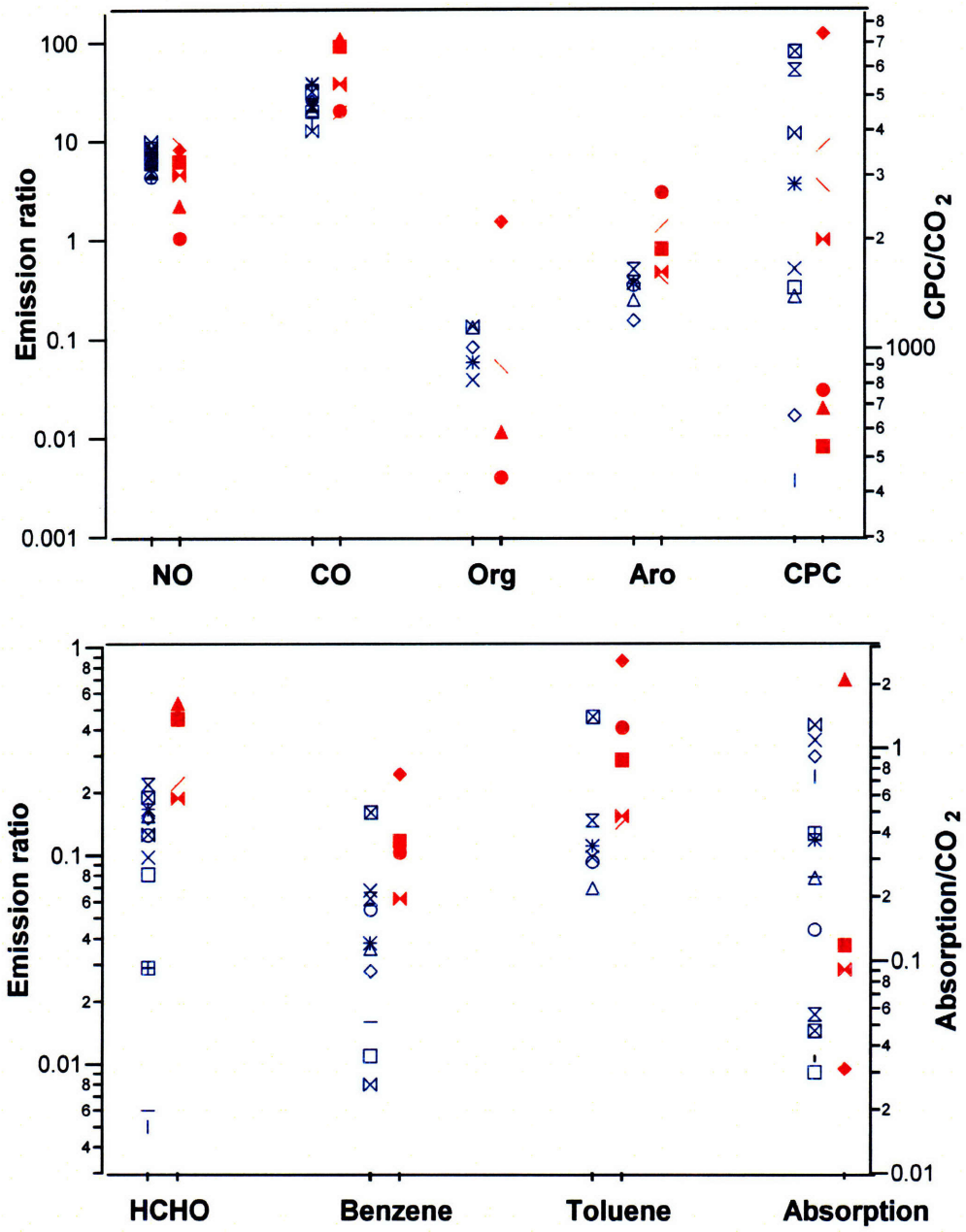

Figure 3.3. Mobile emission ratios measured from gasoline (red) and diesel (blue) vehicles in Mexicali. Each symbol represents an individual vehicle. All units are in [ppb/ppm] except for the measured absorption [1/um/ppm]. Aro refers to the sum of the aromatics: sum of benzene, toluene, C3-benzenes and C2-benzenes. Org refers to the organic component of the fine aerosol mass (less than 1 um in diameter).

Figure 3.3 shows generally higher CO and VOC emission ratios for high emitter gasoline powered vehicles and high variability for almost all other measured parameters. Aldehyde and other VOC emission ratios are particularly high for these gasoline powered vehicles, a probable indication of the malfunctioning of, or the lack of, an emissions control system. Similarly, measured NO emission ratios for the high emitter gasoline vehicles are as large as the HDDT emission ratios. However, although the emitted VOCs are higher for the high emitter gasoline powered vehicles, the organic content in the PM phase of HDDT emissions tends to be higher. This is partially a direct result of the higher content of low volatility hydrocarbon molecules in diesel as compared to gasoline fuels. Diesel engines may also inject a larger fraction of unburned motor oil into their exhaust. Interestingly, the measured variability of the fine particle number density was similar in both types of vehicles but their light absorption, quantifying black carbon content, tends to be smaller for the gasoline vehicles. This is probably also a direct result of the different engine combustion process in the two vehicle classes.

3.2.3 Fleet average emission ratios

In addition to the chase technique, which focuses on a series of selected individual vehicles within a given vehicular class, fleet average on-road emissions can be obtained by processing randomly intercepted vehicle plumes from surrounding traffic. As such, in the fleet average mode the mobile laboratory measured on-road ambient air mixed with emissions of the surrounding vehicles under different experimental settings. These experimental settings included: 1) driving on the road with the rest of the traffic while capturing surrounding vehicle's emissions, 2) stationary sampling of passing vehicles under high traffic load conditions and 3) a semi "open path" approach in which the mobile laboratory drives and samples the emissions along a stationary or semi-stationary line of idling vehicles. For these experimental settings, it is possible to obtain emission ratios classified by driving mode according to the predominant speed of the traffic.

In the fleet average mode, where even merged plumes from multiple vehicles can be processed and included, the sampling time (and therefore the number of vehicle exhaust

plumes interrogated) is normally larger than for chase mode measurements, providing better statistics. Successful application of this method requires a large sample size of mixed emission periods and long enough sampling times so that the number of sampled vehicles is large enough to include a representative number of high emitters. Care must also be taken to avoid situations where the intercepted plumes are dominated by a few nearby vehicles for significant portions of the sampling period. On the basis of the central limit theorem, the emission averages should then be normally distributed if the samples are unbiased and sufficiently large. In such case, symmetric confidence intervals around the average can be established for fleet emissions estimates. The emission ratios obtained in the fleet average operational sampling mode are appropriate to use for comparison with mobile emissions measured with other high sampling volume techniques and for the validation of an emissions inventory.

We accounted for traffic speed of the sampled fleet by qualitatively classifying the sampling periods as: a) IDL for the cases when we used the semi "open-path" approach focused on idling vehicles, b) SAG for cases when the traffic conditions were the type of "Stop and Go", typically under high traffic conditions, c) TRA for cases when there were high traffic conditions but with prevailing moderate speed, and d) CRU for the cases where the sampled fleet was cruising at moderately high to high speeds. The IDL mode measurements were predominantly obtained while sampling the line of vehicles waiting to cross the Mexican-US border at Calexico. In this experiment the mobile laboratory drove by on a traffic free road located beside the border waiting line, entering and re-entering several times, capturing idling and semi-idling emissions from the waiting vehicles.

The measured mobile emission ratios for CO, NO, HCHO, benzene and fine particle number density under the previously described driving mode conditions are presented in Figure 3.4. Similarly, the measured mobile emission ratios for these and the rest of the parameters sampled in fleet average mode are summarized in Table 3.1. In all driving modes gasoline vehicles dominated the type of vehicles sampled. Therefore, we will consider these measurements as representative of the gasoline vehicle fleet, not the

combined gasoline and diesel fleets. Due to difficulties with inappropriate sampling frequency settings for the AMS instrument, there are no available fleet averaged emission PM species partitioning emission ratios for this sampling mode.

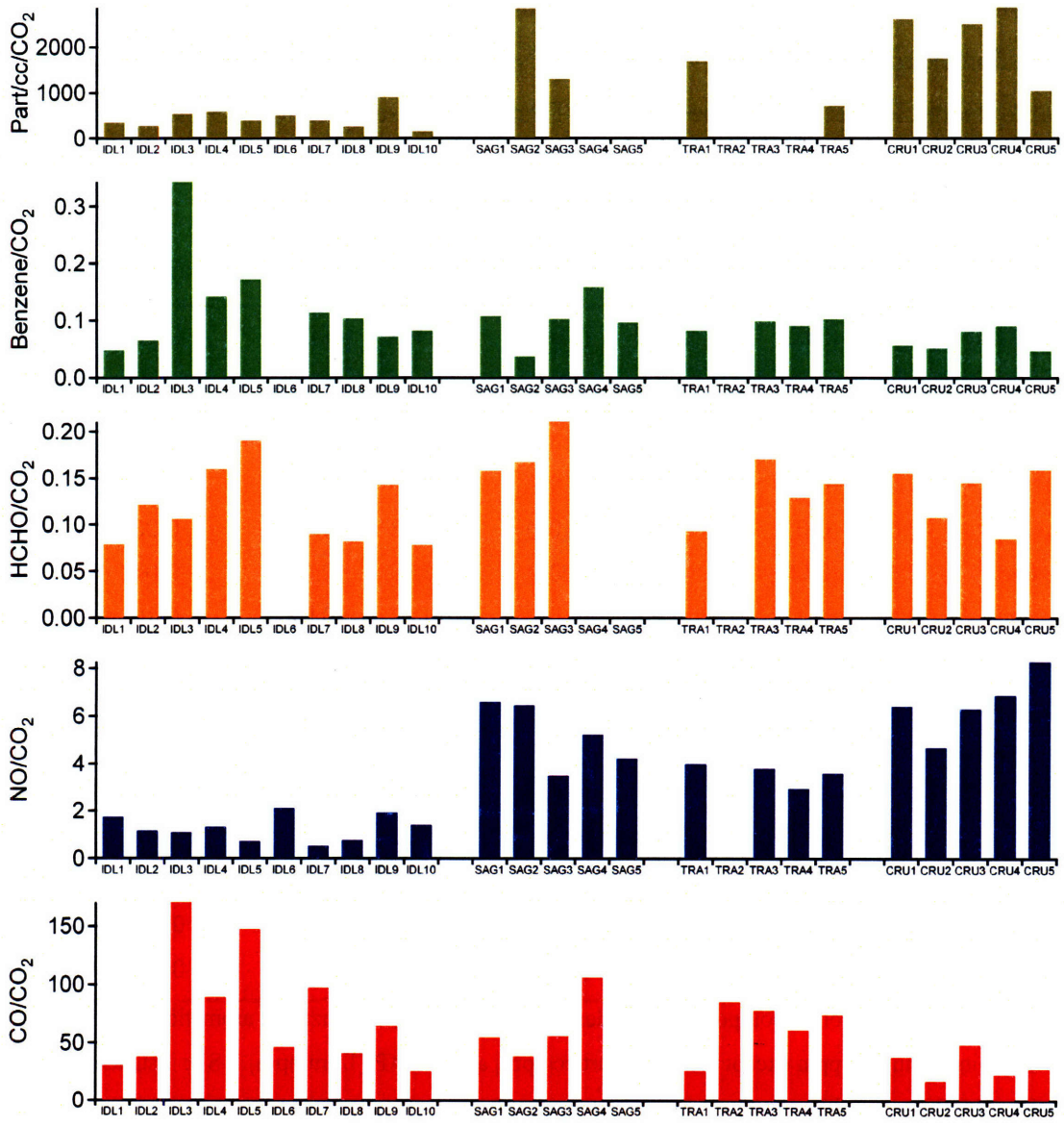

Figure 3.4. Mobile emission ratios for various pollutants measured in fleet average mode for four driving modes (see text for definition of driving modes). All units are in [ppbv/ppmv] except for the number of particles [part/cc/ppmv].

Important differences can be observed in emission ratios by driving mode in Figure 3.4 for NO, CPC (fine PM number density) and CO whereas the effect is less evident for benzene and practically non existent in HCHO emission ratios. This is consistent with other studies on Mexico City fleet averages using the same sampling technique (Zavala et al., 2006). Higher NO emission ratios for higher driving speeds are consistent with the notion of higher engine combustion temperatures and higher availability of oxygen in the combustion chamber of gasoline vehicles at those speeds. Similarly, the production of CO at low vehicle speeds increases as the A/F ratio decreases with less efficient combustion.

Table 3.1. Measured mobile emission ratios during the Mexicali field campaign[a].

Pollutant	IDL	(SD)[b]	SAG	(SD)	TRA	(SD)	CRU	(SD)
CO	74.8	(50.5)	63.7	(29.3)	64.8	(23.3)	30.6	(12.5)
NO	1.28	(0.53)	5.20	(1.35)	3.59	(0.45)	6.50	(1.29)
HCHO	0.12	(0.04)	0.18	(0.03)	0.13	(0.03)	0.13	(0.03)
CH_3CHO	0.04	(0.01)	0.06	(0.01)	0.03	(0.01)	0.03	(0.002)
Benzene	0.13	(0.09)	0.10	(0.04)	0.09	(0.01)	0.07	(0.02)
Toluene	0.17	(0.11)	0.22	(0.09)	0.17	(0.02)	0.10	(0.02)
C2benzenes	0.21	(0.16)	0.24	(0.09)	0.19	(0.02)	0.14	(0.04)
C3benzenes	0.16	(0.11)	0.19	(0.10)	0.13	(0.02)	0.05	(0.03)
Aromatics	0.70	(0.47)	0.79	(0.33)	0.62	(0.07)	0.36	(0.05)
m105	NA[b]	NA	0.01	(0.002)	0.01	(0.002)	NA	NA
m59	0.016	(0.005)	0.024	(0.011)	NA	NA	0.005	(0.002)
CPC	436	(209)	NA	NA	NA	NA	2146	747)
MAAP	0.031	(0.047)	NA	NA	NA	NA	0.069	(0.085)
NH_3	0.032	(0.014)	0.037	(0.006)	NA	NA	0.053	(0.027)

[a] See text for an explanation of compounds considered as C2benzenes, C3benzenes, aromatics, m105, and m59. All units are in ppb/ppm except for CPC [part/cc/ppm] and MAAP [1/um/ppm]. [b] SD: 1 standard deviation, NA: Not available.

Whereas NO_X and CO are direct products of the combustion process, and therefore directly correlated with the A/F ratio –or driving speed, the hydrocarbon emissions result from a variety of other processes. These include *blowby* effects (leakage of gases

escaping through sealing surfaces in the engine) during the compression and power strokes, evaporative emissions (whose amount depends on the fuel volatility, temperature and vehicle maintenance) and the combustion process itself. For these reasons, the hydrocarbon emissions result from a mixture of unburned fuel/oil and partially oxidized exhaust products. The relative proportion of these two types of hydrocarbon exhausts depends on the fleet composition as well as maintenance and fuel characteristics. In general, hydrocarbon emissions increase with heavy load conditions and higher power – that is, a rich A/F ratio is needed.

A more detailed view of the effect of driving speed on selected VOCs, NO and CO is shown in Figure 3.5. In this figure, 75th, 50th, and 25th percentiles are shown for selected VOCs, CO and NO emission ratios under the described driving modes. Figure 3.5 clearly shows that the magnitude and variability of CO and VOCs, which are directly related to the combustion efficiency, reduces with increasing speed whereas the NO emission ratio variability does not decreases with varying speed. C2benzenes and benzene were the highest and lowest abundance aromatic species measured on a mole per mole basis.

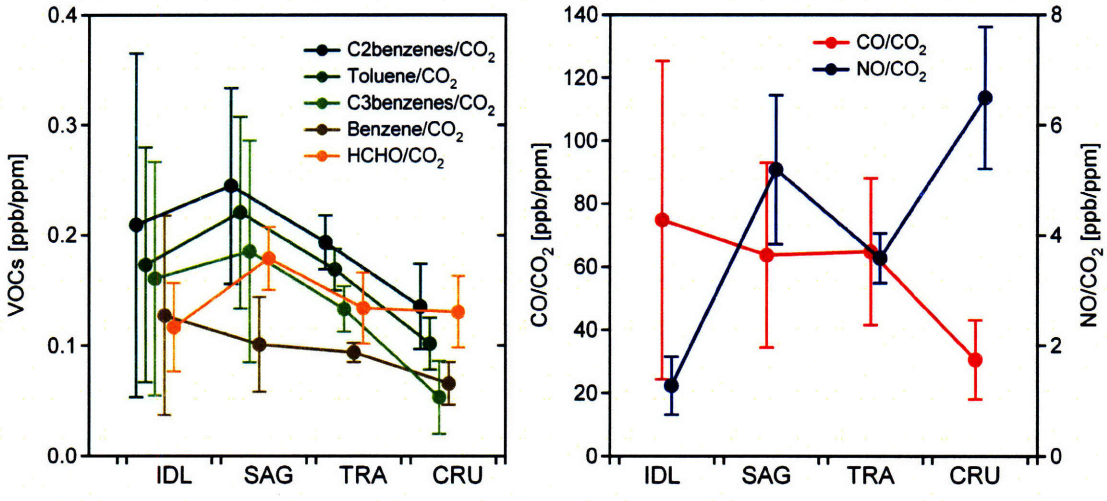

Figure 3.5. Fleet average mobile emission ratios by driving mode for CO, NO and selected VOCs measured in Mexicali. Showing the 75th, 50th, and 25th percentile for each driving mode.

Although, arguable, since the number of samples in some driving mode classifications is relatively small, this sampling technique is much more robust for obtaining fleet average emission conditions and their statistics are more significant than those from individual target vehicle emission measurements. Nevertheless, in the construction of Table 3.1 we did not considered a valid emission ratio average and standard deviation for driving modes with less than four measurements. Most of the standard deviations are smaller than the observed average, a direct effect of the averaging approach of this technique. The values reported in Table 3.1 are used in following sections of this document for the comparison with similar studies done in Mexico City and for the validation of the Mexicali emissions inventory (EI).

3.2.4 Comparison of emission ratios between operational sampling modes

In this section we inter-compare measured mobile emissions ratios from the three previously described experimental modes for selected emitted species. Comparison of emission ratios obtained in different operational sampling modes provides an opportunity to understand the observed variability of the emission data. This is of particular importance when using the observed fleet average emission ratios to estimate fuel-based total emissions for the vehicle fleet. The estimated fuel-based total emissions can be used in turn to assess the validity of traditional "bottom up" emissions inventories.

Figure 3.6 presents the 75^{th}, 50^{th} and 25^{th} percentiles for the fleet average emission ratio measurements as well as all the emission ratios obtained from the chase and the roadside stationary sampling mode measurements of gasoline (GV) and diesel vehicles (DV) plumes. As described above, the four fleet average driving modes in Figure 3.6 are more representative of the gasoline vehicle fleet with no significant representation of diesel vehicles.

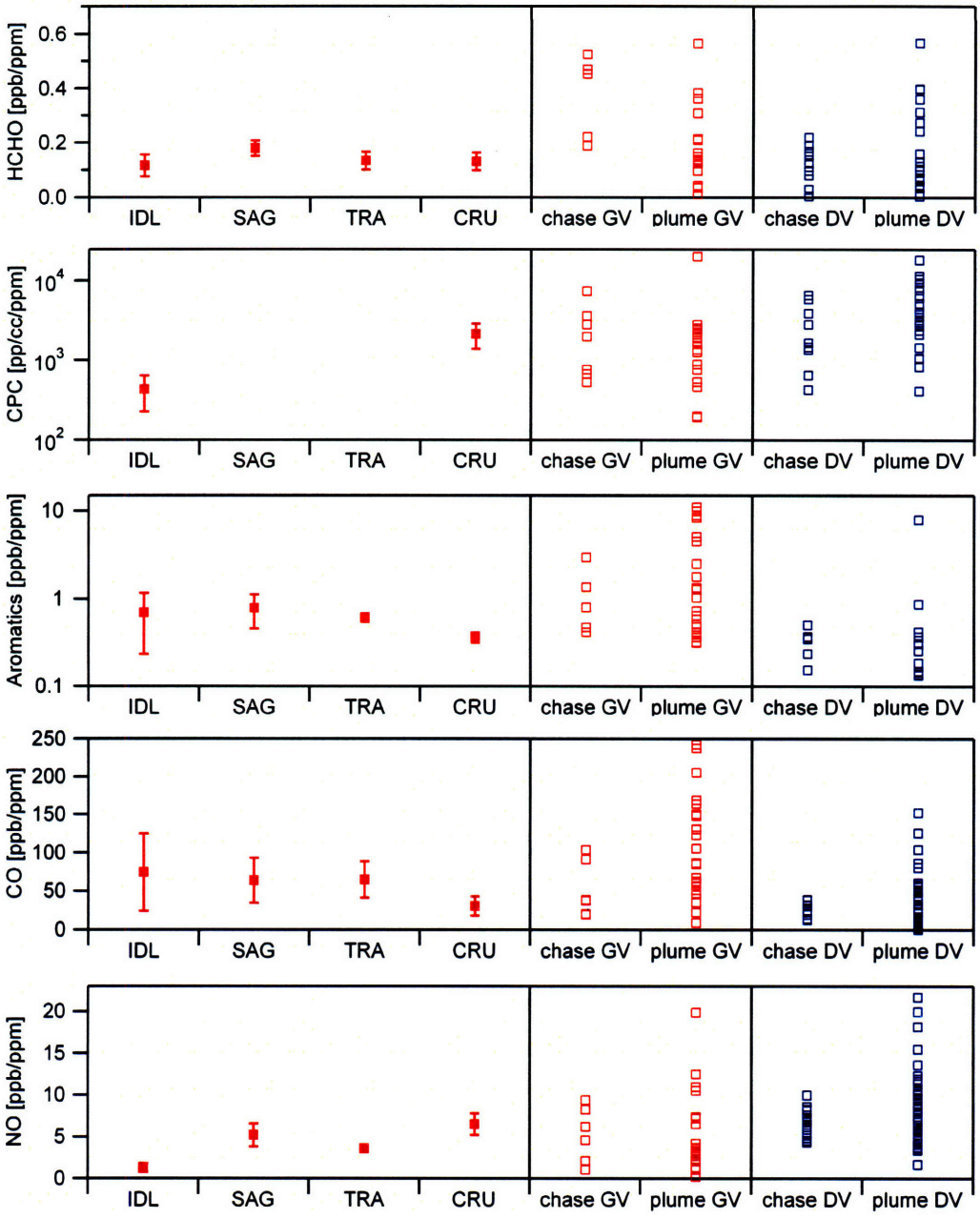

Figure 3.6. Inter-comparison of measured mobile emission ratios for various pollutants by sampling mode.

As expected, Figure 3.6 shows that there is higher variability in the sampling of individual plumes and chased vehicles than for the fleet average mode. Also, the variability of the measured emission ratios is larger for the individual plume samples than

for the chase events both for gasoline and diesel vehicles. The higher variability of the stationary individual plume and the chase modes can readily be explained by the "micro" approach of these measurement techniques where a large number of factors (emission control system, vehicle age, maintenance state, fuel type, etc) may play a major role in determining the emissions from a given vehicle. In the fleet average sampling mode, all these factors are smoothed by averaging (equally weighting) the measured emissions plumes. On the other hand, the variation observed in both the average and the standard deviation in the fleet average sampling mode indicates that the sampling size was large enough to be sensitive to driving mode. Similarly, for emissions of CO, NO and some selected VOCs the resulting consistently smaller standard deviations with respect to the observed emission ratio average in the fleet average mode and the (pronounced in some cases) variation observed with driving mode suggests that the sample size is adequate to represent a true average.

As explained in section 3.2.1, having only a time window of a few seconds for capturing the diluting emission plume in the roadside stationary sampling setup, the use of high time-response instrumentation is required At these short time frames other factors such as time alignment of the signals and intrusion of other non-targeted emission plumes may affect the estimated emission ratio. We have accounted for the differentiation of target plumes from non-target plumes with the analysis procedures described above. Similarly, we have accounted for time alignment issues during the analysis by correcting the time alignment of the signals during the data quality assurance procedures. Nevertheless, although these factors may play a role in the observed magnitude of the individual emission plumes, they can not account for the observed variability within that sampling set up. Engine temperature, driving mode, emission control systems and other major factors are more likely to play a major role in the variability within the individual plume measurements. In some extent, the resulting effects of these factors are more readily observed when continuously measuring the emission plumes of a given vehicle during the chase mode measurements. In that case, the average effect of all these factors is captured for a given vehicle when obtaining an emission ratio for a given speed or driving mode during a period of time of several minutes. The observed variability in Figure 3.6 within

the chase sampling mode data can then be interpreted as the average effect of the noted operational factors for each sampled vehicle.

3.3. Pollutant emission ratios

The ratios of various pollutants may be used to describe vehicle fleet characteristics and to assess the effects of these emissions on the composition of the urban atmosphere. More importantly, fleet average mode emission ratios can be used to inform the design of air quality control measures that target mobile emissions in an urban area. On-road emission ratios can also be compared with similar ratios obtained in semi-diluted and diluted (background) air to assess the oxidation processes during regional pollution episodes. We present the emission ratios for a range of emitted pollutants in this study but their application to the design of air quality control measures are left for future consideration.

We have evaluated emission ratios of CO/NO, HCHO/CH_3CHO, Aromatics/NO, and Benzene/Toluene from the gasoline fleet average emission mode data described in section 3.2.3. Figure 3.7 shows the emission ratios obtained for the four driving modes considered in this study. The standard deviations of the ratios SD_i were obtained with the standard formula for the error propagation of two normal samples with standard deviations SD_1 and SD_2 shown in Equation 1:

$$\frac{SD_i}{X_i} = \sqrt{\left(\frac{SD_1}{X_1}\right)^2 + \left(\frac{SD_2}{X_2}\right)^2} \qquad (1)$$

where X_i, X_1, and X_2 are the average of the ratio and samples 1 and 2, respectively.

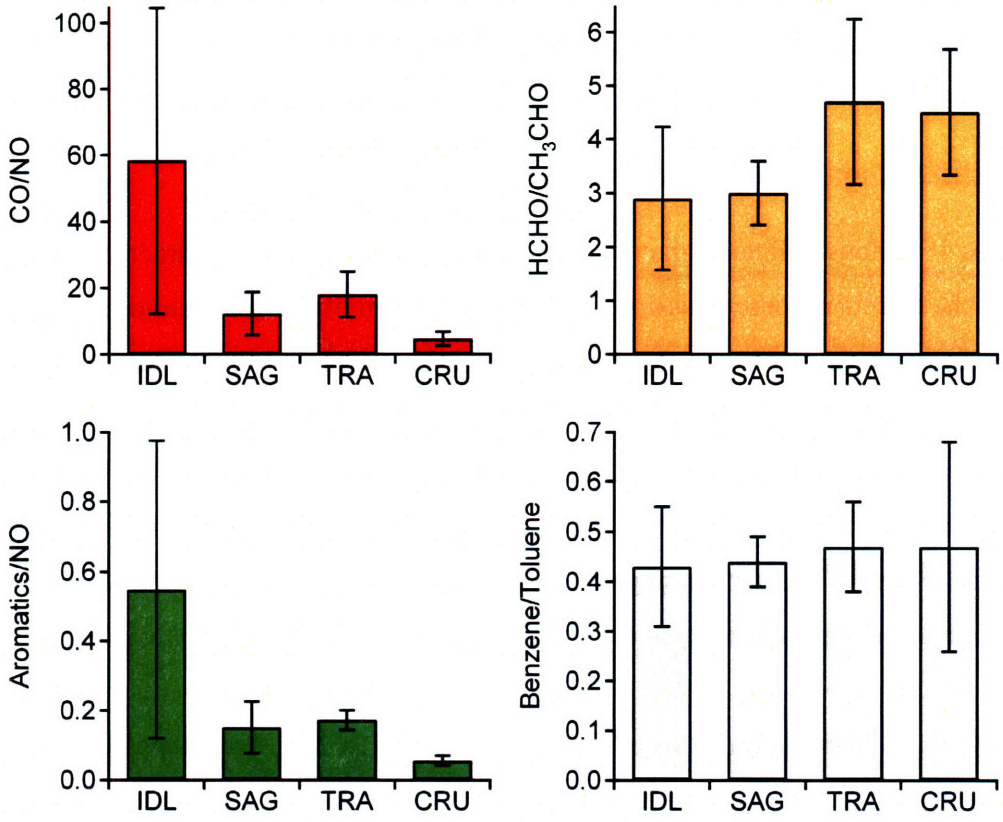

Figure 3.7. Measured fleet average ratios of various emitted pollutants for different driving modes. All units are in [ppbv/ppbv].

A strong negative dependence on driving mode speed is observed for the aromatic/NO and the CO/NO ratios, whereas a week positive dependence is observed for the $HCHO/CH_3CHO$ ratio and no apparent dependence is observed for the benzene/toluene ratio. As explained above, both the aromatic/NO and the CO/NO ratios are directly related to the combustion efficiency of the engine, and it is expected that these ratios vary as the A/F ratio varies with driving mode. Importantly, the quantification of these ratios in Figure 3.7 suggests that the modification of predominant driving modes within urban areas can drastically impact the corresponding ratios of these pollutants in the atmosphere. From the photochemical perspective this is very important as the production of ozone is strongly dependant on the VOC/NO_X ratio of the air mass. In turn, the quantification of photochemical oxidation products has important implications for the evaluation of health impacts of poor air quality.

The benzene/toluene ratio shows a consistent value of around 0.4 ppb/ppb regardless of the driving mode. The ratio of the rate constants for toluene and benzene with respect to reaction with OH, the main oxidation pathway for these aromatic compounds in the atmosphere, is about 4.6 at 298 K. Toluene will react at least 4.6 times faster than benzene in normal conditions. Therefore we would expect the benzene/toluene ratio to increase over time with respect to their at-the-source value of 0.4 ppb/ppb as the air mass is oxidized. Using an average value of $2x10^6$ molecules/cm^3 for OH, we would obtain an average characteristic lifetime for benzene of about 4.7 days whereas that for toluene would be around 1 day. The prevailing meteorological conditions of the region will determine the direction and how far the daily emitted plume is transported downwind. Other non-mobile sources of toluene, particularly painting and solvent emissions may also decrease the observed ambient benzene/toluene ratio. The comparison of the benzene/toluene ratios from different emission sources and their strength could, in principle, be used to device a "clock" for the oxidation history of the air mass in regional transport pollution events.

Using again a typical average value of $2.0x10^6$ molecules/cm^3 for OH, the corresponding characteristic lifetimes for HCHO and CH_3CHO are 14.4 and 8.7 hours, respectively, as CH_3CHO reacts almost 1.7 times faster than HCHO with OH at room temperature. The main importance of this ratio is the facility of aldehydes to produce radicals in the urban atmosphere through photolytic reactions. Having relatively short characteristic times, the direct emission of aldehydes from mobile sources can impact the radical balance of the urban atmosphere in or near the city.

3.4. Comparison with the Emissions Inventory

An important application of the measured mobile emission ratios is the validation of the estimated mobile emissions in an Emissions Inventory (EI). Among other uses, an EI is a very important component of a modeling system that aims to simulate the physical and chemical processes of the atmosphere.

EIs are also an invaluable tool for the design, implementation and follow up of air quality control strategies based on emission controls. Mobile emissions are generally quantified in emissions inventories based on activity factors estimated from a vehicle census or traffic counts, and emissions factors obtained from vehicle exhaust measurements, input into individual vehicle or fleet emission models. Their estimation however may be highly uncertain due to the lack of local information to quantify the required parameters and their inherent high variability due to the multiple factors that affect the combustion process described in the sections above. These conditions highlight the need for measurement techniques that capture real-world vehicle emissions to validate emission inventories.

In this section we compare the mobile emissions estimated in the NEI 2001 combined with the 1999 BRAVO inventory (the result of that combination is denominated here as the Model Emissions Inventory) with the emissions estimated from the fleet average emission ratios reported in this study. We obtain estimates of mobile emissions for selected species using fuel sales estimates for Mexicali in combination with the measured on-road gasoline fleet average mobile emission ratios. To that end it is necessary to convert from ppb/ppm of CO_2 emitted to grams per liter of fuel consumed during the combustion process. We assume complete stoichiometric combustion, a typical value of 54.1 moles of carbon per liter of gasoline and a fuel density of 756 grams/liter. This assumption is reasonably valid because the measured emissions levels of exhaust plume CO and VOCs are small compared to the levels of emitted CO_2 (i.e. generally >90% of fuel carbon is exhausted as CO_2).

For the present study there was no available local information on the gasoline fuel sales or fuel consumption for Mexicali. We estimated the local gasoline sales by using the readily available national total fuel sales data from PEMEX and scaling them using the fraction of vehicles of Mexicali with respect to the national values (data which are readily available). To investigate the validity of this assumption in Figure 3.8 we have plotted the time series of the population and number of vehicles for Mexicali and Mexico along with

the national fuel sales data. The plot shows linear positive monotonic trends in population both nationwide and for Mexicali for the considered periods. The annual population growth rate for Mexicali was, however, about 2.6 times higher than for the rest of the country reflecting the common phenomena of explosive urban growth rates in US-Mexican border cities.

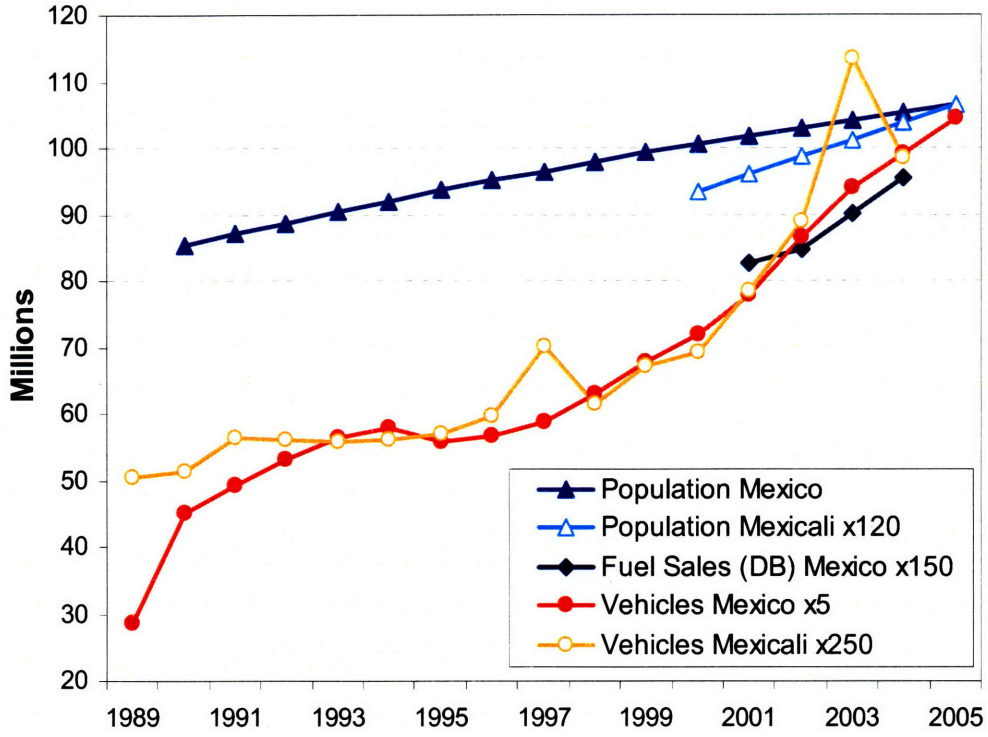

Figure 3.8. Time series of population, and number of vehicles for Mexicali and Mexico (country) and fuel sales for Mexico (country) in daily barrels (DB).

The national number of vehicles shows a positive trend that tends to linear in the last period of available data. The vehicles trend for Mexicali follows the corresponding national trend in some portions of the data, but clearly with a less smoothed behavior due to abrupt changes over short periods of time. These rapid changes (years 1997 and 2003) may be the result of both the high volatility in the population *in transition* in the city and to national political amnesties in which, for a short period of time, Mexican citizens are allowed to buy and legally import US vehicles with limited taxation. That may explain the increase and later reduction of the number of vehicles in a short period of time since,

after the amnesty period ends, many vehicles can be further resold in other regions of the country and not registered in Mexicali any longer. Over the last 13 years the number of Mexicali vehicles followed the corresponding national trend when these "amnesty" periods are not taken into account. Nevertheless, data from more recent years would be desirable to test that assumption and to understand this transitory effect.

The fraction of vehicles in Mexicali with respect to the national number of vehicles is about 2 % when the transitory periods are not taken into account. The corresponding fraction increases to 2.4% in the 2003 transitory period. Therefore, the uncertainty introduced if the transitory period is considered when estimating the local Mexicali fuel sales is of about 17% . Since the base case emission data for comparison is the 2001 Model Emissions Inventory, we use the fraction of 2% as the scaling factor of the national fuels sales, obtaining an estimated local fuel sale of 11,230 barrels of gasoline per day. As an external check on the magnitude of this local fuel sales estimation, we can use data from an urban area for which both the number of vehicles and the fuel sales are known and to compare the obtained average fuel economy value of the two fleets. We did that exercise for Mexico City and obtained an average of 5.6 liters/day per vehicle with data for 1999 taken from (Molina and Molina, 2002). With the estimated local fuel sales for Mexicali we obtain a corresponding value of 5.72 liters/day per vehicle for the base case year 2001. This suggests that the magnitude of the estimated local fuel sales is about right but, due to the necessary assumption of complete consumption by the gasoline fleet alone, certainly it will imply an upper limit estimate of the calculated emissions.

We extracted emission information for CO, NO_X, HCHO and CH_3CHO from the Model Emissions Inventory from the 12 km grid domain shown in Figure 3.9. Based on these emissions, the location of Mexicali is readily visible in the upper left corner of the domain, as well as the effect of two major roads in the domain. To some extent the emissions from Yuma are reflected in the CO and NO estimations, but were not accounted in the aldehyde emissions. The geographical extent of the city of Mexicali is of about 15 km by 17 km and, as such, its emissions can be accounted in 1 or 2 of the 12 km cells domain. Nevertheless, we have extracted the emissions information from three

adjacent cells ([3, 1], [4, 1] and [4, 2]) to account for the poor resolution of the spatial distribution.

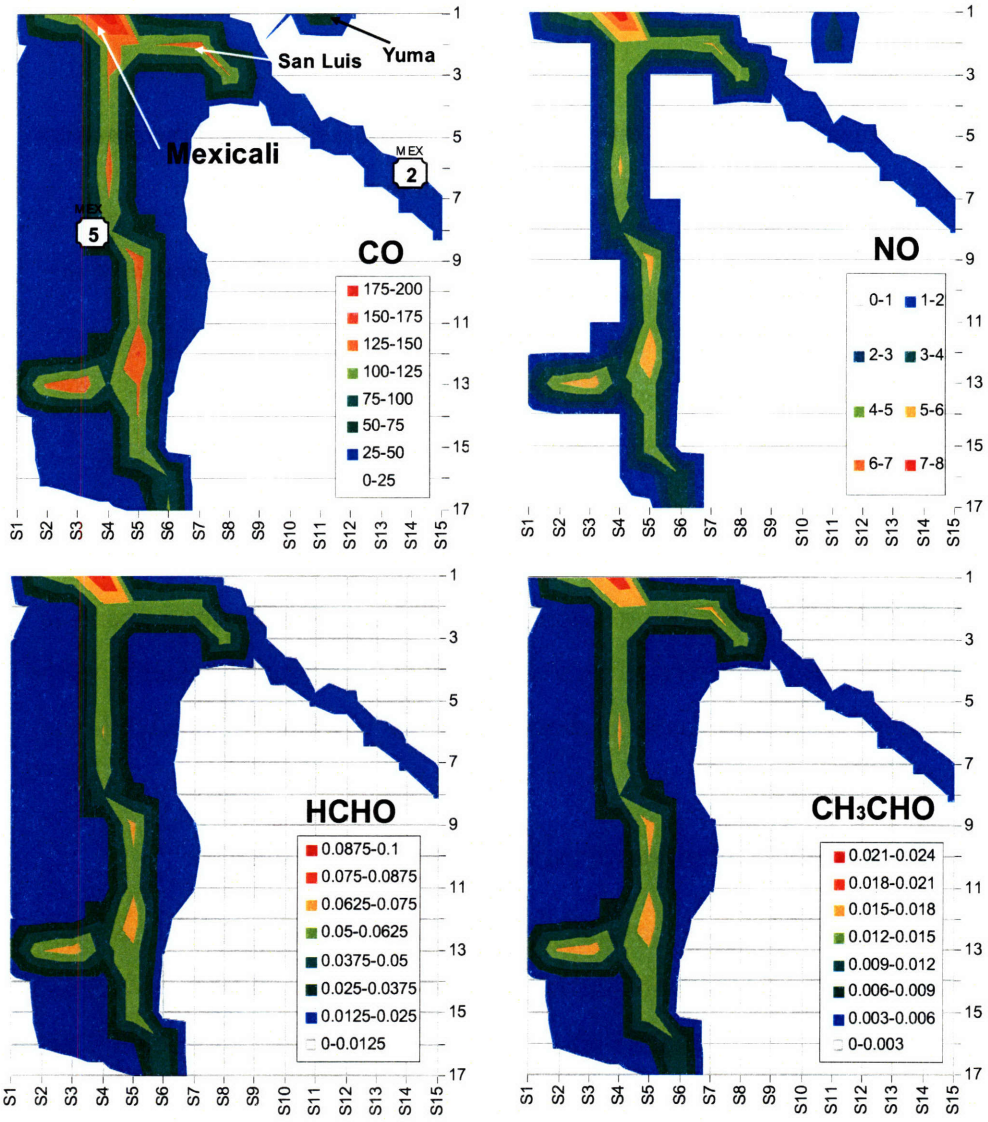

Figure 3.9. Daily emission maps of CO, NO, HCHO and CH_3CHO constructed from 24 hourly spatial distribution maps in moles/sec units. The grid cell is of 12 km.

A comparison between the extracted emission information from the Model Emissions Inventory and the calculated emissions with the use of the fuel sales data and the measured mobile emission ratios is shown in Table 3.2. The pollutant mass emissions in this study were obtained using the gasoline fleet average TRA driving mode as it is

assumed it is the prevailing driving condition in the city and the error range was set at one standard deviation of the average emission ratio. Table 3.2 indicates a severe underestimation for aldehyde emissions and a large underestimation for NO and CO emissions.

Table 3.2. Comparison between the Model Emissions Inventory and the emissions estimated in this study [tons/day] for gasoline vehicle fleet in Mexicali.

Pollutant	Model Emissions Inventory	This study	Underestimation
CO	46.1	175 +/- 62	3.8
NO	1.9	10.4 +/- 1.3	5.4
HCHO	0.0227	0.39 +/- 0.09	17.1
CH_3CHO	0.0076	0.12 +/- 0.03	15.9

The significantly higher mobile emissions based on our on-road measurements in Mexicali suggest that future modeling studies should use a much broader range on input emissions when attempting to model the photochemistry of the Mexicali region.

3.5. Comparisons with measurements in other cities

In this section we compare the gasoline vehicle fleet measured obtained during the Mexicali campaign with those obtained in Mexico City during the MCMA-2003 field campaign in which the ARI mobile laboratory also participated. The mobile emission ratios for MCMA-2003 are reported in Zavala et al., (2006) and were obtained using the same analysis procedures adopted for Mexicali study. As such, differences in the reported emission ratios directly reflect the differences in fleet characteristics and composition between the two urban areas rather than differences in instrumentation, measurement techniques or data analysis procedures. In addition, we compare the diesel on-road emission ratios from HDDTs measured in Mexico City, Mexicali and Austin, TX. These represent emissions from a limited number of vehicles and it is possible that there is no sufficient number of samples for obtaining diesel fleet-average emission conditions.

In Table 3.3 we present the comparisons of the measured mobile emission ratios during the MCMA-2003 and the Mexicali campaigns. We do not report CO emission ratios for Mexico City because the response time of the CO instrument used during the MCMA-2003 field campaign was not short enough to fully resolve individual emission plumes.

Table 3.3. Comparison of measured fleet-average mobile emission ratios between Mexicali and Mexico City[a].

Pollutant	SAG (SD)		TRA (SD)		CRU (SD)	
	Mexicali	Mexico City	Mexicali	Mexico City	Mexicali	Mexico City
NO	5.20 (1.35)	2.92 (0.9)	3.59 (0.45)	4.58 (2.2)	6.50 (1.29)	4.33 (1.7)
H_2CO	0.18 (0.03)	0.23 (0.06)	0.13 (0.03)	0.23 (0.07)	0.13 (0.03)	0.20 (0.07)
CH_3CHO	0.06 (0.01)	0.04 (0.02)	0.03 (0.01)	0.04 (0.02)	0.03 (0.002)	0.04 (0.01)
H_2CO/ CH_3CHO	3.0 (0.59)	6.2 (1.3)	4.7 (1.54)	6.2 (2.0)	4.5 (1.17)	6.4 (1.8)
Benzene	0.10 (0.04)	0.14 (0.04)	0.09 (0.01)	0.10 (0.03)	0.07 (0.02)	0.10 (0.04)
Toluene	0.22 (0.09)	0.28 (0.07)	0.17 (0.02)	0.18 (0.06)	0.10 (0.02)	0.18 (0.08)
C2benzenes	0.24 (0.09)	0.32 (0.11)	0.19 (0.02)	0.22 (0.09)	0.14 (0.04)	0.19 (0.09)
C3benzenes	0.19 (0.10)	0.24 (0.09)	0.13 (0.02)	0.15 (0.05)	0.05 (0.03)	0.15 (0.08)
NH_3	0.037 (0.006)	0.09 (0.05)	NA	0.09 (0.06)	0.053 (0.027)	0.11 (0.07)

[a] See ext for an explanation of compounds considered as c2-benzenes, c3-benzenes, aromatics, m105, and m59. All units are in ppb/ppm except for H_2CO/CH_3CHO [ppb/ppb]. NA: Not available, SD: 1 standard deviation.

Interesting differences can be found in the data emissions reported in Table 3.3. NO emission ratios seem to be around 20 % higher in Mexicali than in Mexico City whereas HCHO emission ratios are higher almost by a factor of 2 in Mexico City as compared to Mexicali. However, emission ratios of acetaldehyde in Mexicali do not seem to be significantly different as compared to Mexico City and the corresponding $HCHO/CH_3CHO$ ratio varies accordingly.

The selected VOCs (aromatics) emission ratios measured in the Mexicali gasoline vehicle fleet are slightly, but consistently, smaller than those measured in Mexico City. Nevertheless, the variability in the selected VOCs emission ratios seems to be higher in the Mexico City measurements and the difference may not be statistically significant. The variability may be due to the difference in the sampling size (almost a factor of 4 higher in Mexico City) between the two experimental settings. Emission ratios of NH_3 seem to be higher in Mexico City than in Mexicali by a factor of 2 or more. The variability of the different NO and selected VOCs emission ratios with respect to driving mode seems to be consistent in both datasets although a bit more pronounced in Mexicali than in Mexico City, particularly at cruising speeds.

Among the major factors that may play a role in explaining the observed differences between the two measurements are the fleet age, the distribution of vehicle-types, the fraction of vehicles with emission control technology and the fuel composition. Other local parameters that may play a role in the differences between the emissions measured in the two urban areas are the temperature, altitude (ambient pressure) and to some extent the relative humidity. As the mobile emissions clearly play an important role in the formation of ozone and secondary organic aerosols, it would be of major interest to design a follow up study aimed at exploring in detail each of these factors and parameters influencing the differences between the two cities and their correlation with ambient pollution levels.

Figure 3.10 shows the comparison of NO_Y/CO_2 emission ratios obtained in the three cities. The figure indicates that, on average, NO_Y emission ratios from HDDTs in

Mexicali and the MCMA were significantly higher than in Texas and that the variability (indicated here as the 1-sigma standard of the measurements) is similar in all three locations. As explained, however, the limitation of this comparison is the limited number of samples in Texas, and in some respect in Mexicali, as compared to measurements in the MCMA. The large variability observed in the NO_Y emission ratios is in fact a reflection of the large number of conditions affecting the emissions of the HDDTs sampled. Figure 3.11 shows the NO_Y/CO_2 and NO_2/NO_Y on-road mobile emissions - colored by vehicle speed- of individual HDDTs measured in Austin TX. The figure clearly indicates a large variability of NO_Y emission ratios between individual vehicles. The observed variability correlated to vehicle speed is an indication of enhanced thermally-induced NO_X formation at higher engine temperatures. The strong correlation between NO_X emission ratios and vehicle speed suggests the possibility for impacting NO_X emissions from HDDTs by controlling the A/F ratio, similar to the findings obtained for the gasoline fleet. However, these measurements were obtained in highway conditions rather than in the city, where much more variation in driving more are expected.

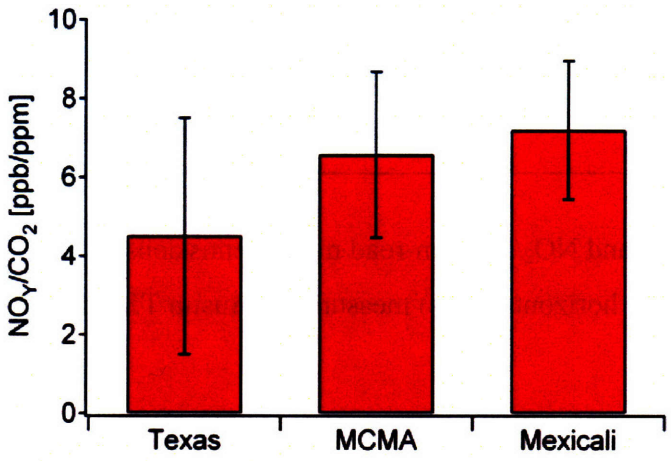

Figure 3.10. Comparison of HDDTs on-road NO_Y/CO_2 emission ratios measured in Austin, Mexicali and the MCMA.

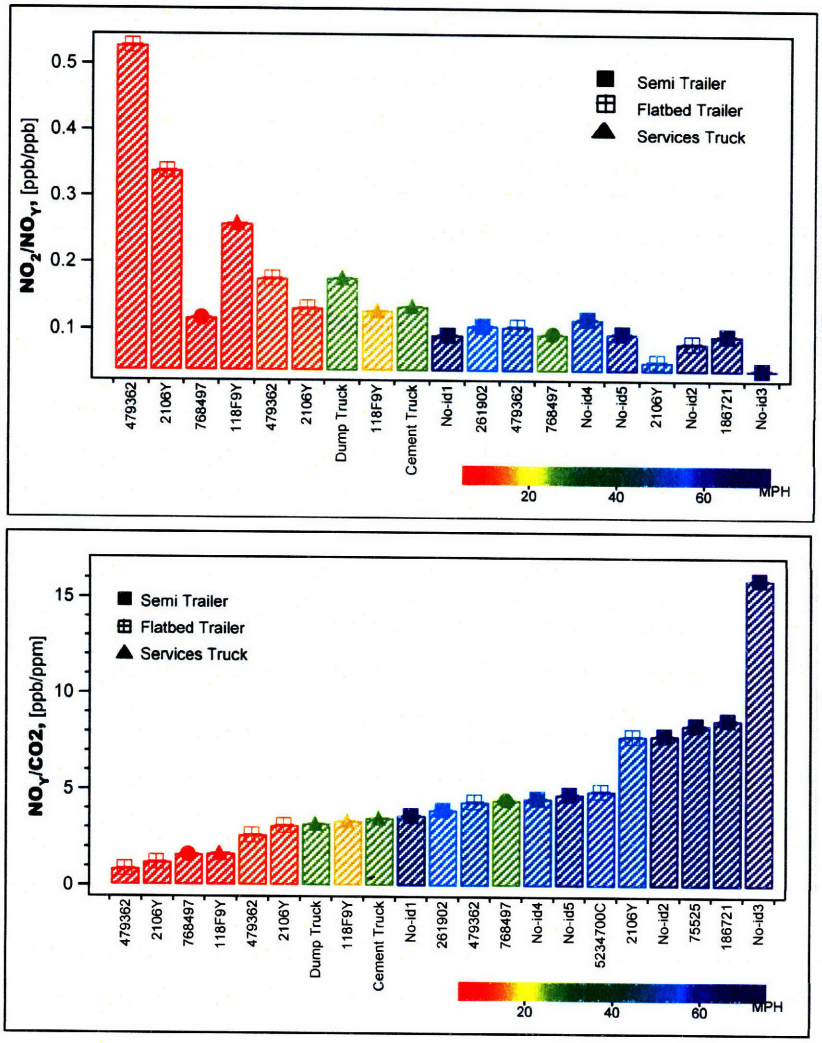

Figure 3.11. NO_Y/CO_2 and NO_2/NO_Y on-road mobile emissions of individual HDDTs (license plates are in the horizontal axes) measured in Austin TX colored by vehicle speed.

Chapter 4. Linking historical changes of mobile emissions to changes in photochemistry levels in the MCMA

4.1. Introduction

Past and recent field campaigns held in Mexico City have shown the strong influence of mobile emissions on the photochemical pollutant levels within the basin. Similarly, the impacts of regional transport events of both primary and secondary gaseous pollutants and aerosol particles are also directly related to the mass fluxes, temporal patterns, reactivity, phase partitioning, composition and other emission characteristics of mobile sources in the city. In addition to its effects on both the photochemical processes and particle loadings within the city and, consequently, its impacts at regional scales, mobile emissions are also significant contributors to high concentration levels of unregulated toxic species (Zavala et al., 2006). This suggests that significant benefits for human health, ecosystem vitality and climate can be obtained by policies directed toward controlling mobile emission sources. To effectively mitigate air pollution levels, mobile emissions-based air quality control policies in urban areas should be directly based on the characterization and quantification of mobile sources emissions.

The emission characteristics of mobile sources in the MCMA have significantly changed over the course of the past few decades in response to emission control policies, advancements in emission control technologies, and improvements in fuel quality and vehicle inspection and maintenance programs (Molina and Molina, 2004). In addition, increases on the renewal rates of the vehicle fleet in combination with the introduction of better technologies in new and in-use vehicles, have decidedly impacted the emissions characteristics of mobile sources in the MCMA. Along with these changes, concurrent non-linear changes in photochemical pollutant levels as well as aerosols, toxic and criteria pollutants have been observed. The observed large perturbations of mobile emission sources suggest that the VOC/NO_X ratio in the city has also been modified as a result of these changes.

The amount, quality and frequency of measurements of both mobile emissions and air quality levels during the past two decades in the MCMA represent a unique opportunity to understand the effects of perturbations of mobile emission levels on the photochemistry of the region. It will be demonstrated that current mobile source emission levels in the city have already been significantly "perturbed" (referred here as the fractional change from a given emissions base case) compared to past emission levels. By knowing the size of the emission perturbations, observed "natural" sensitivity effects represent a rare opportunity to evaluate "artificial" sensitivity tests using complex air quality models. This suggest the possibility of quantifying the contribution of mobile emissions to photochemical pollutant levels (a non linear effect) by evaluating both measurement and modeling approaches.

In this chapter we quantify the observed effects from perturbations of mobile sources on the photochemical pollutant levels in the city. We first describe the historically observed effects on ozone, CO and NO_X trends in the urban area. The analysis uses historical data from the local ambient monitoring network. The observed effects will be the basis for evaluating the sensitivity results obtained with the modeling techniques in the next chapter. In this chapter we also compare the historical trends of CO, NO_X and hydrocarbons (HCs) derived from mobile emission studies in the MCMA from 1991 to 2006 with pollutant trends of hourly data of CO, NO_X, and the CO/NO_X ratio from the monitoring network during peak traffic hours. We use this approach to estimate the magnitude of the perturbations in mobile source emissions in the MCMA. Approximate historical trends of the HC/NO_X ratio from mobile sources in the MCMA are defined using these data. Finally, the inferred emission trends are compared with observed trends of O_3 to quantify the impact of changes of mobile source emissions on the photochemical pollutant levels in the city.

4.2. Observed effects on O_3, CO and NO_X

The atmospheric monitoring network in Mexico City, RAMA (for Red Automatica de Monitoreo Atmosferico), has continuously measured ozone and other gaseous criteria pollutants since 1986. PM10 has been continuously measured since 1988 and PM2.5 since 2003. The network consists of about 32 stations located in the metropolitan area and is administered, supported and maintained by the Mexican federal environmental agency SEMARNAT (for Secretaria del Medio Ambiente y Recursors Naturales). The data is reported hourly and is publicly available at http://www.sma.df.gob.mx/simat/.

4.2.1 Effects on ozone trends

To investigate the observed effects of the perturbations of mobile source emissions on the photochemical levels in the urban area, we have analyzed the changes in ozone formation using the monitoring network data. In our analysis, we have included all hourly data with a valid reading for each day that meets the following criteria. First, to minimize the effects of inter-annual seasonal variability of meteorological parameters on ozone formation (e.g. solar radiation, mixing height, and temperature), we have included in our trend analysis only the months of March and April of each year. These months, for which high pollution levels are typically registered, are also the periods in which the monitoring campaigns of MCMA-2003 and MILAGRO-2006 were deployed in Mexico City. Second, to minimize the "weekend effect" on the analysis of the ozone trends we have excluded all data from Saturdays and Sundays. Third, we have also excluded all major holidays (March 21 and April 30) and, particularly, the corresponding days for the Holy Week for each year. The exclusion of these days filters out in our analysis the effects on ozone formation due to atypical variations of anthropogenic emissions.

In the analyzed period of 21 years of data, filtered with the exclusion criteria aforementioned, significant and interesting trends on the magnitude, timing and spatial allocation of ozone are clearly discernible. Figure 4.1 shows ozone box plots of hourly ozone concentration profiles corresponding to the 10^{th}, 25^{th}, 50^{th}, 75^{th}, and 90^{th} percentiles of all stations with valid data for a given hour. Four years are chosen in Figure 4.1 to

represent spans of 5 to 6 years, but the following analyses are qualitatively similar using other years. The data from Figure 4.1 suggests a significant decrease of the peak ozone levels and a moderate decrease of the median ozone diurnal levels. These changes are concurrent with a decrease in the spatial variability of the ozone fields (that is, the differences between the ozone levels measured by all the stations –e.g. the difference between the 90th and 10th percentiles- have decreased over time), mainly due to smaller ozone peaks in recent years. Smaller nighttime concentration levels are also observed in recent years, probably linked to particular trends in NO_X emissions, as shown later.

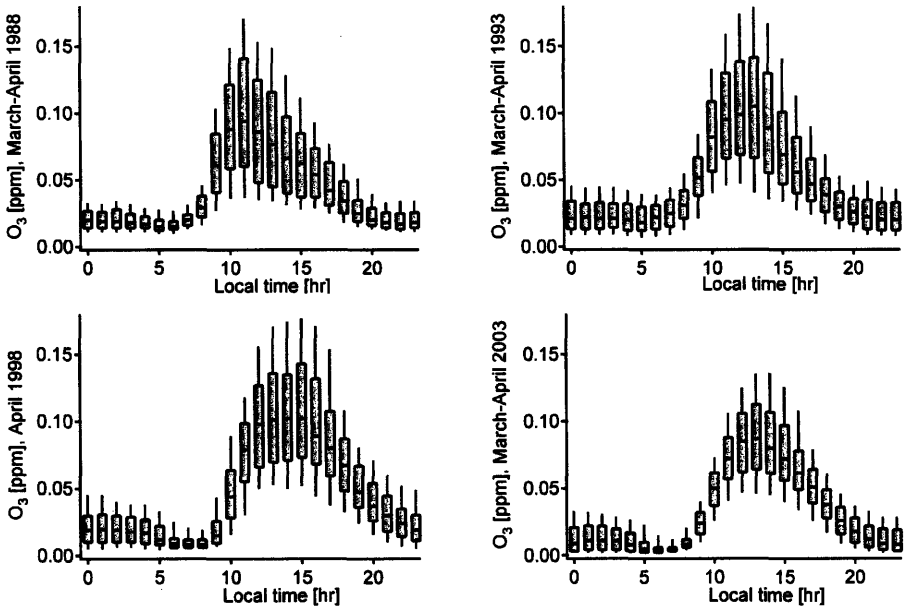

Figure 4.1. Ozone box plot profiles for 4 years of data during March and April.

These trends are also evident in Figure 4.2 where the 50th percentile ozone concentration profiles for each year are plotted. In addition, there seems to be some changes in the diurnal profile patterns of ozone, particularly before and after the mid 90's. The annual variability for the first 5 years of data, from 1986 to 1991, seems to be higher than for the rest of the years. Actually, median ozone concentrations initially increased during this period before starting a steady downward trend. Also, the magnitude and spatial variability of ozone has been drastically reduced in the early hours, and night time values

seem in general lower in recent years. Overall, comparing the early 90's with recent years there seems to be a reduction of about 25 ppb in median ozone concentrations.

The median ozone data for the year 1992 seems to have higher ozone values compared to any other data year, particularly at night. Corresponding NO_X values for this year do not seem particularly different from others, indicating that the higher ozone values may be due to differences in data acquisition protocols or miscalibration of the instruments rather to changes in the ozone formation process. Apparently, during the first five or six years of its existence the network was characterized by poor quality assurance protocols for some instrumentation that may be responsible for some of the large data variability during these years[4]. After that period, the network has maintained the highest standards and quality assurance protocols.

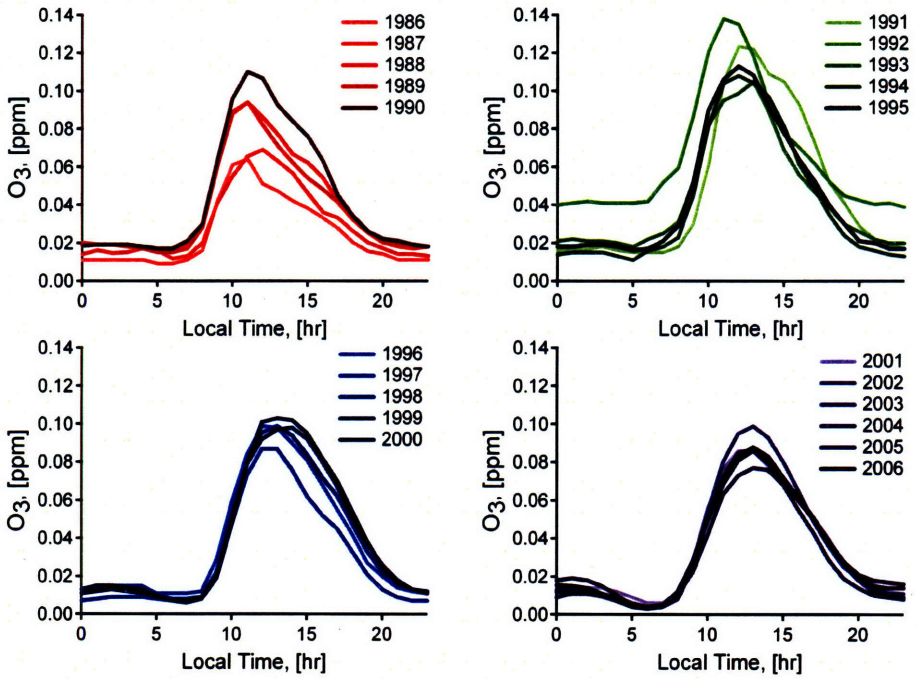

Figure 4.2. Ozone 50th percentile concentration profiles for the months of March and April for a given year.

[4] Armando Retama, (RAMA director) personal communication.

Besides the analysis of the median ozone profiles, maximum concentrations also provide useful insights for understanding the anthropogenic impacts on ozone during this data period. Figure 4.3 shows the trends for the maximum ozone concentrations and the average –local hour- timing for the occurrence of these maximums for all monitoring stations. The figure also shows a comparison with the corresponding trends obtained using data from the Holy Friday of each year (probably the day of the year with the lowest anthropogenic emissions-activities in Mexico City). As expected, there is no discernible trend in the Holy Friday data series, since its ozone levels are more likely to be governed by the particular meteorological conditions of each day rather than differences in emission activity levels between years.

Figure 4.3 also indicates that a rapid increase in maximum concentration levels occurred up to 1992 (with an alarming rate of 12 +/- 1.3 ppb/year), followed by a steady decrease of about 2.7 +/- 0.5 ppb/yr. We will show later in this chapter that this "breathing effect"[5] is strongly related to changes in anthropogenic emissions, with mobile sources playing a significant role. Overall, the observed variability of the maximum ozone concentrations trends has not significantly changed, indicating that high concentrations are still common in the city. Another interesting feature of the observations plotted in Figure 4.3 is the changes in ozone formation rates. Figure 4.3 shows that the average local time occurrence, of the maximum ozone concentrations is delayed from about 11 AM in the early years to about 1 PM in recent years. We will discuss in more detail the apparent time delay in the ozone formation rates in subsequent sections, with particular attention in the possible effect of anthropogenic perturbations.

[5] "Breathing effect" is meant to figuratively represent the upward-plateau-downward behavior of the data series, similar to the registered by CO_2 levels during the respiratory process.

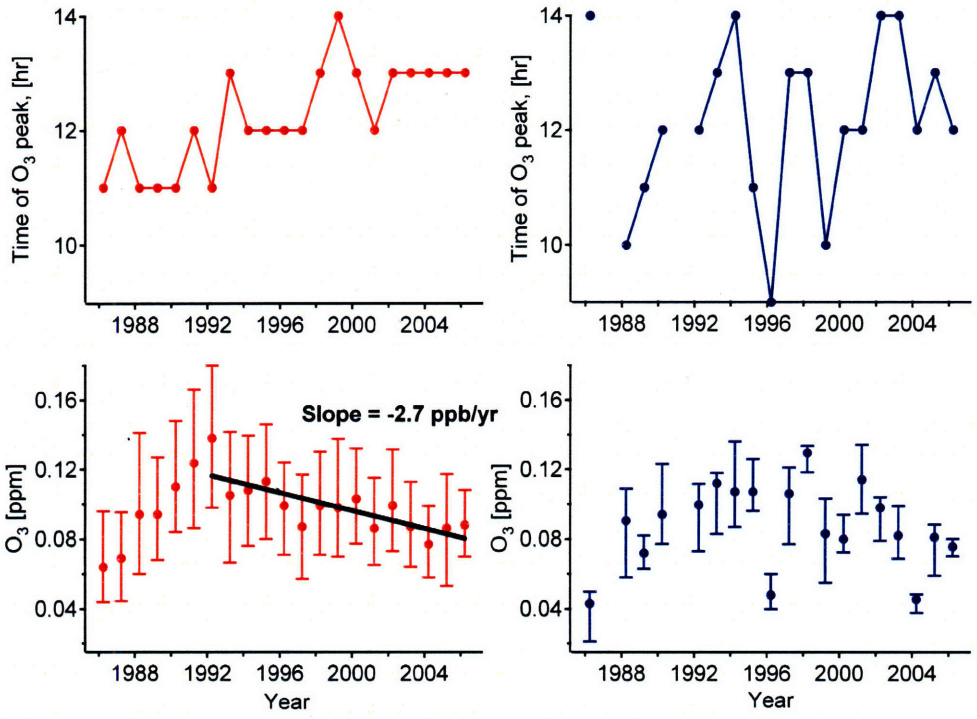

Figure 4.3 Lower figures: 50th, 75th, and 25th ozone percentiles of the ozone maximums for all monitoring stations for March and April (left) and for the Holy Friday (right) of each year. Upper figures: time of the day for the maximum of the 50th ozone percentile for March and April (left) and the Holy Friday (right) for all stations.

Another way to quantify the effects on ozone is plotting the daily domain-wide ozone peak concentrations (that is, the daily maximum of the maximums registered by each monitoring station) over time as shown in Figure 4.4. This figure shows a drastic reduction of more than 100 ppb for ozone peak concentrations. This reduction is clearly larger than the reductions observed in the median and maximum ozone concentration levels. This is further evidence that while the ozone peak has been reduced significantly, high median and maximum concentrations still persists throughout the day. This observation is particularly important because these two metrics have different implications when assessing the impacts of air quality policies based on human exposure to ozone levels.

As further evidence of the drastic changes that ozone formation has experienced in the analyzed period, Figure 4.5 shows the daily domain-wide ozone peak concentrations versus its local timing (that is, the local time at which the domain-wide ozone peak occurred in a given monitoring station) colored by time. The figure shows also the drastic reduction of the ozone peak and gives further evidence of a "delay" in the ozone peak formation by 2 to 3 hrs with respect to present years, in accordance with Figure 4.3.

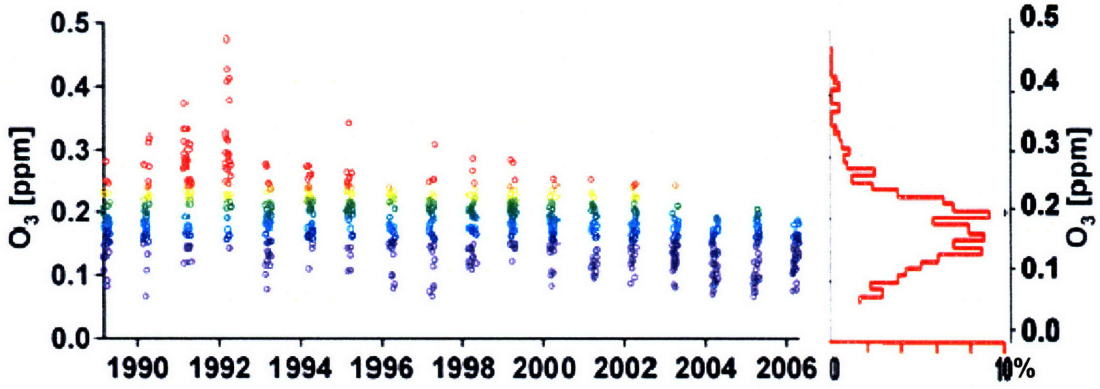

Figure 4.4. Domain-wide daily ozone peak trend and associated frequency distribution for the MCMA.

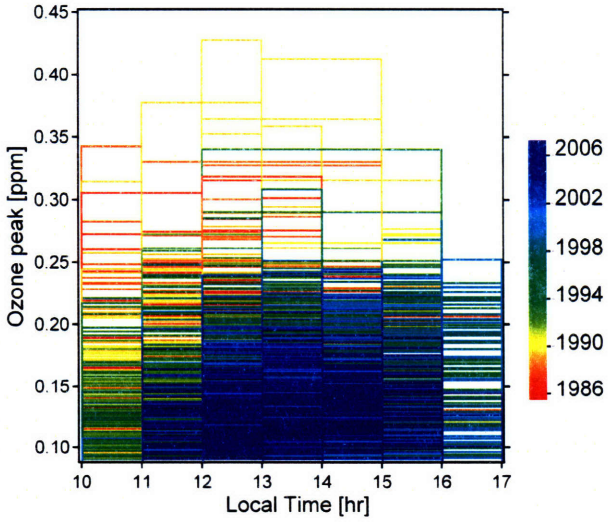

Figure 4.5. Domain-wide daily ozone peak vs its occurrence in local time for each monitoring station for all years during March and April.

As a consequence of the observed time delay in high ozone concentrations, including the ozone peak, it is natural to expect changes in the spatial allocation of the maximum ozone concentrations as well. One way to assess this effect is to obtain frequency maps for the allocation of the ozone peak and observe its changes over time. That is difficult to do in other than in time-varying digital format, for example a movie[6]. In any event, an attempt to do it in paper format is shown in Figure 4.6a where each circle represents the allocation of a daily domain-wide ozone peak (that, is the daily highest ozone concentration measured by the network) and the size of the circle is proportional to time. Larger circles represent recent time measurements and the smaller circles represent early past time measurements.

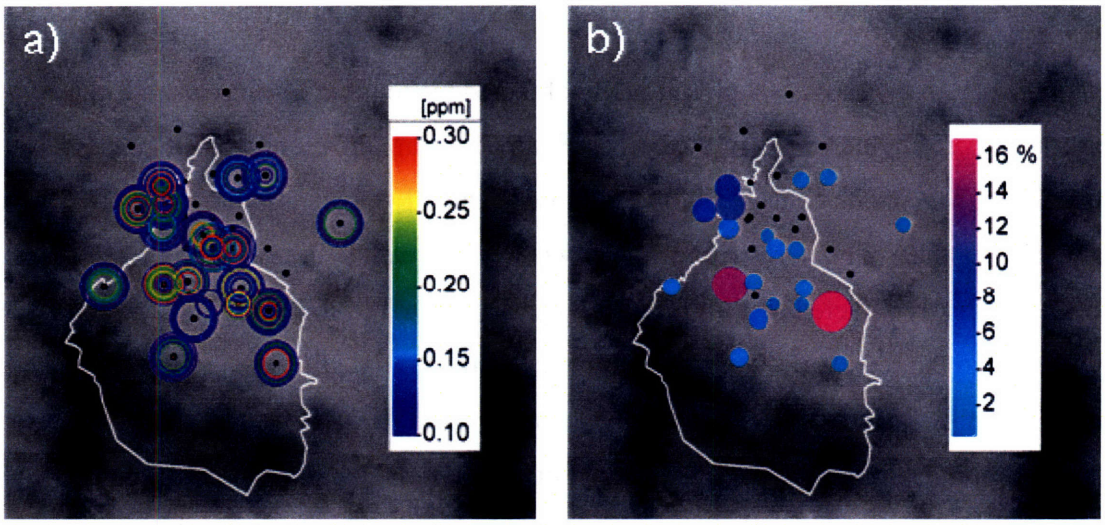

Figure 4.6. a) Daily spatial-time allocation of the domain-wide ozone peak colored by concentration. The size of the circles represents time, linearly increasing from 1986 (smaller circles) to 2006 (larger circles). b) Frequency map of the spatial-time allocation ozone map. Black dots are also monitoring stations, white perimeter is the political boundary for the Federal District and the background image is the topography of the region.

A "core-to-skirt" effect, in which the ozone peak concentrations are gradually more frequently registered in time in more peripheral stations, is already observed from Figure

[6] A movie has been created that clearly shows the observed "core-to-skirt" effect described here.

4.6a. This effect is in clear accordance with the delay in peak concentrations observed in Figure 4.5 since the air masses containing core city emissions have traveled longer distances by the time the ozone peak occurs, as registered by the network.

However, another important aspect that Figure 4.6a reveals is that the reductions in ozone as observed by the network, particularly impressive for the peak, may in fact not be as large as thought in terms of "real" reductions. This is simply because the network is being "blinded" to the real (basin-wide) ozone peak which may be occurring at places where there are no monitoring stations. This is an aspect that can –and will- be explored with detail in our modeling exercise due to the advantage of the larger spatial domain of the simulation.

The frequency map in Figure 4.6b (basically obtained by counting the circles in Figure 4.6a and converting them to percentages) shows that, during the months of March and April, the highest ozone concentrations are more frequently located in three clusters: southwest, southeast and northwest of the city core. The magnitude and spatial variability of ozone is clearly affected by multi-day wind patterns that are coupled to synoptic circulations in the region. As such, the frequency of the spatial allocation of the ozone peak is probably linked to the prevailing wind patterns (in frequency terms) occurring in those two months. Indeed, a trend analysis of historical wind data registered from the monitoring stations is in remarkable agreement with this picture (de Foy and Molina, 2007).

Finally, another aspect that we have explored is the influence of temperature variability on the spatial allocation of the ozone peak concentrations. Figure 4.7 show that the daily domain-wide peak temperature (that is, the highest daily temperature record measured by the network) does not have a discernible trend in the data period. In addition, its allocation is frequently centered on thin latitudinal and longitudinal bands around the center of the city. The heat island effect has already been observed in the city (Jauregui, 2005) and this figure suggests that it has been a prevailing feature of the city in the past two decades. Both the lack of apparent trend in peak temperature as well as the different

spatial allocation of temperature peaks, as compared to the spatial allocation of ozone peaks, suggests that the observed trend in ozone is not influenced by the long term variability of temperature. Still, short term variability of temperature not explored here is likely to be correlated with ozone levels (warmer/cooler days versus daily ozone levels). Although as we will show in the next section the observed ozone trends actually have a strong correlation (not linear) with perturbations of anthropogenic emission sources, we have not explored the effects of changes in biogenic emission sources (e.g. land use alterations) over time on ozone levels.

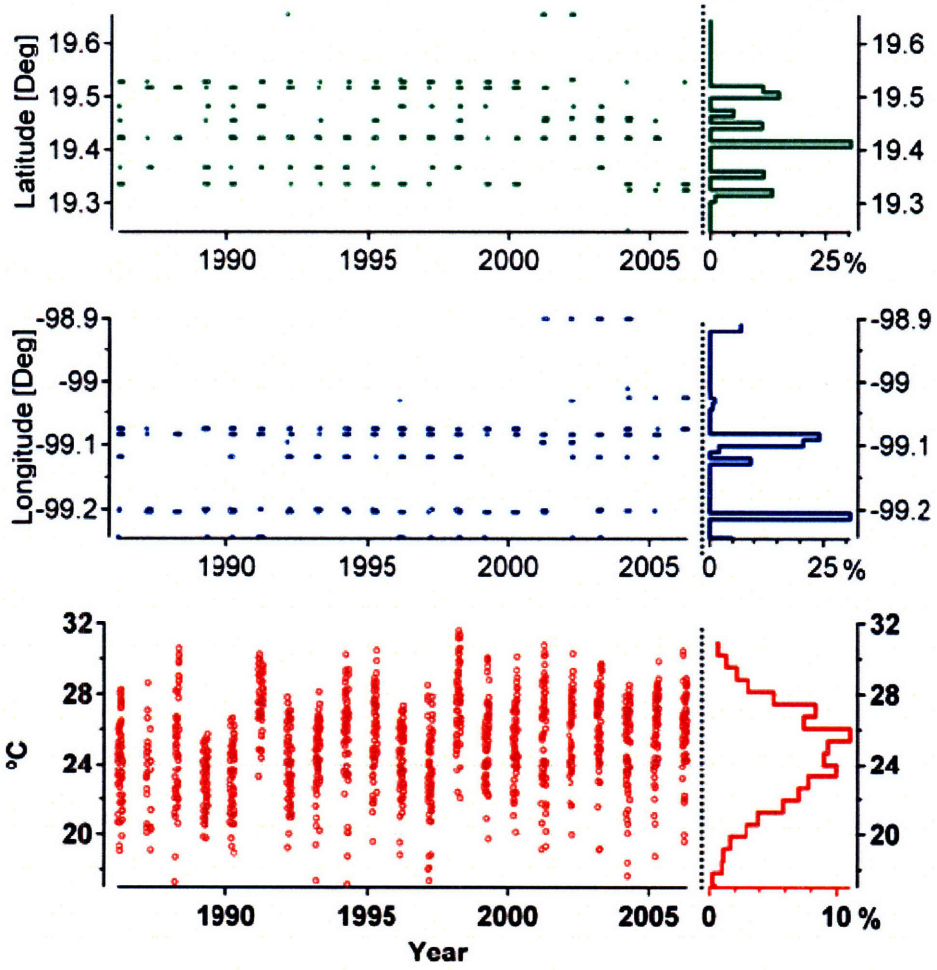

Figure 4.7. Daily domain-wide peak temperature and its corresponding spatial allocation trends for the MCMA with associated frequency distributions.

In summary, our analyses indicate that significant changes have occurred in the diurnal pattern profiles of ozone for night, early morning, diurnal and peak concentrations. From the early 1990s, a decrease rate of 2.7 +/- 0.5 ppb/yr has been observed in maximum ozone concentrations after an in impressive increase rate of 12 +/- 1.3 ppb/yr from the start of measurements through 1992. Peak ozone concentrations have drastically been reduced in the city while high median concentrations still persist. We have shown, however, that a "core-to-skirt" effect caused by the observed delay in photochemical formation rates may in fact be overstating such decreases since the monitoring network may simply no longer be capturing the real basin ozone peak.
We will see in turn that the observed delay (of 2 to 3 hours) in the formation rate of ozone has a strong anthropogenic signature. Frequency allocation maps of peak ozone show distinctive clusters that are likely related to the prevailing meteorological patterns occurred during the months of March and April.

4.2.2. Effects on CO and NO_X trends

In this section we analyze the historical trends in CO and NO_X profiles that have occurred concurrently with the observed ozone trends. Emitted by mobile sources, these species, particularly CO, are dominated by primary anthropogenic emission sources urban areas. Thus, their long term variability is likely to be directly influenced by emission sources perturbations. Figures 4.8 and 4.9 show the temporal concentration profiles in box plots (constructed from the 10^{th}, 25^{th}, 50^{th}, 75^{th}, and 90^{th} percentiles) with data from all stations for CO and NO_X, respectively. The same three exclusion criteria aforementioned for ozone were also used for the construction of these figures, minimizing the effects of atypical emission conditions and intra-annual variability of meteorological parameters.

Whereas Figure 4.8 shows a drastic reduction of CO concentration profiles, Figure 4.9 indicates that NO_X concentrations have not been reduced significantly over time. As indicated by the changes between the 75^{th} and 25^{th} percentiles, the spatial variability of the CO concentration fields seems to have been also reduced over time, but the variability

of NO_X has not. Similarly, large reductions are observed for the high CO concentrations in early morning hours whereas high NO_X concentrations have persisted over time.

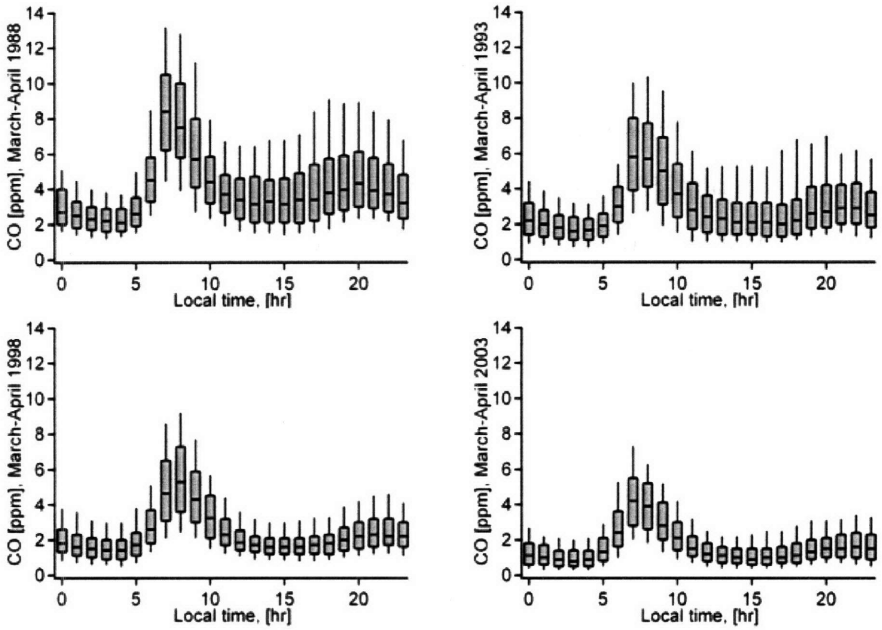

Figure 4.8. CO box plot profiles for 4 years of data during March and April.

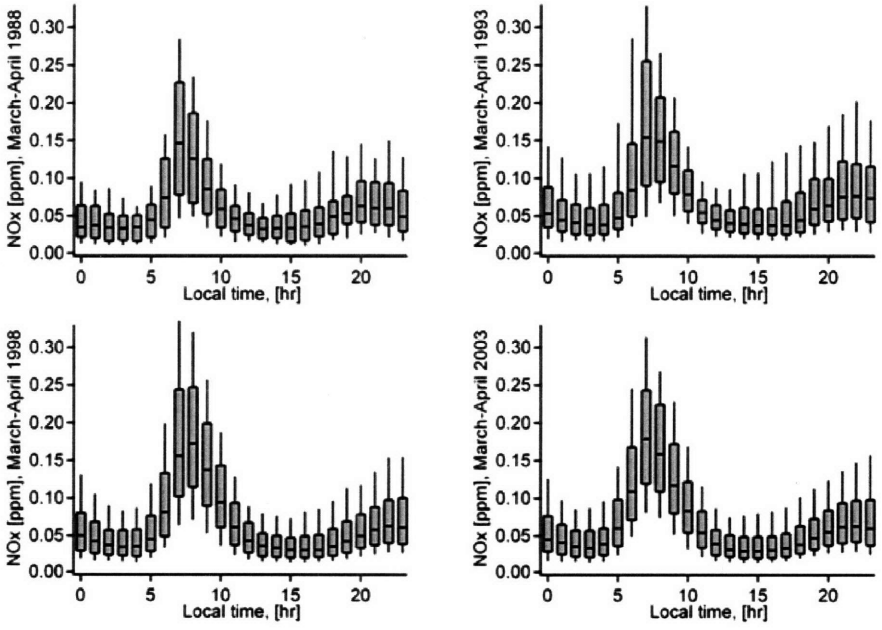

Figure 4.9. NO_X box plot profiles for 4 years of data during March and April.

Figure 4.10 shows the median concentration profiles for CO and NO_X for each year of the period analyzed. The CO median concentration profiles in Figure 4.10 show a much larger relative reduction than the reductions in median ozone concentrations in Figure 4.2, perhaps due to the fact that ozone is a secondary pollutant. The variability of the median NO_X concentration profiles of recent years is basically the same as in early years, indicating that the balance between sources and sinks of NO_X has not changed significantly over this period. However, CO shows a clear indication of the "breathing effect", albeit of much larger magnitude than the ozone trend analysis predicted in section 4.2.1. In the next section we will discuss the possible relationship of these changes to trends in mobile emission characteristics.

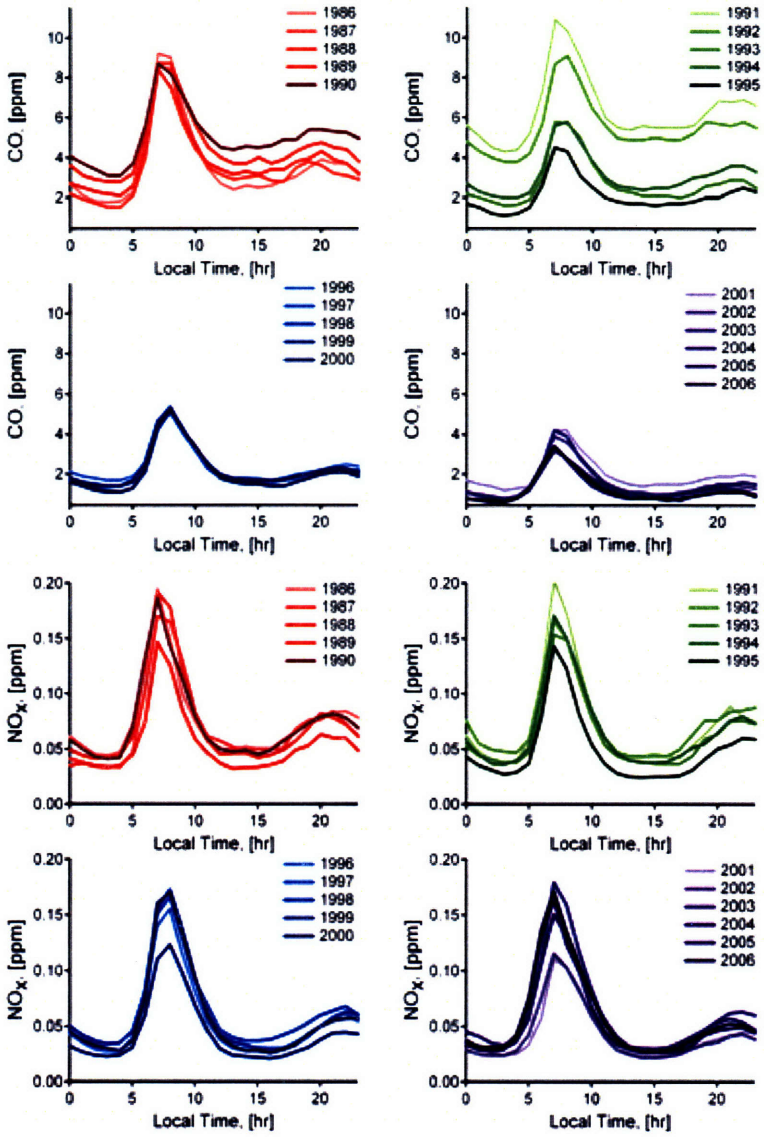

Figure 4.10. CO and NO_X 50th percentile profiles for the months of March and April for a given year.

Another very interesting result obtained from the analysis of the median profile concentration trends of Figure 4.10 is with respect to probable changes in the temporal emission patterns of mobile emissions. Figure 4.11 shows the normalized (converted to percentage) temporal profiles for median CO and NO_X. In the figure, each hourly value represents the percentage contribution to the total accumulated daily concentration. The figure shows what seems to be a negative shift in time of 1 to 2 hours of the median concentration patterns during the early morning hours. Since we expect that the mixing

height characteristics are similar over these years (because we have used only the months of March and April of each year in the analysis), this effect can only be explained by changes in the temporal emission patterns in the city. As traffic increases due to large increases of vehicle fleet with little changes in road infrastructure, residents need to leave home earlier to arrive to work on time. The effect of prolonged rush hours over time is clearly captured by the monitoring stations.

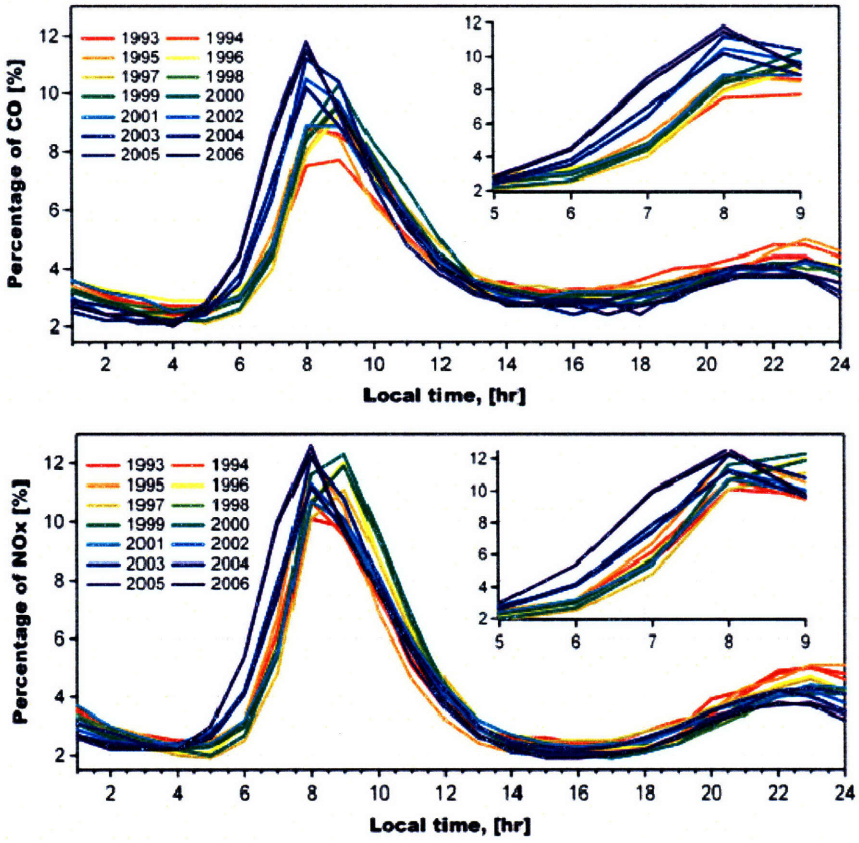

Figure 4.11. Median CO and NO_X temporal profiles in hourly-percentage contribution.

4.3. Estimating historical changes in mobile emissions

4.3.1. Direct measurements of mobile emissions trends

Mobile emissions in the MCMA have been studied since the early 1990's with several measurement techniques that include remote sensing (Bishop et al., 1997; Schifter et al., 2003a), dynamometer (Schifter et al., 2003b) and tunnel studies (Mugica et al., 1998)

and more recently with the on-road sampling techniques (Zavala et al., 2006). An emissions monitoring study using a PEMS (Portable Emission Monitoring System) is currently underway for a limited number of vehicles in the city (Jazcilevich, A., personal communication).

Chassis dynamometer studies are controlled-conditions experiments in which the vehicle is forced to follow a pre-established driving cycle while its emissions are monitored after collection trough a dilution tunnel. In PEMS studies, on-board diagnosis instruments are mounted on individual vehicles for measuring a number of emitted species while driving (Cadle et al., 2006), allowing the direct measurement of emissions in real driving conditions. The applicability of these two techniques for obtaining fleet-average emission characteristics is, however, limited mainly by the necessary assumption of a pre-established driving cycle to represent real world driving conditions (dynamometer studies) and for the small sampling size during the extrapolation to other types of vehicles (PEMS studies).

Remote sensing, tunnel studies and on-road sampling (chase and fleet average) experiments are emissions measurement techniques that can be used to obtain on-road vehicle emissions produced by real world driving conditions. A description of the methods, instrumentation, and assumptions made using these techniques is given in Chapter 2. Nevertheless, due to their sampling size and measurement characteristics, these techniques are more suited for obtaining fleet-average emission conditions than dynamometer or PEMS studies. Fleet-average mobile emission estimates have also been recently obtained using long-path measurement techniques by analyzing the buildup of emitted species/CO_2 ratios during early morning rush hours (Volkamer et al., 2005b). However, necessary assumptions, sampling times and frequencies as well as the sampling size of measurements vary significantly among these techniques. There has been considerable efforts to intercompare studies using the aforementioned techniques, with some comparisons more successful than others (Cadle et al., 2006). Nevertheless, these techniques have been applied in the MCMA at different times in the past two decades and important information has been gathered for obtaining fleet-average emission

characteristics. We have performed a literature review of these studies to obtain fleet-average emission estimates for the MCMA and have converted the reported data to fuel-based estimates[7], (grams of emitted species by liter of fuel consumed). As a result of this analysis, an interesting picture of historical emission trends of mobile sources for HC, NO_X and CO has emerged, see Figure 4.12.

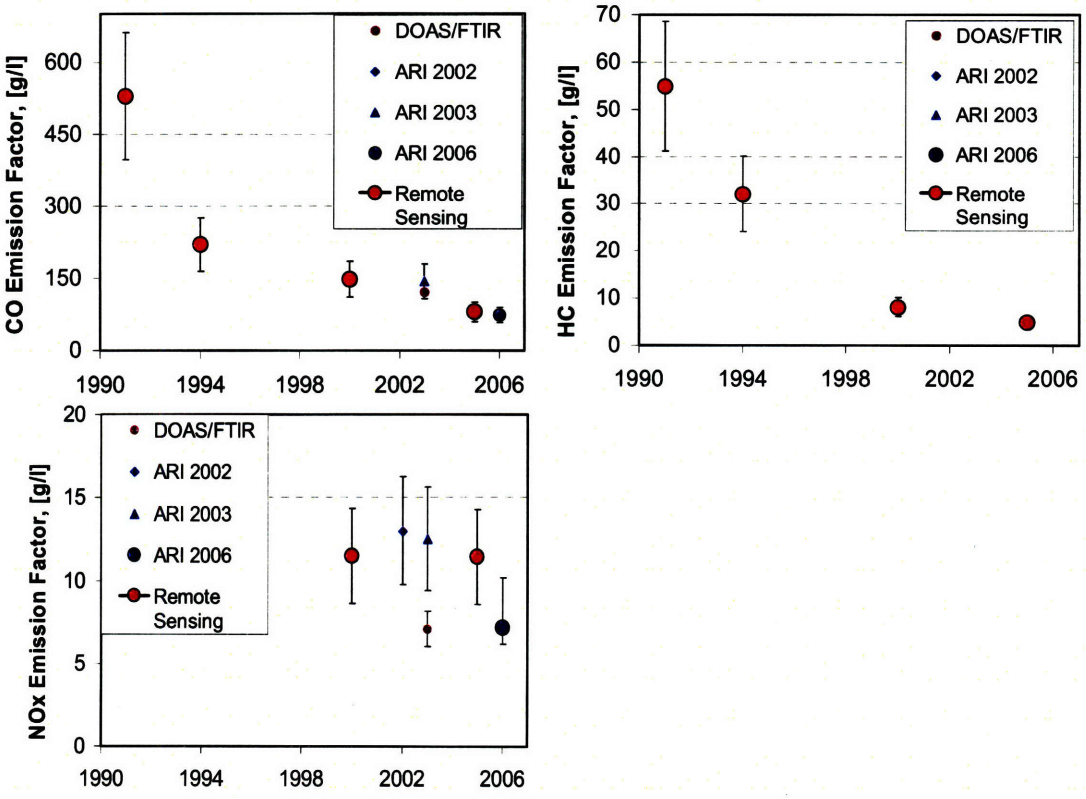

Figure 4.12. Emission factors trends for CO, NO_X and HC (in propane equivalents) in the MCMA from DOAS/FTIR (Volkamer et al., 2005b), on-road plume sampling using the Aerodyne mobile lab in 2002, 2003 and 2006 (Zavala et al., 2006) and crossroad remote sensing studies in the MCMA (GDF-SMA, 2006).

Figure 4.12 shows that fleet average emission factors have drastically decreased for CO and HC over the past two decades whereas NO_X emission factors show no strong trend. Decreases in CO and HC are likely due to improvements in vehicle and emission control

[7] We used a fuel density of 0.75 kg/l and considered 70.3 moles of C per kg of fuel for gasoline. Fuel economy was assumed as 10 km/l for gasoline.

technologies over time, which are in turn related to regulation policies through the implementation of more stringent emission standards for new vehicles. The fact that these measured fleet-average emission factors show a significant decrease over time despite the linear increases in fuel consumption (see Figure 4.13) and population and -associated- vehicle fleet growth (see Figure 4.14) is remarkable. This implies that technology improvements have –so far- overcome the increases in vehicle fleet for CO and HC emissions.

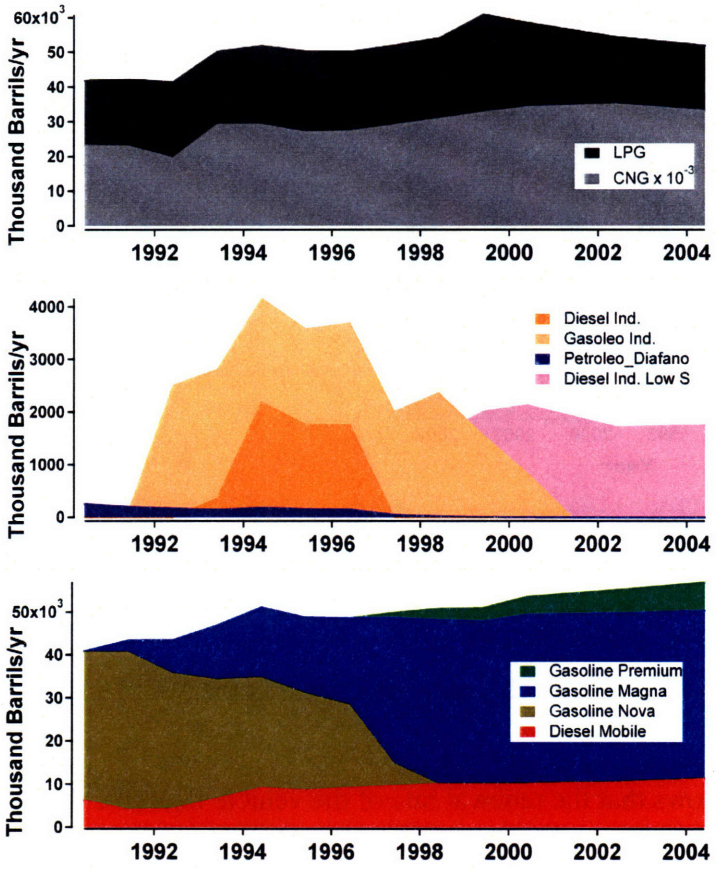

Figure 4.13. Gasoline, diesel, LPG and NG sale trends in the MCMA (CAM, 2006).

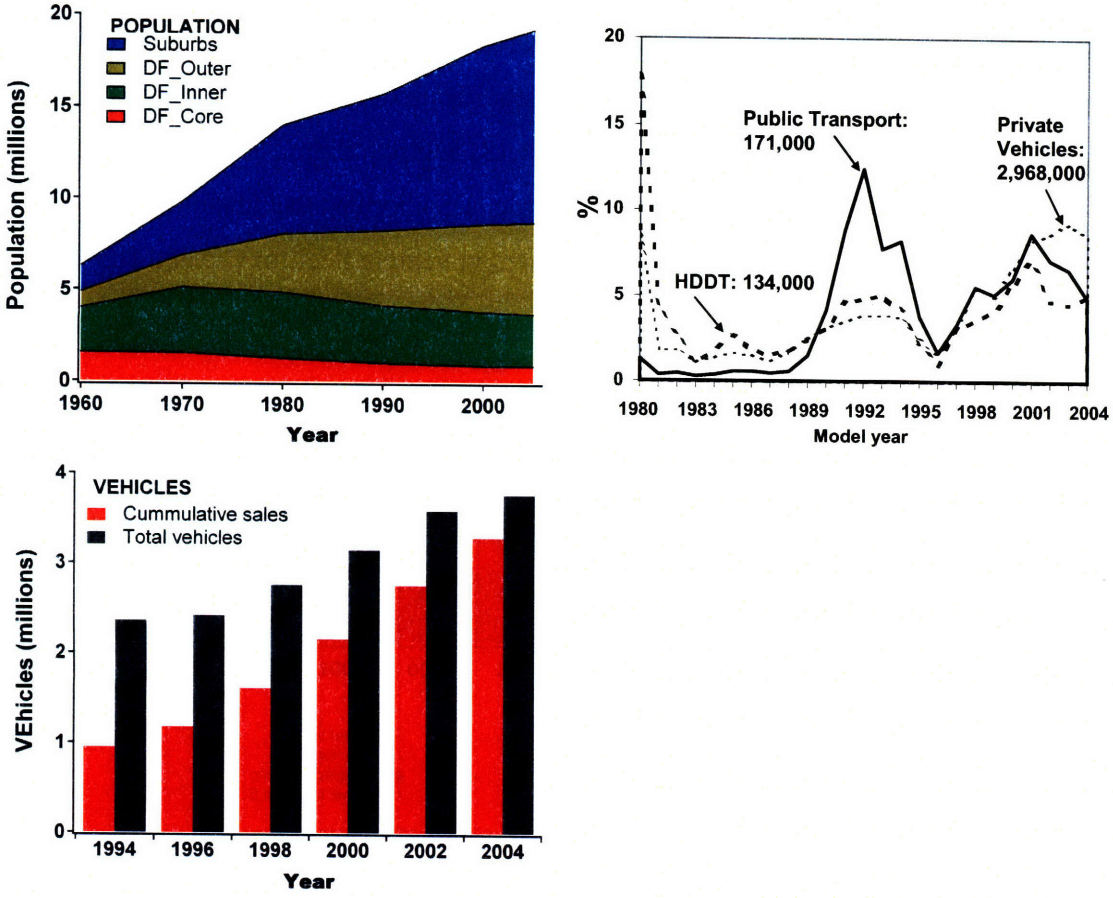

Figure 4.14. Upper left: population trends colored by geographical location - from core to suburbs- of MCMA municipalities (Demographia, 2007). Upper right: vehicle fleet distributions in percentage for the year 2004 (CAM, 2006). Lower left: cumulative vehicle sales and number of vehicles for a given year in the MCMA (CAM, 2006).

Figure 4.14 also shows that the renewal rate of the vehicle fleet (the difference between the cumulative vehicle sales and the number of vehicles between two given periods) has significantly increased in recent years. With more new vehicles in the fleet every year, the fleet tends to homogenize faster because older vehicles are more rapidly taken out of the fleet. Interestingly, this can explain the decrease in the magnitude of the variability bars of Figure 4.12, which suggest that the fleet is homogenizing over time with respect to CO and HC emissions. Similarly, the observed reduction of CO and HC variability is, in turn, in good agreement with the observed downward trends in variability for ambient concentration profiles of CO in Figures 4.8 and 4.10.

In the case of NO_X trends, unfortunately the earliest fleet-average NO_X emission measurements where performed in year 2000, and it is therefore possible that there are simply not sufficient measurements in the time span of Figure 4.12 to observe any trend. However, a larger variability seems to be observed for NO_X than for CO. Although the observed decrease of the magnitude and variability of CO and HC emission factors over time may be an indication of a homogenization process of the combustion efficiency of the fleet, it is also possible that the large variability of measured NO_X emission factors may be due to other causes. In order to obtain a better picture of NO_X emission trends, we will go back to this point after introducing a second approach for estimating the perturbation of mobile emissions.

4.3.2. Indirect measurements of mobile emissions trends

In addition to the literature research presented above, we have investigated the magnitude of the perturbations of mobile sources over the past two decades using an indirect measurement approach. This consists in obtaining the trends of the CO and NO_X concentrations, as well as their CO/NO_X ratio, using only the 6 to 9 AM values measured by the RAMA monitoring stations in the city, see Figure 4.15. Due to the developing stage of the mixing height at these hours and to the coincidence of the rush hour traffic during typical weekdays, this data period contains the largest signature of emissions from mobile sources in the measured diurnal profiles. In addition, at this time of the day the pool of emitted NO_X molecules are not significantly catalytically active in the photochemical cycle, as NO_2 photolysis peaks around local noon, and there is therefore a stronger signal of primary nature. Furthermore, the use of the ratio of CO to NO_X accounts for dilution effects due to vertical mixing and transport during the analysis of emission intensity trends. This represents an interesting indirect method for linking a particularly important emission source with data from a monitoring network.

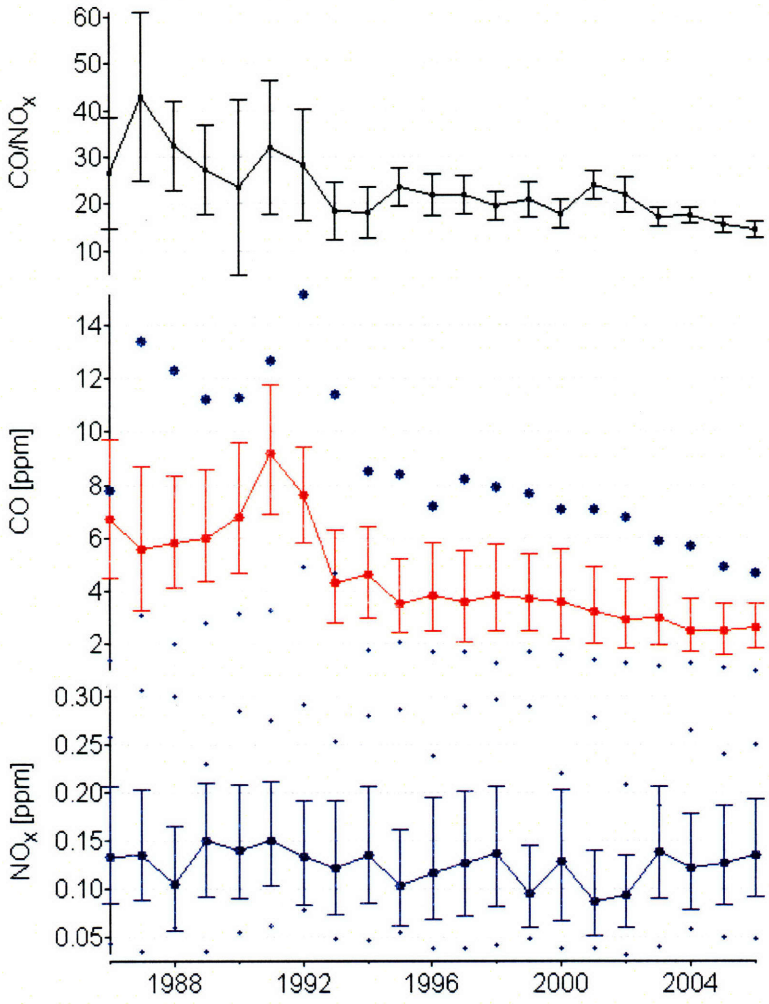

Figure 4.15. CO, NO_X concentration and CO/NO_X trends of 6 to 9 AM values in the MCMA. Middle dots are the averages, lower and upper bars are the 25th and 75th percentiles, and upper and lower dots for CO and NO_X are the minimum and maximum values of all monitoring stations.

Clearly, this indirect method is only reliable if long term data sets are used so that the natural short-term daily variability does not affect the trend. This second approach may be particularly useful for understanding the trends of NO_X emissions, for which much less direct information is available for the MCMA. Similar to the previously described exclusion criteria used for the ozone, CO and NO_X analysis, we have further filtered out the effects of short-term perturbations of mobile emissions, such as weekends and holiday effects, by excluding such days from the analysis. Additionally, we have

accounted for the inter-annual variability of the species by considering only data from the months of March and April of each year. Using these filtering criteria, the 6 to 9 AM concentration and ratio trends are more likely to be result of the long term variability of anthropogenic emissions, mobile sources in particular, rather than the result of natural variability.

Figures 4.15 and 4.15 show similar downward trends for the magnitude and variability, providing further evidence that the fleet is homogenizing in its CO (and therefore HC) emission characteristics by reducing the number of high emitters. The concurrent reduction of the magnitude and variability of ambient CO concentrations shown in Figures 4.8 and 4.10 with the trends of CO and HC mobile emission factors and morning concentration trends shown in Figures 4.12 and 4.15 also indicate that mobile emission sources, rather than point and area sources, are largely responsible for the observed downward concentration trends. Even more, Figure 4.15 suggests that the "breathing effect" shown in the trend analysis of ambient concentrations has been largely the result of changes in mobile emission sources.

What caused the "breathing effect"? The balance between sources and sinks of various pollutants was drastically altered around 1991-1992 in Mexico City. Air pollution in Mexico City started to draw public attention in the early 1980's as a result of the evident deterioration of visibility and concerns on human health[8]. Rapid population growth (particularly in the suburbs, see Figure 4.14) and its associated increases in vehicle fleet, industrial and services sectors, were experienced at that time with little or no control measures. As a result, air pollutant concentrations increased continuously at explosive rates. It was then clear that aggressive control measures needed to be taken and, at the end of 1990, a series of air quality control actions started to be implemented through a program called PICCA (Programa Integral Contra la Contaminación Atmosférica en el

[8] In December 19th of 1985 a large pollution episode caused by a thermal inversion of several days produced a dramatic decrease of visibility in the city, alarming the public and bringing the media attention. Several massive public demonstrations demanding governmental actions followed. Similarly, in February of 1987 thousands of birds were found dead in the south of Mexico City. Accounts in media assumed that air pollution was in part the culprit and public awareness further increased, perhaps prompting authorities to aggressively implement control measures.

Valle de México). Some of the most important actions that PICCA implemented included: 1) the introduction of 2-way catalytic converters for new vehicles in 1991, 2) gasoline lead content started to be drastically reduced until it was finally eliminated in 1997, 3) sulfur content in industrial diesel was reduced from 3.8% to 0.05% in 1997, 4) The "Hoy No Circula"[9] ("A day without a car") program, first started in 1989, was continued as mandatory throughout the year, 5) a Vehicle Emissions Verification Program mandated the inspection and maintenance (I/M) of all vehicles twice a year, 6) in 1993 three-way catalytic converters were first introduced as mandatory for new vehicles, 7) oxygenated gasoline was first introduced with 5% MTBE, 8) changes in fuel quality included the reduction of Reid Vapor Pressure and limits on olefins (<10% v), aromatics (<25% v), and benzene (<1% v) content in gasoline in 1996, 9) the substitution of heavy oil by natural gas started for thermoelectric stations and major industries in the city, 10) a large refinery ("Refineria 18 de Marzo") located in the middle of the city was shut down in 1990.

4.3.3. Hydrocarbon trends in the MCMA

The major actions listed in the previous section definitely started the plateau-decline trends in gaseous air pollutant levels from the early 1990's. CO and HC levels responded particularly promptly to control measures. CO and HC emissions are co-byproducts of incomplete combustion and, therefore, the reductions in ambient concentrations of CO should be accompanied by reductions in ambient HC concentrations (if sinks and other sources are constant over time). Nevertheless, although CO is measured continuously with the monitoring network and therefore its trends are easily tractable, until recently HC levels were not measured continuously. Intensively measured only during field campaigns, hydrocarbon data is scarce and trends are difficult to interpret. In the following paragraphs, we describe briefly the major findings of major field campaigns related to hydrocarbon concentrations.

[9] At first, the program's objective was to restrict the circulation of all cars one day per week during the winter months, when the highest ozone levels occur. Later the program became year-round. In addition, during contingency episodes only the least polluting vehicles are allowed to circulate. This is done by issuing a certificate to each vehicle according to its emission-technology level.

During the MARI project (LANL/IMP, 2004), in February of 1991 measurements of total hydrocarbons and aldehydes were made using adsorption cartridges. In addition, canister samples were also collected in 1992 and 1993 and analyzed using GC/MS at several sites within the MCMA. These measurements revealed non-methane hydrocarbon concentrations ranging from 2 to 7 ppmC, clearly indicating much higher levels than those found in polluted cities in the U.S. The speciation of VOCs showed that propane, butane, toluene, ethane and acetylene together accounted for between 25 and 45 percent of the total VOCs.

Another major field campaign held in Mexico City, IMADA (Edgerton et al., 1999), during February and March of 1997 found the highest hydrocarbon concentrations about 4.1 ppmC at the La Merced monitoring station (in the center of the city) during the early morning hours. The measurements also showed that the most abundant hydrocarbons were propane and butane (together 35 percent by mass), toluene, m-xylenes, p-xylenes and benzene (10 percent by mass), and ethane, acetylene and propene (together 6 percent by mass).

During various weeks in 1993, canister samples were taken at several locations in the MCMA and analyzed using cryogenic separation followed by gas chromatography, (Blake and Rowland, 1995). They also found high concentrations of alkanes relative to other hydrocarbons along with ethylene and acetylene from mobile sources. The highest maximum total concentration for C2 to C10 HCs was 4ppmC in February 1993. They also compared the chemical composition of LPG sold in the MCMA versus that sold in Los Angeles, and showed that the Mexico City LPG contained more olefins and butane. Since these compounds are much more reactive in producing ozone than propane (more abundant in the LPG composition of Los Angeles), this prompted to changes in the LPG composition in the MCMA.

In the 90s, other independent studies of even shorter duration also measured hydrocarbon concentrations in the atmosphere of the MCMA but focused on the HC speciation of individual species, not total hydrocarbons (Young et al., 1997; Serrano Trespalacios,

1999). As in previous studies, these measurements also showed high concentrations of alkenes, aromatics and aldehydes in early morning samples.

During the MCMA-2002 and MCMA-2003 field campaigns a wide variety of VOC measurements were conducted within the city as well as in rural and boundary sites (Velasco et al., 2007). Four distinct analytical techniques were used: whole air canister samples with Gas Chromatography/Flame Ionization Detection (GC-FID), on-line chemical ionization using a Proton Transfer Reaction Mass Spectrometer (PTR-MS), continuous real-time detection of olefins using a Fast Olefin Sensor (FOS), and long path measurements using UV Differential Optical Absorption Spectrometers (DOAS). In addition, a novel conditional sampling technique using canisters was developed to collect samples dominated by fresh on-road vehicle exhaust using the Aerodyne mobile laboratory. From these observations, the VOC composition (in ppbC) was dominated by alkanes (60%), followed by aromatics (15%) and olefins (5%). The remaining 20% was a mix of alkynes, halogenated hydrocarbons, oxygenated species (esters, ethers, etc.) and other unidentified VOCs. The highest early morning HC concentrations of about 2.5 ppmC were measured inside the city and significant spatial gradients of HC concentrations were found towards rural and boundary sites.

During the MILAGRO-2006 field campaign, extensive HC measurements with a multitude of measurement techniques, including those techniques used in the MCMA-2003 field campaign, were obtained at three lagrangian-arranged supersites (the so-called T0 at the center of the city, T1 at the northeast peripheral limits of the city, and T2 at a northeast boundary site). HC measurements included traditional point sampling (e.g. canisters, cartridges, PTR-MS), horizontal distributions (e.g. FTIR and DOAS) and vertical distributions (e.g. tethered balloons, DOAS, FOS in a flux tower). In addition, PTR-MS and canister samples obtained with the Aerodyne mobile laboratory allowed HC concentration measurements at other sites, including boundary sites and rural areas. Numerous HC measurements were also obtained with various instrumentations onboard several airplanes to obtain the regional distribution of key hydrocarbon species. Numerous groups participated in the HC measurements and a large effort will have to be

made in the coming months/years to compile the numerous results, which at the present are still preliminary. A description of the multiple ongoing results from the field campaign can be found at http://mce2.org/milagromex/.

In one particular study also part of MILAGRO, Prof. Blake's group from the University of California, Irvine took canister measurements of VOCs during the campaign (Baker et al., 2007) and the results were compared with similar VOC measurements made during 1993 (Blake and Rowland, 1995). They found a significant decrease in all major VOC mixing ratios and attribute such decrease to reductions in vehicular emissions. However, the benzene to toluene ratios representative of mobile emissions did not change between the 1993 and the 2006 samples. In general, despite the decrease in VOC concentrations, the relative composition of the mayor VOC fractions did not change significantly, suggesting that changes in fuel composition have not had a large impact on the fleet average VOC composition of the exhaust from mobile sources. However, this comparative analysis has not been made for other components, such as aldehydes, that due to their reactivity may have a much larger relative importance in ozone formation.

Besides the previously described field campaigns, there are two sources of data with semi-continuous measurements of hydrocarbons in the MCMA. In the first one, canister measurements conducted between 1992 and 2001 by the IMP (Mexican Petroleum Institute) for the C2 for C12 hydrocarbons (over 100 species) showed a slight but statistically significant decrease for that period (Arriaga-Colina et al., 2004). The canister samples, analyzed using GC/FID, were collected at three sites (Xalostoc in the north, La Merced in the center and Pedregal in the southwest of the city) and showed significant north to south spatial gradients of HC concentrations within the city. They also report similar hydrocarbon fractions: 50 to 60 percent of total HC were alkanes, 14 to 19 percent were aromatics, and 9 to 12 percent were alkenes. The second semi-continuous measurements of HC have been made by CENICA (Centro Nacional de Investigación y Capacitación Ambiental) at its headquarters (near downtown of the city) since 1998. The samples are taken using a cryogenic trap and are analyzed by GC-FID. The results of this ongoing study, still unpublished, also show a strong diurnal profile of HC concentrations

and highlight propane as one of the mayor components (B. Cardenas, CENICA director, personal communication).

The ambient concentration measurements described above are in qualitative agreement with a decreasing time for HC levels in the city, although perhaps not as large as those observed for CO. As seen from the estimated HC emission trends in the previous section, perturbations of mobile emission sources have likely played a significant role in such downward trends. Nevertheless, as opposed to CO, which is mainly emitted from mobile sources within the city, other large non-combustion emission sources also contribute to HC levels. Normally, the contributions from these other area emissions sources (such as paints, solvent consumption, cleaners, CNG leakages, etc.) are estimated using population-based scaling factors. As such, the contributions from these sources tend to increase over time as population increases. Even more, other unmeasured emission sources (e.g. street-food vendors and informal commerce) have also likely contributed in a still quantitatively-unknown measure to HC trends.

The resulting picture is that HC emissions from mobile sources have decreased over time (mainly due to improvements in vehicle and emission control technologies as well as to the increasing renewal of the fleet) despite the vehicle population growth; on the other hand, HC area emission sources have increased over time probably linearly with population grow rates. The decreasing ambient concentrations of HC levels suggest that the mobile source decreases have, so far, overcome the increases of other non-combustion related HC emission sources. However, VOCs from different sources have characteristically different reactivities and it is critical to evaluate the effects of these trends on the chemical composition of overall HC emissions. Of particular importance will be to fully characterize ambient HC levels measured in 2006 during MILAGRO. Such highly characterized HC data (in time and spatial distributions as well as in HC composition), along with the semi-continuous measurements done at CENICA and IMP may allow a better determination of long term HC concentrations and chemical composition trends.

4.3.4. NO_X trends in the MCMA

As noted in section 4.3.2, Figure 4.15 suggests that overall NO_X emissions from mobile sources have not experienced a constant, long term, downward trend in the past two decades. However, given the large NO_X variability observed, it is possible that a trend is hidden in the NO_X data series. NO_X data series, similar to those in Figure 4.15, were obtained using data from individual monitoring stations and they show basically the same trends, albeit with different magnitudes, so the results seem to be spatially consistent. Still, if present, these downward trends are probably not as large as those for CO and HC (see for example the NO_X downward periods of 1991 to 1996 and 1998 to 2002 in Figure 4.15).

Here we enumerate some possible explanations for the observed NO_X levels and emission trends:

1) One possibility is that vehicle technology has apparently been more effective in controlling CO and HC than NO_X levels in the MCMA. Vehicle technology is in turn directed by the establishment of emission standards. The first emission standards, particularly during the 90's, for new vehicles in the MCMA were focused on aggressively reducing HCs and CO as compared to NO_X, see Figure 4.16. Similarly, for in-use vehicles, in 1999 the I/M Program mandated a maximum HC limit of 300 ppm for all light-duty gasoline vehicles model year 1990 and before, with a limit of 200 ppm for 1991-1992 vehicles, and 100 ppm for the 1993 up to present day model years. The CO limit was set at 3.0 vol % for vehicles up to the 1990 model year, 2.0 % for 1991-1992 models, and 1 % for 1993 and later cars. In January 2000, for the first time in the MCMA, limits of 2500 ppm were fixed for NO_X emissions up to 1990 model year, 1500 ppm for 1991-1992 model year, and 1200 ppm for 1993 and later models. Moreover, 1993-1995 model years were obliged to replace their used three way catalyst to meet the 2000 I/M exhausts limits. A much more stringent emission standard (particularly for NO_X) is under negotiation that will replace the current NOM-042-ECOL-2003 standard.

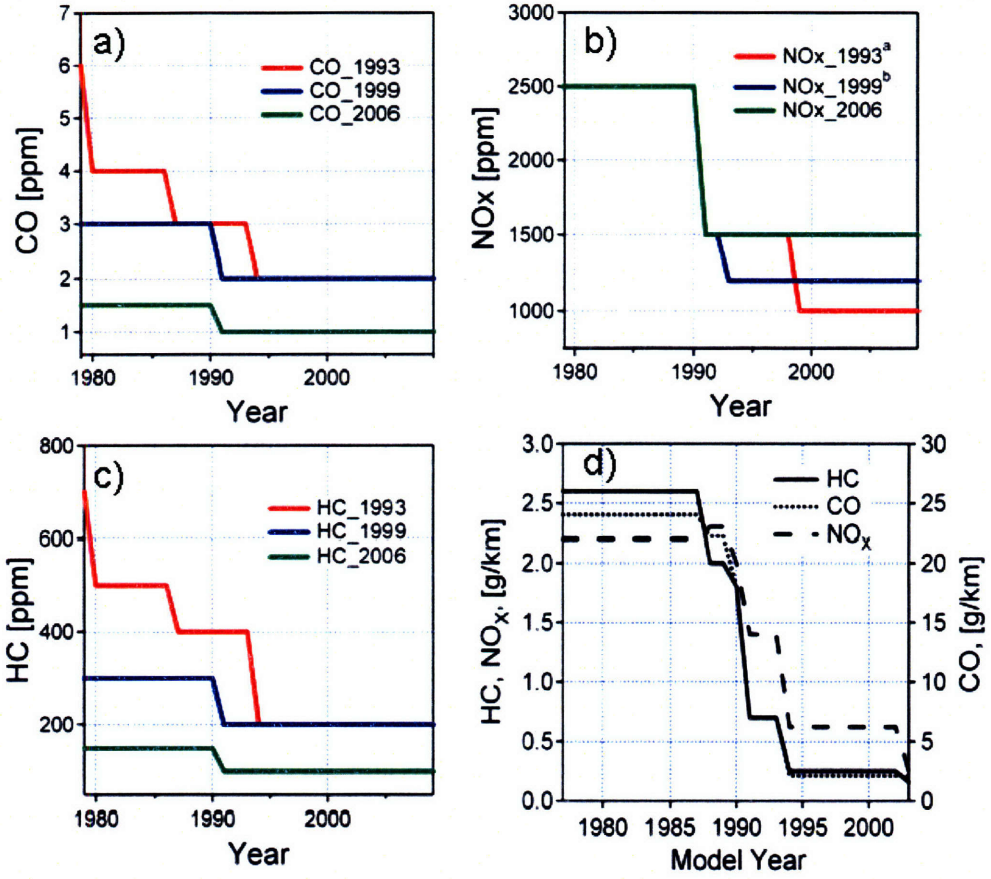

Figure 4.16. Evolution of Mexican emission standards for in use vehicles (panels a to c. Source: NOM-041-ECOL-1993, NOM-041-ECOL-1999, and NOM-041-SEMARNAT-2003) and new vehicles (panel d. Source: for 1970 to 1994 data from (Fernandez, 2004), later from NOM-042-ECOL-1999 and NOM-042-SEMARNAT-2003). [a] refereed to "cruising" speed; [b] standards modified for the MCMA.

2) Different decreases in efficiency for reducing NO_X than for oxidizing HC and CO emissions by catalytic converters. It is possible that emission control technologies, (i.e. catalytic converters) which are, in a way, a response to the implementation of emission standards, may be losing their ability to reduce NO faster than their ability to oxidize CO and HC (G. Bishop and D. Stedman, personal communication). It is also possible that lifetimes of catalytic converters be significantly affected by fuel quality. Shorter life of NO_X emission control devices

(~5 years for catalytic converters), may help to explain the shorter cycles of increase-decrease NO_X levels originated by the continuous renewal of the fleet.

3) Changes in driving mode patterns. As explained in Chapter 2 and 3, higher combustion temperatures are related to higher thermally-formed NO_X species whereas fuel-formed NO_X tends to vary with the type of fuel burned. Thermally formed NO_X emissions are in turn highly dependent on driving mode (see the emissions factors in Chapter 2 obtained for SAG "Stop and Go", TRA "Traffic" and CRU "Cruising" conditions for the MCMA). Figure 4.11 gave evidence of a transition in driving patters in the city probably caused by prolonged rush traffic hours.

4) Faster growth rates of the diesel fleet than the gasoline fleet. Figure 4.17 indicates that annual fuel sales growth rates for mobile sources have widely varied during the observed period, although a stabilization seems to be happening in recent years. This is in part the result of the changes on the different gasoline formulations (Nova, Magna and Premium) used in the city. Premium gasoline is the preferred gasoline for newer vehicles and its higher growth rates may be an indication of the rapid change of the age of the gasoline fleet. Nova gasoline is now discontinued and Magna gasoline sales maintain a small but negative annual sales growth rate, again perhaps as a result of the renewal of the gasoline fleet. Except for the periods of 1995 and 2000, however, in general seems that annual sales rates for diesel have always been higher than for gasoline (total). This may be an indication of faster annual growing rates of the diesel fleet than those of the gasoline fleet. Since diesel vehicles, in general, are significantly higher NO_X emitters than gasoline vehicles, this would imply increases of annual NO_X emissions that may balance the effect of the introduction of new lower-emitting gasoline vehicles.

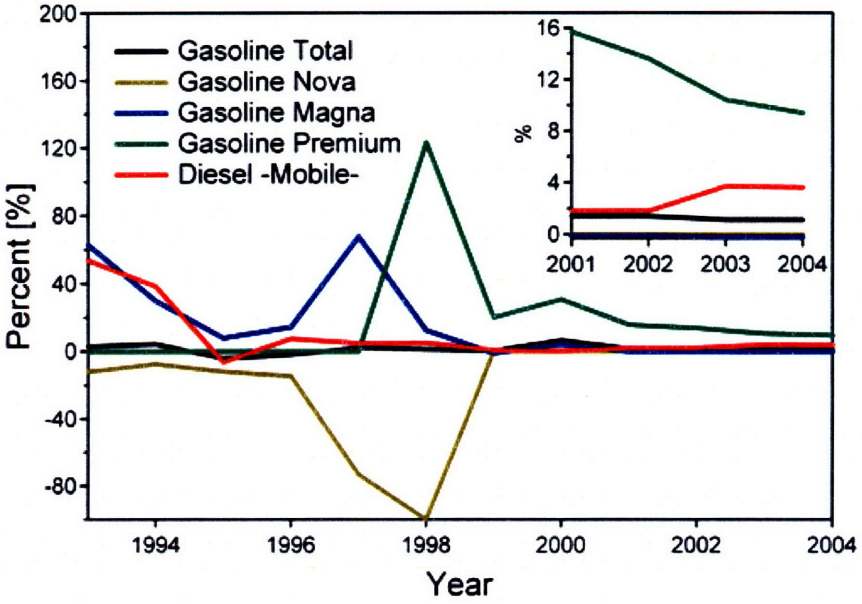

Figure 4.17. Annual fuel sales growth rate –in percent- for gasoline and diesel mobile sources in the MCMA

4.4. Summary

In this chapter we first described the observed concentration trends of CO, NO_X and ozone over the past 21 years in the urban area. Significant changes have occurred for the variability and the diurnal temporal profiles of these species. The changes in the night, early morning and peak concentrations are particularly evident for CO and ozone. Peak ozone concentrations have been drastically reduced in the city while high median concentrations still persist. From the early 90s, a decrease rate of 2.7 +/- 0.5 ppb/yr has been observed in maximum ozone concentrations after an in impressive growth rate of 12 +/- 1.3 ppb/yr from the start of the measurements until 1992. Using direct measurements of emissions and a new indirect approach, we further showed that these changes are strongly linked to concurrent perturbations of anthropogenic source emissions, and of mobile emissions in particular. We also provided evidence for the existence of a "core-to-skirt" effect caused by the observed delay in photochemical pollutant formation rates. This also suggest that the monitoring network may be no longer be capturing the real (domain-wide) ozone peak of the basin. Frequency maps for the allocation of the ozone peak show distinctive clusters that are likely related to the prevailing meteorological

patterns occurring during the months of March and April. These effects, along with the observed trends, will be explored in the sensitivity modeling techniques described in the next chapter.

Chapter 5. Model sensitivity and uncertainty analyses in the Mexico City Metropolitan Area

5.1. Introduction

Emission-based air quality control strategies in an urban area or region are typically directed towards the regulation of NO_X and/or VOCs from various emission sources. However, determining the causes of high particulates and ozone concentrations is not simple. Emitted NO_X and VOCs are transformed in the presence of sunlight to produce ozone, nitric acid and other oxidants in a complex series of chemical reactions that occur along the transport of air masses. These photochemical reactions also are involved in the generation of secondary organic, nitrate and sulfate particle matter. In Mexico City, these secondary processes constitute 70 to 80 % of PM2.5 mass (Salcedo et al., 2006), demonstrating that gas-to-particle conversions can contribute significantly to the total particle loadings in an urban area.

Controlling high levels of particulates and ozone is challenging because the relationship between NO_X, VOCs and air quality is nonlinear: high levels of NO_2 scavenge hydroxyl (OH) radicals that initiate the oxidation of VOCs leading to ozone and aerosol production. In turn, the rate of formation of OH radicals is dictated by reactions such as the photolysis of ozone, HONO and key VOC species (e.g. aldehydes), as well as the reactions of ozone and key VOC species (e.g. alkenes). Ozone, itself a powerful oxidant of VOCs in the atmosphere, can also be destroyed in the presence of high NO_X levels through titration reactions. This coupling of key chemical species, occurring at very different reaction rates, is an important source of nonlinearity in the system. Thus, reductions of NO_X or VOC emissions may have little or no effect on -or may even increase- ozone concentrations. Understanding the particular rates at which these processes occur is required to evaluate an emission-based air quality control strategy.

A common approach used in the design of emission-based air quality control strategies is the application of Air Quality Models (AQMs) that aim to reproduce the dynamic physicochemical processes that produce air pollution. With estimated emission scenarios, these models are used to predict concentration profiles of key atmospheric pollutants. AQMs make air quality predictions by incorporating current knowledge of emissions, meteorology and atmospheric chemistry in a mathematical framework. Nevertheless, the representation of these processes is, in various degrees, limited and therefore uncertain. In addition, the input data needed for the construction of these models is itself uncertain due to insufficient and uncertain measurements. Such uncertainties are propagated through the model to the results. Consequently, model predictions are uncertain because of uncertainties in the input data and the parameters used in their formulation. Therefore, when model predictions are used to evaluate control strategies, there may be significant scientific uncertainties about the environmental impacts of such strategies.

One way to assess the uncertainty of the model predictions is to perform sensitivity and uncertainty propagation analyses. Sensitivity analyses estimate model responses to changes in the model inputs (parametric sensitivity analysis) or to changes in the model formulation (structural sensitivity analysis). Uncertainty analyses probabilistically estimate the uncertainty of the model outputs by quantifying the uncertainty of the inputs and their contributions to the model uncertainty outputs. As we will see in this chapter, the two are related because the product of an observable sensitivity coefficient and a parameter uncertainty is often taken as a measure of the parameter's contribution to uncertainty in the model output.

The first part of this chapter describes the evaluation of the performance of the model for the MCMA using a base case simulation event. A high pollution episode period ("Ozone-South") during April of 2003 is chosen along with the construction of a base case emission scenario. The construction of a base case simulation period using measured local data and a thorough evaluation of its performance against key observational data (such as hydrocarbon species, photochemical products and radical concentrations) are essential for any attempt to use an AQM for sensitivity and uncertainty propagation

studies. In the second part of this chapter we perform a sensitivity analysis and study the propagation of uncertainties from mobile emission sources inputs. The sensitivity studies are carried out using the mathematical Decoupled Direct Method (DDM) and the results are validated using the standard Brute Force Method (BFM).

5.2. Base case photochemical simulation for the MCMA

The MCMA is surrounded by mountain ridges on the west, south and east, with a broad opening to the north and a narrow gap to the south-southwest. The area of the basin is about 2400 km^2; it is located in a subtropical latitude of 19°25'N and at an altitude of 2240 m a.s.l.. With a fleet of about 4 million vehicles, a population of about 20 million inhabitants and associated commercial, services and industrial activities, significant rates of anthropogenic pollutants are daily injected into the atmosphere. Due to its location and altitude, the basin receives intense sunlight throughout the year. The enhanced solar radiation in combination with a complex topography and less efficient combustion processes induced by a decrease in atmospheric oxygen content with altitude, contribute to high rates of photochemical smog formation.

Over the past decade, several modeling studies in the MCMA have been conducted aimed at understanding important aspects of the air pollution formation processes in the basin. Simulations based on a Lagrangian model were used to estimate the variations of ozone concentrations as a function of the VOCs composition of emissions (Bugajny et al., 1993). Los Alamos National Laboratory (LANL) and Instituto Mexicano del Petróleo (IMP) used a 3D transport model to simulate the meteorology and photochemistry during the MARI campaign (Williams et al., 1995). A multi-level photochemical box model was used to estimate hydrocarbon speciation of emissions as well as NO_X emissions (Young et al., 1997). Meteorological processes associated with inhomogeneous ozone concentrations over Mexico City were examined using observations from the IMADA-AVER field campaign with a dispersion modeling system (Fast and Zhong, 1998). Air pollution regimes were simulated showing that the complex topography induces confluence lines and significant vertical transport over the region (Jazcilevich et al.,

2003; Jazcilevich et al., 2005). A high pollution episode during March of 1997 was simulated with a 3D transport model (CIT) with adjusted official emissions of CO and VOCs by 2 and 3, respectively, but no formal treatment of uncertainty was performed (West et al., 2004). It has also been suggested that the basin ventilates relatively rapidly so that there is very little pollution carry over from day to day (de Foy et al., 2006b; Fast and Zhong, 1998).

More recently, the urban plume outflow was simulated with a box model and a detailed gas phase chemistry mechanism (Madronich, 2006). The results showed that the reactivity of the urban plume persisted for several days, suggesting potential impacts on the tropospheric chemistry at regional and continental scales. In another recent study, the official estimates of CO and SO_2 from the Emissions Inventory (EI) were evaluated using a combination of trajectory and 3D models (de Foy et al., 2007). The results suggest that current official CO estimates are about right, whereas SO_2 estimates need to include the emissions from nearby industrial regions and the Popocatepetl volcano. The magnitude and timing of ozone, CO and NO_X were also recently studied with the newly developed regional chemical/dynamical model WRF-Chem, (Tie et al., 2007). The model was able to reproduce the concentration and diurnal cycles of these species when compared with surface measurements from the local ambient monitoring network. Finally, in a recent application of the Comprehensive Air Quality Model with extensions (CAMx) the ozone production rates in the MCMA were investigated (Lei et al., 2007). The results indicated that ozone formation in the urban region is VOC limited. The formulation of the base case simulation period used in our sensitivity and uncertainty analysis is based on the findings of Lei et al (2007).

5.2.1. Model and model inputs

The 3D CAMx chemical transport model (version 4.30) employed in this study is an Eulerian photochemical grid model designed to investigate air quality issues on urban and regional scales (ENVIRON, 2002). CAMx simulates the emission, transport, chemistry, and deposition processes of pollutants in the troposphere. The model is driven by hourly

meteorological output fields from the Penn State /National Center for Atmospheric Research (PSU/NCAR) Mesoscale Modeling System (MM5) (Grell et al., 1995), including wind, temperature, water vapor, cloud/rain and land use. The vertical diffusion coefficients were deduced from the MM5 output based on the O'Brien scheme (O'Brien, 1970), and the minimum values were set to 2 - 4 m^2/s (day-varying) in the MCMA based on the findings of (de Foy et al., 2007). MM5 was configured to three one-way nesting with grid resolutions of 36, 12 and 3 km and 23 sigma levels in the vertical, and was run with the NOAH soil model, MRF boundary layer scheme, K-F convection scheme, simple ice microphysics, and cloud radiation scheme (de Foy et al., 2006a). The CAMx model domain is the same as the MM5 domain, with 15 vertical layers extending from the surface to 5 km a.g.l. with the bottom layer interface of about 64 m a.g.l.

The boundary conditions were carefully examined using measurements taken at the boundary sites during the MCMA-2003 Campaign (Molina et al., 2007). A sensitivity run with a 50% change of the chemical boundary conditions (which basically covered the variations of the boundary measurements for most important species) did not show significant effects on O_3 and other photochemically active species. Chemical initial conditions were taken from (West et al., 2004) but the first simulation day was considered only as spin up of the model. The SAPRC99 gas phase chemical mechanism (Carter, 2000) was used in this study. Photolysis rate frequencies for clear sky were pre-computed with the Tropospheric Ultraviolet and Visible radiation model (TUV) (Madronich and Flocke, 1998). In the computation, the aerosol loading was scaled to match those measured in the MCMA-2003. In highly polluted areas the aerosol optical depth at 340-nm wavelength was set to 0.8, comparable to the concurrent LIDAR aerosol extinction measurements (Frey et al., 2004). The effects of cloud presence on photolysis rates were taken into account by using the approach of Chang et al., (1987).

5.2.2. Base case emission estimates and episode selection

The emission input fields for the 2003 simulation period were constructed with the interpolation between the 2004 official emissions inventory (EI) (CAM, 2006) and the

2002 EI (CAM, 2004) emission estimates. Interpolated total annually emitted masses of VOCs, CO and NO_x were distributed across mobile, point and area emission source categories considered in the EI and were transformed into spatially and temporally resolved and chemically speciated emission fields. Updated fine resolution population maps, road, street and highway digital data along with the digitalization of point sources and most of the area emission sources considered in the EI, were input to a Geographical Information System (GIS). With the information digitized in GIS format, we constructed spatially distributed 2.25 km gridded emission maps that were temporally distributed using activity data taken during MCMA-2003. When information from area source-specific emission categories was not available, updated population-based distributions were used as proxies. The emission input fields described above are referred to as the initial emission estimates henceforth. A summary of the total basin-wide initial emissions by source category and pollutant type is given in Table 5.1. Selected key VOC initial emissions shown in Table 5.1 were subsequently scaled using the scaling factors described in Velasco et al., (2007) that used the distribution of measured ambient concentrations from canister samples to estimate adjustments in the distribution of emissions by species classes. The resulting mass-based VOC emissions, referred here as reference emissions, increased by about 65 %.

A 4-day period (13-16 April 2003) was selected for the evaluation of performance of the model. However, for our sensitivity analysis we focused on the April 15 simulation event as our base case. In that way, we allow the model base case to become less sensitive to initial conditions. We selected this "Ozone –South" episode[10] for several reasons. First, during "Ozone-South" days, meteorological conditions are characterized by weak synoptic forcing, stagnant surface winds and clear skies, which are conductive to the occurrence of high ozone levels. Second, the basin flow is governed by a thermally-driven northerly flow from the Mexican plateau during the day and southerly gap flow from the southeast passage in the late afternoon and early evening, this leads to the highest ozone levels in the southern part of the city. In addition, in Chapter 4 we

[10] The term "Ozone-South", as well as "Ozone-North" and "Cold-Surge", was introduced by (de Foy et al., 2005) to describe prevailing meteorological conditions that lead to the formation of ozone in given spatial characteristics.

calculated the frequency of the historical location of the ozone peak in the city for the months of March and April. We showed that the ozone peak location at this time of the year has the highest frequencies with the spatial characteristics of "Ozone-South" episodes, indicating that this episode represents typical meteorological/pollution conditions.

Table 5.1. Annual base case emissions inventory used in this study.

Emission source	CO		NMHC		NO_X		SO_2		NH_3	
	ktons	(%)	ktons	(%)	ktons	(%)	ktons	(%)	Ktons	(%)
LDGV	1038	55.7	106	18.7	66	36.2	2	32.0	3	15.4
HDDT	424	22.7	44	7.7	60	33.0	1	14.0	0	1.6
Taxis	152	8.1	17	3.0	13	7.2	0	5.6	0	2.9
Public transport*	239	12.8	25	4.4	14	7.5	0	2.7	0	1.2
All mobile**	1853	**99.3**	191	**33.9**	152	**83.8**	4	**54.4**	4	**21.0**
Electricity generation	2	0.1	0	0.0	11	6.3	0	0.2	0	0.4
Other Industries**	6	0.3	97	17.1	10	5.4	3	45.1	0	0.8
All Indus. sources	8	**0.4**	97	**17.2**	21	**11.6**	3	**45.3**	0	**1.3**
Residential cooking	0	0.0	0	0.0	3	1.6	0	0.0	0	0.0
Airports	3	0.2	2	0.3	2	1.2	0	0.0	0	0.0
Solvents	0	0.0	79	14.0	0	0.0	0	0.0	0	0.0
LPG leakage	0	0.0	65	11.5	0	0.0	0	0.0	0	0.0
Other area**	2	0.1	114	20.1	2	1.3	0	0.3	13	77.7
All area sources	5	**0.3**	259	**46.0**	8	**4.2**	0	**0.3**	13	**77.7**
Biogenic	0	0.0	17	3.0	1	0.3	0	0.0	0	0.0
Total	1865	**100**	564	**100**	181	**100**	8	**100**	17	**100**

* Public transport refers to combis, microbuses and colectivos.

** The official EI considers 51 emission source categories: 10 for mobile, 10 for industrial, 30 for area sources and 1 for biogenic sources. These categories are lumped here for simplicity of illustration.

5.2.3. Base case model results and performance evaluation

The performance of the MM5 model for simulating the meteorological patterns of the selected period has been described in detail elsewhere (de Foy et al., 2006a,b). Briefly, the main features of the Mexico basin flow are well represented by the model including the northerly flow from the Mexican plateau during the day, up-slope flows on the basin edges and the southerly gap flow from the southeast passage in the late afternoon and early evening. Weak synoptic forcing leads to surface winds that are weak and variable and are particularly challenging to model. The main difference between the model and the observations is the timing of the increase in surface wind speeds and the wind shift on April 14. This affects the location of the horizontal wind convergence zone, and can have a large impact on pollutant dispersion predictions.

The performance of CAMx was evaluated by comparing near surface ozone, NO_Y and CO concentrations with data from the RAMA monitoring network and data obtained during the MCMA-2003 field campaign. In particular, we compared model VOC concentrations with measurements from canister samples (Velasco et al., 2007) and DOAS measurements of selected VOCs (Volkamer et al., 2005b). In addition, and of prime relevance to our sensitivity analysis, we compared model concentrations of key radical species such as OH and HO_2 with corresponding measurements obtained at the CENICA supersite (Shirley et al., 2006).

We have selected eight stations from the RAMA monitoring network for comparisons with the model outputs. These monitoring stations (denoted as EAC, AZC, TAC, MER, PLA, BJU, UIZ, CES in the official classification by RAMA) represent urban conditions with less influence from nearby local emission sources. Figure 5.1 compares measured and simulated concentrations of ozone, NO_Y, and CO averaged over these 8 stations within the urban area. We have used the NO_Y model predictions for comparison with NO_X measurements from RAMA since the chemiluminescence technique used by the network most accurately represents NO_Y. The model using the reference emissions correctly reproduces the diurnal variation of ozone in the first 3 days, although the peak ozone on April 14 is overestimated by about 30 ppb, most likely due to difficulties in

reproducing the meteorological fields for that day (Lei et al., 2007). On the other hand, the model using the initial emissions clearly underpredicts the ozone level over the whole episode, supporting the necessity of increasing VOC emissions.

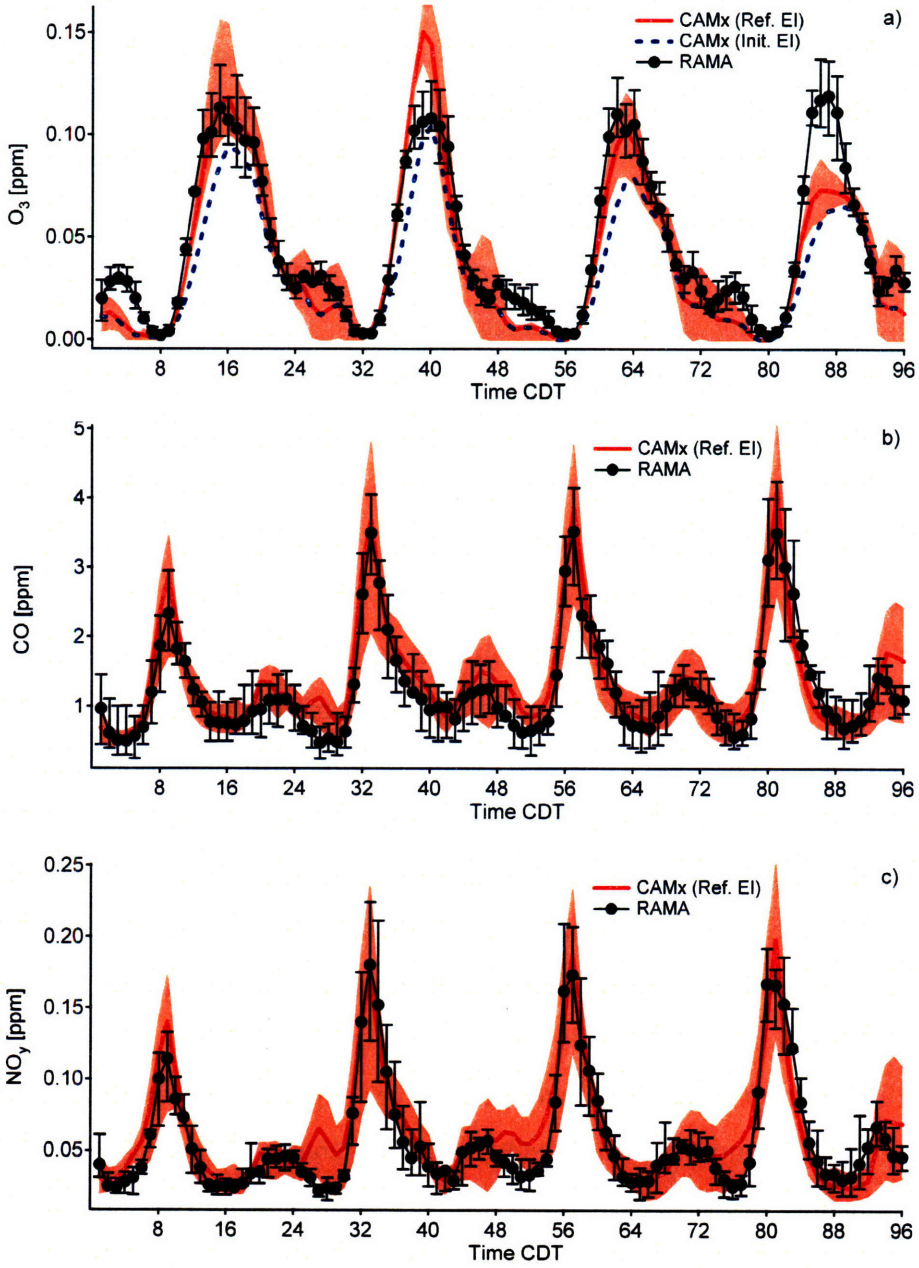

Figure 5.1. Comparison of measured (black) and simulated (red) diurnal variation of near surface hourly concentrations of (a) ozone, (b) CO, and (c) NO_Y averaged over the 8 monitoring stations. Error bars and shaded areas envelop the 25% and 75% percentiles of

measurements and simulations, respectively. Also shown in Panel (a) is the modeled ozone time series using the initial emissions. Time in the x-axis is the end hour in CDT (central daylight time) starting at 01 CDT April 13, 2003.

Figure 5.1 also shows that simulated CO and NO_Y agree well with the measurements from the monitoring network within the modeled and experimental variability, and there are no systematic biases between modeled and observed daytime CO and NO_Y. However, there are some hangovers of simulated CO and NO_Y during the late night and very early morning. Most of the hangover can be explained by the underprediction of nighttime planetary boundary layer (PBL) height affecting vertical mixing. The larger NO_Y hangover is due to the relative higher nighttime NO_X emission fractions as compared to CO. This gives us confidence in model performance and in the accuracy of the emissions of CO and NO_X used in the model.

Figure 5.2 shows measured and predicted surface ozone concentrations over all RAMA stations during the simulated episode, with the cutoff value set to 40 ppb of measured concentrations, indicating good agreement between the measured and the predicted ozone concentrations. The figure also presents some ozone performance statistics, such as the normalized bias (the percentage difference between the predicted and observed ozone concentrations paired in time and site with observed values above a 40 ppb threshold), the normalized gross bias (the percentage of the absolute difference between the predicted and observed ozone concentrations paired in time and site with observed values above the threshold), and the average accuracy of the peak (the percentage difference between the predicted and observed peak ozone concentrations paired in site). These statistical values also indicate a satisfactory performance in the ozone simulation.

We also compare predicted VOC species with a comprehensive array of available observations described in detail in Velasco et al. (2007) and Volkamer et al. (2005). As shown in Figure 5.3 panels (a) to (e), the predicted concentrations of alkenes and speciated alkanes agree very well with measured concentrations (30-min average) from canister samples. Figure 5.3 also shows the comparison of predicted concentrations of

aromatics and formaldehyde with those obtained by DOAS. There is good agreement between modeled and measured concentrations for aromatics on April 15 with no systematic bias. Observed ARO1 (Figure 5.3f) was constructed from DOAS measurements of toluene and benzene, and observed ARO2 (Figure 5.3g) was derived from DOAS measurements of xylenes using a scaling factor obtained from the canister data in which the contribution of xylenes to ARO2 can be estimated. The measured aromatic concentrations on April 13 are much higher than the rest of the measurement period, and the model is unable to reproduce this particular day. However, the phenomenon of much higher measured APRIL 13th aromatic concentrations compared to other days is not found in the CO, NO_X or HCHO species data.

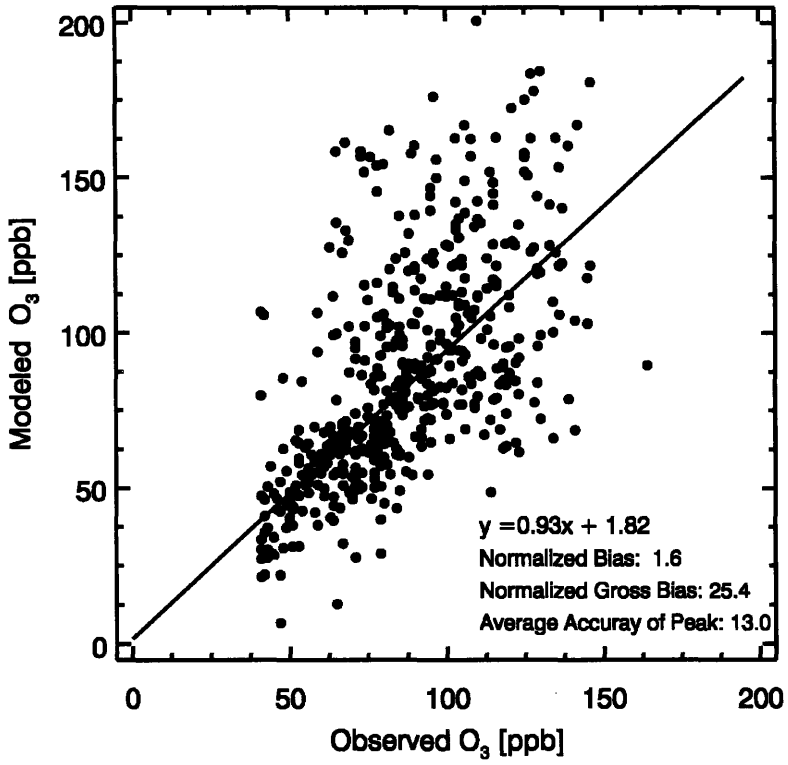

Figure 5.2. Scatter plot of observed and simulated near surface ozone concentrations over all RAMA stations during 13-15 April 2003 when observed ozone values are above 40 ppb. Also shown are the linear fitting parameters and performance statistics.

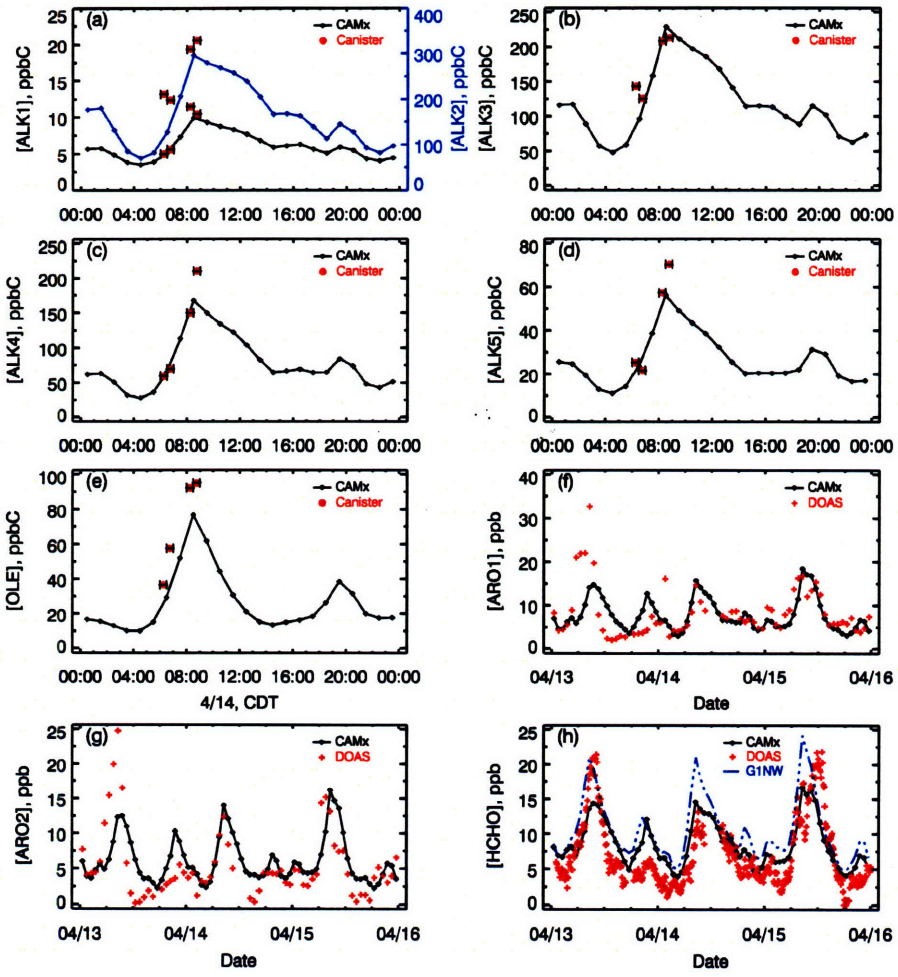

Figure 5.3. Comparisons of modeled VOC concentrations with canister and DOAS measurements at CENICA supersite. Canister data are 30-minute averages. The legend G1NW denotes one model (3km) grid northwest of CENICA.

HCHO is somewhat underestimated during the morning hours at CENICA site even with an adjustment factor to the HCHO emissions. Nevertheless, Figure 5.3 also shows that grid cells a few kilometers north and west of CENICA were predicted to have much higher HCHO concentrations, suggesting an uncertainty in the spatial distribution of HCHO emissions. CENICA site is located at the edge of a high vehicular emission area in the current emission estimates; the total emission estimates may need to be allocated over a broader area, considering the growth of the city.

Based on these comparisons, it seems that emissions of some VOC species are underestimated by a factor of 2-3 in the EI, but not all VOCs are underestimated. Overall mass emissions of VOCs are underestimated by about 65%. This result is consistent with the conclusions from Velasco et al. (2007a), which are based on comparisons of 1998 EI with canister data of early morning VOC abundance at several sampling sites. It should be noted, however, that the adjustments of VOC emissions in this study were solely based on comparisons at only one station (CENICA), over a few days (one day for alkanes and alkenes), with limited dataset, and with assumptions that the spatial and temporal distribution of emissions in the EI were accurate.

In the base case simulation of Lei et al (2007) several other aspects of the photochemical characteristics for the MCMA were investigated. These included estimations of the photochemical ozone formation rate as a function of NO_X levels ($P(O_X)$ values ranged between 10 and 80 ppb/hr) and its dependence on radical sources. The results suggested that O_X formation is VOC-limited in the urban area and largely dependant on the VOC reactivity composition and radical sources. Using the product of speciated VOCs and their reaction rates with OH, the VOC reactivity (total reactivity was estimated larger than 25 s^{-1}) analysis indicated that alkanes, alkenes and aromatics contribute comparably to the VOC reactivity, with alkanes dominating slightly. During the early morning rush hour, alkenes dominate the total VOC reactivity in the MCMA. As time evolves, relatively lower contribution to VOC reactivity would be expected from the more reactive alkenes in the afternoon due to their shorter lifetimes.

An important characteristic of the evaluation of the model's performance is a comparison with observed radical concentrations. Figure 5.4 shows the comparison between observed and modeled OH and HO_2 radicals corresponding to the base case simulation of April 15, 2003 at the CENICA supersite. The figure indicates that OH is over predicted by about 25 % at the peak and under predicted by a similar magnitude from early in the morning until the local noon. OH concentrations at night are largely under predicted, suggesting missing non-photolytic radical sources in the model.

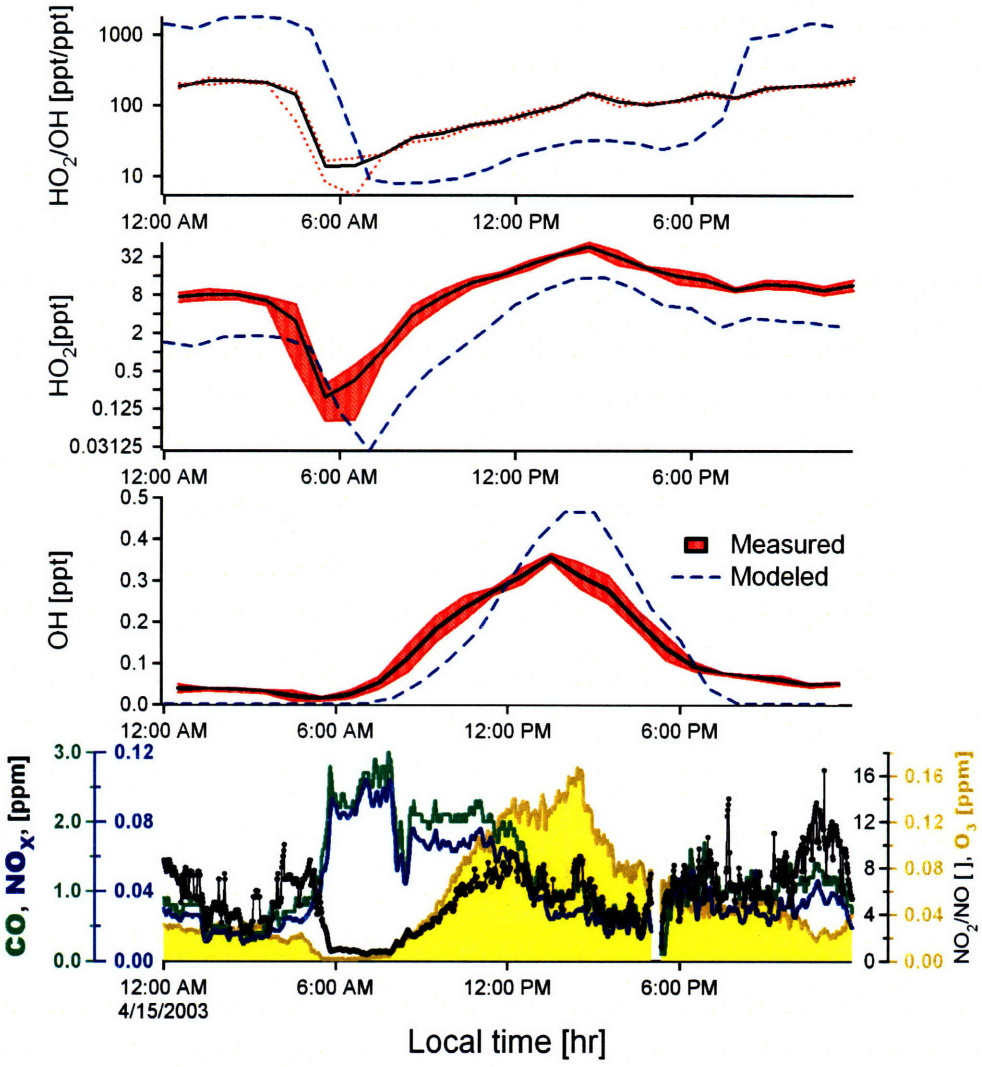

Figure 5.4. Comparison between modeled and measured HO_X radicals on April 15, 2003 at the CENICA supersite. Red areas correspond to 1 standard deviation of measurements. The upper panel shows observed and modeled HO_2/OH ratios and the lower panel shows concurrently measured CO, NO_X, ozone, and the NO_2/NO ratio.

Figure 5.4 also suggests that modeled HO_2 radicals are severely under predicted by a factor of 2 to 3, and the under estimation is constant throughout the profile. Reasons for such under predictions are not clear. Since ozone and VOCs and reasonably reproduced, one possibility is that the model is compensating for the missing HO_2 with organic peroxy radicals in the SAPRC99 chemical mechanism. Unfortunately we do not have RO_2 measurements to compare with the model. The temporal profile for HO_2 is

accurately captured by the model, whereas the predicted OH shows a delay of about 1.5 hours in early in the morning, which propagates to the timing of the local peak. The moderate over-prediction of OH radicals and the large under-prediction of HO_2 radicals results in a substantially lower modeled HO_2/OH ratio compared to the measured ratio.

The HO_2/OH and the NO_2/NO ratios largely determine the efficiency of ozone production. This can be seen using the simplified general mechanism described in Seinfeld and Pandis, (2006) for tropospheric ozone formation. Considering the OH radical as the dominant species oxidizing hydrocarbons (RH), the alky radicals (R) formed can rapidly combine with oxygen to generate alkyl peroxy radicals (RO_2):

$$\left.\begin{array}{l} RH + OH \rightarrow R + H_2O \\ R + O_2 + M \xrightarrow[fast]{} RO_2 + M \end{array}\right\} \quad RH + OH \xrightarrow{O_2} RO_2 + H_2O \qquad R.1.$$

For completeness, the reaction of CO with OH is also considered:

$$CO + OH \xrightarrow{O_2} CO_2 + HO_2 \qquad R.2.$$

The peroxy radicals in reactions 1 and 2 subsequently react with NO, NO_2, HO_2 and themselves. For urban conditions where NO_X is abundant, a good assumption is that the alkyl peroxy radicals predominantly react with NO and HO_2:

$$RO_2 + NO \rightarrow RO + NO_2 \qquad R.3,$$
$$RO_2 + NO \rightarrow RONO_2 \qquad R.4,$$
$$RO_2 + HO_2 \rightarrow ROOH + O_2 \qquad R.5.$$

The yield of alkyl nitrate radicals formed in reaction 4 increases with the size of the parent hydrocarbon molecule and can undergo photolysis or further react with OH (Becker and Wirtz, 1989). Reaction 3 is then the predominant channel of NO and RO_2 radical reactions contributing to NO_2 formation. The alkoxy radicals (RO) generated in reaction 3 rapidly react with oxygen to form aldehydes and hydroperoxy radicals:

$$RO + O_2 \xrightarrow[fast]{} RCHO + HO_2 \qquad R.6.$$

The aldehydes produced by reaction 6 are also oxidized by OH radicals or undergo photolysis, further contributing to the propagation of radicals. The hydroperoxy radicals formed in reactions 2 and 6 can react with NO to regenerate OH:

$$HO_2 + NO \rightarrow NO_2 + OH \qquad R.7.$$

The NO_2 formed in reactions 3 and 7 can then participate in the formation of ozone through its photolysis:

$$NO_2 + h\nu \xrightarrow{O_2} NO + O_3 \qquad R.8,$$
$$O_3 + NO \rightarrow NO_2 + O_2 \qquad R.9,$$

and the ozone concentration is governed by the NO_2/NO ratio in the photostationary state relation:

$$[O_3] = \frac{j_{NO_2}[NO_2]}{k_9[NO]} \qquad Eq.1,$$

in which the conversion of NO to NO_2 is given not only by reaction 9 but also from reactions 3 and 7 involving peroxy radicals. The radicals provided in this mechanism are created by reactions such as the photolysis of ozone, HONO and key carbonyl compounds, as well as by reactions of ozone with alkenes. These radicals are created in substantial amounts but their production is offset by equally large sink pathways that involve radical-radical reactions:

$$RO_2 + HO_2 \rightarrow ROOH + O_2 \qquad R.5,$$
$$HO_2 + HO_2 \rightarrow H_2O_2 + O_2 \qquad R.10,$$

and the HO_X-NO_X termination pathway:

$$OH + NO_2 \xrightarrow{O_2} HNO_3 \qquad R.11.$$

Therefore, the rate of production of radicals is balanced by their destruction rates through reactions 5, 10 and 11 as:

$$HHL = 2k_{10}[HO_2]^2 + k_5[RO_2][HO_2] \qquad Eq.2,$$

$$NHL = k_{11}[OH][NO_2] \qquad Eq.3.$$

There are other removal processes for NO_2 that involve the production of alkyl nitrates and peroxyacyl nitrates (PANs) but they tend to be temporary reservoirs since they rapidly undergo photolysis, react with OH or thermally decompose.

From this simplified general mechanism we observe that ozone production, $P(O_3)$, directly depends on the availability of NO_2, which is governed by the rate of NO to NO_2 conversions by the HO_2 and RO_2 radicals. We calculate $P(O_3)$ from the mechanism described above as:

$$P(O_3) = k_7[HO_2][NO] + k_3[RO_2][NO] \qquad Eq.4.$$

The ozone production efficiency (OPE), defined as the number of ozone molecules formed per each NO_2 molecule that is removed from the system, is estimated from Equations 3 and 4:

$$OPE = \frac{P(O_3)}{NHL} = \frac{k_7[HO_2][NO] + k_3[RO_2][NO]}{k_{11}[OH][NO_2]} = \left[\frac{k_7}{k_{11}}\frac{[HO_2]}{[OH]} + \frac{k_3}{k_{11}}\frac{[RO_2]}{[OH]}\right]\frac{NO}{NO_2} \qquad Eq.5.$$

Equation 5 shows the importance of the HO_X and NO_X ratios in controlling the efficiency of ozone production. In turn, their ratios are interrelated through the production and destruction rates of the HO_X and NO_X families. To illustrate this, let's assume that the RO_2 generated in reaction 1 rapidly and predominantly converts to HO_2 via reactions 3 and 6 (which is plausible in urban conditions) and that within the HO_X family the HO_2 radicals rapidly interconvert with OH so that we can represent the steady state balance for HO_2 radicals:

$$k_1[OH][RH]+k_2[OH][CO]=k_7[HO_2][NO]+2k_{10}[HO_2]^2+k_5[RO_2][HO_2] \qquad Eq.6.$$

Equation 6 can be arranged in the form:

$$\frac{[HO_2]}{[OH]}=\frac{k_1\frac{[RH]}{[NO]}+k_2\frac{[CO]}{[NO]}}{k_7+2k_{10}\frac{[HO_2]}{[NO]}+k_5\frac{[RO_2]}{[NO]}} \qquad Eq.7,$$

that shows the nonlinear process involved in the ozone formation process encountered when the emission levels of hydrocarbons [RH], [CO] and [NO_X] are perturbed in an urban area by altering the radical levels. Equation 7 is an upper limit estimate of the HO_2/OH ratio because it assumes that all RO_2 radicals from equation 1 will rapidly produce HO_2 radicals. The last two terms in the denominator of equation 7 reflect the termination pathways due to radical-radical reactions and tend to be small in urban environments with high NO_X emissions.

Figure 5.5 shows ozone production $P(O_3)$, OPE and the important radical sink pathways HHL and NHL calculated using equations 4, 5, 2 and 3, respectively. For the calculation of these parameters, we have not considered radical termination pathways of RO_2, since they were not measured. Rate constants for the calculation of the sink pathways were adjusted for the local values of pressure (altitude) and temperature as a function of time following the formula described by Sander et al., (2003). Figure 5.5 shows that the radical-radical sink pathway is an order of magnitude smaller than the NO_X radical sink pathway, indicating that in the MCMA the abundance of NO_X predominantly controls the destruction of radicals and that O_X production is NO_X saturated (VOC limited) most of the time within the urban area.

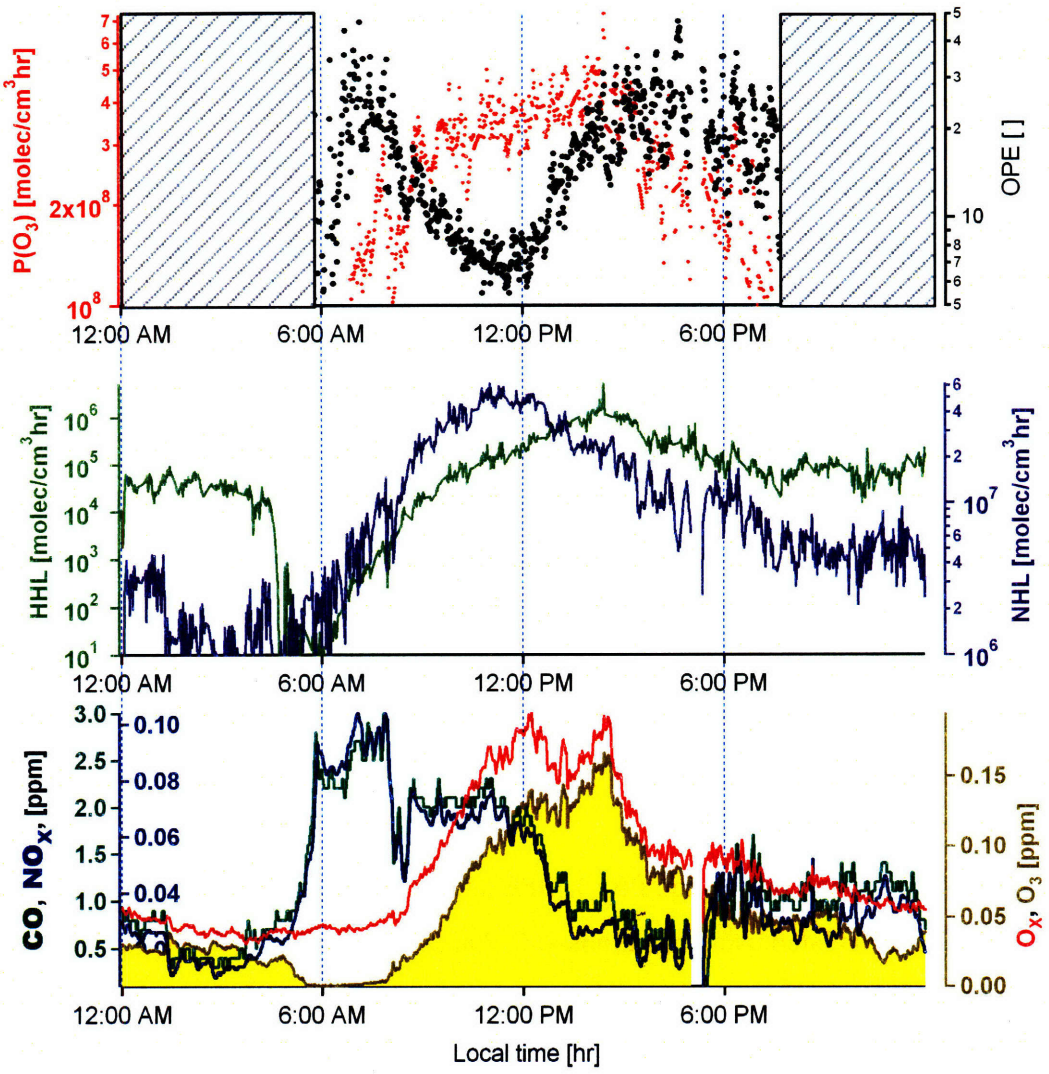

Figure 5.5. Calculated ozone production $P(O_3)$, ozone production efficiency (OPE), radical-radical sinks (HHL), NO_X-radical sinks(NHL) at the CENICA site in April 15, 2003. Lower panel shows measured CO, NO_X, ozone and O_X (ozone + NO_2).

The reactions in the chemical mechanism described above and the equations derived can be used in conjunction with Figures 5.4 and 5.5 to understand the role of radical budgets in the formation of ozone in the MCMA. The following is a chronological description of the ozone formation process from the perspective of radical production and destruction pathways.

4:30 to 6:00 AM. Mobile emissions are rapidly injected into a shallow boundary layer creating a sharp increase of CO and NO_X concentrations[11], and presumably in both burned and unburned RH. The injection of NO_X emissions quickly titrates all the remaining O_3 carried over from nighttime chemistry and transport. The observed sharp decrease in the NO_2/NO ratio is due to the massive injection of emissions: mobile sources are rich in NO compared to NO_2 (our measurements of NO_2/NO ratios from mobile sources suggested ratios of 2 to 30%). The decrease in the HO_2/OH ratio is concurrent with a decrease of the NO_2/NO ratio; the HO_2/OH ratio decreases (see equation 7) because HO_2 reacts rapidly with NO (abundantly present) but is not rapidly regenerated. The reaction of HO_2 with NO will deplete HO_2 and generates OH. However, we do not observe a build-up of OH because of an increased flux in the NHL pathway, and due to reaction with NO to form HONO. The HONO accumulates until its photolysis becomes significant, i.e. at sunrise around 6:00 AM.

6:00 to 8:00 AM. At about 6:00 AM the HO_X radicals reach their minimum values due to the abundance of NO_X and limited sources of radicals. The low values of radicals and their ratios translate to low OPE values, as described in equation 5. From that low point there is a rapid increase in OPE from 6:00 to about 7:00 AM that results from both the decrease of the NO_2/NO ratio -still dominated by emissions from combustion sources- and a small but persistent increase in the HO_2/HO ratio. The increase of the HO_2/OH ratio indicates that OH is being taken out of the system faster than HO_2, possibly due to the formation and accumulation of HONO in addition to the NHL termination channel that produces HNO_3. However, this low point and the subsequent increase in OPE "artificially" results from its definition in equation 5, in the sense that ozone is not being really produced (because NO_2 photolysis is still not significant). At about 7:00 AM the balance of radicals starts to change significantly, increasing the HO_2/OH ratio due to the increase of the NHL pathway and possibly to the photolysis of emitted aldehydes producing peroxy radicals. The production of ozone starts to increase (but still somewhat

[11] This early injection of emissions before 5:00 AM is in accordance with the observed probable change - presented in Chapter 4- regarding driving times in the city as compared to 15 or 20 years ago. Basically the change indicates that at present residents leave home much earlier than before to account for the increase in periods of traffic congestion. As we will see, this massive injection of emissions in "dark" conditions has profound implications on the chemistry in subsequent hours.

artificially) because HO_2 concentrations start to increase, but ozone itself is low due to the chemical scavenging by NO and also because NO_2 photolysis is still slow.

8:00 AM to 12:00 PM. The thermal energy accumulated from sunrise, which initiated a moderate rise in the boundary layer in the previous period, finally allows a significant expansion of the boundary layer at about 8:00 AM. Ozone production is now rapidly growing as a result of the increase of NO_2 photolysis. Ozone production is also favored by the (linear) increase of the HO_2/OH ratio that allows rapid oxidation of NO through reaction 7. The increase in the HO_2/OH ratio is, in turn, caused by the contribution of peroxy radicals from the photolysis and photochemical oxidation of emitted hydrocarbons and by the increase of the NHL pathway. Aldehydes, which as was presented in Chapter 2 appear to be emitted in excess in the MCMA, may be particularly important as an early morning source of new radicals. As a result, the HO_2/OH further increases due to the (now significant) radical cycling induced by the oxidation of VOCs. In this period, OPE decreases and starts to converge to its noon values due to the rapid increase of the NHL loss pathway, see equation 5, which is still larger that the rate of increase ozone production. In addition, the NO_2/NO ratio grows as a result of increased oxidation of NO, caused in turn by the increase of peroxy radical concentrations (reflected in the linear increase of HO_2/OH). As such, the noon value of OPE coincides with the peak of the NO_2/NO ratio and the peak of the NHL pathway.

12:00 to 6:00 PM. At noon O_X reaches its first peak due to the rapid interconversion between ozone and NO_2, indicating that large amounts of oxidants are already present. OPE has now a value of about 7 which is significantly higher than values in US cities at the time of their peak ozone production (Kleinman et al., 2002). Figure 5.6 shows that OPE is significantly higher than the values reported by Kleinman et al. for 5 U.S cities, even though NO_X concentrations are more than double in the MCMA. After NO_2/NO reaches its peak around noon, it decreases until about 2:30 PM when a short but significant increase is observed. The decrease of the NO_2/NO ratio from local noon is possible due to the peak of NO_2 photolysis -as reflected in the peak of O_X. At this time there is large production of peroxy radicals (as indicated by the increase of the HHL

pathway) that can also react with NO_2 to create peroxynitrates $ROONO_2$ and $HOONO_2$ but these are rapidly photodissociated reforming radical reactants. The PEAK abundance of HO_2 radicals coincides with the second peak of O_X and ozone, around 2:30 PM, because the oxidation of NO is favored with the increase of peroxy radicals. From that time to about 6:00 PM, the balance of radicals is changed again because OH is being depleted faster than HO_2 via the NHL channel and because photolytic reactions start to slow down. The decrease of photolytic reaction rates is still compensated by the excess of HO_2 radicals, allowing the conversion of NO to NO_2 and the formation of ozone. These processes maintain high levels of ozone until 5:30 PM or so.

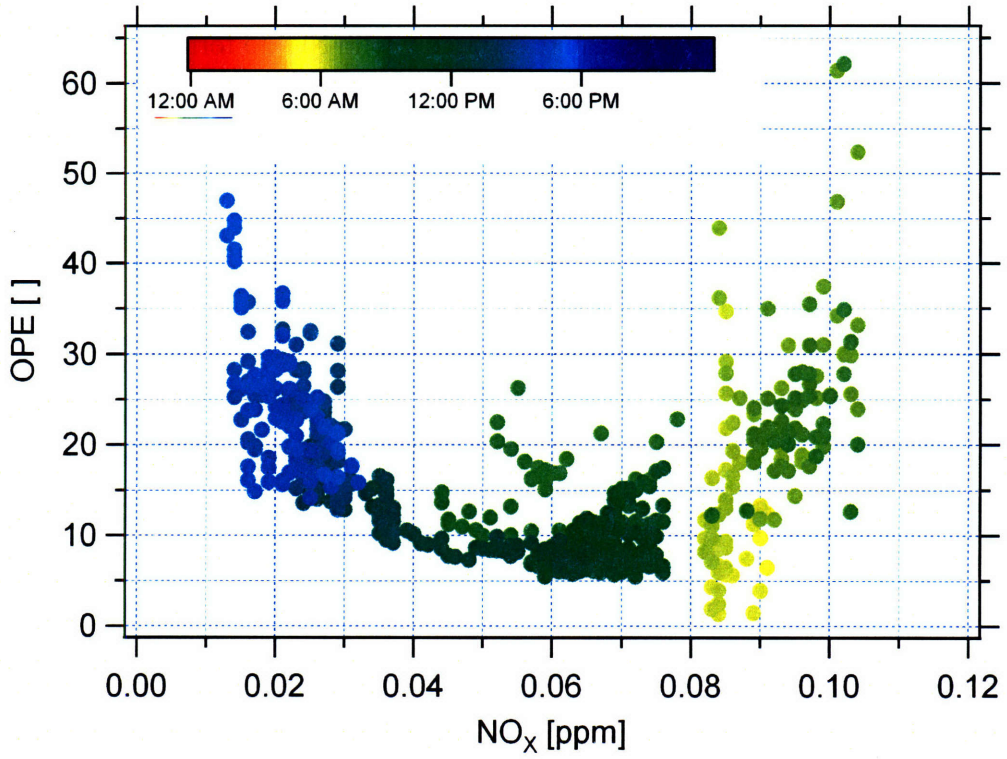

Figure 5.6. OPE as a function of NO_X levels for April 15th, 2003.

6:00 PM to 4:30 AM. After 6:00 PM the production of NO_2 induced by the excess of peroxy radicals is no longer able to generate high ozone concentrations because the NO_2 photolysis rate is drastically decreased. However, the abundance of peroxy radicals still promotes the oxidation of NO to NO_2, increasing the NO_2/NO ratio. At about 7:00 PM the CO and NO_X concentrations start to increase again as a result of both the sustained

emissions from mobile sources and the lowering of the boundary layer. In the absence of sunlight, the NO present reacts rapidly with ozone, further increasing the NO_2/NO ratio. In turn, the NO_2 reacts with ozone to produce nitrate radicals:

$$NO_2 + O_3 \rightarrow NO_3 + O_2 \qquad R.12.$$

which are now more stable because there is no photolysis and because NO concentrations are lower, slowing the reaction

$$NO_3 + NO \rightarrow 2NO_2 \qquad R.13.$$

However, the nocturnal nitrate radical can react rapidly with NO_2 to form N_2O_5 which can reach equilibrium concentrations through the reactions:

$$NO_2 + NO_3 + M \rightarrow N_2O_5 + M \qquad R.14.$$
$$N_2O_5 + M \rightarrow NO_2 + NO_3 + M \qquad R.15.$$

Since both NO_2 and O_3 concentrations remain high at night, reaction 12 can provide significant amounts of nitrate radicals. In turn, the low temperatures and high concentrations of NO_2 shift the equilibrium of reactions 14 and 15 to N_2O_5, which may act as a reservoir of oxidized nitrogen directly or through the production of HNO_3 from hydrolysis:

$$N_2O_5 + H_2O(s) \rightarrow 2HNO_3 \qquad R.16.$$

The nitric acid formed may deposit rapidly on surfaces making nitrogen species unavailable for the formation of ozone the following day.

Besides the reaction of ozone with alkenes, the high production of nitrate radicals may also help explain the relatively high observed HO_X concentrations at night. NO_3 reacts with alkenes and some aromatics (Atkinson and Arey, 2003) either by hydrogen abstraction or by addition to the double-bond producing peroxy and nitro-peroxy radicals which then react with NO, HO_2 or other peroxy radicals. The reaction of these products

with NO leads to the formation of OH. In this way the nitrate radical acts as a source of HO_X during the night, when ozone and aldehydes photolysis, the main sources of HO_X radicals during the day, are absent.

5.3. Model sensitivity study

We use two methods for investigating the sensitivity of the model to perturbations in its input emission fields, with emphasis on mobile emission sources. In the first method, the Brute Force Method (BFM), we select the magnitude of the perturbations and observe the results on the model predictions one parameter at the time. In the second method, the Decoupled Direct Method (DDM), we employ Taylor series to develop a first order local sensitivity expression that is applied to all inputs of the model. To determine the uncertainties in the model outputs using a local sensitivity approach (as the DDM method) requires variations in the input variables small enough to use a low-order Taylor series expansion. In that way, it is important to verify that a first-order expansion is adequate to represent the sensitivity of the model for a given magnitude of the perturbation. In our case, the BFM is used to verify this approximation. We introduce these two methods and present the results from their application along with an inter-comparison of their estimated model sensitivities in the following subsections.

5.3.1. Model sensitivities using the Brute Force Method

The BFM is conceptually the simplest sensitivity analysis method since each model input parameter is perturbed one at the time and the model output is evaluated for each control run. The change in model output is quantified from the difference between the perturbed case and the base case and this process in then repeated for each input parameter investigated. In AQM applications this process can rapidly become time consuming and computationally expensive. Besides being computationally inefficient for most AQM applications, the sensitivities estimated with the BFM depend upon the magnitude of the perturbation if the model response is nonlinear. In addition, for small model input perturbations the estimated sensitivities may contain significant levels of uncertainties introduced by numerical noise. Still, since the method is in principle applicable to any

model input parameter and the results are easy to explain and interpret, the BFM is often used for the validation of more complex mathematical-based sensitivity methods (Hamby, 1994).

Figure 5.7 shows the perturbations as scaling factors performed in the VOC and NO_X emission fields to our base case simulation. Each cross in Figure 5.7 represents a model control run with a given perturbation in emissions. We analyze the sensibility of the model to emission perturbations for light-duty gasoline vehicle fleet (LDGV), diesel fleet, all mobile (LDGV plus diesel) and all emission sources. The base case emissions for these and other emission sources were introduced previously in Table 5.1.

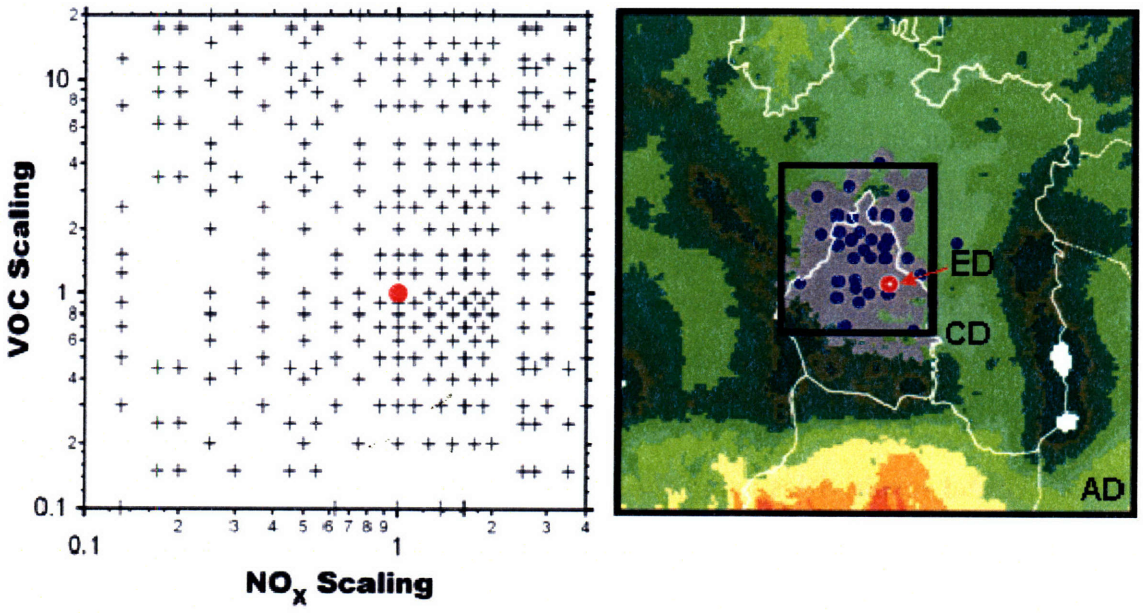

Figure 5.7. Left panel: emission perturbations performed using the BFM method for the April 15, 2003 base case (red dot). Right panel shows the domains for which isopleths are constructed: domain-wide (AD, biggest square), city-domain (CD, surrounding the urban area), and the CENICA site (ED, red symbol). Blue dots show the location of the RAMA monitoring stations and white lines show the political boundaries of the region.

We define a "sensitivity coefficient" S which represents the change in concentration c with respect to some input parameter λ, evaluated relative to the base case ($\lambda = \lambda_0$):

$$S = \left.\frac{\partial c_p}{\partial \lambda}\right|_{\lambda=0} \qquad Eq.8.$$

In general, λ can be a vector that contains multiple parameters related to processes in the model (e.g., rate constants) or inputs to the model (e.g., emissions). We will focus in more detail on the derivation of S in the next section. In the case of the BFM the sensitivity coefficients are obtained by the two-side finite difference approximation:

$$\left.S_p^{BFM}\right|_{\lambda=0} = \frac{c_p(\lambda=+\delta)-c_p(\lambda=-\delta)}{2\delta} = \left.\frac{\partial c_p}{\partial \lambda}\right|_{\lambda=0} + O(\delta^2) \qquad Eq.9.$$

The sensitivity coefficients of the model are analyzed in terms of the peak and diurnal average (6:00 AM to 6:00 PM) predicted concentrations with respect to three spatial domains (indicated in Figure 5.7): AD that refers to all cells of the first layer of the model domain, CD that refers to surface cells corresponding only to the urban area, and ED that corresponds to the surface cell of the location of the CENICA supersite. In the case of the peak concentrations results, we have also analyzed the effects on the positions and the occurrence of the local timing of the specie's peak as a result of perturbations in emissions. The comparison of the model results under these domains will allow us to investigate the spatial response of the model's sensibility.

Figures 5.8 and 5.9 show the isopleths obtained using the BFM method for peak and average ozone concentrations, respectively, for each of the three domains studied. These figures reveal several interesting characteristics of the model's sensitivity to emission perturbations of specific sources. The shape of both peak and average concentration isopleths are remarkably similar for each corresponding emission source category, indicating that the directional sensitivity of the model is similar for the ozone peak and average concentrations for the perturbations of a given emission source. However, the magnitudes of the sensitivities for the peak and ozone concentrations are significantly different. As an illustration, peak ozone concentrations reduce more than 150 ppb from a control run of perturbations to LDGV emissions of the order: (VOC, NO_X)= (7, 1.25)

(corresponding to an emissions scenario of around 12 to 15 years from the base case, see Figures 4.2 and 4.4) with respect to the base case (VOC, NO_X)= (1, 1). The same perturbation reduces the ozone diurnal average concentrations only about 30 ppb. The figures indicate that the model successfully reproduces the corresponding relative changes in historical observations of ozone peak and diurnal average concentrations described in Chapter 4.

As suggested by the historical changes of mobile emissions described in Chapter 4, the isopleths of Figures 5.8 and 5.9 also indicate that the ozone production in the MCMA has changed from a highly VOC sensitive regime to a slightly VOC sensitive regime over a period of 15 to 20 years. The comparison of the isopleths for the different emission source categories also suggests that mobile emission sources (and LDGV in particular) have largely contributed to that change. Isopleths obtained from the perturbations in the diesel fleet show a predominant NO_X sensitive regime since these sources contribute strongly to NO_X emissions. On the other hand, although they are directionally equal, the sensitivity of the model to perturbations of different mobile emission source categories is not equal in magnitude to the sum of the individual sensitivities for each emission categories:

$$S_{mobile} \neq S_{diesel} + S_{LDGV} \qquad Eq.10,$$

because these source categories have characteristic different VOC/NO_X emission ratios. As such, these sources contribute differently to the radical propagation cycling described in the previous section and their effects on ozone formation are non linear.

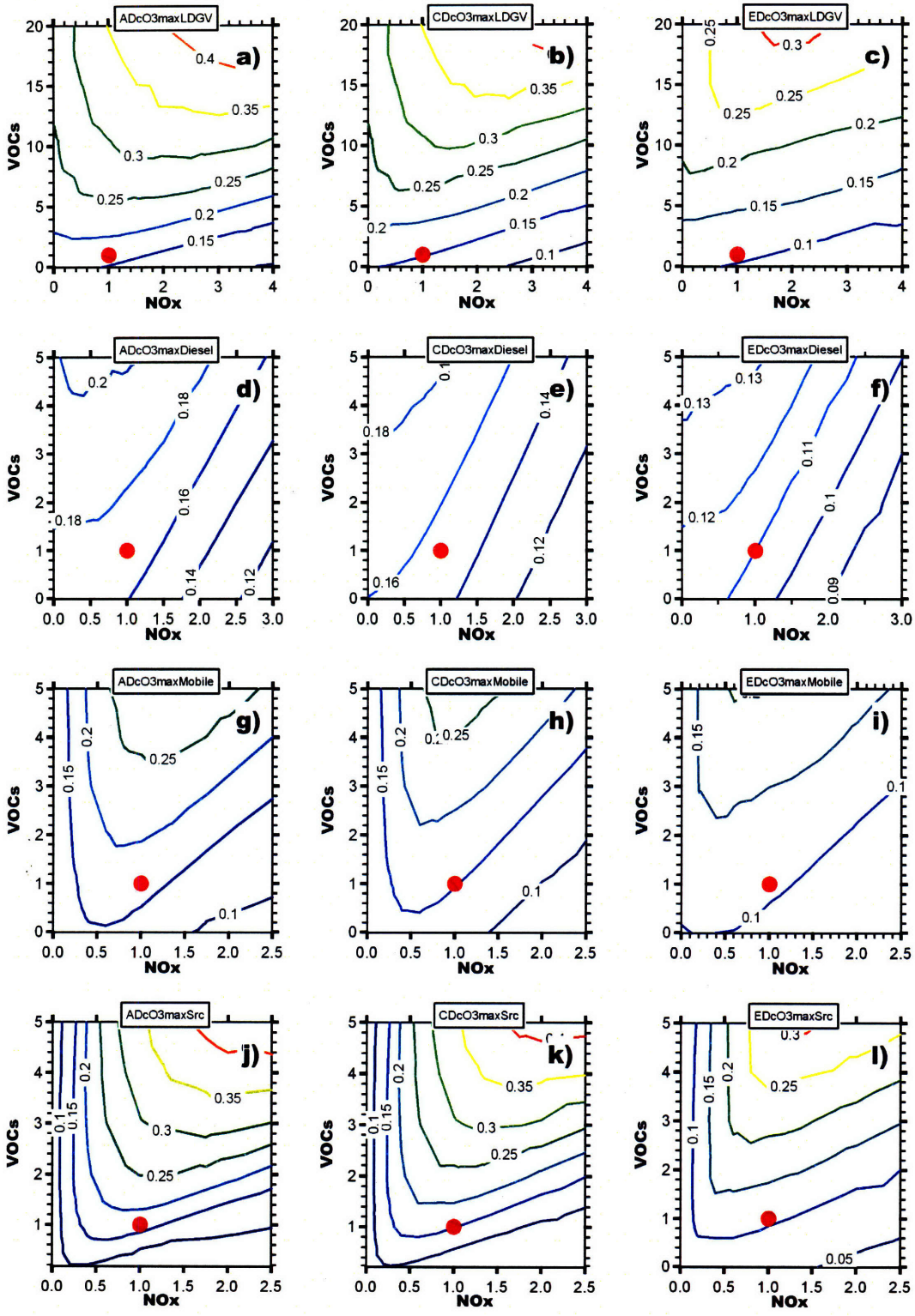

Figure 5.8. Peak ozone isopleths [ppm] for domain-wide (AD), city domain (CD) and CENICA site (ED) for emissions perturbations in LDGV (a, b, c), diesel (d, e, f), all mobile (g, h, i), and all sources (j, k, l). The axes represent mass-based scaling factors of VOC and NO_X emissions from the base case simulation (red dot).

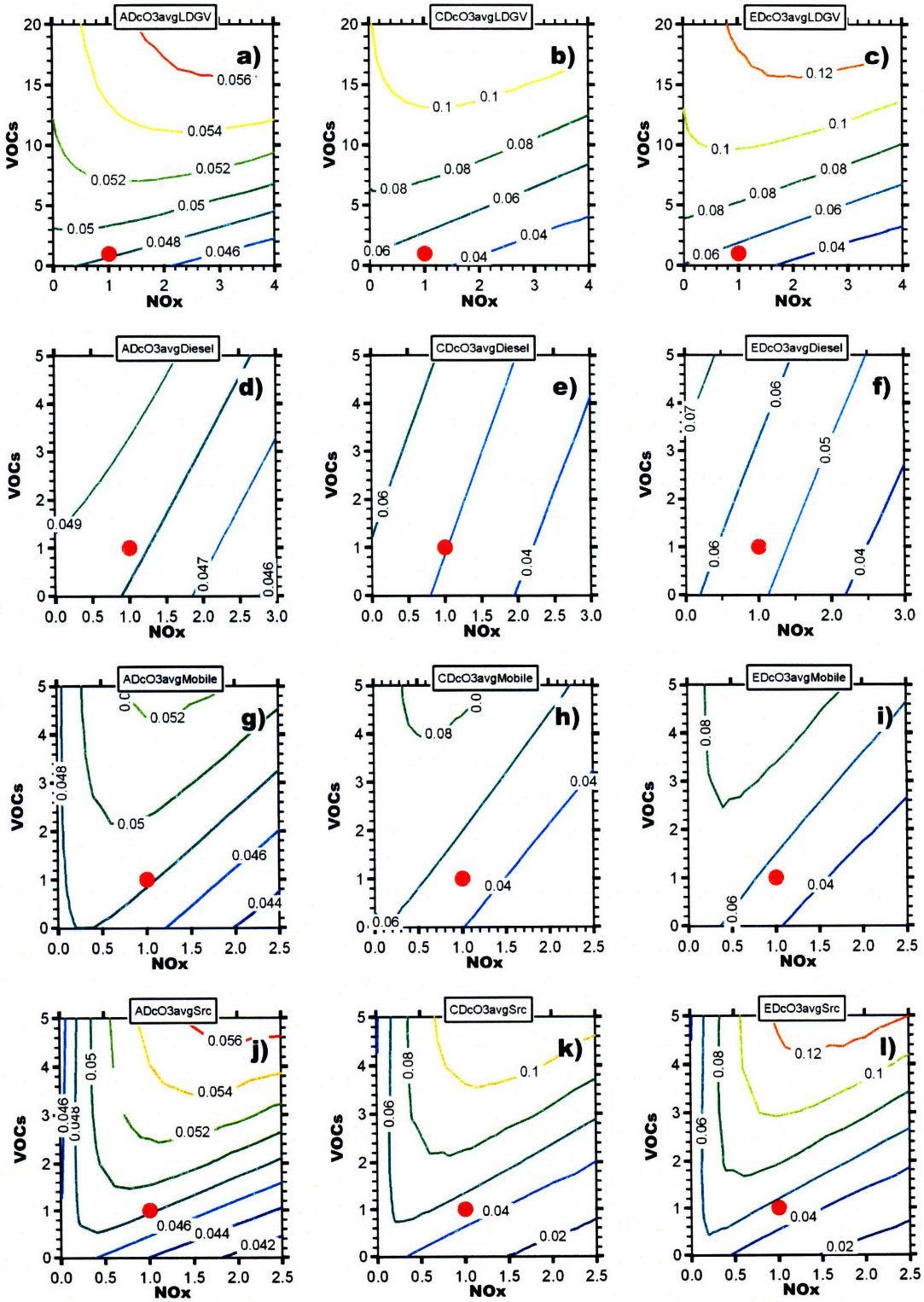

Figure 5.9. Diurnal average ozone isopleths [ppm] for domain-wide (AD), city domain (CD) and CENICA site (ED) for emissions perturbations in LDGV (a, b, c), diesel (d, e, f), all mobile (g, h, i), and all sources (j, k, l). The axes represent mass-based scaling factors of VOC and NO_X emissions from the base case simulation (red dot).

For both the peak and diurnal average ozone concentrations, the shape of the ozone isopleths for each emission source category perturbed is remarkably similar among the three spatial domains studied. This suggests that a given emission control policy directed towards the reduction of ozone in the MCMA can have directionally the same effects within the urban area and the surroundings. Nevertheless, the figures show that the sensitivity of the model with respect to the ozone peak concentrations is larger in the AD (domain-wide) domain, independent of the emission source category. However, that is not the case when assessing the changes in the diurnal average concentrations, for which the model is most sensitive within the CD (city-wide) domain. These results suggest that significant benefits can be achieved simultaneously inside the city (CD domain) and outside the city (AD domain) as a result of controlling anthropogenic emissions, particularly VOCs.

Table 5.2 shows a comparison of first order ozone sensitivity coefficients calculated for several VOC-varying control runs: (VOC, NO_X)=(λ,1), where the size of the perturbation λ is indicated in the same table. The sensitivity coefficients shown in Table 5.2 were calculated using equation 9 and they represent a particular example of the characteristics of the model's sensitivity behavior described previously in Figures 5.7 and 5.8. The model predicts sensitivities three to four times higher with respect to the ozone peak in the city than the average concentrations when perturbing mobile emissions. The ozone sensitivity of the model is in general higher for perturbations of all sources than for mobile sources alone. Similarly, the sensitivity to perturbations in the gasoline and diesel fleets emissions do not add up linearly to the sensitivities of all mobile sources. Table 5.2 also indicates that the ozone model sensitivity response to the size of the perturbation, λ, is relatively linear up to λ =1. This information is particularly useful when comparing results with the DDM method, which in our application only estimates first order sensitivity coefficients.

Table 5.2. First order ozone sensitivity coefficients [ppb] using the BFM method for the three studied domains and four emission categories perturbations.[a]

	Diesel	LDGV	Mobile	All sources	Diesel	LDGV	Mobile	All sources	Diesel	LDGV	Mobile	All sources
	AD, λ=0.25				CD, λ=0.25				ED, λ=0.25			
Ozone average	0.34	0.84	1.49	3.66	2.16	5.61	9.75	27.74	2.65	6.87	11.93	29.84
Ozone peak	8.07	20.15	35.21	115.2	6.94	18.11	32.72	108.9	6.16	15.35	26.48	58.91
	AD, λ=1.0				CD, λ=1.0				ED, λ=1.0			
Ozone average	0.34	0.85	1.52	3.59	2.23	5.60	9.91	25.29	2.74	6.83	12.11	27.88
Ozone peak	8.30	21.79	38.44	87.87	7.63	18.95	32.69	83.07	6.34	13.65	23.02	51.95
	AD, λ=5.0				CD, λ=5.0				ED, λ=5.0			
Ozone average	0.26	0.55	0.85	1.29	1.76	4.18	6.83	12.44	2.12	4.95	7.99	13.79
Ozone peak	6.47	14.53	23.02	33.66	6.03	13.30	25.34	37.10	4.26	8.66	16.11	35.62

[a] Perturbations in λ correspond to VOC emissions only.

Another aspect that Figures 5.8 and 5.9 as well as Table 5.2 reveal is that, given the current slightly VOC sensitive regime, currently the model is more sensitive to perturbations of emissions others than mobile. This suggests that larger benefits could be achieved with emission control policies directed to the regulation of VOC emissions from area sources. As indicated in Table 5.1, solvent consumption and cooking activities are possibly good candidates for such reductions given their large contribution to VOC emissions. In Appendix A we show the isopleths obtained for several species including olefins, alkanes, NO_X, HNO_3, HCHO and higher aldehydes predicted by the model as a result of perturbations in emissions. Not surprisingly, NO_X and VOC species isopleths tend to be NO_X and VOC sensitive, respectively, as they have a direct contribution from primary sources. Higher aldehydes and HCHO are also mostly VOC sensitive but they tend to have some NO_X sensitivity regimens (particularly under low NO_X conditions) as a result of the carbonyls contribution from the VOC oxidation process.

Another aspect that we can explore using the BFM is the effect of emissions perturbations on the position and local timing of the ozone peak. In Chapter 4, we

provided evidence for the existence of a historical "core-to-skirt" effect caused by the observed delay in photochemical pollutant formation rates. This effect also suggested that the ambient monitoring network may be no longer capturing the real (domain-wide) ozone peak of the basin. As described previously, our base case simulation corresponds to an ozone-south meteorological pattern, characteristic of the months March and April in the MCMA. As such, the analysis of the changes in ozone location and local peak timing due to emissions perturbations (under the same meteorological scenario) not only provides another way of evaluating the model's performance, but also a way of quantifying the role of different emission sources on the observed changes in concentration, location and timing of the ozone peak.

Figure 5.10 shows the isopleths of the latitudinal and longitudinal ozone peak position (shown as the difference of the number of cells of a control run with respect to the cell position of the ozone peak in the base case) and local timing of the ozone peak (shown as the difference in hours of the occurrence of the local ozone peak for a control run and the local timing of the base case). Having the grid model a cell size of 3 km, the isopleths suggest that the ozone peak has moved about significantly southward. Taking again the illustrative control run of (VOC, NO_X)= (7, 1.25) (corresponding to an emissions scenario of around 12 to 15 years from the base case, see Figures 4.2 and 4.4), the isopleths suggest that the position of the ozone peak has moved about 15 to 20 km southward.

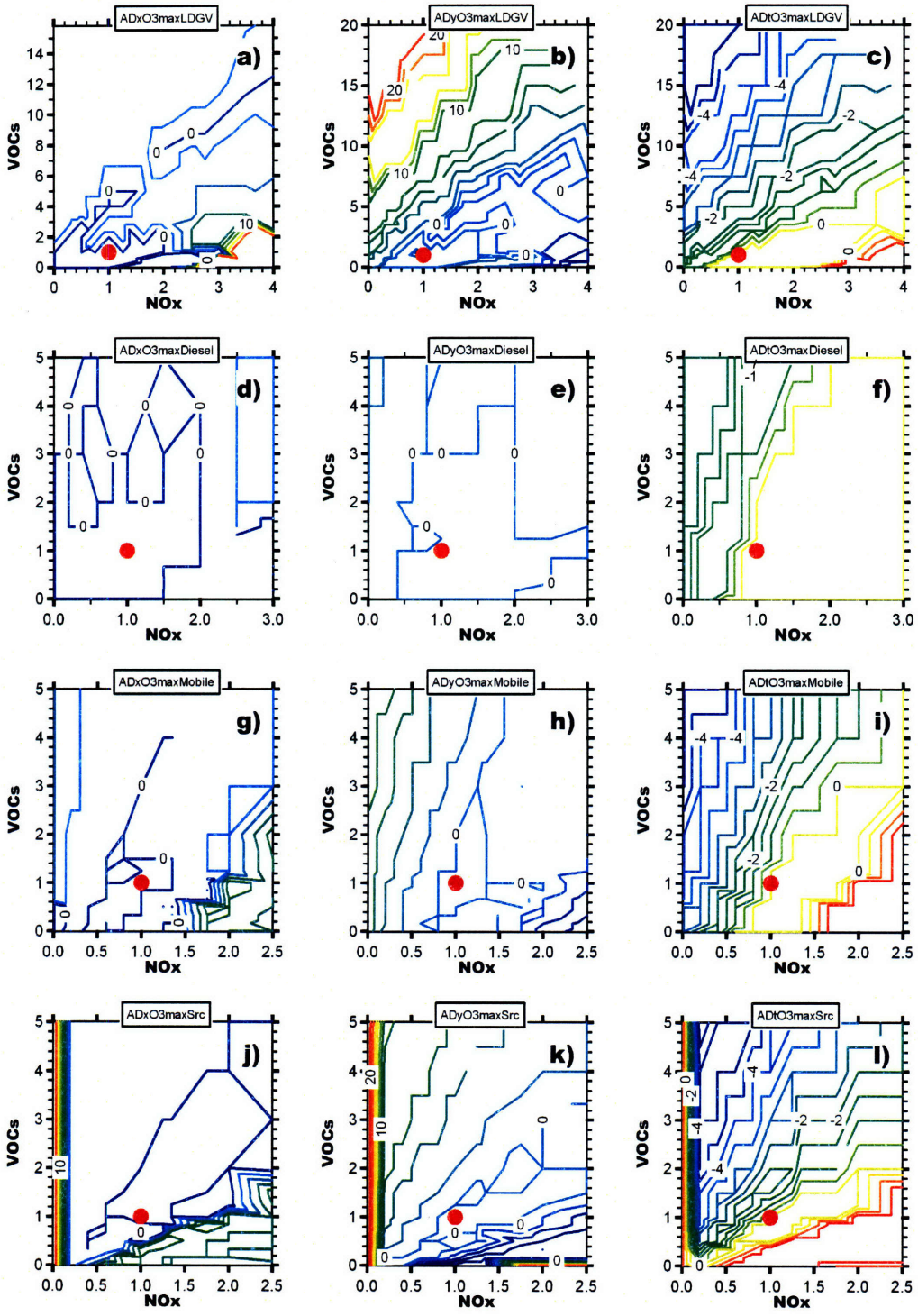

Figure 5.10. Isopleths of position [num. cells] and timing [hrs] for the domain-wide peak ozone. Longitudinal (first column plots), latitudinal (second column plots) and timing (third column plots) isopleths are referenced to the base case (e.g. timing[control run] – timing[base case]) and correspond to emissions perturbations in LDGV (a, b, c), diesel (d, e, f), all mobile (g, h, i), and all sources (j, k, l). Axes represent mass-based scaling factors of VOC and NO_X emissions from the base case (red dot).

Similarly, the isopleths show that the model can reproduce the lag in the local timing occurrence of the ozone peak by about 2 hrs with respect to a past VOC rich scenario. The fact that the model reproduces both spatial and temporal historical effects in ozone peak, (in addition to the observed changes in concentrations), suggests that the model sensitivities to emission perturbations, and mobile sources in particular, are accurately captured. Although the ozone sensitivity of the model behaves relatively linear for a given emission source category even with large perturbations (see Table 5.2), and this gives some confidence to the magnitude of the observed change in ozone location and timing, nevertheless, this analysis is only illustrative because we are limited to one meteorological scenario.

Figures 5.11 and 5.12 show the isopleths obtained with the emission source perturbations using the BFM method for peak OH and HO_2 concentrations, respectively, for each of the three studied domains. Similarly, in Appendix A we show the isopleths obtained for peak and average values of OH, HO_2, O_X production $P(O_X)$, O_X loss (O_X), and net ozone production. Figures 5.11 and 5.12 indicate that the model is significantly more sensitive regarding peak and average concentrations of HO_2 than OH. For the same control run mentioned above (VOC, NO_X)= (7, 1.25) with respect to the base case in the city domain, OH peak concentrations increase 25 % whereas HO_2 peak decreased more than 200 %. Also, as oppose to the previously described model ozone sensitivity, the sensibility of HO_X species vary significantly spatially. The isopleths of Figures 5.11 and 5.12 show that HO_X concentrations tend to vary much less outside than inside the urban area as a result of the emission perturbations (OH is particularly insensitive in the AD domain, except for very rich NO_X conditions).This effect can be explained by considering the fact that the HO_X concentrations are the result of the balance between very large magnitudes of sources (particularly VOC distributions) and sinks (particularly NO_X distributions) of radicals resulting in very short lifetimes (~ 1 sec) for these species. Having a short lifetime implies that these species are much less influenced by transport and more influenced by the spatial allocation of the radical sources and sinks. As such, the effects of emissions perturbations for these species will be observed much closer to the location of the perturbations, which in this case were only made inside the urban area.

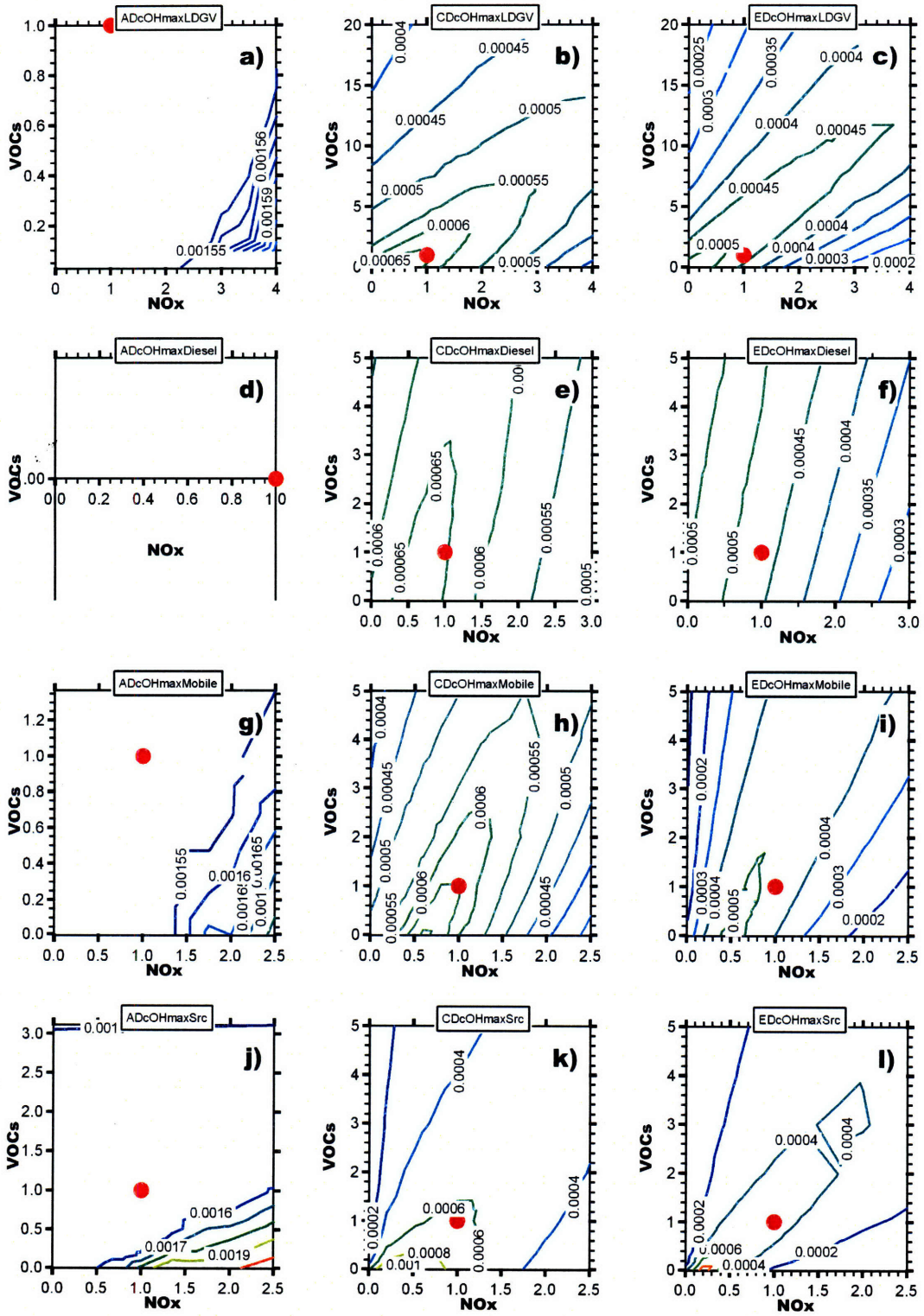

Figure 5.11. Peak OH isopleths [ppb] for domain-wide (AD), city domain (CD) and CENICA site (ED) for emissions perturbations in LDGV (a, b, c), diesel (d, e, f), all mobile (g, h, i), and all sources (j, k, l). The axes represent mass-based scaling factors of VOC and NO_X emissions from the base case simulation (red dot).

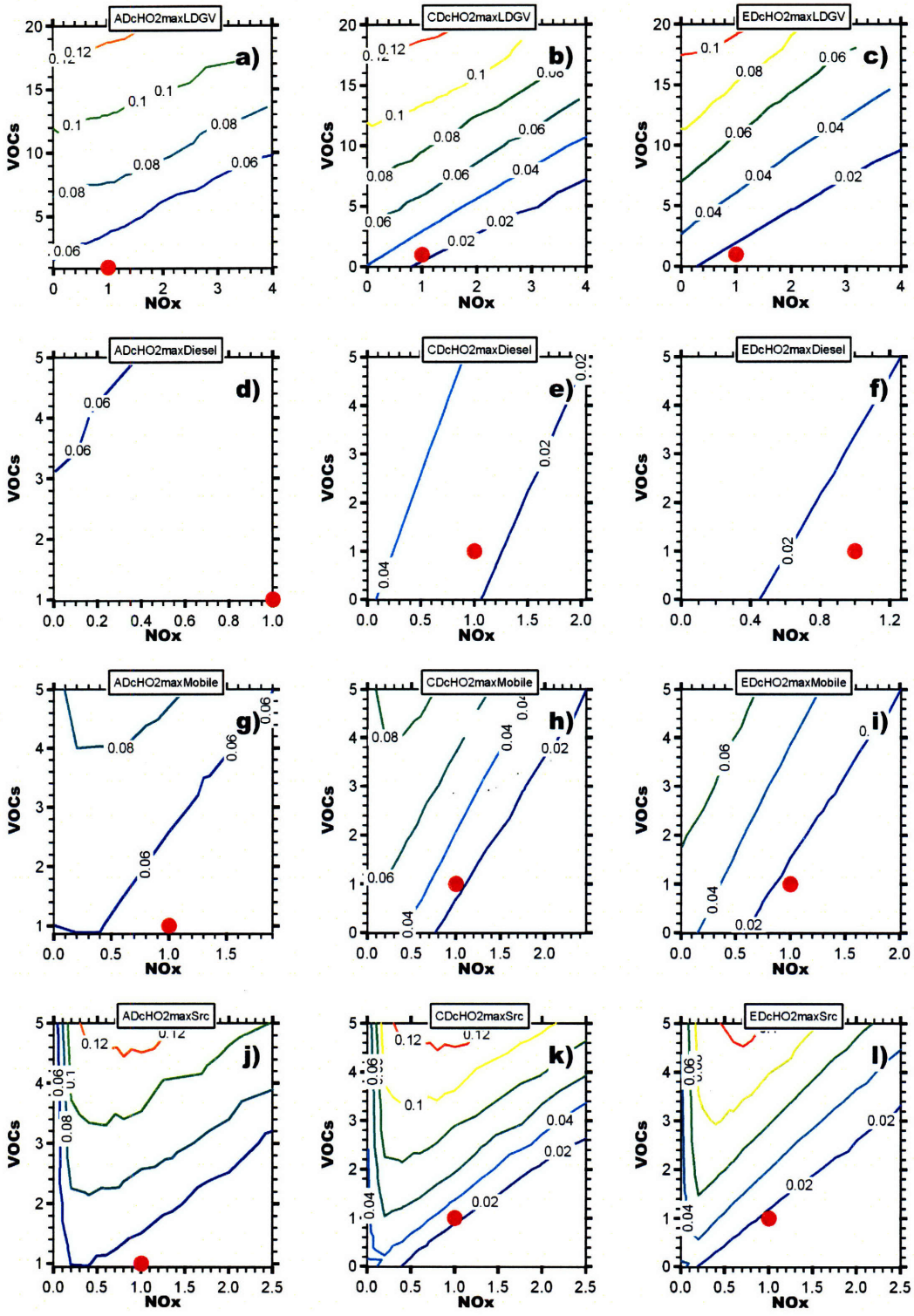

Figure 5.12. Peak HO_2 isopleths [ppm] for domain-wide (AD), city domain (CD) and CENICA site (ED) for emissions perturbations in LDGV (a, b, c), diesel (d, e, f), all mobile (g, h, i), and all sources (j, k, l). The axes represent mass-based scaling factors of VOC and NO_X emissions from the base case simulation (red dot).

Tables 5.3 and 5.4 show the sensitivity coefficients for OH, and HO_2, respectively, estimated for various degrees of perturbations, λ, of VOC emissions: (VOC, NO_X)=(λ,1). The table indicates that the radical concentrations in the model are much more sensitive to perturbations to all emission sources than to mobile sources alone. As described above, HO_2 sensitivities are much higher than OH sensitivities and they are non-linearly additive (similar to equation 10). Domain-wide and city-wide OH sensitivities also vary significantly, even directionally, due to impacts of the spatial allocation of the radical sources and sinks. With the variation of λ, we observe that the OH sensitivity of the model is much more nonlinear compared to ozone and HO_2 model sensitivities for very large perturbations (λ=5) but still comparable for large ones (λ=1). This suggests that first order perturbations with the BFM would be valid only for small to moderate perturbations of the emissions when assessing the effects on OH radicals. Note, however, that directionally the OH sensitivities are consistent and therefore even for very large perturbations the qualitative analysis of the model behavior can be relevant.

Table 5.3. First order OH sensitivity coefficients [10^3 ppt] using the BFM method for the three studied domains and four categories of emission perturbations.[a]

	Diesel	LDGV	Mobile	All sources	Diesel	LDGV	Mobile	All sources	Diesel	LDGV	Mobile	All sources
	AD, λ=0.25				CD, λ=0.25				ED, λ=0.25			
OH average	-2.6	-8.3	-10	-58.5	6.2	14.1	19.6	57.2	7.3	16.4	23.6	59.6
OH peak	0	0	0	-20.9	3.8	-4.3	17.2	-68.0	13.9	26.3	32	72.8
	AD, λ=1.0				CD, λ=1.0				ED, λ=1.0			
OH average	-2.8	-8.3	-14.1	-59.1	6.3	14.3	26.2	65	7.4	16.5	30.8	73.9
OH peak	0	0	0	-149	4.1	-2	5.2	-104.7	13.2	25.0	47.9	128.4
	AD, λ=5.0				CD, λ=5.0				ED, λ=5.0			
OH average	-2.3	-6.2	-9.9	-26.1	4.2	6.3	7.0	-4.9	4.6	5.5	4.7	-11.7
OH peak	0	-0.02	-0.02	-15.9	-4.2	-23.0	-31.0	-54.8	7.7	0.34	-9.9	-42.8

[a] Perturbations in λ correspond to VOC emissions only.

Table 5.4. First order HO_2 sensitivity coefficients [ppt] using the BFM method for the three studied domains and four categories of emission perturbations.[a]

	Diesel	LDGV	Mobile	All sources	Diesel	LDGV	Mobile	All sources	Diesel	LDGV	Mobile	All sources
	AD, λ=0.25				CD, λ=0.25				ED, λ=0.25			
HO_2 average	0.14	0.31	0.39	0.99	0.48	1.26	1.42	6.47	0.66	1.69	1.92	7.95
HO_2 peak	-0.2	-0.44	-0.46	8.32	3.22	7.97	10.12	37.86	1.61	4.13	5.09	21.93
	AD, λ=1.0				CD, λ=1.0				ED, λ=1.0			
HO_2 average	0.15	0.31	0.57	0.99	0.50	1.25	2.22	6.17	0.67	1.68	2.95	7.46
HO_2 peak	-0.1	0.70	3.51	11.47	3.30	8.01	13.80	27.9	1.64	4.51	8.41	19.7
	AD, λ=5.0				CD, λ=5.0				ED, λ=5.0			
HO_2 average	0.11	0.24	0.40	0.64	0.45	1.28	2.47	7.22	0.59	1.60	2.99	8.12
HO_2 peak	1.29	3.66	6.96	16.23	2.68	6.14	9.56	20.7	1.71	4.05	6.68	17.3

[a] Perturbations in λ correspond to VOC emissions only.

Changes in the average concentrations of HO_X are more relevant for understanding the changes in radicals in the MCMA as a result of emission perturbations. This is because the local effects of particular emission sources (i.e. point and area sources that can affect peak concentrations locally) in HO_X concentrations are smoothed. The analysis of diurnal average HO_X isopleths (shown in Appendix A) and Tables 5.3 and 5.4 suggest that the historical reductions of mobile emission in the MCMA has resulted in a substantial decrease in HO_2 and a small decrease in OH (note that the previously described *increase* in OH was with respect to the AD domain).

This remarkable result regarding the changes in HO_X concentrations suggests that induced reductions in OH radical sources (mainly through the observed and predicted moderate reductions in ozone) has been compensated by about the same rate of decrease of the radical sinks induced by the reduction of VOC concentrations (via reaction 1). Opposite to that, HO_2 sources are drastically reduced because, through radical cycling, they depend on VOC levels at more than one step during the cycling process: first by the reduction of the reaction of OH radicals with VOCs and also by the reduction of carbonyl

compounds acting as a source of peroxy radicals through their photolysis. Moreover, not only the sources of peroxy radicals are drastically reduced but also their sinks are not significantly reduced because they depend only indirectly on VOC levels (mainly the HHL pathway in equation 2). As a result, for the VOC/NO_X conditions in the MCMA, HO_2 has been much more sensitive to perturbations in VOC emissions than OH.

The predicted substantial reduction in HO_X concentrations (as HO_X is predominantly HO_2) would suggest that the ability of the atmosphere to clean itself –the so called *oxidative capacity*- has been significantly reduced as a result of the historical emission perturbations in the MCMA. However, rather than using the HO_X concentrations alone, a better measure of the oxidative capacity of the atmosphere in an urban environment is the intensity of the oxidation process of ambient pollutant species. An approximation is given by the HO_X chain length, defined as the number of oxidation cycles completed by the average HO_X radical before leaving the system. Every time an OH radical propagates via a chain of reactions and reforms OH (or HO_2 propagates back to HO_2) may be considered as one cycle of HO_X propagation. The HO_X chain length can be calculated as a function of time simply as the ratio of total HO_X reacted during the oxidation to the new radicals produced (by HONO, ozone and carbonyls photolysis and by reaction of ozone with alkenes).

For every model control run we have tracked the number of radicals reacted and the radicals newly formed. By doing this, we have estimated the changes in HO_X chain length as a result of the emissions perturbations using the BFM. Figure 5.13 shows the isopleths of HO_X chain length peak. The peak of the HO_X chain length corresponds to the period of maximum radical propagation efficiency as more radicals are formed by each new radical that enters the system. Figure 5.13 reveals that the drastic reductions of VOC/NO_X ratios experienced in the MCMA, has not significantly changed the HO_X chain length. No more than a small decrease (if any) in HO_X peak chain length can be attributed to perturbations in emissions.

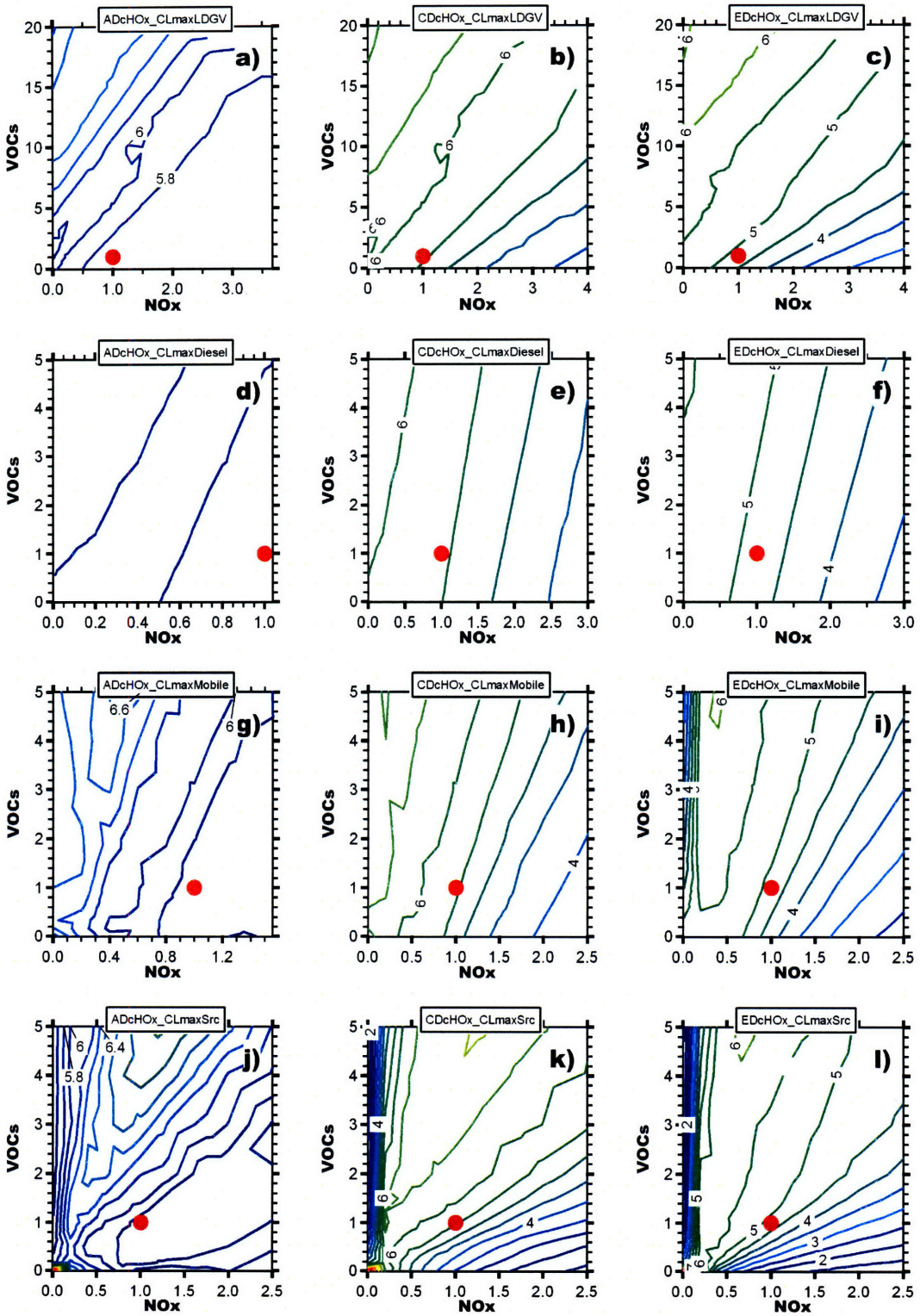

Figure 5.13. Peak HO_X chain length isopleths [ppb-hr/ppb-hr] for domain-wide (AD), city domain (CD) and CENICA site (ED) for emissions perturbations in LDGV (a, b, c), diesel (d, e, f), all mobile (g, h, i), and all sources (j, k, l). Axes represent mass-based scaling factors of VOC and NO_X emissions from the base case simulation (red dot).

The observation that the peak HO_X chain decreases slightly, if at all, due to changes in historical emission perturbations (whereas HO_2 is drastically reduced and OH is only slightly reduced) implies that the rate of propagation of radicals rapidly adjusts to the (decreasing) rate of formation of new radicals. While the formation of new radicals depends mostly on ozone and VOC levels (through their photolysis), the propagation of radicals depends strongly on NO_X (see reactions 3 and 7) and also on the initiation of the VOC oxidation (reaction 1). With VOC concentrations drastically reduced, the initial rate of formation of peroxy radicals is drastically reduced and, since the NO_X levels have not been significantly reduced (see Chapter 4), the rate of propagation of new radicals has adjusted to the decreasing rate of formation of new radicals. Note, however, that this analysis corresponds only to the range of historical emission perturbations. In fact, the isopleths show that the HO_X chain length can be drastically reduced under both very rich NO_X and very rich VOC conditions. Very small HO_X chain lengths means that nearly all newly produced HO_X radicals terminate rapidly at their first reactions (few cycles are completed). The terminations pathways can be done either by the HHL or NHL channels described in equations 2 and 3, respectively. Under VOC rich conditions, NO_X is scarce and radicals cannot propagate via reactions 3 and 7 and radicals are terminated through the HHL channel. Under very rich NO_X conditions NO_2 is very high and radicals are scavenged via the NHL channel, ending the propagation of radicals. Fast OH or HO_2 termination results in decreased ozone production.

5.3.2. Model sensitivities using the Decoupled Direct Method

The Decoupled Direct Method (DDM) was first used in the calculation of sensitivity coefficients in a three-dimensional air quality model (the Urban Airshed Model, UAM) by Alan M. Dunker in the early 1980s (Dunker, 1981). The DDM was also applied to the California/Carnegie Institute of Technology (CIT) airshed model, an application termed DDM-3D (Yang et al., 1997). More recently, the implementation of the DDM in CAMx to calculate first-order sensitivities with respect to emissions and initial and boundary concentrations has been reported (Dunker et al., 2002). In that study, the accuracy of the

DDM sensitivities were investigated by comparing with sensitivities estimated using the BFM. The DDM was found to be highly accurate for calculating the sensitivity of the 3D-model for perturbations up to 40% in reductions from the base case. The DDM has also been used in CAMx to estimate PM sensitivities (Napelenok et al., 2006) PM source apportionment of linear systems (Yarwood et al., 2004).

The detailed mathematical basis for the implementation of the DDM in CAMx is presented elsewhere (Dunker et al., 2002). Briefly, the method is implemented by defining:

$$F_i(x,t) = f_i(x,t) + \lambda_i G_i(x,t) \qquad Eq.11,$$

where f_i represents some set of base case input function (e.g. base case emissions) in space and time and $\lambda_i G_i$ is the perturbation of the base case f_i. The perturbation is performed by applying a scaling parameter λ_i to a new set of input function G_i. Each input parameter and chemical species can, in principle, be defined by a unique function. As such, the method provides information on how the model would respond if the input f_i is replaced by F_i.

The DDM calculates the sensitivity coefficient $S_i(x,t)$, defined previously as:

$$S = \left.\frac{\partial c_p}{\partial \lambda}\right|_{\lambda=0} \qquad Eq.8,$$

with respect to the scalar parameter λ_i by approximating the output concentration variable c with a Taylor series:

$$c(x,t;\lambda) = c(x,t;\lambda_0) + \sum_{i=1}^{n} \left.\frac{\partial c}{\partial \lambda_i}\right|_{\lambda_0} (\lambda_i - \lambda_{i0}) + \\ + \frac{1}{2}\sum_{i=1}^{n}\sum_{j=1}^{n} \left.\frac{\partial^2 c}{\partial \lambda_i \partial \lambda_j}\right|_{\lambda_0} (\lambda_i - \lambda_{i0})(\lambda_j - \lambda_{j0}) + \ldots \qquad Eq.12.$$

The expansion is done around the base case λ_0 and the sensitivity coefficients are not normalized (e.g. by mass of emissions) but absolute. As the magnitude of the input perturbation tends to zero, the output response will become dominated by the first-order sensitivity element. Therefore, the Taylor series to first order approximation gives the estimate:

$$c_i(x,t;\lambda_i) = c_i(x,t;\lambda_0) + \lambda_i S_i(x,t) \qquad Eq.13,$$

where $c_i(x;t;\lambda_i)$ is the estimated model result for species i when $F_i(x,t)$ is used as input, and $c_i(x;t;\lambda_0)$ is the base case model result when $f_i(x,t)$ is used as input. To obtain the first order sensitivity coefficients to the perturbation λ by the DDM, the Advection-Diffusion Equation (ADE) for trace pollutants in the atmosphere:

$$\frac{\partial c_i}{\partial t} + \nabla \cdot (uc_i) = \nabla \cdot (K \nabla c_i) + R_i + E_i \qquad Eq.14,$$

is differentiated with respect to λ:

$$\frac{\partial S_i}{\partial t} + \nabla \cdot (uS_i) = \nabla \cdot (K \nabla S_i) + JS_i + E_i' \qquad Eq.15.$$

In equations 14 and 15, K represents the turbulent diffusion coefficient vector, u is the average horizontal wind speed considered in the advection term, $E_i[x, t]$ represents the emission input fields and E_i' is the unperturbed emission rate (G_i in equation 11). Including photolytic reactions, all chemical reactions are aggregated into the volume term R_i, whereas J is the Jacobian matrix $J = (\partial R / \partial c)$ of the reaction rates. The sensitivities defined in and obtained from equations 8 and 15, respectively, are absolute, not semi-normalized, because λ is dimensionless as defined by equation 11. The semi-normalized sensitivities are scaled with respect to the unperturbed function. In the case of emission sensitivities:

$$S^* = \frac{S}{E_i'} \qquad Eq.16.$$

An important advantage of the DDM method, equations 14 (for concentrations) and 15 (for sensitivities) are solved with the same spatial grid, time steps, and algorithms in the program's model. The DDM application was not included in the version of the CAMx model (4.30) with the SAPRC99 chemical mechanism that we used for obtaining the BFM results. However, a subroutine containing the DDM specifically for the SAPRC99 chemical mechanism was kindly provided by Dr. Yarwood at ENVIRON. The subroutine was then edited, included and successfully compiled with the main base case.

Figure 5.14 shows the ozone sensitivity coefficients to perturbations in VOC, NO_X and all emission sources obtained with the application of the DDM in CAMx for the base case of April 15, 2003 in the MCMA. Similar to the results with the BFM, the sensitivities depicted in Figure 5.14 indicate that ozone is reduced when reductions in VOC emissions alone are implemented. Correspondingly, reductions in NO_X emissions alone lead to ozone increase and the magnitude of both VOC and NO_X sensitivities are similar.

The results from the DDM also indicate that simultaneous reductions of all emissions will also lead to ozone reductions, albeit with a factor of around 4 smaller than VOC (or NO_X) emission reductions, but only after around 11 AM local time. The transition between the two regimes suggests that the balance between the radical production and sink pathways is changed at that time. As seen in the previous section, during the period from 8 AM to about 12 PM the production of radicals is largely determined by the magnitude of the NHL sink pathways (Eq. 3), whereas after midday the production of radicals is largely dependant on the sources of radicals (VOC oxidation and photolysis). As the cycling of radicals during the ozone formation process depends on the specific reactivity of the air masses, both the magnitude of the regimes and the timing of their transition observed in Figure 5.14 are the results of the characteristic VOC/NO_X ratios of the city. Nighttime ozone levels are entirely linked to NO_X levels in the model as the titration pathway represents the main sink of ozone at night.

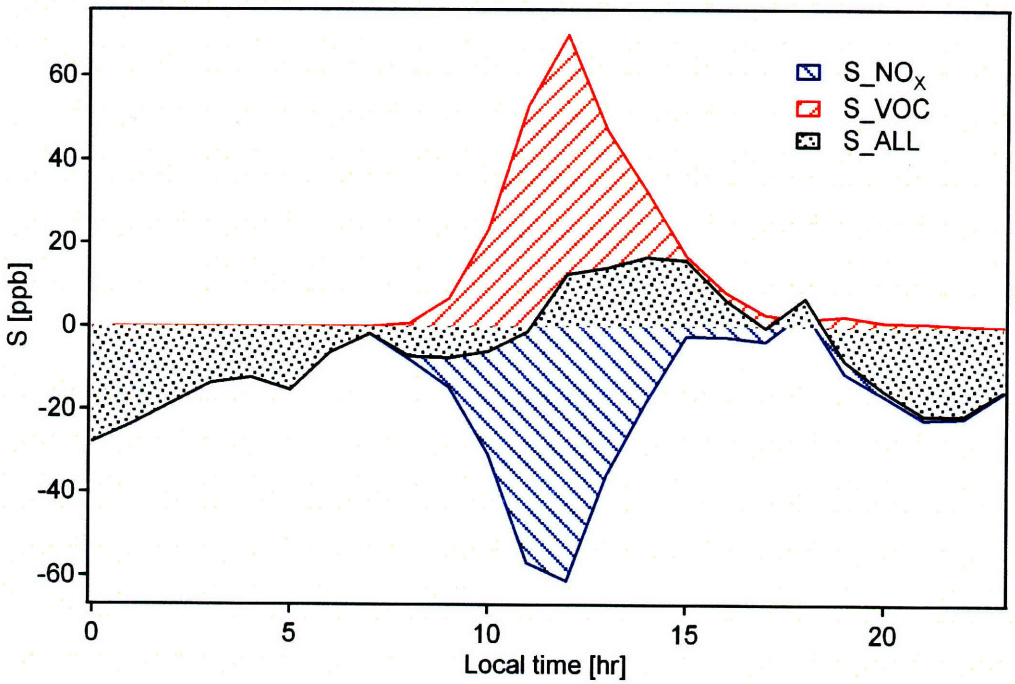

Figure 5.14. Absolute sensitivity coefficients for NO_X, VOC and all emissions obtained using the DDM method.

Another major advantage of applying the DDM as compared to the BFM is that the sensitivity coefficients of multiple input parameters can be estimated during the same run. Producing isopleths as those depicted in Figures 5.8 to 5.13 and those included in Appendix A for input emissions of individual VOC species would be extremely expensive and cumbersome. With the DDM, however, we can obtain first order sensitivity coefficients to emissions of individual VOC species groups at relatively low computational burden[12].

We obtained the sensitivity coefficients for each of the VOC emission groups included in the VOC speciation of the SAPRC99 chemical mechanism in the model. Figure 5.15 indicates that ozone in the current base case episode is highly sensitive to emissions of aromatics and alkenes, which have large contributions from mobile sources. When

[12] Still, the computer time using the DDM with 19 input parameters perturbed in CAMx for 1 simulation day increased by a factor of about 12 as compared to the base case simulation in a 2 Intel ® processors Xeon ™ CPU 2.00 GHz station.

considering semi-normalized sensitivity coefficients (obtained using Eq. 16 with the corresponding emissions of each VOC emission group) we observe, however, that in a mass-emitted-basis HCHO has the largest sensitivity coefficient followed by ethane. Both of these species have also large contributions from mobile sources (other sources of ethane include biomass burning and industrial sources). These results suggest significant benefits in ozone abatement in the city can be achieved by controlling sources that are high emitters of alkenes, aromatics and aldehydes. Mobile sources are clearly significant contributors to these emissions, but area sources such as painting and solvent consumption are also typically large contributors to these compound's emissions (but not to NO_X emissions). A specific source apportionment study using data collected during the MILAGRO-2006 field campaign for identifying the primary sources of these compounds will be desirable.

The comparison of Figures 5.15 a) and b) shows the importance of the reactivity of the different VOC species on the formulation of ozone abatement strategies based on VOC emission controls. For example, propane (most of ALK2) has an absolute sensitivity coefficient only 30% smaller than formaldehyde, mainly due to its larger emissions. However, on a mass per mass basis, 1 kg of formaldehyde will produce more than 40 times more ozone than 1 kg of propane, as indicated by Figure 5.15 b).

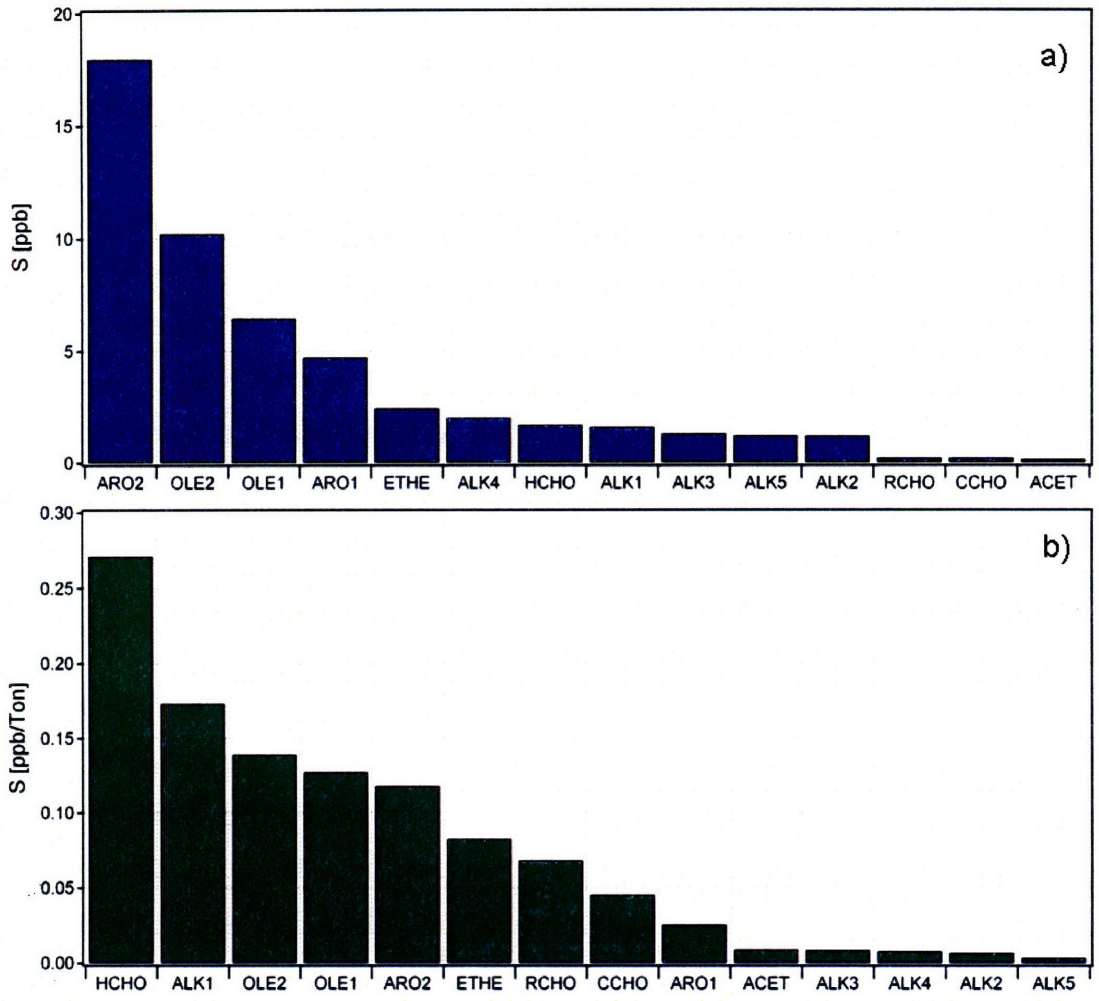

Figure 5.15. a) Absolute sensitivity coefficients and b) semi-normalized sensitivity coefficients for lumped classes of VOCs according to the SAPRC99 chemical mechanism[a].

[a] The detail species composition of each VOC lumped class is given elsewhere (Carter, 2000). Briefly, as the number specification of each group grows (e.g. ALK1 to ALK5), the magnitude of the rate constant of the species with OH increases. The number of individual VOC species in each group can be significant. As an approximation in molar weighting, however, we can consider that ALK1 is primarily ethane, ALK2 is primarily propane and acetylene, ALK3 is mostly n-Butane and isobutene, ALK4 is mostly iso-pentane, n-pentane and 2-methyl pentane, ALK5 is a large mixture of pentanes to decanes, ARO1 is primarily toluene, benzene, n-propyl benzene and ethyl benzene, ARO2 is primarily m, p, and o xylenes, OLE1 are primarily terminal alkenes, OLE2 are mostly internal alkenes, CCHO are acetaldehyde and clycolaldehyde, RCHO are lumped C3+ aldehydes and TERP are biogenic alkenes other than isoprene. Explicitly emitted compounds include ETHE as ethene, HCHO (formaldehyde), ISOP as isoprene and ACET as acetone.

5.3.3. Comparison of sensitivities obtained using the DDM and BFM

We have compared the sensitivities of the model using the BFM and the DDM methods for perturbations of NO_X, VOC and all emission sources. The comparison allows testing the consistency of the two techniques and gives an estimate of the first order accuracy of the sensitivities provided by the DDM. For the comparison we performed two types of analysis. The first type of analysis investigates the magnitude and the temporal distribution of the sensitivity coefficients obtained by the two techniques. The corresponding BFM and DDM sensitivities were calculated with equations 9 and 15 and represent a first order approximation of the sensitivity of the model to input emission perturbations. The second type of analysis consists on the comparison of the spatial distributions of the sensitivities between the two techniques and their effect on the spatial distribution of ozone. This is done by comparing the predicted ozone spatial distributions of the two techniques (directly in the BFM and by equation 13 in the DDM).

Figure 5.16 shows the comparisons between the BFM and the DDM for various magnitudes of the perturbation of VOC, NO_X and all emission sources. The figure shows that the BFM sensitivities converge to the DDM sensitivities as the magnitude of the perturbation decreases in all three cases. The results suggest that the model sensitivity to these emissions types behaves relatively linear for perturbations of up to 40% of the base case emissions. The model sensitivity becomes rapidly non-linear, particularly for NO_X after that magnitude. However, the response of ozone to simultaneous perturbations of NO_X and VOC emissions is more nearly linear than perturbations of any of these two alone.

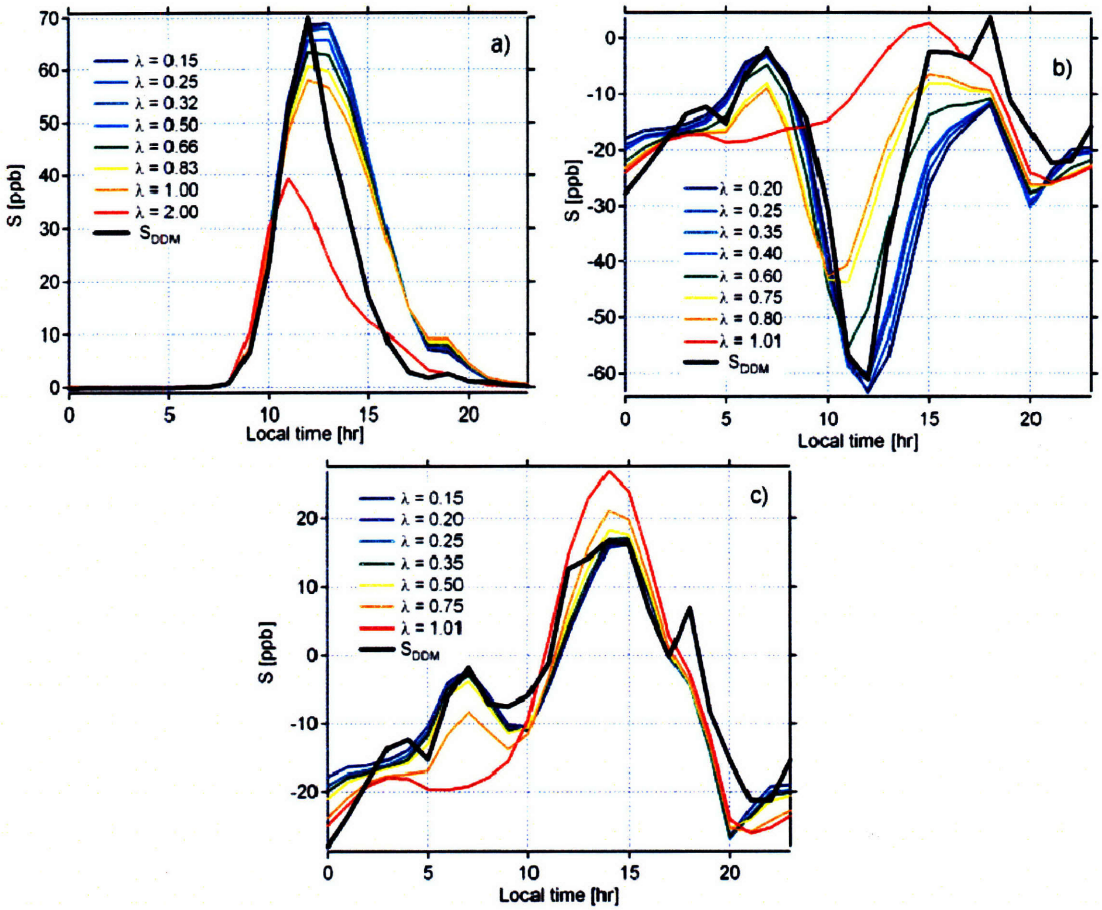

Figure 5.16. Comparison of absolute sensitivity coefficients between the DDM and the BFM methods for perturbations of: a) VOC, b) NO_X, and c) VOC and NO_X emissions.

The comparison of the spatial distributions of ozone concentrations predicted by the two sensitivity techniques is illustrated in Figure 5.17. Whereas the spatial distribution of ozone is predicted directly in the BFM, the spatial distribution of ozone with the DDM was constructed using the first order approximation given in equation 13. Figure 5.17 shows that both sensitivity techniques predict similar spatial effects on ozone distribution at remarkable precision when increasing the conrresponding input emission parameters by 25% from the base case.

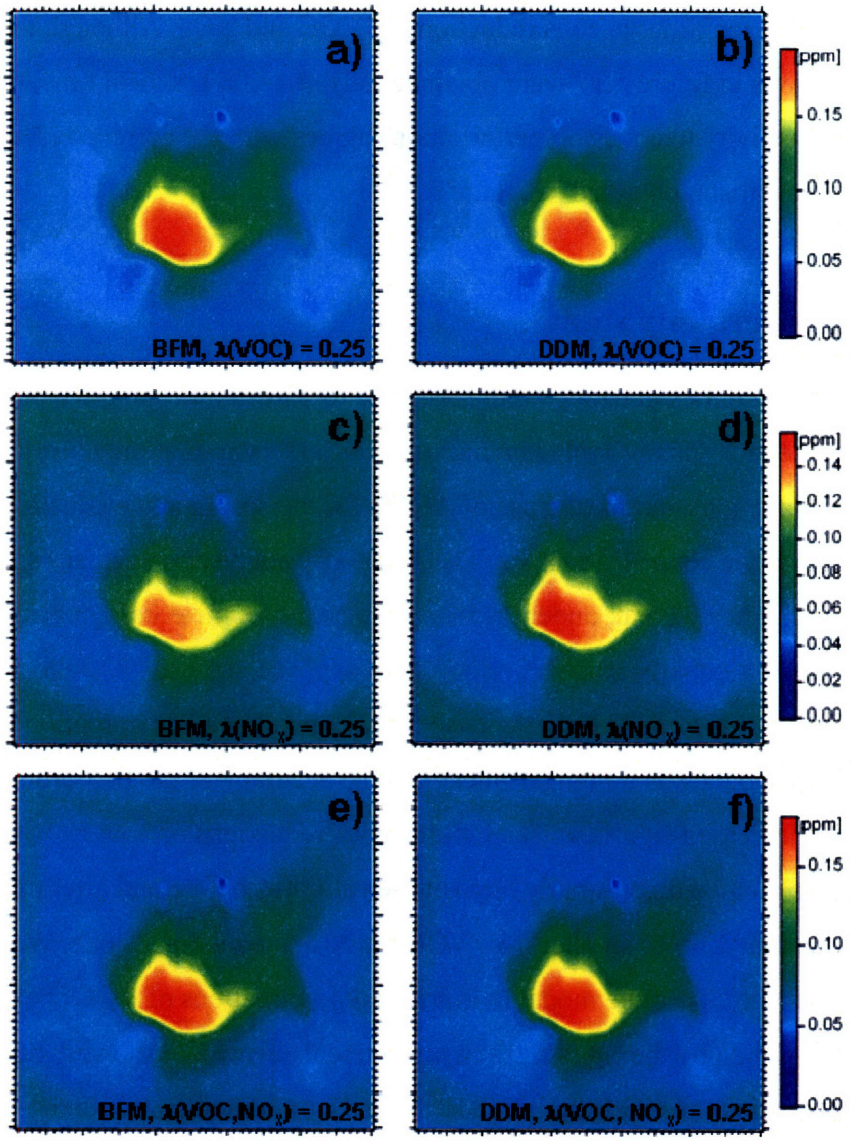

Figure 5.17. Comparison of estimated ozone concentration fields obtained with the DDM and the BFM for perturbations of VOC (a and b), NO_X (c and d), and simultaneous VOC and NO_X emissions (e and f). Maps correspond to 14:00 hrs local time.

Although the spatial distributions between the two techniques seem to agree reasonably well, the comparison indicates that there are some differences in the magnitude of the ozone predictions. The DDM seems to predict slightly less ozone than the BFM when considering VOC sensitivity alone. The opposite occurs for NO_X sensitivities: the DDM under-predicts ozone reductions (i.e. predicts higher concentrations) compared to the BFM. The magnitude and spatial allocation of ozone predicted by the two techniques is

remarkably similar for simultaneous reductions of VOC and NO_X. Although the ozone spatial distributions in figure 5.17 were obtained only at 14:00 hrs local time, the effects of the model sensitivity to emission perturbations agrees with the corresponding temporal distributions comparison obtained in Figure 5.16.

5.4. Model uncertainty study

What are the uncertainties in ozone predictions due to uncertainties in the input emission precursor parameters? This is a relevant question for understanding the uncertainties of ozone model predictions and for the use of AQMs for the design and evaluation of emission-based ozone control strategies. The sensitivity analyses presented in the previous section indicated that, under the base case emission/meteorological scenario studied, the model is equally sensitive (albeit with opposite sign) to NO_X and VOC emission reductions up to 50% from the base case. Beyond those perturbation levels, the sensitivity of the model was no longer linear and the accuracy of the first order approximation decreased significantly. Simultaneous reductions of both NO_X and VOC emission groups yielded directionally opposite sensitivities before and after midday with magnitudes of about 4 times smaller than VOC (or NO_X) reductions alone. We also quantified the sensitivity of the model to individual perturbations of VOC species lumped in groups as described by the SAPRC99 chemical mechanism. We showed that the model is particularly sensitive to aromatics, higher alkenes, and formaldehyde emissions.

The estimated sensitivities are very useful for understanding the possible effects on ozone formation when particular emission sources are perturbed as well as to estimate the likely valid range of application of such emission changes. However, a sensitivity analysis alone does not provide information about the uncertainties of the ozone predictions due to uncertainties of a given emission group. An input emission parameter with large uncertainties in its estimation may have a large effect on the uncertainty of the model predictions even if the sensitivity of the model to that parameter is small. On the other hand, an input emission parameter that is relatively well known may have a small effect on the uncertainties of the model predictions even if the model is highly sensitive to that

parameter. Clearly, the uncertainty of the input estimate must be known or estimated prior to conducting uncertainty analysis with parametric sensitivity coefficients.

The uncertainty of the input parameters is best described by probability density functions (PDFs) over the range of probable occurrences of the input parameter. Often, the PDFs of key parameters are not known and the uncertainty is estimated by running the model under a range of possible values of input parameters. These multiple simulations produce model output probability distributions that reflect the model uncertainty due to the parameter uncertainties. The choice of the input parameter for each simulation can be defined by sampling algorithms using random or quasi-random Monte Carlo techniques or by constrained sampling schemes such as Latin hypercube sampling (Fine et al., 2003). An alternative for determining model uncertainty due to parametric uncertainty consists in approximating the model response with orthogonal polynomial in the parameters where the weighting functions of the polynomials are the PDFs of the input parameter (Tatang et al., 1997).

Another way of investigating the uncertainties of model outputs is to use a "descriptor" that relates the parametric uncertainties and the sensitivity of the model to the input parameter (Pun, 1998). By describing the input parameter with a particular PDF and associated mean and variance (σ^2), the measure of the uncertainty effect is the contribution of the uncertain parameter to the variance of the output:

$$VC_{p_j}^{c_i} = \sigma_{p_j}^2 \left(\frac{\partial c_i}{\partial p_j} \right)^2 \qquad Eq.17.$$

The descriptor $VC_{p_j}^{c_i}$ represents the variance contribution (VC) of the input parameter p_j to the variance of the model output species c_i. In equation 17, $\sigma_{p_j}^2$ represents the variance of the input parameter p_j and the term inside the parenthesis is the sensitivity coefficient of the model to perturbations of p_j. The method allows the comparison of the relative importance of the uncertain inputs in terms of their effects on the uncertain outputs. The major limitation of this method is that it presupposes knowledge of the variance of the

input, which in most cases is not known, and the sensitivity of the model to the input parameter must be also determined. Fortunately, we can provide a reasonable estimation of the variance of important input emission parameters under two circumstances. First, by analyzing data from the MCMA-2003 field campaign we have obtained measured-based emission factors for key emitted species. As explained in Chapter 2, such emission factors have been converted to fuel-based emission estimates and the corresponding PDFs have been obtained. Second, fuel consumption values are relatively well know for the MCMA because there is only one corporate fuel provider and records are available. As a result, all the variability (variance) for the estimated emissions can be attributed to the measured variability (variance) of the fuel-based emission factors.

These circumstances allow us to directly estimate the variance for emissions of NO_X, formaldehyde, acetaldehyde, benzene, toluene and higher aromatics using measured fuel-based emission factors as described in Chapter 2. It is not possible to estimate the variance of alkanes, alkenes, acetone and higher aldehydes emissions from the available measurements. However, one can assume that the dispersion (that is, the variance σ^2) of the emission data with respect to their mean is equal for two given emission parameters:

$$\frac{\mu_{EF1}}{\sigma^2_{EF1}} = \frac{\mu_{EF2}}{\sigma^2_{EF2}}; \qquad \frac{\mu_{E1}}{\sigma^2_{E1}} = \frac{\mu_{E2}}{\sigma^2_{E2}} \qquad Eq.18.$$

Where (μ_{EF1}, μ_{E1}) and (μ_{EF2}, μ_{E2}) represent the mean of emission factors (*EF*) and emissions (*E*) of species 1 and 2, respectively. Equation 18 assumes that the PDF of species 1 and 2 are similar and works only because *EF*s are given in fuel-based units and the variability of *E* is assumed to be all related to *EF*. From equation 18 the following approximation can be obtained:

$$\sigma^2_{E2} = (fc)^2 \left(\sigma^2_{EF1}\right)\left(\frac{\mu_{E2}}{\mu_{E1}}\right) \qquad Eq.19.$$

In equation 19 *fc* represents the associated fuel consumption rate. With the approximation given by equation 19, we can estimate the variance of VOC groups for which we do not have measurements of fuel-based emission factors by assuming that the dispersion of

their data in their PDF behaves similarly to the dispersion of a given (measured) VOC species. We have applied such approximation for the estimation of the variance of the species groups RCHO, ARO2 and ARO1 using the measured variance of acetaldehyde, c2-benzene and benzene, respectively. This is a good approximation because these species are mostly co-emitted with the other species that form those VOC groups.

For all the other VOC species groups considered (mainly alkanes and olefins) we cannot use the approximation described above because there are no available measurements of emission ratios of co-emitted species in these groups. To provide an estimation of their probable contribution to the uncertainties in the ozone predictions, and for purposes of comparison with those *VC*s directly obtained, we have considered a large range of possible dispersion of their PDFs equivalent to standard deviations of 50 % and 200 % of their base case mean. That range, corresponding to variances of $0.25(\mu_E)^2$ and $4.0(\mu_E)^2$, respectively, is large enough to explore the possible contribution of these species groups to uncertainties in the model's ozone predictions.

Table 5.5 shows the variance contributions from the different VOC groups to variance of ozone predictions estimated with the above described procedures. The table indicates that alkenes and large aromatics are possibly large sources of uncertainties of ozone predictions. Interestingly, aldehydes emissions show a small contribution to uncertainty despite the relatively large sensitivity of the model to such emissions. Uncertainties of olefins emission can potentially contribute significantly to uncertainties in ozone predictions. Sensitivity coefficients of nearly equal magnitudes and opposite sign can provide information about compensating errors. For example, uncertainties in VOC emission estimates can contribute about half to 6 times or more compared to uncertainties of NOx emission estimates, depending on the limits of the ranges chosen, to uncertainties in ozone production predictions.

Table 5.5. Variance contribution (VC) estimation for different emission inputs.[a]

VOC species	S* [ppb/ton]	σ^2 [ton^2][b]	VC [ppb^2] [b]
OLE2	1.4E-01	312 - 4988	6.02 - 96.4
OLE1	1.3E-01	99 - 1583	1.58 - 25.3
ARO2[c]	1.2E-01	1175	16.5
ALK4	7.8E-03	5674 - 90785	0.34 - 5.47
ETHE	8.3E-02	25 - 407	0.17 - 2.78
ALK1	1.7E-01	3 - 47	0.09 - 1.41
ALK3	8.4E-03	893 - 14286	0.06 - 1.02
HCHO	2.7E-01	4	0.28
ALK2	6.6E-03	348 - 5568	0.02 - 0.24
ALK5	3.4E-03	1156 - 18502	0.01 - 0.21
ARO1[d]	2.6E-02	98	0.06
CCHO	4.5E-02	0.377	0.001
RCHO[e]	6.8E-02	0.100	0.0005
ACET	9.0E-03	0.27 - 4.259	0.00002 - 0.0003
Sum OLE			7.61 - 121.7
Sum ARO			16.53
Sum ALK			0.52 - 8.35
Sum ALD			0.28
VOC	1.9E-02	64612 - 1033792	24.1 - 386.1
NO_x	-9.6E-02	6398	58.7

[a] See captions in Figure 5.15 for definition of the different VOC species groups.

[b] Shown ranges of σ^2 and VC correspond to standard deviations with magnitudes of 50 and 200 % of the base case emissions for each group.

[c] Obtained using Equation 19 with toluene as species 1.

[d] Obtained using Equation 19 with benzene as species 1.

[e] Obtained using Equation 19 with acetaldehyde as species 1.

Similar to the sensitivity coefficients estimates, the variance contributions of the different species groups shown in Table 5.5 are not linearly additive. As such, the sum of the different emission groups sensitivities shown in the table are merely illustrative of the overall contributions of these groups to uncertainties in ozone predictions. Note also that we have not explored cross-correlated sensitivities of the model to various input parameters or emission groups. That is, the sensitivity of the model to simultaneously

reducing (or increasing) two or more emission groups has not been explored in our application.

Another consideration in the interpretation of the variance contributions shown in Table 5.5, is that the results are based on the assumption that the model formulation is structurally correct. For example, the model assumes that all but major point sources are emitted at the surface and instantaneously mix in the cell's volume. All the emissions for a given species are summed in the model and treated with this "instant mixing" assumption. Since actually the photochemistry is often nonlinear, the chemistry can be distinctly different at locations both near and far from emission source, even within a model's cell. It would be desirable to conduct uncertainty analyses of the model that include uncertainties introduced by this assumption. However, the results from Table 5.5 provide an initial ranking of the variance contributions of given emission groups to ozone predictions uncertainties. As in the case of the sensitivity results, a source apportionment study using the VOC data collected during the MILAGRO-2006 field campaign is desirable for identifying those emission sources that contribute the most to particular VOC groups.

5.5. Summary

In the first part of this chapter we presented the evaluation of the base case simulation corresponding to April 15, 2003 in the MCMA using the CAMx model version 4.30. The model's performance was investigated by comparing simulated near surface concentrations of ozone, NO_X, CO, OH and HO_2 radicals and selected VOC with data from the local ambient monitoring network as well as the data collected during the intensive field campaign of MCMA-2003. The base case simulation corresponded to a "ozone-south" meteorological scenario, which appears to be predominant during the months of March and April in the MCMA basin. The model reproduces reasonable concentrations of ozone and VOCs and more accurate those of CO and NO_X. The model over predicts OC concentrations by about 25% and severely under-predicts HO_2 by a

factor of 2 to 3 suggesting that the radical formation pathways in the current state-of-the art AQMs should be reevaluated.

In the second part of this chapter we investigated the sensitivity of the model to various input parameters using the BFM and the DDM sensitivity techniques. The results indicated that, under the base case emission/meteorological scenario studied, the model is equally sensitive (albeit with opposite sign) to NO_X and VOC emission reductions up to 50% from the base case. Beyond those perturbation levels, the sensitivity of the model was no longer linear and the accuracy of the first order approximation decreased significantly. Using the DDM, we model sensitivity coefficients to individual perturbations of VOC species lumped in groups as described by the SAPRC99 chemical mechanism. We showed that the model is particularly sensitive to aromatics, higher alkenes, and formaldehyde emissions. Using a "descriptor" technique and available measurement data of fuel-based emission factors, we obtained the variance contributions of NO_X and various VOC species groups to uncertainties in ozone predictions. We found that NO_X, olefins and aromatic species can potentially contribute significantly to uncertainties in ozone predictions whereas aldehydes (whose input emission uncertainties have been reduced due to available measurements) contribute much less uncertainties despite the higher sensitivity of the model to these species. The range of applicability of sensitivity results is limited by the level of the model performance in representing key physical and chemical phenomena, as well as on the size and quality of the supporting database employed to develop the inputs. As such, considerable care is necessary to determine the applicability of the findings in a regulatory regional air quality modeling context.

Chapter 6. Conclusions and future work

6.1. Introduction

Model predictions are inherently uncertain because of uncertainties in both the input data and the chemical and physical processes represented in their formulation, which are often a reflection of insufficient scientific understanding of the physicochemical processes involved. When model predictions are used for the evaluation of control strategies, there may be significant scientific uncertainties about the environmental impacts of such strategies. It is imperative, therefore, to address the following two fundamental questions when using AQMs to design and evaluate emission-based air quality management policies aiming to improve air quality levels in an urban area:

1) What is the ability of the model to simulate interactions of complex chemical, meteorological and pollutant emissions processes?
2) What is the uncertainty in the model predictions as a response to changes in determined input emission parameters?

Answers to these questions require the compilation of comprehensive data sets of parameters needed to solve the numerical equations representing the physical and chemical phenomena that lead to air pollution. These parameters are rarely measured concurrently in the same place, making it difficult to implement and thoroughly evaluate the AQM's performance. As a result, uncertainty analyses of urban air quality model predictions are not commonly performed. When performed, the uncertainty analyses are normally limited to emissions, meteorology, chemistry, resolution, or observational data (for initial and boundary conditions). In addition, uncertainties can be inherently associated with model formulations such as erroneous or simplified/incomplete representations and insufficiently accurate numerical solution techniques.

For the MCMA we are fortunate to have a fairly comprehensive set of concurrent measurements of key physical and chemical parameters obtained in several past and recent field campaigns held within the city and the region. These data sets allow the

possibility to constrain an AQM with further detail and assess the parametric uncertainty of important model predictions.

This thesis focuses on quantifying the effects of parametric uncertainties of input emission fields on model uncertainties of ozone predictions. To that aim, we first analyzed direct measurements of mobile emission sources in the MCMA, quantifying the magnitude and variability of key pollutant species using a fuel-based approach. This analysis allowed a direct evaluation of the emissions inventory used in AQMs for the MCMA. We then constructed a base case simulation period constraining the model with available locally measured data during the MCMA-2003 field campaign. The performance of the model during the base case simulation was evaluated using key ambient pollutant species. In addition, we evaluated the model's ability to reproduce historical changes in ozone formation as a result of perturbations of anthropogenic sources, and mobile emissions in particular. Finally we performed sensitivity and uncertainty analyses of the model ozone predictions due to uncertainties in emission parameters using the BFM and the DDM techniques. The following section presents the major findings of this work.

6.2. Conclusions

In Chapter 2 we described the analyses and results of the on-road measurements of mobile emission sources obtained in the MCMA using the Aerodyne mobile laboratory during the MCMA-2003 field campaign. The analyses allowed us to obtain fleet-average emission measurements of key species emitted at various driving modes in the MCMA. By converting to fuel-based units and using readily available fuel consumption data, we were able to estimate annual emissions of mobile NO_X and selected VOCs and to evaluate the current official emissions inventory estimates. Measurements of selected VOCs and NO_Y showed a strong dependence on traffic mode, suggesting the possibility for designing air quality control strategies based on the modification of the driving modes and the retrofitting of public transport vehicles in urban areas. Our measurements also

indicated a larger than expected burden of emitted NO_X and aldehydes, particularly from the public transport sector.

We estimated annual emissions of benzene, toluene, formaldehyde, and acetaldehyde in the MCMA for the first time using a fuel-based approach. The results indicate that the emissions of these toxic pollutants are similar or higher than the corresponding estimated toxic VOC emissions for Los Angeles, even though the size of the vehicle fleet and fuel consumption in Los Angeles are more than 3 times higher than in the MCMA. The large burden of toxic VOCs in the MCMA is likely linked to an older vehicle fleet and the smaller fraction of vehicles with emission control technologies, both characteristics that are likely shared by many urban areas in the developing world. The high yield of aldehyde emissions from MCMA vehicles may have important impacts on the photochemistry of the region and the high emissions of aromatic and aldehyde air toxics may have important health implications.

In chapter 3 we presented an inter-comparison of on-road measurements of mobile sources obtained in Mexicali and Austin, TX with those in the MCMA described in chapter 2. The measurements in the three cities were obtained using the Aerodyne mobile laboratory using the same on-road sampling technique, constituting a unique opportunity to compare the vehicle fleet emission characteristics of a megacity with two smaller urban areas that have distinct vehicle fleet characteristics. In addition, the comparison could be useful for understanding the fast-evolving characteristics of the vehicle fleet in a US-Mexican border city.

Similar to the results obtained in the MCMA, the measurements of mobile emissions in Mexicali showed a strong correlation with driving mode and large variability of emission ratios. The large variability of measured emissions for NO_X, CO and selected VOC species suggests the prevalence of high emitters in the fleet that may be the result of malfunctioning of, or the lack of, emission control systems by a significant fraction of the fleet. Interestingly, similar to the results obtained for the MCMA, formaldehyde emissions showed a slight dependence on driving mode. However, measured

formaldehyde emission ratios in the MCMA were higher than in Mexicali by a factor of 2 whereas acetaldehyde emission ratios in Mexicali do not seem to be significantly different from Mexico City. In addition, the selected aromatic VOCs emission ratios measured in the Mexicali gasoline vehicle fleet are slightly, but consistently, smaller than those measured in Mexico City whereas emission ratios of NH_3 seem to be higher in Mexico City than in Mexicali by a factor of 2 or more.

The measurements also indicated that NO_Y emission ratios from HDDTs in Mexicali and the MCMA were significantly higher than in Texas and that the variability (1-sigma standard of the measurements) is similar in all three locations. The main limitation in the comparison is the smaller number of vehicles sampled in Texas, and to some respect in Mexicali, compared to the number of measurements in the MCMA. However, comparisons of NO_Y/CO_2 and NO_2/NO_Y on-road mobile emissions of individual HDDTs for the three cities indicated large variability of NO_Y emission ratios that correlated with vehicle speed for individual vehicles. The observed variability correlated to vehicle speed is an indication of enhanced thermal NO_X formation at higher engine temperatures. The strong correlation between NO_X emission ratios and vehicle speed suggests the possibility of impacting NO_X emissions from HDDTs by controlling the A/F ratio in the vehicles.

Following the procedure described in Chapter 2 for obtaining fuel-based estimates of emissions from mobile sources, we evaluated the 2001 National Emissions Inventory (NEI) combined with the 1999 BRAVO inventory for the Mexicali region. The results indicated a severe underestimation of aldehyde emissions and a large underestimation of NO and CO emissions in the inventory, suggesting that modeling studies using such inventory should use a much broader range of input emissions when attempting to model the photochemistry of the Mexicali region.

In chapter 4 we quantified the observed effects from perturbations of mobile sources on the photochemical pollutant levels in Mexico City. We first presented a trend analysis of historical ambient measurements in the MCMA in which we applied appropriate filtering

criteria that minimized the effects of inter-annual seasonal variability of meteorological parameters as well as atypical variations of anthropogenic emissions on ambient pollutant levels. The results showed that significant changes have occurred in the MCMA for ozone, CO and NO_X concentration levels over the past 21 years. From the early 1990s, a decrease rate of 2.7 +/- 0.5 ppb/yr has been observed in maximum ozone concentrations after an in impressive growth rate of 12 +/- 1.3 ppb/yr from the start of the measurements until 1992. Since then, peak ozone concentrations have been drastically reduced in the city while high median concentrations still persist.

Using direct measurements of emissions and a new indirect approach, we further showed that the observed changes in CO, NO and ozone concentration levels are strongly linked to concurrent perturbations of anthropogenic source emissions, and of mobile emissions in particular. Our analysis indicates that fleet average emission factors have drastically decreased for CO and HC over the past two decades whereas NO_X emission factors do not show strong long term trend. Decreases in CO and HC are likely due to improvements in vehicle and emission control technologies over time, which are in turn related to regulation policies through the implementation of more stringent emission standards for new vehicles. Possible explanations of the different behavior of NO_X emissions trends from mobile sources as compared to CO and HC emissions include: 1) more effective vehicle engine technologies for reducing CO and HC than for NO_X, 2) lower efficiency for NO_X reduction than for HC and CO oxidation by catalytic converters, 3) changes in driving modes in the city, and 4) a faster growth of diesel fleet activity compared to the gasoline fleet activity.

Estimating the size of the perturbations of mobile sources allowed us to quantify a "natural" sensitivity effect on ozone formation in the urban area. In addition, the analysis revealed the existence of a "core-to-skirt" effect caused by the observed delay in historical photochemical pollutant formation rates. These results suggest that the ambient monitoring network may no longer be capturing the real (domain-wide) ozone peak of the basin. Frequency maps constructed for the allocation of the ozone peak showed

distinctive clusters that are likely related to the prevailing meteorological patterns occurring during the months of March and April in the city.

In chapter 5 we presented an evaluation of the base case simulation corresponding to April 15, 2003 in the MCMA using the CAMx model version 4.30. We evaluated the model's performance by comparing simulated near surface concentrations of ozone, NO_X, CO, OH and HO_2 radicals and selected VOCs with data from the local ambient monitoring network as well as the data collected during the intensive MCMA-2003 field campaign. The base case simulation corresponded to an "ozone-south" meteorological scenario which, according to the analysis presented in chapter 4, appears to be predominant during the months of March and April in the MCMA basin. The model reasonably reproduces concentrations of ozone and VOCs and accurately those of CO and NO_X. The model largely underestimates the concentrations of HO_X radicals at night, suggesting the need for including non photolytic radical sources in the model. The large concentrations of ozone and NO_X at night suggest that significant concentrations of NO_3 radicals are formed. In turn, the presence of NO_3 would induce the formation of N_2O_5 which can reach equilibrium due to the large concentrations of NO_2. In this way, the N_2O_5 may act as a significant reservoir of oxidized nitrogen directly or through the production of HNO_3 from its hydrolysis. The nitric acid formed may deposit rapidly on surfaces making nitrogen species unavailable for the formation of ozone the following day.

The model under predicts OH concentrations by about 25% from sunrise to the diurnal peak and over predicts it by the same magnitude afterwards until sunset. On the other hand, the model severely under-predicts HO_2 by a factor of 2 to 3 suggesting that the radical formation pathways in current state of the art AQMs should be revised. Because the model reasonably reproduces ozone, CO, NO_X and key VOCs, it is possible that the model compensate with organic peroxy radicals to account for the missing HO_2 radicals. The analysis of the data also suggests that HONO accumulates in the early morning until its photolysis becomes significant. The HONO accumulated in the early morning would act as an important source of radicals for the initiation of VOC oxidation. Free radicals

(in additions to ozone and photolysis reactions) initiate the oxidation of hydrocarbons in the gas phase and are key participants in the formation of Secondary Organic Aerosols (SOA) which is formed from low volatility products of the VOC oxidation.

We also investigated the sensitivity of the model to various input parameters using the BFM and the DDM sensitivity techniques. The results of the BFM indicate that the model reproduces successfully the corresponding relative changes in historical observations of ozone peak and diurnal average concentrations described in Chapter 4. This provides further evidence that ozone production in the MCMA has changed from a high VOC-sensitive regime to a moderate VOC-sensitive regime over a period of 15 to 20 years. The results also indicated that, under the base case emission/meteorological scenario studied, the model is equally sensitive (albeit with opposite sign) to NO_X and VOC emission reductions below about 40 to 50 % from the base case. Beyond those perturbation levels, the sensitivity of the model was no longer linear and the accuracy of the first order approximation decreased significantly. Using the DDM, we obtained sensitivity coefficients of the model to individual perturbations of VOC species lumped in groups as described by the SAPRC99 chemical mechanism. We showed that the model is particularly sensitive to aromatics, higher alkenes, and formaldehyde emissions. Using a "descriptor" technique and available measurement data to compute fuel-based emission factors, we obtained the variance contributions of NO_X and various VOC species groups to uncertainties in ozone predictions. We found that NO_X, olefins and aromatic species can potentially contribute significantly to uncertainties in ozone predictions whereas aldehydes (whose input emission uncertainties have been reduced due to available measurements) contribute much less uncertainty despite the higher sensitivity of the model to these species.

6.3. Future work

Based on the results of this work, some directions for future research that can help to improve our understanding of the atmospheric pollution phenomena in urban areas are suggested.

1. Emissions need to be treated as variables, rather than point estimates. As shown in chapter 4, mobile emissions may vary significantly daily, as well as intra and inter annually in an urban area. The variability of emissions is the result of competing and variable space/time factors that include: vehicle's emissions control technologies, fuel consumption and fuel composition, emission's control policies (e.g. "a-day-without-a-car", I&M programs, etc.), and fleet size, age and renewal rate, among many others. Due to the combination of these factors, emissions vary continuously in time within an urban area. Estimated emissions in official emissions inventories should include variability estimates of their variability in addition to base case estimates. Due to their importance for determining the uncertainty in the predictions of the model, both the magnitude and variability of emissions need to be investigated with continuous direct measurements of mobile emissions.

2. The effects of the assumptions in the models' formulation of emission processes should be investigated. Model sensitivity studies tend to be local parametric analyses that rely on the model being structurally correct. However, structural sensitivity/uncertainty analysis, particularly for investigating the assumption of "instantaneous" mixing in AQM's grid cells, is desirable.

3. Global sensitivity and uncertainty studies that concurrently investigate the uncertainties of the model predictions due to uncertainties in meteorological and emission parameters need to be performed. Such studies can help elucidate the relative importance of these processes in model predictions.

4. Sensitivity and uncertainty analyses of the reaction rates represented in the chemical mechanism used in the model for the base case simulation in the MCMA also need to be performed. The analyses would identify the most relevant chemical parameters in the chemical mechanism for the VOC/NO_X conditions in the MCMA.

5. Model sensitivities to concurrent perturbations of various VOC emission groups should be evaluated. Cross-sensitivities and higher order sensitivities and their associated uncertainties of various VOC groups were not investigated in this work. These types of sensitivities may be important when evaluating mitigation strategies that directly target VOC emissions (such as solvent, paint and dry cleaning emissions, etc.), where more than one VOC emission species are affected.

6. The sink and source budgets for organic peroxy radicals in the SAPRC99 chemical mechanism in the model should also be evaluated. Since the model reasonably predicts ozone, NO_X, CO and selected VOCs, but severely underestimates HO_2 radicals (OH is overestimated only about 25%), one possibility is that the model compensates for the missing HO_2 radicals with organic peroxy radicals.

Appendices

Isopleths of key model predictions.

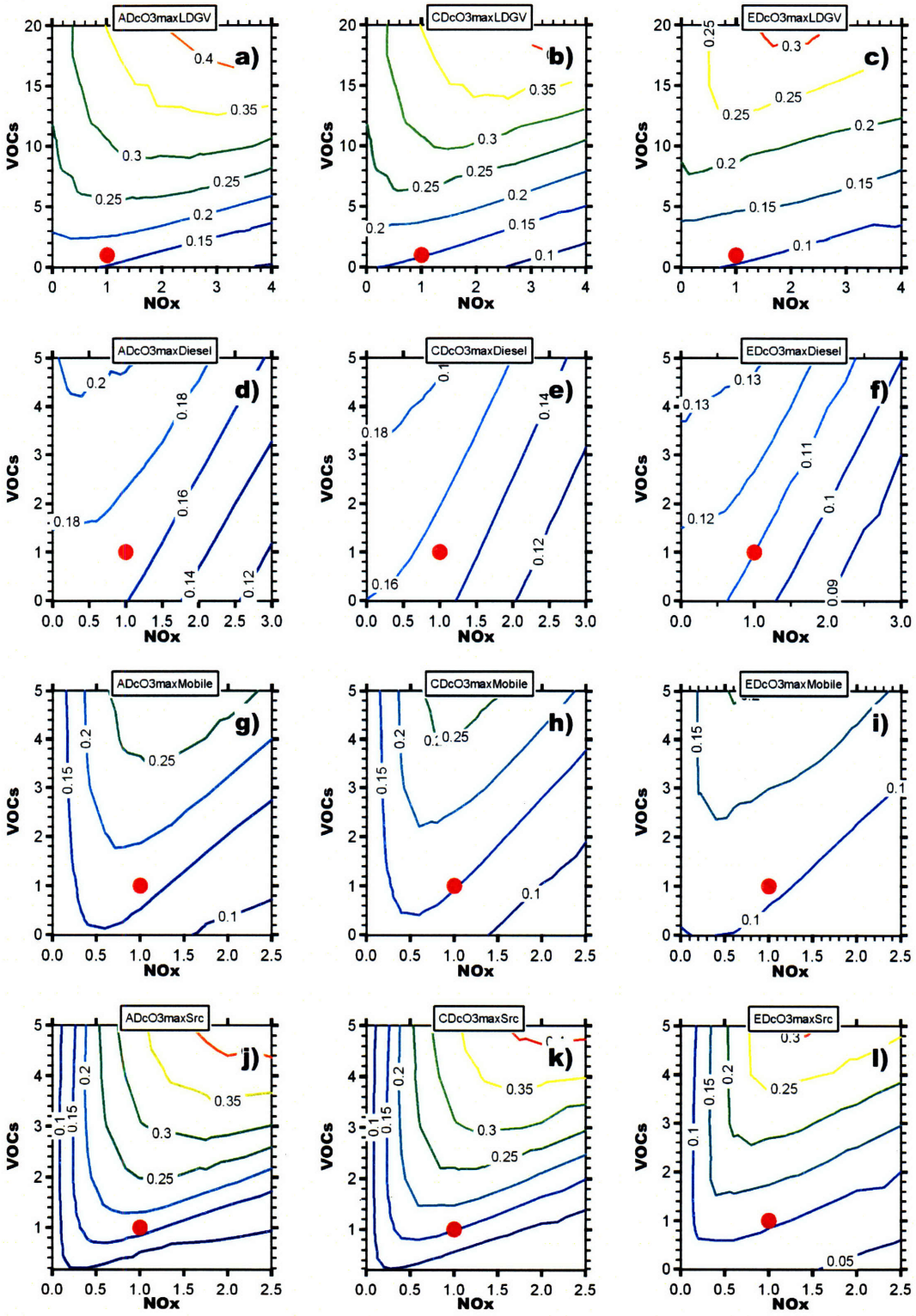

Figure A.1. Peak ozone isopleths [ppm] for domain-wide (AD), city domain (CD) and CENICA site (ED) for emissions perturbations in LDGV (a, b, c), diesel (d, e, f), all mobile (g, h, i), and all sources (j, k, l). Axes represent mass-based scaling factors of VOC and NO_X emissions from the base case simulation (red dot).

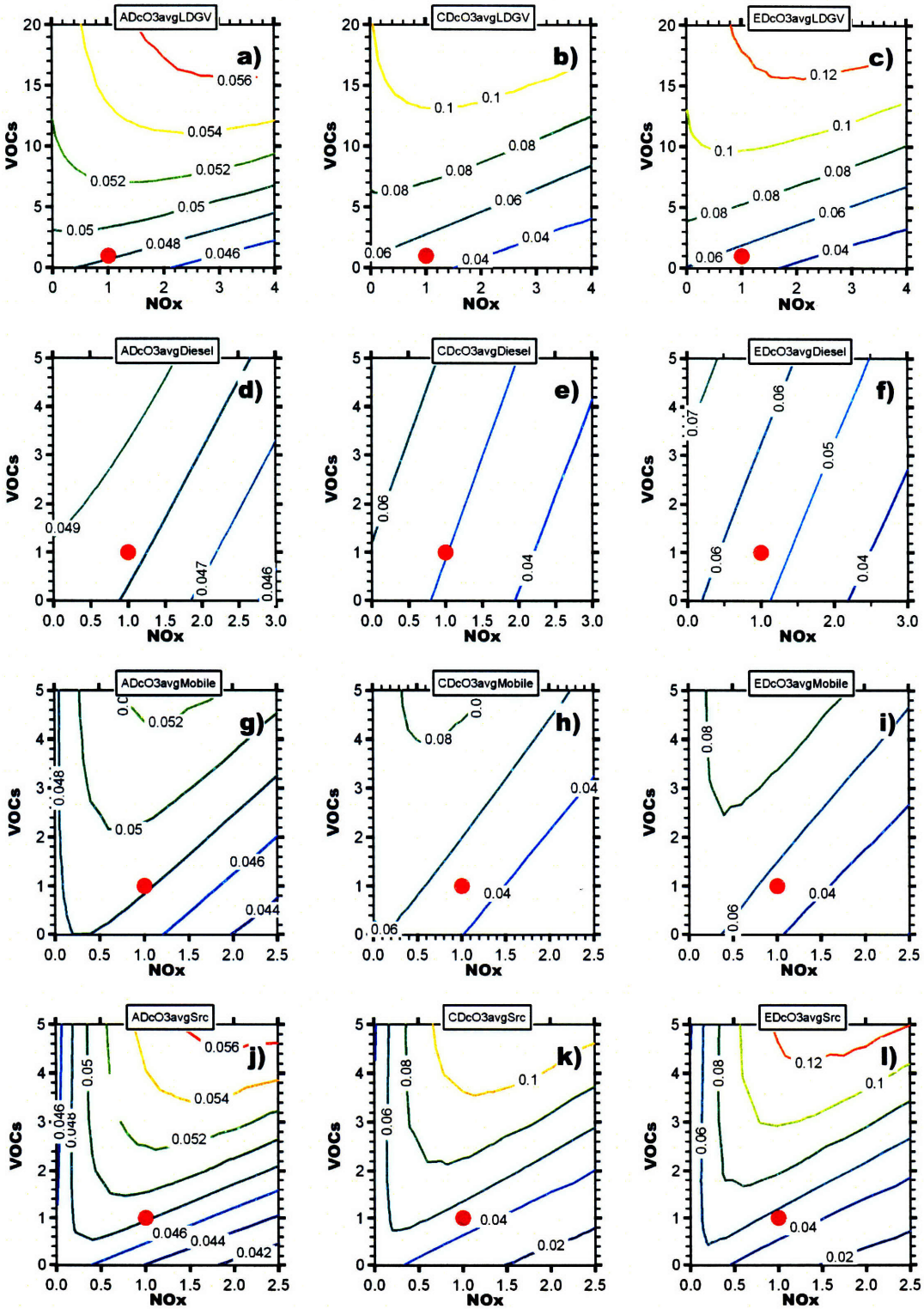

Figure A.2. Diurnal average ozone isopleths [ppm] for domain-wide (AD), city domain (CD) and CENICA site (ED) for emissions perturbations in LDGV (a, b, c), diesel (d, e, f), all mobile (g, h, i), and all sources (j, k, l). Axes represent mass-based scaling factors of VOC and NO_X emissions from the base case simulation (red dot).

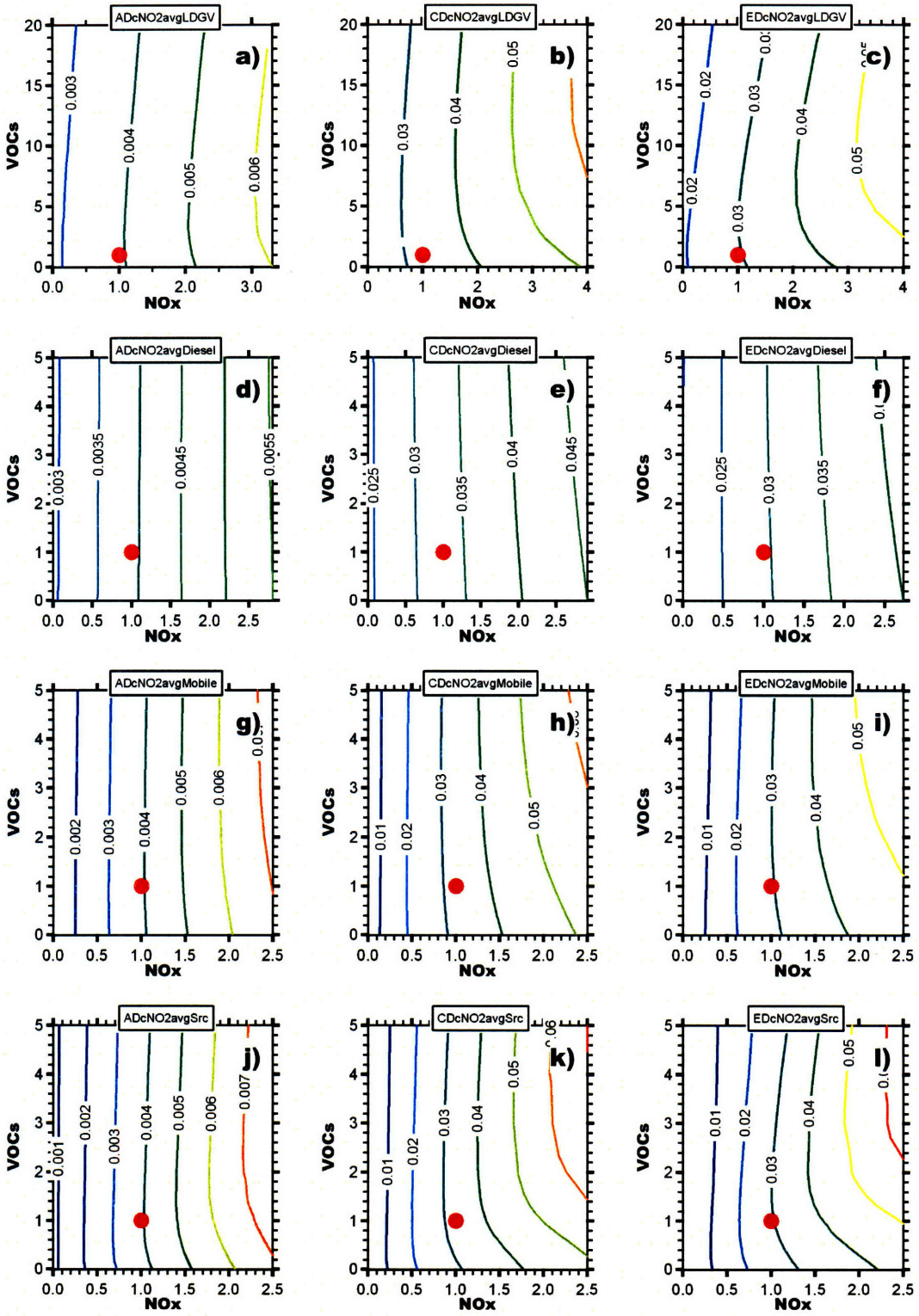

Figure A.3. Diurnal average NO_2 isopleths [ppm] for domain-wide (AD), city domain (CD) and CENICA site (ED) for emissions perturbations in LDGV (a, b, c), diesel (d, e, f), all mobile (g, h, i), and all sources (j, k, l). Axes represent mass-based scaling factors of VOC and NO_X emissions from the base case simulation (red dot).

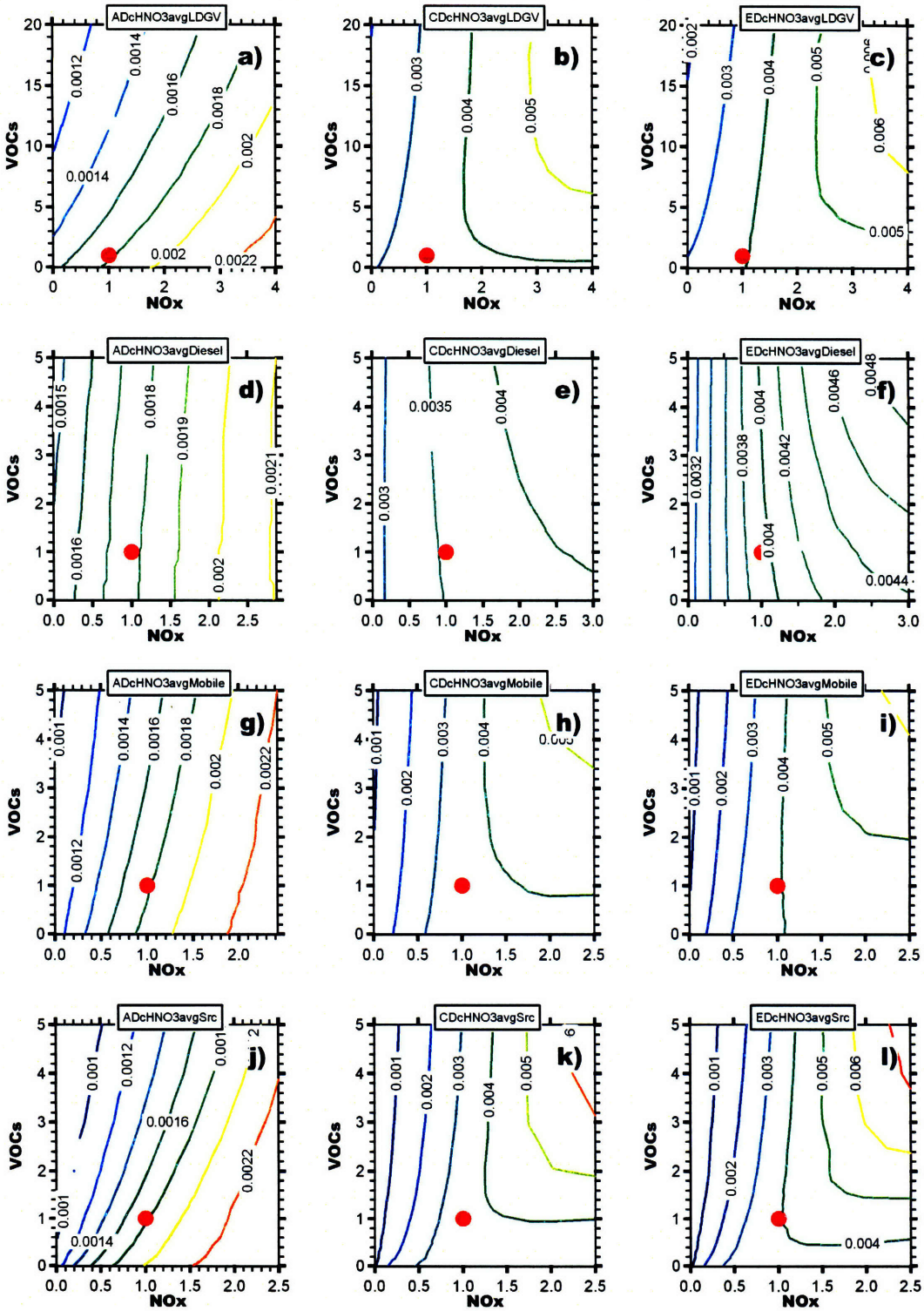

Figure A.4. Diurnal average HNO_3 isopleths [ppm] for domain-wide (AD), city domain (CD) and CENICA site (ED) for emissions perturbations in LDGV (a, b, c), diesel (d, e, f), all mobile (g, h, i), and all sources (j, k, l). Axes represent mass-based scaling factors of VOC and NO_X emissions from the base case simulation (red dot).

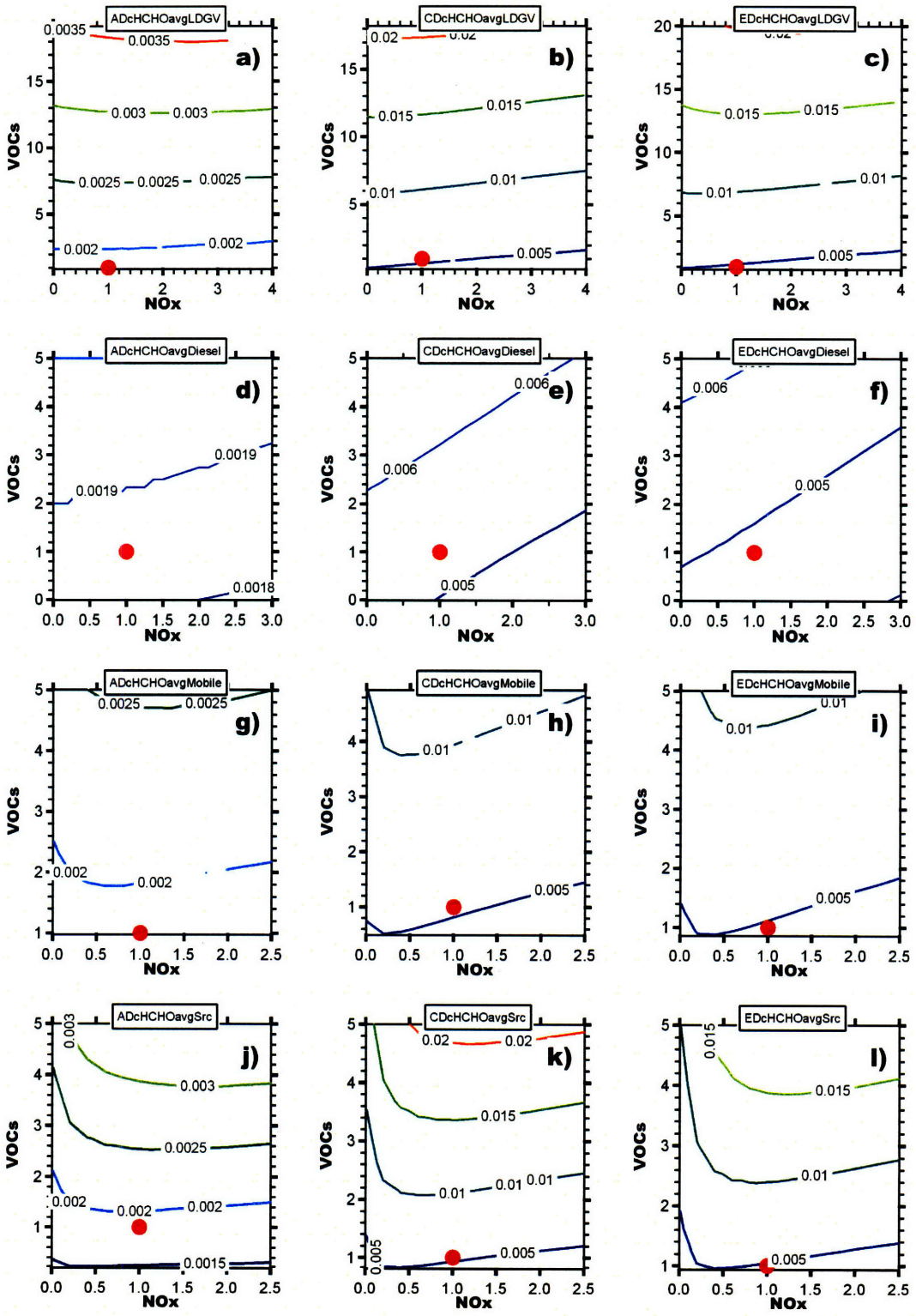

Figure A.5. Diurnal average HCHO isopleths [ppm] for domain-wide (AD), city domain (CD) and CENICA site (ED) for emissions perturbations in LDGV (a, b, c), diesel (d, e, f), all mobile (g, h, i), and all sources (j, k, l). Axes represent mass-based scaling factors of VOC and NO_X emissions from the base case simulation (red dot).

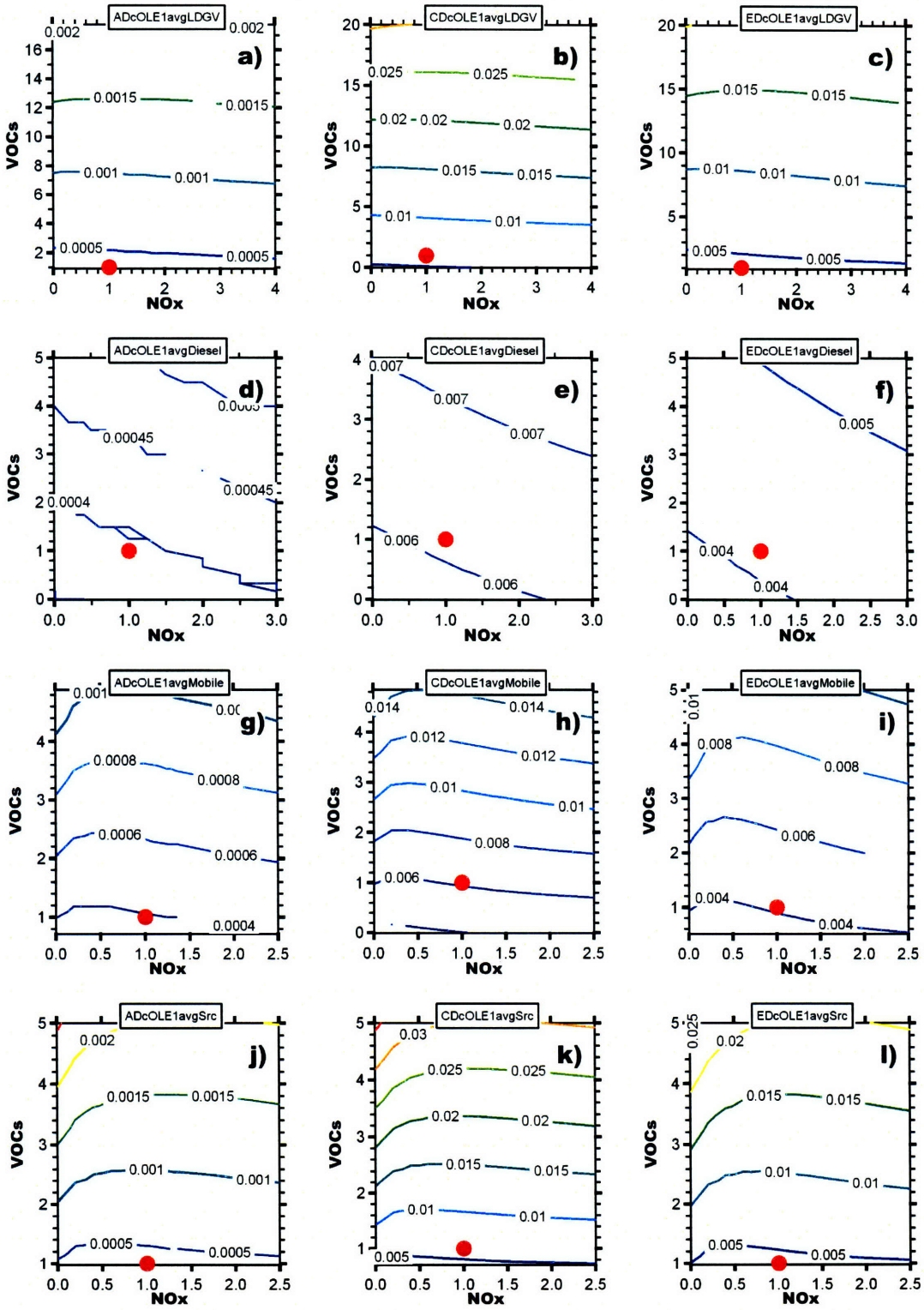

Figure A.6. Diurnal average OLE1 isopleths [ppm] for domain-wide (AD), city domain (CD) and CENICA site (ED) for emissions perturbations in LDGV (a, b, c), diesel (d, e, f), all mobile (g, h, i), and all sources (j, k, l). Axes represent mass-based scaling factors of VOC and NO_X emissions from the base case simulation (red dot).

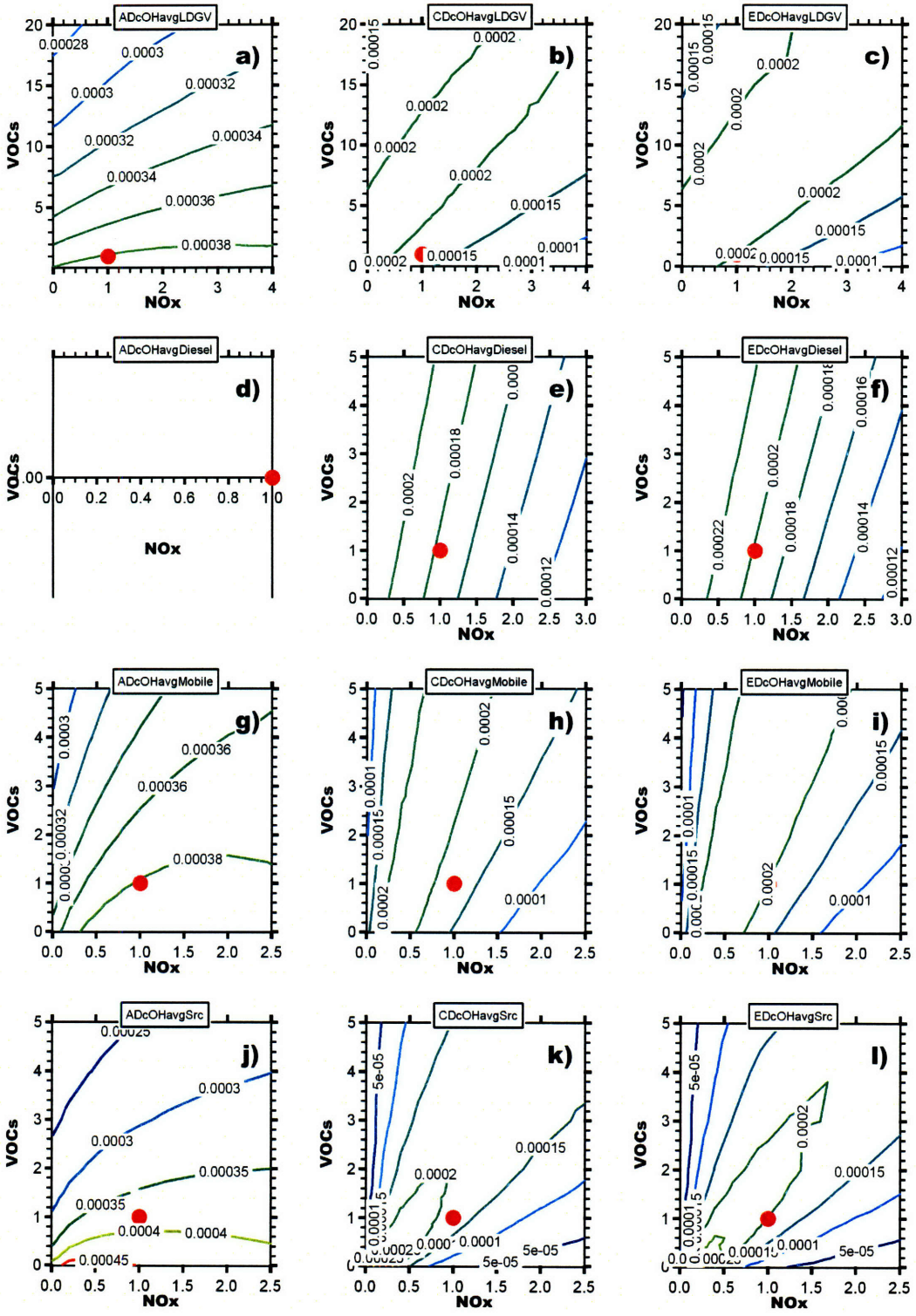

Figure A.7. Diurnal OH isopleths [ppb] for domain-wide (AD), city domain (CD) and CENICA site (ED) for emissions perturbations in LDGV (a, b, c), diesel (d, e, f), all mobile (g, h, i), and all sources (j, k, l). Axes represent mass-based scaling factors of VOC and NO_X emissions from the base case simulation (red dot).

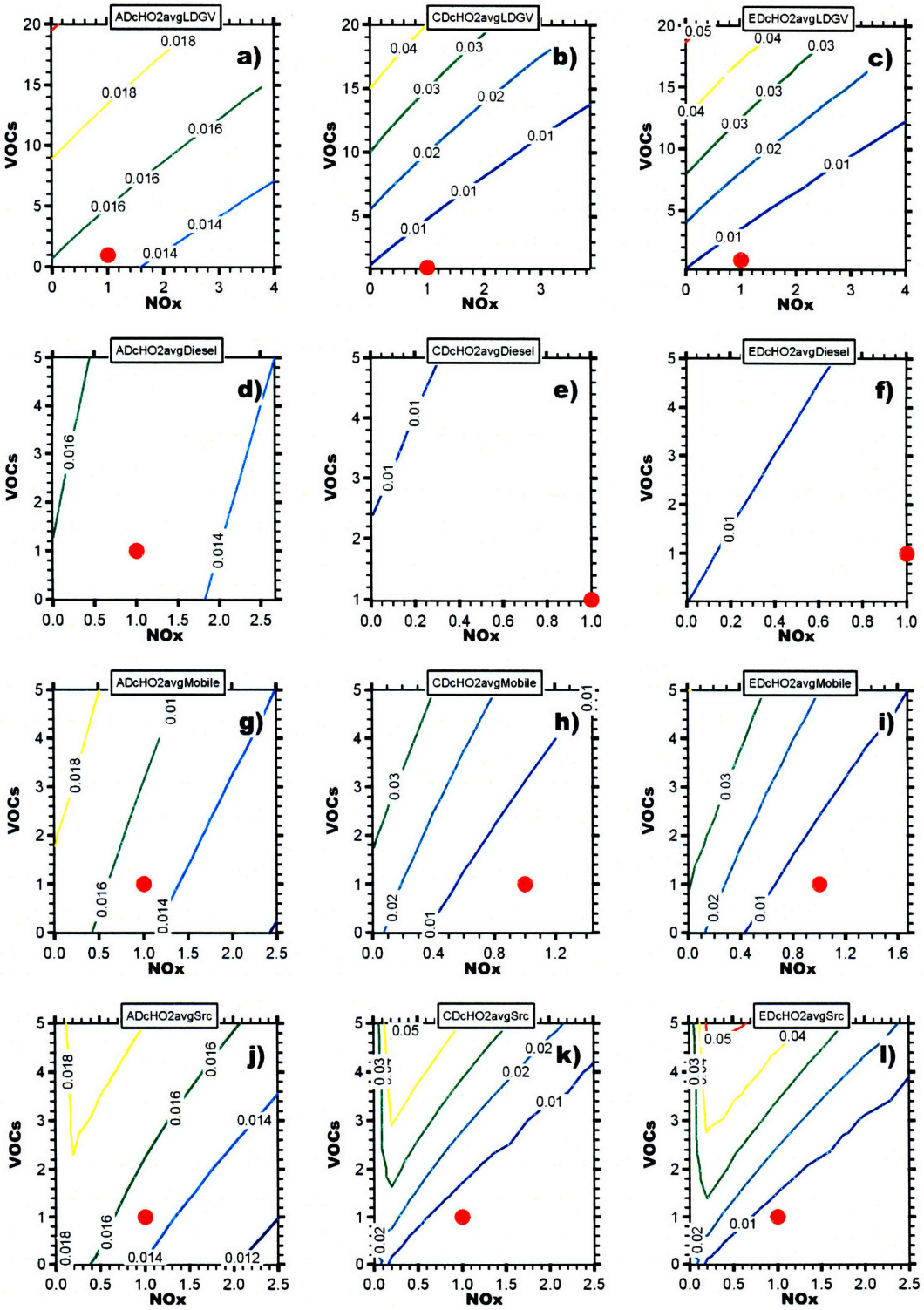

Figure A.8. Diurnal average HO_2 isopleths [ppm] for domain-wide (AD), city domain (CD) and CENICA site (ED) for emissions perturbations in LDGV (a, b, c), diesel (d, e, f), all mobile (g, h, i), and all sources (j, k, l). Axes represent mass-based scaling factors of VOC and NO_X emissions from the base case simulation (red dot).

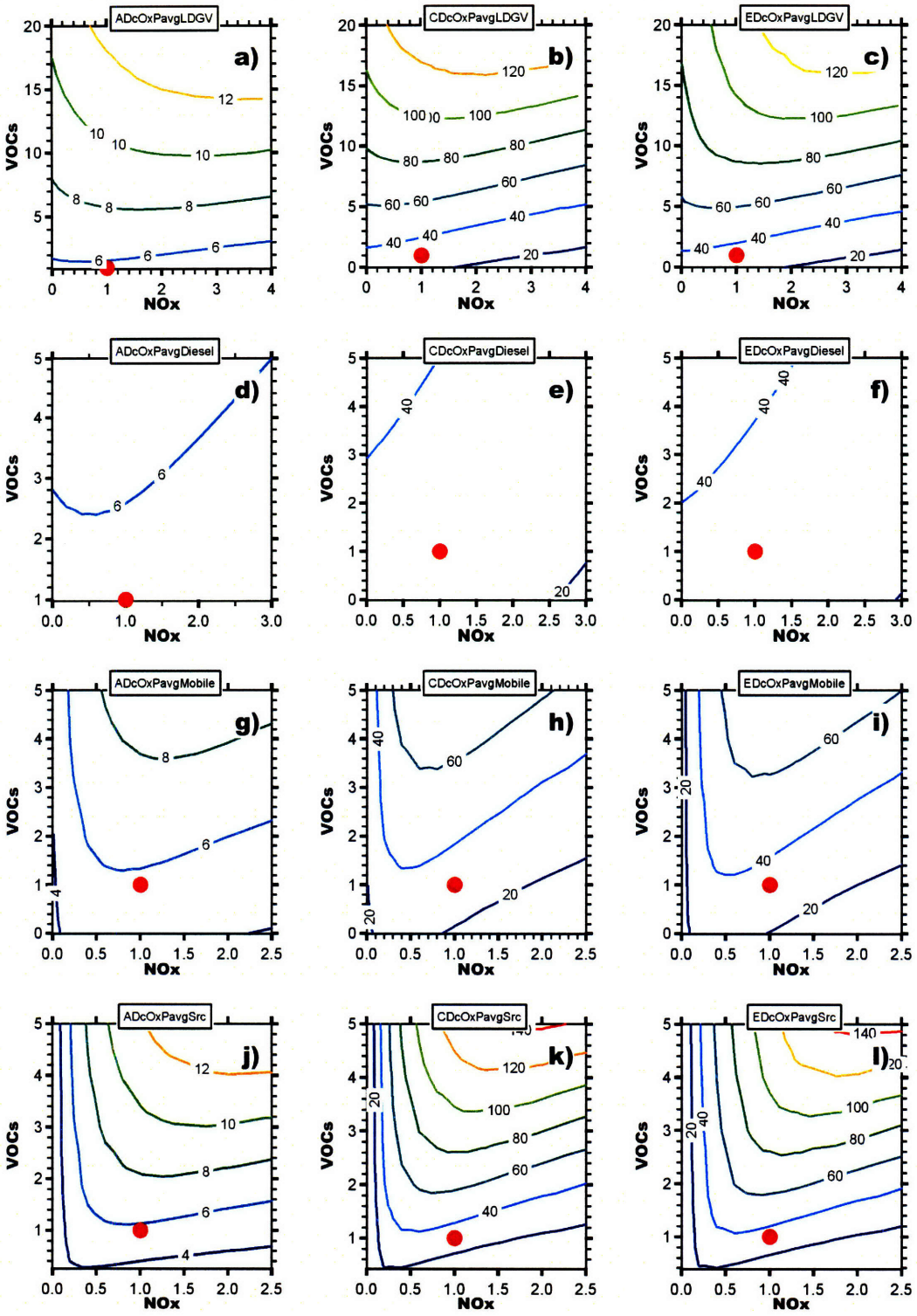

Figure A.9. Diurnal average O_X production -P(O_X)- isopleths [ppb/hr] for domain-wide (AD), city domain (CD) and CENICA site (ED) for emissions perturbations in LDGV (a, b, c), diesel (d, e, f), all mobile (g, h, i), and all sources (j, k, l). Axes represent mass-based scaling factors of VOC and NO_X emissions from the base case simulation (red dot).

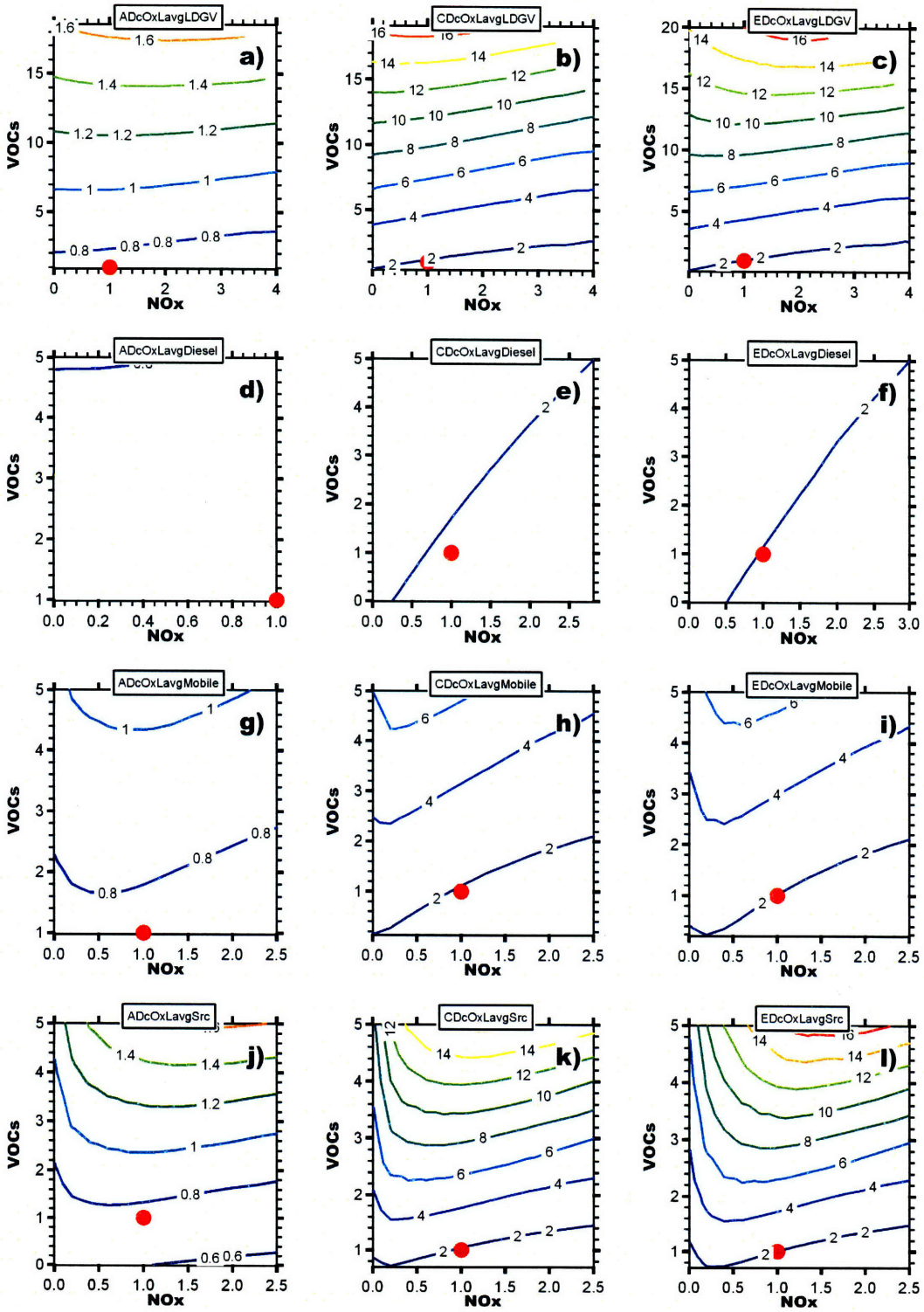

Figure A.10. Diurnal average O_X Loss -L(O_X)- isopleths [ppb/hr] for domain-wide (AD), city domain (CD) and CENICA site (ED) for emissions perturbations in LDGV (a, b, c), diesel (d, e, f), all mobile (g, h, i), and all sources (j, k, l). Axes represent mass-based scaling factors of VOC and NO_X emissions from the base case simulation (red dot).

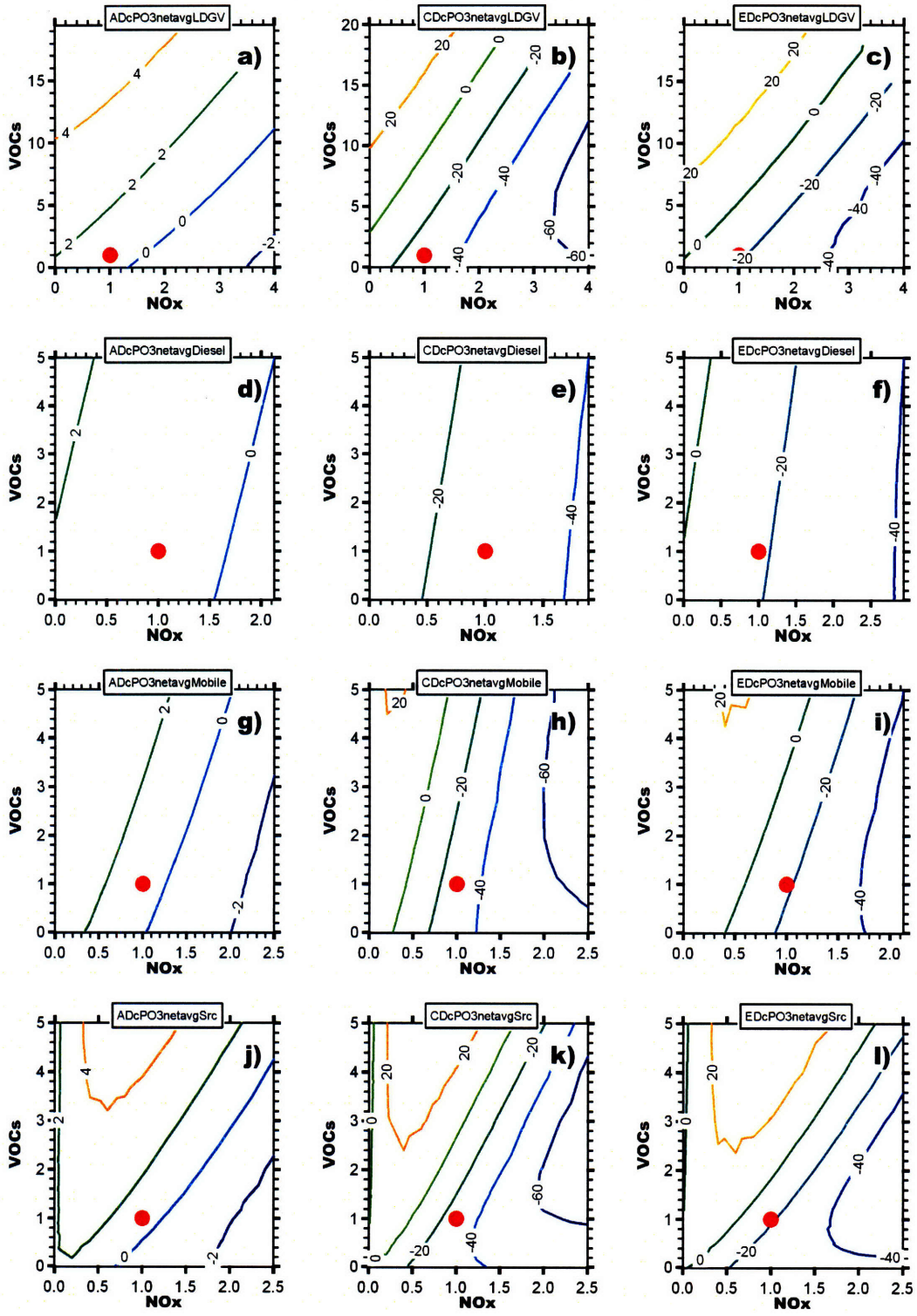

Figure A.11. Diurnal average net ozone production isopleths [ppb/hr] for domain-wide (AD), city domain (CD) and CENICA site (ED) for emissions perturbations in LDGV (a, b, c), diesel (d, e, f), all mobile (g, h, i), and all sources (j, k, l). Axes represent mass-based scaling factors of VOC and NO_X emissions from the base case simulation (red dot).

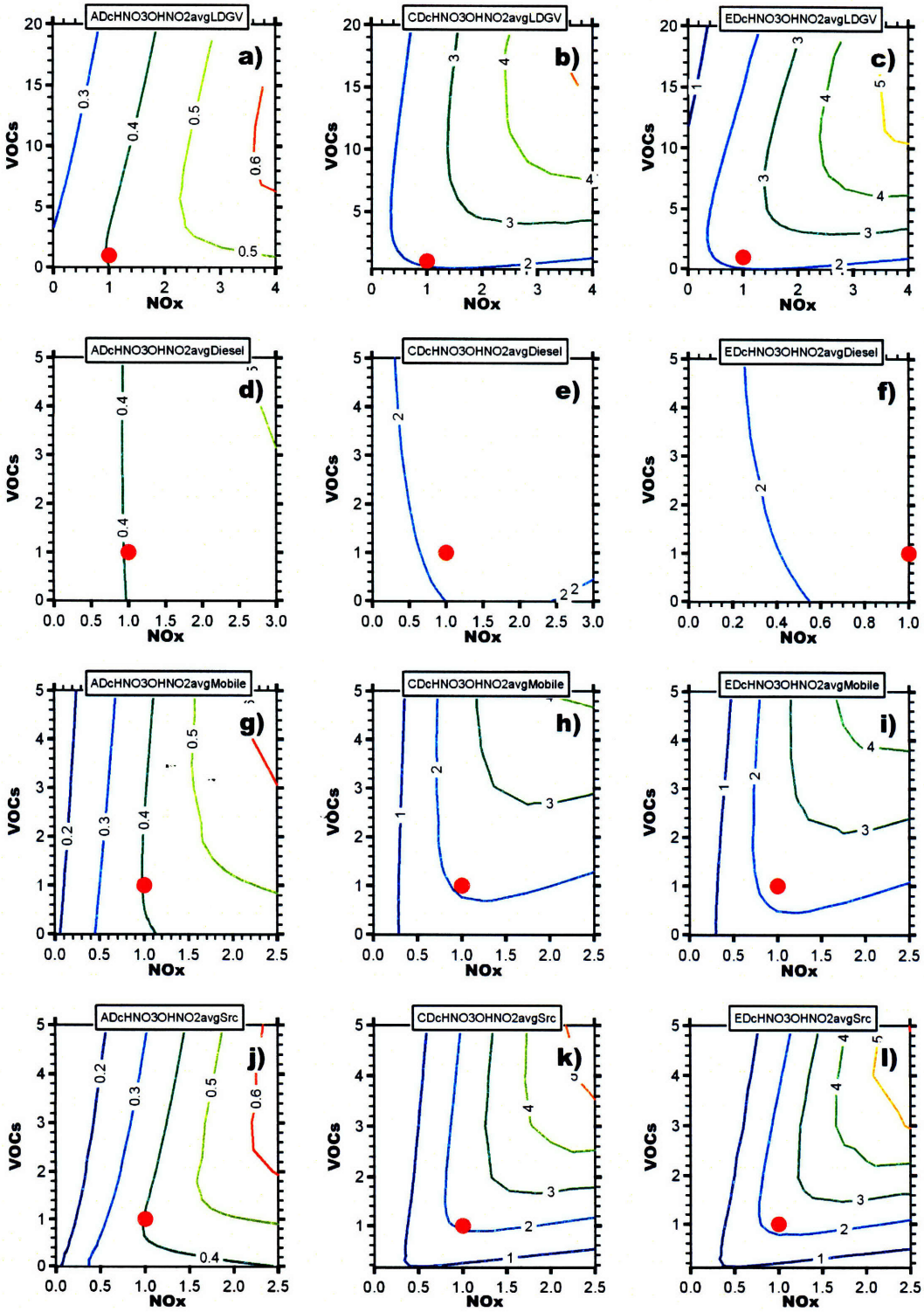

Figure A.12. Diurnal average OH + NO_2 reaction isopleths [ppb] for domain-wide (AD), city domain (CD) and CENICA site (ED) for emissions perturbations in LDGV (a, b, c), diesel (d, e, f), all mobile (g, h, i), and all sources (j, k, l). Axes represent mass-based scaling factors of VOC and NO_X emissions from the base case simulation (red dot).

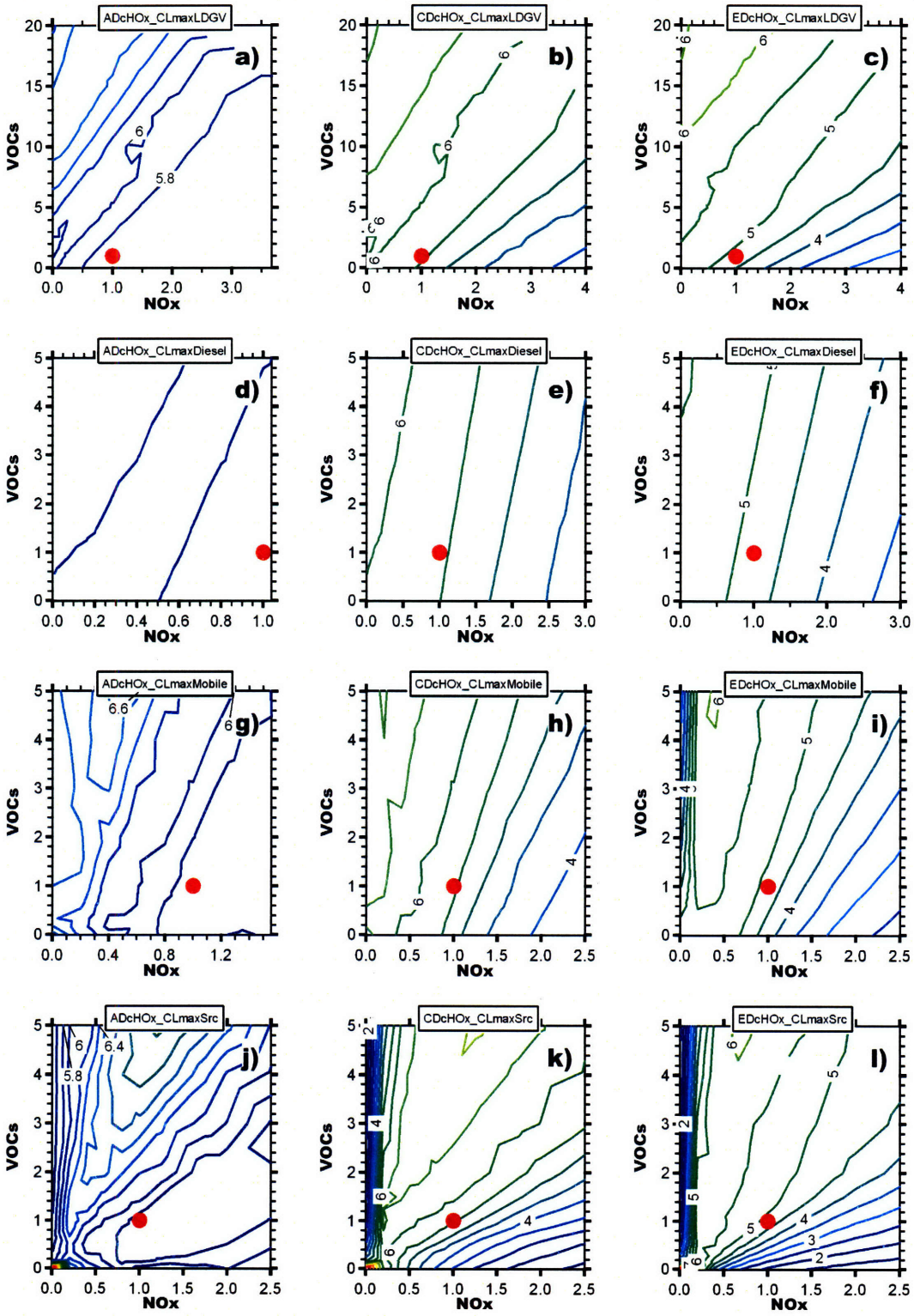

Figure A.13. Peak HO_X chain length isopleths [ppb-hr/ppb-hr] for domain-wide (AD), city domain (CD) and CENICA site (ED) for emissions perturbations in LDGV (a, b, c), diesel (d, e, f), all mobile (g, h, i), and all sources (j, k, l). Axes represent mass-based scaling factors of VOC and NO_X emissions from the base case simulation (red dot).

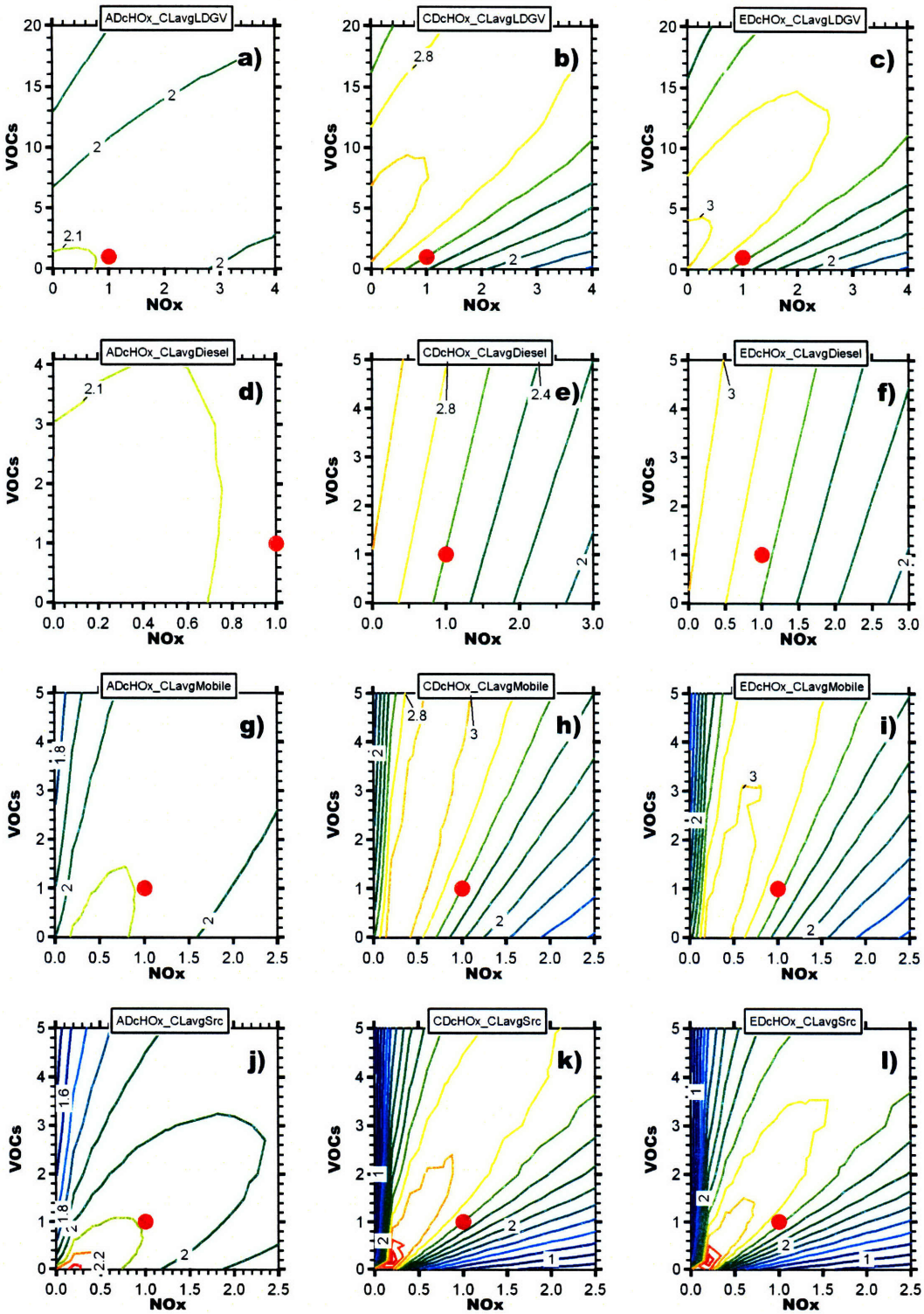

Figure A.14. Diurnal HO_X chain length isopleths [ppb-hr/ppb-hr] for domain-wide (AD), city domain (CD) and CENICA site (ED) for emissions perturbations in LDGV (a, b, c), diesel (d, e, f), all mobile (g, h, i), and all sources (j, k, l). Axes represent mass-based scaling factors of VOC and NO_X emissions from the base case simulation (red dot).

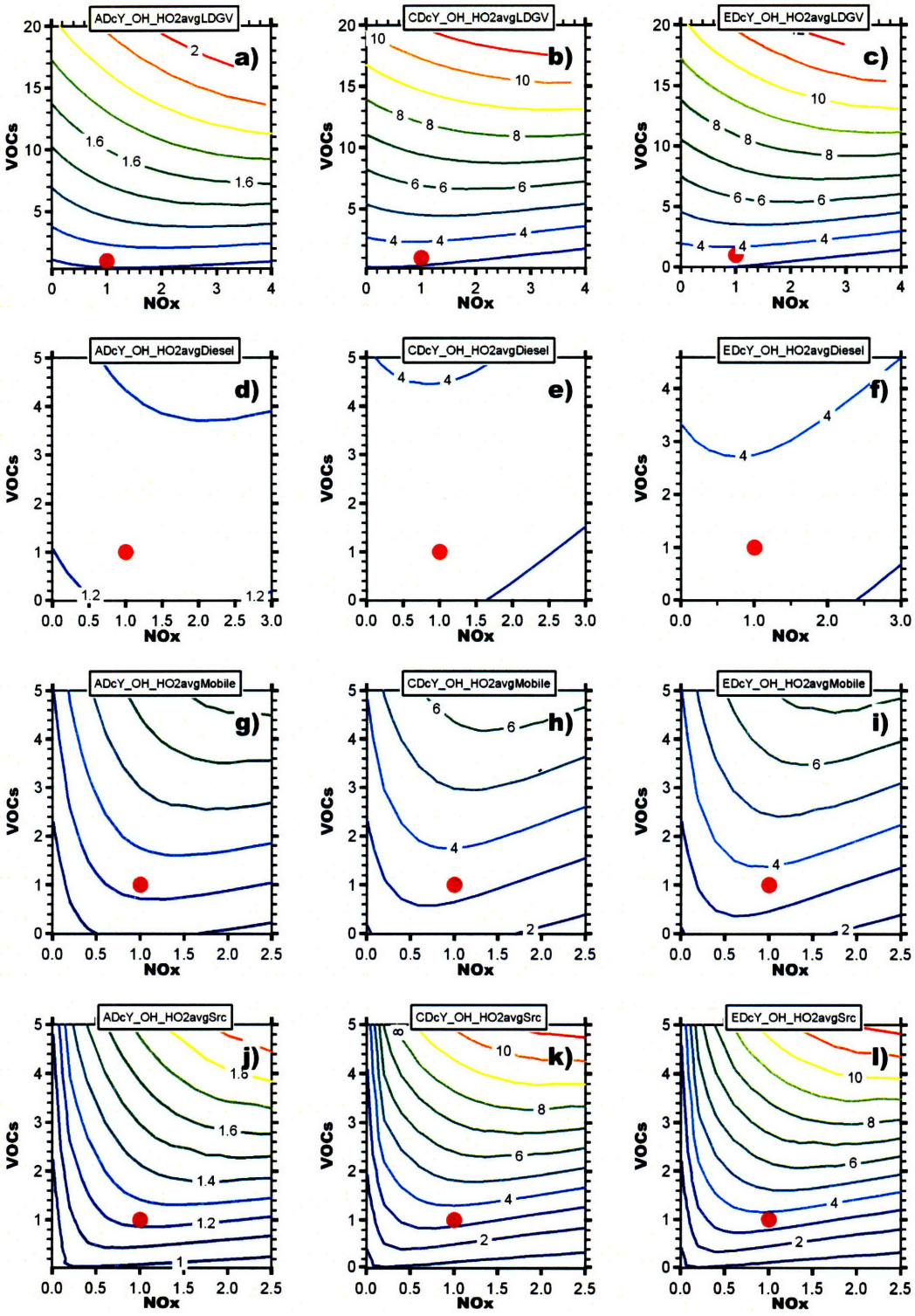

Figure A.15. Diurnal average yield of OH per HO_2 reacted isopleths [] for domain-wide (AD), city domain (CD) and CENICA site (ED) for emissions perturbations in LDGV (a, b, c), diesel (d, e, f), all mobile (g, h, i), and all sources (j, k, l). Axes represent mass-based scaling factors of VOC and NO_X emissions from the base case simulation (red dot).

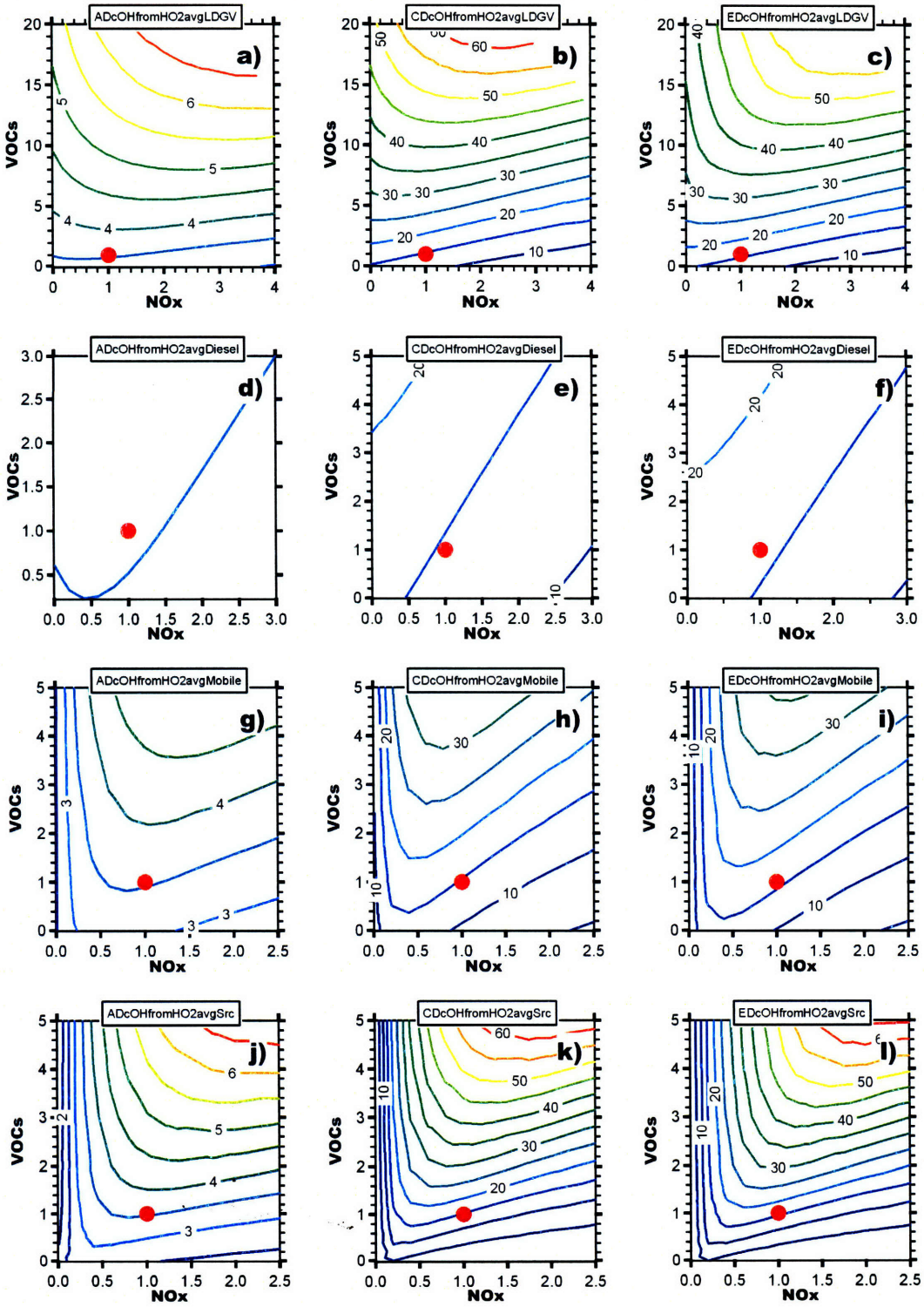

Figure A.16. Diurnal average OH produced from reactions of HO_2 isopleths [] for domain-wide (AD), city domain (CD) and CENICA site (ED) for emissions perturbations in LDGV (a, b, c), diesel (d, e, f), all mobile (g, h, i), and all sources (j, k, l). Axes represent mass-based scaling factors of VOC and NO_X emissions from the base case.

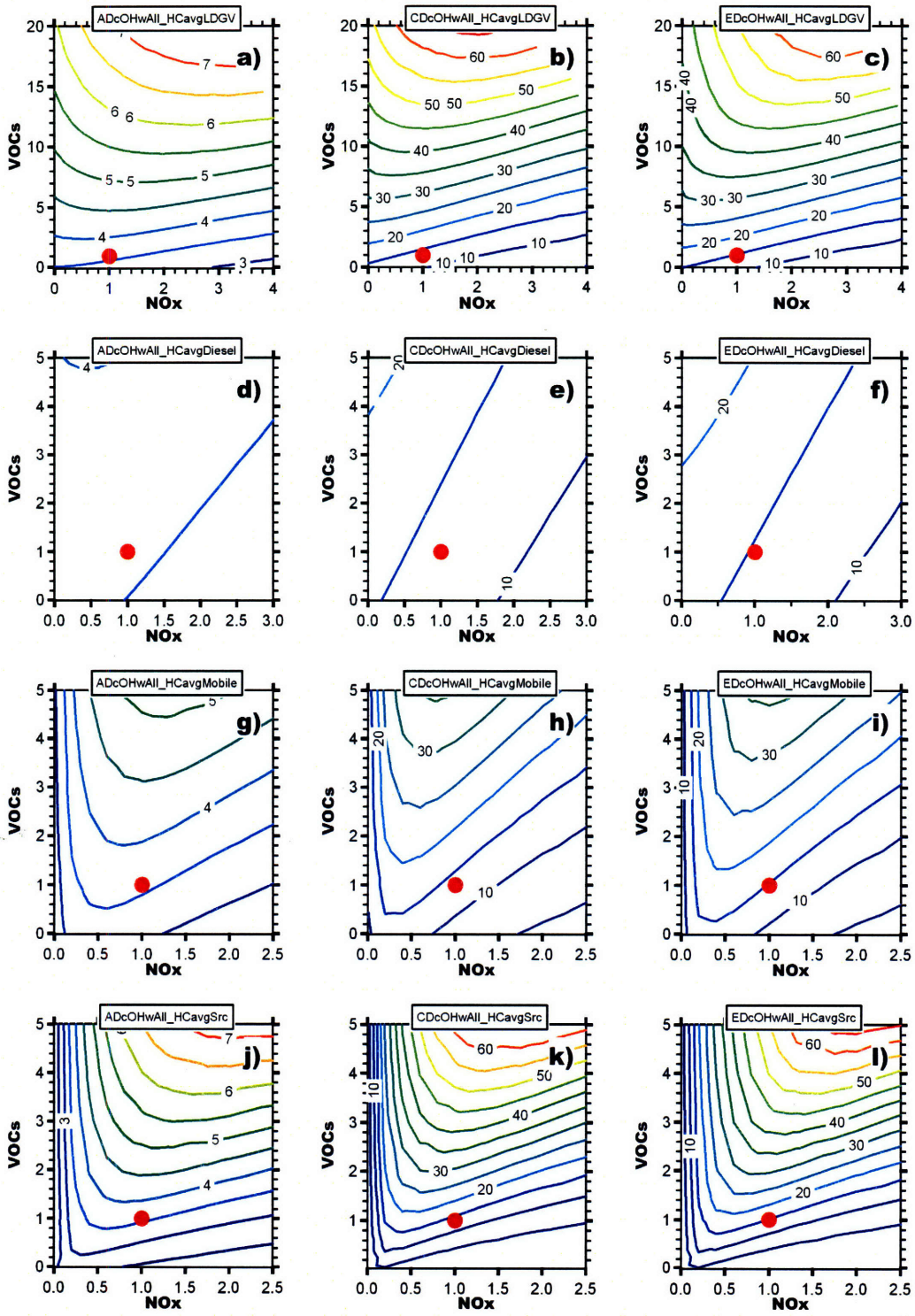

Figure A.17. Diurnal average OH reacted with all organic compounds (including CO) isopleths [] for domain-wide (AD), city domain (CD) and CENICA site (ED) for emissions perturbations in LDGV (a, b, c), diesel (d, e, f), all mobile (g, h, i), and all sources (j, k, l). Axes represent mass-based scaling factors of VOC and NO_X emissions from the base case simulation (red dot).

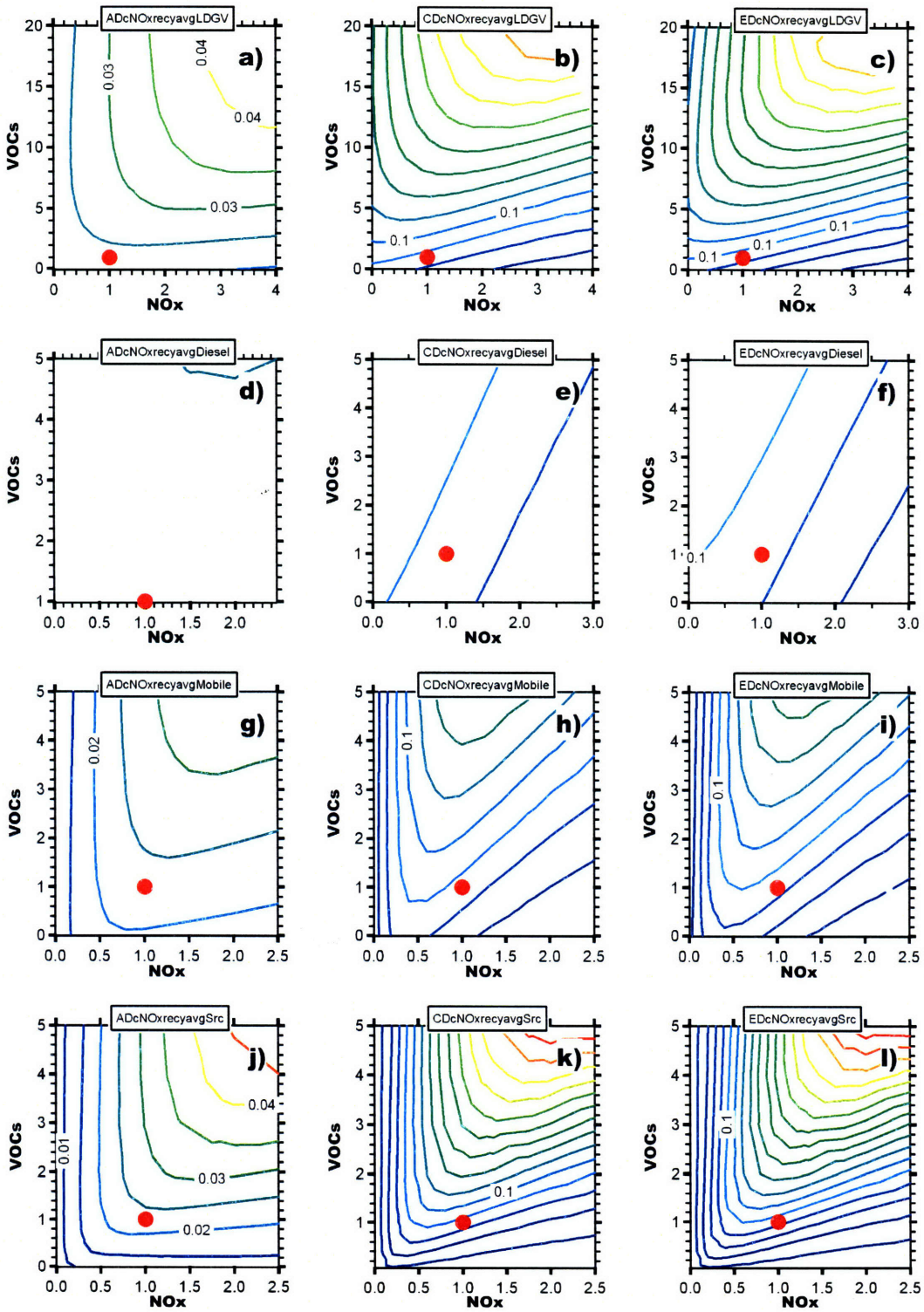

Figure A.18. Diurnal average nitrates recycled to NO_X isopleths [ppb/hr] for domain-wide (AD), city domain (CD) and CENICA site (ED) for emissions perturbations in LDGV (a, b, c), diesel (d, e, f), all mobile (g, h, i), and all sources (j, k, l). Axes represent mass-based scaling factors of VOC and NO_X emissions from the base case simulation (red dot).

References

Arriaga-Colina, J. L., West, J. J., Sosa, G., Escalona, S. S., Ordunez, R. M., and Cervantes, A. D. M., 2004, Measurements of VOCs in Mexico City (1992-2001) and evaluation of VOCs and CO in the emissions inventory: Atmospheric Environment, **38,** 2523-2533.

Atkinson, R. and Arey, J.. Atmospheric degradation of volatile organic compounds. Chem.Rev 103, 4605-4638. 2003.

Bachmann, J., 2007, Will the circle be unbroken: A history of the U.S. National Ambient Air Quality Standards: Journal of the Air & Waste Management Association, **57,** 652-697.

Baker, A., Beyersdorf, A., Blake, N. J., Meinardi, S., Atlas, E., Rowland, F. S., and Blake, D. R.. Measurements of VOCs in Mexico City during MILAGRO. 2007. Proceedings of the Second MILAGRO meeting, Mexico . 2007

Becker, K. H. and Wirtz, K., 1989, Gas-Phase Reactions of Alkyl Nitrates with Hydroxyl Radicals Under Tropospheric Conditions in Comparison with Photolysis: Journal of Atmospheric Chemistry, **9,** 419-433.

Bishop, G. A., Morris, J. A., and Stedman, D. H., 2001, Snowmobile contributions to mobile source emissions in Yellowstone National Park: Environmental Science & Technology, **35,** 2874-2881.

Bishop, G. A., Starkey, J. R., Ihlenfeldt, A., Williams, W. J., and Stedman, D. H.. IR long-path photometry: a remote sensing tool for automotive emissions. Analytical Chemistry 61[10], 671-677. 1989.

Bishop, G. A., Stedman, D. H., Castro, J. D., and Davalos, F. J., 1997, On-road remote sensing of vehicle emissions in Mexico: Environmental Science & Technology, **31,** 3505-3510.

Blake, D. R. and Rowland, F. S., 1995, Urban leakage of liquefied petroleum gas and its impact on Mexico City air quality: Science, **269,** 953-956.

Bugajny, C., Guillermo, R., and Dechaux, J. C., 1993, Study on Air-Pollution Due to Photochemical Oxidants in Mexico-City: Science of the Total Environment, **134,** 81-91.

Cadle, S. H., Belian, T. C., Black, K. N., Carlock, M. A., Graze, R. R., Minassian, F., Murray, H. B., Nam, E. K., Natarajan, M., and Lawson, D. R., 2006, Real-world vehicle emissions: A summary of the 15th Coordinating Research Council on-road vehicle emissions workshop: Journal of the Air & Waste Management Association, **56,** 121-136.

Cadle, S. H., Gorse, R. A., Bailey, B. K., and Lawson, D. R., 2002, Real-world vehicle emissions: A summary of the Eleventh Coordinating Research Council On-Road Vehicle Emissions Workshop: Journal of the Air & Waste Management Association, **52,** 220-236.

CAM. Inventario de Emisiones 2002 de la Zona Metropolitana del Valle de México. 2004. Mexico, Secretaria del Medio Ambiente.

-----. Inventario de Emisiones 2004 de la Zona Metropolitana del Valle de México. 1-270. 2006. Mexico, Secretaria del Medio Ambiente.

Canagaratna, M. R., Jayne, J. T., Ghertner, D. A., Herndon, S., Shi, Q., Jimenez, J. L., Silva, P. J., Williams, P., Lanni, T., Drewnick, F., Demerjian, K. L., Kolb, C. E., and Worsnop, D. R., 2004, Chase studies of particulate emissions from in-use New York City vehicles: Aerosol Science and Technology, **38,** 555-573.

Carter, W. P. L.. Documentation of the SAPRC-99 chemical mechanism for VOC reactivity, final report to California Air Resources Board. 2000. CA, Calif. Air Res. Board, Sacramento. Contract 92-329 and 95-308.

Chang, J. S., Brost, R. A., Isaksen, I. S. A., Madronich, S., Middleton, P., Stockwell, W. R., and Walcek, C. J., 1987, A three-dimensional Eulerian acid deposition model: Physical concepts and formulation: J. Geophys. Res., **81,** 421-423.

Cohan, D., Hakami, A., Hu, Y., and Russel, A. G., 2005, Nonlinear response of ozone to emissions: Source apportinoment and sensitivity analysis: Environmental Science & Technology, **39,** 6739-6748.

de Foy, B., Caetano, E., Magana, V., Zitacuaro, A., Cardenas, B., Retama, A., Ramos, R., Molina, L. T., and Molina, M. J., 2005, Mexico City basin wind circulation during the MCMA-2003 field campaign: Atmos. Chem. Phys, **5,** 2267-2288.

de Foy, B., Clappier, A., Molina, L. T., and Molina, M. J., 2006a, Distinct wind convergence patterns due to thermal and momentum forcing of the low level jet into the Mexico City basin: Atmos. Chem. Phys, **6,** 1249-1265.

de Foy, B., Lei, W., Zavala, M., Volkamer, R., Samuelsson, J., Mellqvist, J., Galle, B., Martinez, A. P., Grutter, M., Retama, A., and Molina, L. T., 2007, Modelling constraints on the emission inventory and on vertical dispersion for CO and SO2 in the Mexico City Metropolitan Area using Solar FTIR and zenith sky UV spectroscopy: Atmospheric Chemistry and Physics, **7,** 781-801.

de Foy, B. and Molina, L.. Basin-Scale Lagrangian Transport and Meteorological Episodes during MILAGRO. Proceedings of the Second MILAGRO meeting, Mexico . 2007.

de Foy, B., Varela, J. R., Molina, L. T., and Molina, M. J., 2006b, Rapid ventilation of the Mexico City basin and regional fate of the urban plume: Atmospheric Chemistry and Physics, **6,** 2321-2335.

Demographia. Mexico City Metropolitan Area Population Change from 1960 by Sector. 2007. Available at http://www.demographia.com/db-mxcpop.htm

Dunker, A. M.. Efficient calculation of sensitivity coefficients for complex atmospheric models. Atmospheric Environment 15[1155], 1161. 1981.

Dunker, A. M., Yarwood, G., Ortmann, J. P., and Wilson, G. M., 2002, The Decoupled Direct Method for Sensitivity Analysis in a Three-Dimensional Air Quality Model--Implementation, Accuracy, and Efficiency: Environmental Science & Technology, **36,** 2965-2976.

Dunlea, E., Volkamer, R., Johnson, K. S., Zavala, M., Molina, L. T., Molina, M. J., Lamb, B., Allwine, E., Rogers, T., and Knighton, B., 2004, Nitrogen Oxides (NOy) in the Mexico City Metropolitan Area: American Geophysical Union, Fall Meeting.

Edgerton, S. A., Bian, X., Doran, J. C., Fast, J. D., Hubbe, J. M., Malone, E. L., Shaw, W. J., Whiteman, C. D., Zhong, S., Arriaga, J. L., Ortiz, E., Ruiz, M., Sosa, G., Vega, E., Limon, T., Guzman, F., Archuleta, J., Bossert, J. E., Elliot, S. M., Lee, J. T., Mcnair, L. A., Chow, J. C., Watson, J. G., Coulter, R. L., Doskey, P. V., Gaffney, J. S., Marley, N. A., Neff, W., and Petty, R., 1999, Particulate air pollution in Mexico City: A collaborative research project: Journal of the Air & Waste Management Association, **49,** 1221-1229.

ENVIRON. User's guide to the comprehensive air quality model with extensions (CAMx). Version 3.10. ENVIRON Int.Corp. 2002. CA.

EPA. The benefits and costs of the Clean Air Act, 1970 to 1990. 1997. Washington, DC, Report prepared for the U.S. Congress.

Fast, J. D. and Zhong, S. Y., 1998, Meteorological factors associated with inhomogeneous ozone concentrations within the Mexico City basin: Journal of Geophysical Research-Atmospheres, **103,** 18927-18946.

Fernandez, A.. Emissions standards for new vehicles: a negotiation analysis approach. 12-2-2004. **Sao Paulo, Brazil**. Conference Proceeding.
Fine, J., Vuilleumier, L., Reynolds, S., Roth, P., and Brown, N., 2003, Evaluating uncertainties in regional photochemical air quality modeling: Annu. Rev. Environ. Resour., **28,** 59-106.

Fraser, M. P. and Cass, G. R., 1998, Detection of excess ammonia emissions from in-use vehicles and the implications for fine particle control: Environmental Science & Technology, **32,** 1053-1057.

Frey, S., Molina, L. T., Molina, M. J., and Wöste, L.. Design and Implementation of a Compact Raman-Lidar for Ozone and Aerosol Measurements. 561, 151-154. 2004. European Space Agency (Special Publication).

Gakenheimer, R., Molina, L. T., Sussman, J., Zegras, C., Howitt, A., Makler, J., Lacy, R., Slott, R., Villegas, A., and Molina, M. J., 2002, The MCMA transportation system: Mobility and air pollution: Air Quality in the Mexico Megacity: An Integrated Assessment, edited by: Molina, LT and Molina, M. J. , Kluwer Academic Publishers, Dordrecht, The Netherlands, 213-284.

Garcia, A. R., Volkamer, R., Molina, L. T., Molina, M. J., Samuelson, J., Mellqvist, J., Galle, B., Herndon, S. C., and Kolb, C. E., 2006, Separation of emitted and photochemical formaldehyde in Mexico City using a statistical analysis and a new pair of gas-phase tracers: Atmospheric Chemistry and Physics, **6,** 4545-4557.

GDF. Agenda estadística del distrito federal-Transporte, Gobierno de México. 2000. Gobierno del Distrito Federal.

GDF-SMA. Campañas de monitoreo ambiental a distancia de vehículos. Gobierno del Distrito Federal, Secretaria del Medio Ambiente. 2006. Mexico.

Giechaskiel, B., Ntziachristos, L., Samaras, Z., Scheer, V., Casati, R., and Vogt, R., 2005, Formation potential of vehicle exhaust nucleation mode particles on-road and in the laboratory: Atmospheric Environment, **39,** 3191-3198.

Grell, G. A., Dudhia, J., and Stauffer, D. R.. A Description of the Fifth-Generation Penn State/NCAR Mesoscale Model (MM5). NCAR. 1995. NCAR/TN-398+STR.

Hamby, D. M., 1994, A review of techniques for parametric sensitivity analysis of environmental models: Environmental Monitoring and Assessment, **32,** 135-154.

Herndon, S. C., Jayne, J. T., Zahniser, M. S., Worsnop, D. R., Knighton, B., Alwine, E., Lamb, B. K., Zavala, M., Nelson, D. D., McManus, J. B., Shorter, J. H., Canagaratna, M. R., Onasch, T. B., and Kolb, C. E., 2005a, Characterization of urban pollutant emission fluxes and ambient concentration distributions using a mobile laboratory with rapid response instrumentation: Faraday Discussions, **130,** 327-339.

Herndon, S. C., Shorter, J. H., Zahniser, M. S., Wormhoudt, J., Nelson, D. D., Demerjian, K. L., and Kolb, C. E., 2005b, Real-time measurements of SO2, H2CO, and CH4 emissions from in-use curbside passenger buses in New York City using a chase vehicle: Environmental Science & Technology, **39,** 7984-7990.

Herndon, S. C., Shorter, J. H., Zahniser, M. S., Nelson, D. D. J., Jayne, J. T., Brown, R. C., Miake-Lye, R. C., Waitz, I. A., Silva, P., and Lanni, T., 2004, NO and NO2 emission

ratios measured from in-use commercial aircraft during taxi and takeoff: Environ. Sci. Technol, **38,** 6078-6084.

Huai, T., Durbin, T. D., Rhee, S. H., and Norbeck, J. M., 2003, Investigation of emission rates of ammonia, nitrous oxide and other exhaust compounds from alternative-fuel vehicles using a chassis dynamometer: International Journal of Automotive Technology, **4,** 9-19.

Jauregui, E., 2005, Possible impact of urbanization on the thermal climate of some large cities in México: Atmosfera, **18,** 249-252.

Jazcilevich, A. D., Garcia, A. R., and Caetano, E., 2005, Locally induced surface air confluence by complex terrain and its effects on air pollution in the valley of Mexico: Atmospheric Environment, **39,** 5481-5489.

Jazcilevich, A. D., Garcia, A. R., and Ruiz-Suarez, L. G., 2003, A study of air flow patterns affecting pollutant concentrations in the Central Region of Mexico: Atmospheric Environment, **37,** 183-193.

Jiang, M., Marr, L. C., Dunlea, E. J., Herndon, S. C., Jayne, J. T., Kolb, C. E., Knighton, W. B., Rogers, T. M., Zavala, M., Molina, L. T., and Molina, M. J., 2005, Vehicle fleet emissions of black carbon, polycyclic aromatic hydrocarbons, and other pollutants measured by a mobile laboratory in Mexico City: Atmospheric Chemistry and Physics, **5,** 3377-3387.

Jimenez, J. L., Koplow, M. D., Nelson, D. D., Zahniser, M. S., and Schmidt, S. E., 1999, Characterization of On-Road Vehicle NO Emissions by a TILDAS Remote Sensor: Journal of the Air & Waste Management Association, **49,** 463-470.

Jimenez, J. L., McManus, J. B., Shorter, J. H., Nelson, D. D., Zahniser, M. S., Koplow, M., Mcrae, G. J., and Kolb, C. E., 2000, Cross road and mobile tunable infrared laser measurements of nitrous oxide emissions from motor vehicles: Chemosphere Global Change Science, **2,** 397-412.

Johnson, K. S., Zuberi, B., Molina, L. T., Molina, M. J., Iedema, M. J., Cowin, J. P., Gaspar, D. J., Wang, C., and Laskin, A., 2005, Processing of soot in an urban environment: case study from the Mexico City Metropolitan Area: Atmos. Chem. Phys, **5,** 3033-3043.

Kado, N. Y., Okamoto, R. A., Kuzmicky, P. A., Kobayashi, R., Ayala, A., Gebel, M. E., Rieger, P. L., Maddox, C., and Zafonte, L., 2005, Emissions of Toxic Pollutants from Compressed Natural Gas and Low Sulfur Diesel-Fueled Heavy-Duty Transit Buses Tested over Multiple Driving Cycles: Environmental Science & Technology, **39,** 7638-7649.

Kirchstetter, T. W., Singer, B. C., Harley, R. A., Kendall, G. R., and Traverse, M., 1999, Impact of California reformulated gasoline on motor vehicle emissions. 1. Mass emission rates: Environmental Science & Technology, **33,** 318-328.

Kittelson, D., Johnson, J., Watts, W., Wei, Q., Drayton, M., Paulsen, D., and Bukowiecki, N., 2000, Diesel Aerosol Sampling in the Atmosphere: Government/Industry Meeting, Washington, DC (US), 06/19/2000--06/21/2000.

Kleinman, L. I., Daum, P. H., Imre, D., Lee, Y.-N., Nunnermacker, L. J., Springston, S. R., Weinstein-Lloyd, J., and Rudolph, J., 2002, Ozone production rate and hydrocarbon reactivity in 5 urban areas: A cause of high ozone concentration in Houston: Geophys. Res. Lett., **29**.

Kolb, C. E., Herndon, S. C., McManus, B., Shorter, J. H., Zahniser, M. S., Nelson, D. D., Jayne, J. T., Canagaratna, M. R., and Worsnop, D. R., 2004, Mobile laboratory with rapid response instruments for real-time measurements of urban and regional trace gas and particulate distributions and emission source characteristics: Environmental Science & Technology, **38,** 5694-5703.

LANL/IMP. Mexico City ar quality research initiative. Los Alamos National Laboratoy and Instituto Mexicano del Petroleo. 2004. Los Alamos, NM.

Lei, W., de Foy, B., Zavala, M., Volkamer, R., and Molina, L. T., 2007, Characterizing ozone production in the Mexico City Metropolitan Area: a case study using a chemical transport model: Atmospheric Chemistry and Physics, **7,** 1347-1366.

Madronich, S., 2006, Chemical evolution of gaseous air pollutants down-wind of tropical megacities: Mexico City case study: Atmospheric Environment, **40,** 6012-6018.

Madronich, S. and Flocke, S., 1998, The role of solar radiation in atmospheric chemistry *in* Handbook of Environmental Chemistry: Springer-Verlag, Ed., P. Boule, Heidelberg, Germany.

Mobley, D., 2005, Improving Emission Inventories for Effective Air Quality Management Across North America.

Molina, L. T., Kolb, C. E., de Foy, B., Lamb, B. K., Brune, W. H., Jimenez, J. L., Ramos-Villegas, R., Sarmiento, J., Paramo-Figueroa, V. H., and Cardenas, B., 2007, Air quality in North America's most populous cityûoverview of the MCMA-2003 campaign: Atmospheric Chemistry and Physics, **7,** 2447-2473.

Molina, L. T. and Molina, M. J., 2002, Air Quality in the Mexico Megacity: An integrated Assessment: Kluwer Academic Publishers.

Molina, L. T., Molina, M. J., Slott, R. S., Kolb, C. E., Gbor, P. K., Meng, F., Singh, R. B., Galvez, O., Sloan, J. J., and Anderson, W. P.. Air quality in selected megacities, critical review complete online version,http://www.awma.org. 2004.

Molina, M. J. and Molina, L. T., 2004, Megacities and atmospheric pollution: Journal of the Air & Waste Management Association, **54,** 644-680.

Mugica, V., Vega, E., Arriaga, J. L., and Ruiz, M. E., 1998, Determination of motor vehicle profiles for non-methane organic compounds in the Mexico City metropolitan area: Journal of the Air & Waste Management Association, **48,** 1060-1068.

Napelenok, S. L., Cohan, D., Hu, Y., and Russell, A. G.. Decoupled direct 3D sensitivity analysis for particulate matter (DDM-3D/PM). Atmospheric Environment 40[32], 6112-6121. 2006.

O'Brien, J. J., 1970, A note on the vertical structure of the eddy exchange coefficient in the planetary boundary layer: J. Atmos. Sci., **27,** 1214-1215.

Pirjola, L., Parviainen, H., Hussein, T., Valli, A., Haemeri, K., Aaalto, P., Virtanen, A., Keskinen, J., Pakkanen, T. A., and Maekelae, T., 2004, Sniffer'; a novel tool for chasing vehicles and measuring traffic pollutants: Atmospheric Environment, **38,** 3625-3635.

Popp, P. J., Bishop, G. A., and Stedman, D. H., 1999, Development of a high-speed ultraviolet spectrometer for remote sensing of mobile source nitric oxide emissions: Journal of the Air & Waste Management Association, **49,** 1463-1468.

Prinn, R. G., 2003, Ozone, Hydroxyl Radical, and Oxidative Capacity *in* Treatise On Geochemistry.

Pun, B. K.. Treatment of Uncertainities in Atmospheric Chemical Systems: a combined Modeling and Experimental Approach. 1-2-1998. Massachusetts Institute of Technology. 1-2-1998. Thesis/Dissertation.

Rogers, T. M., Grimsrud, E. R., Herndon, S. C., Jayne, J. T., Kolb, C. E., Allwine, E., Westberg, H., Lamb, B. K., Zavala, M., Molina, L. T., Molina, M. J., and Knighton, W. B., 2006, On-road measurements of volatile organic compounds in the Mexico City metropolitan area using proton transfer reaction mass spectrometry: International Journal of Mass Spectrometry, **252,** 26-37.

Salcedo, D., Onasch, T. B., and Canagaratna, M. R., 2007, Technical Note: Use of a beam width probe in an Aerosol Mass Spectrometer to monitor particle collection efficiency in the field: Atmos. Chem. Phys., **7,** 549-556.

Salcedo, D., Onasch, T. B., Dzepina, K., Canagaratna, M. R., Zhang, Q., Huffman, J. A., DeCarlo, P. F., Jayne, J. T., Mortimer, P., Worsnop, D. R., Kolb, C. E., Johnson, K. S., Zuberi, B., Marr, L. C., Volkamer, R., Molina, L. T., Molina, M. J., Cardenas, B., Bernabe, R. M., Marquez, C., Gaffney, J. S., Marley, N. A., Laskin, A., Shutthanandan, V., Xie, Y., Brune, W., Lesher, R., Shirley, T., and Jimenez, J. L., 2006, Characterization of ambient aerosols in Mexico City during the MCMA-2003 campaign with Aerosol Mass Spectrometry: results from the CENICA Supersite: Atmospheric Chemistry and Physics, **6,** 925-946.

Sander, S. P., Golden, D. M., Kurylo, M. J., Huie, R. E., Orkin, V. L., Moortgat, G. K., Ravishankara, A. R., Kolb, C. E., Molina, M. J., and Finlayson-Pitts, B. J.. Chemical

kinetics and photochemical data for use in atmospheric studies. Evaluation 14. 2003. Pasadena, CA, Jet Propulsion Laboratory.

Schifter, I., Diaz, L., Duran, J., Guzman, E., Chavez, O., and Lopez-Salinas, E., 2003a, Remote sensing study of emissions from motor vehicles in the metropolitan area of Mexico City: Environmental Science & Technology, **37,** 395-401.

Schifter, I., Diaz, L., Mugica, V., and Lopez-Salinas, E., 2005, Fuel-based motor vehicle emission inventory for the metropolitan area of Mexico city: Atmospheric Environment, **39,** 931-940.

Schifter, I., Diaz, L., Vera, M., Castillo, M., Ramos, F., Avalos, S., and Lopez-Salinas, E., 2000, Impact of engine technology on the vehicular emissions in Mexico City: Environmental Science & Technology, **34,** 2663-2667.

Schifter, I., Diaz, L., Vera, M., Guzman, E., Duran, J., Ramos, F., and Lopez-Salinas, E., 2003b, Evaluation of the vehicle Inspection/Maintenance Program in the Metropolitan Area of Mexico City: Environmental Science & Technology, **37,** 196-200.

Schifter, I., Diaz, L., Vera, M., Guzman, E., and Lopez-Salinas, E., 2004, Fuel formulation and vehicle exhaust emissions in Mexico: Fuel, **83,** 2065-2074.

Seinfeld, J. H. and Pandis, S. N., 2006, Atmospheric Chemistry and Physics: From Air Pollution to Climate Change.

Serrano Trespalacios. Indicadores ambientales de compuestos organicos volatiles ene el aire de la Ciudad de Mexico. CONSERVA. 58-64. 1999. Mexico. Estudios 1998.

Shirley, T. R., Brune, W. H., Ren, X., Mao, J., Lesher, R., Cardenas, B., Volkamer, R., Molina, L. T., Molina, M. J., Lamb, B., Velasco, E., Jobson, T., and Alexander, M., 2006, Atmospheric oxidation in the Mexico City Metropolitan Area (MCMA) during April 2003: Atmos. Chem. Phys., **6,** 2753-2765.

Shorter, J. H., Herndon, S., Zahniser, M. S., Nelson, D. D., Wormhoudt, J., Demerjian, K. L., and Kolb, C. E., 2005, Real-time measurements of nitrogen oxide emissions from in-use New York City transit buses using a chase vehicle: Environmental Science & Technology, **39,** 7991-8000.

Singer, B. C. and Harley, R. A., 2000, A fuel-based inventory of motor vehicle exhaust emissions in the Los Angeles area during summer 1997: Atmospheric Environment, **34,** 1783-1795.

Stedman, D. H., Bishop, G. A., Aldrete, P., and Slott, R. S., 1997, On-road evaluation of an automobile emission test program: Environmental Science & Technology, **31,** 927-931.

Tatang, M. A.. Direct Incorporation of uncertainty in chemical and environmental engineering systems. 1994. Massachusetts Institute of Technology. Thesis/Dissertation.

Tatang, M. A., Pan, W., Prinn, R. G., and Mcrae, G. J., 1997, An efficient method for parametric uncertainty analysis of numerical geophysical models: J. Geophys. Res, **102,** 21-925.

Tie, X. X., Madronich, S., Li, G. H., Ying, Z. M., Zhang, R. Y., Garcia, A. R., Lee-Taylor, J., and Liu, Y. B., 2007, Characterizations of chemical oxidants in Mexico City: A regional chemical dynamical model (WRF-Chem) study: Atmospheric Environment, **41,** 1989-2008.

Velasco, E., Lamb, B., Westberg, H., Allwine, E., Sosa, G., Arriaga-Colina, J. L., Jobson, B. T., Alexander, M. L., Prazeller, P., Knighton, W. B., Rogers, T. M., Grutter, M., Herndon, S. C., Kolb, C. E., Zavala, M., de Foy, B., Volkamer, R., Molina, L. T., and Molina, M. J., 2007, Distribution, magnitudes, reactivities, ratios and diurnal patterns of volatile organic compounds in the Valley of Mexico during the MCMA 2002 & 2003 field campaigns: Atmospheric Chemistry and Physics, **7,** 329-353.

Vogt, R., Scheer, V., Casati, R., and Benter, T., 2003, On-Road Measurement of Particle Emission in the Exhaust Plume of a Diesel Passenger Car: Environmental Science & Technology, **37,** 4070-4076.

Volkamer, R., Molina, L. T., Molina, M. J., Shirley, T., and Brune, W. H., 2005a, DOAS measurement of glyoxal as an indicator for fast VOC chemistry in urban air: Geophysical Research Letters, **32**.

Volkamer, R., Zavala, M., Molina, L., Molina, M., Flores, E., Grutter, M., Samuelsson, J., Mellqvist, J., Galle, B., and Knighton, B.. Open-path emission factors derived from DOAS and FTIR Measurements in the Mexico City Metropolitan Area. Poster contribution to "Air Pollution as a Climate Forcing: A second Workshop", April 4-6 2005, Honolulu, Hawaii . 4-6-2005b.

Wenzel, T., Singer, B. C., and Slott, R., 2000, Some issues in the statistical analysis of vehicle emissions: Journal of Transportation and Statistics, **3,** 1-14.

West, J. J., Zavala, M. A., Molina, L. T., Molina, M. J., San Martini, F., Mcrae, G. J., Sosa-Iglesias, G., and Arriaga-Colina, J. L., 2004, Modeling ozone photochemistry and evaluation of hydrocarbon emissions in the Mexico City metropolitan area: Journal of Geophysical Research-Atmospheres, **109**.

Whitfield, J. K. and Harris, D. B., 1998, Comparison of Heavy-Duty Diesel Emissions from Engine and Chassis Dynamometers and On-Road Testing: Eighth CRC On-Road Vehicle Emissions Workshop, San Diego, CA. , Coordinating Research Council.

Williams, M. D., Brown, M. J., Cruz, X., Sosa, G., and Streit, G., 1995, Development and testing of meteorology and air dispersion models for Mexico City: Atmos. Environ., **29,** 2929-2960.

Yang, Y. J., Wilkinson, J. G., and Russell, A. G.. Fast, direct sensitivity analysis of multidimensional photochemical models. Environmental Science & Technology 31, 2859-2868. 1997.

Yanowitz, J., Graboski, M. S., Ryan, L. B. A., Alleman, T. L., and Mccormick, R. L., 1999, Chassis dynamometer study of emissions from 21 in-use heavy-duty diesel vehicles: Environmental Science & Technology, **33,** 209-216.

Yarwood, G., Morris, R. E., and Wilson, G. M., 2004, Particulate Matter Source Apportionment Technology (PSAT) in the CAMx Photochemical Grid Model: International technical Meeting. Banff, Canada. October.

Young, A. T., Betterton, E. A., and DeRueda, L. S., 1997, Photochemical box model for Mexico City: Atmosfera, **10,** 161-178.

Zahniser, M. S., Nelson, D. D., McManus, J. B., Kebabian, P. L., and Lloyd, D., 1995, Measurement of Trace Gas Fluxes Using Tunable Diode Laser Spectroscopy [and Discussion]: Philosophical Transactions: Physical Sciences and Engineering, **351,** 371-382.

Zavala, M., Herndon, S. C., Slott, R. S., Dunlea, E. J., Marr, L. C., Shorter, J. H., Zahniser, M., Knighton, W. B., Rogers, T. M., Kolb, C. E., Molina, L. T., and Molina, M. J., 2006b, Characterization of on-road vehicle emissions in the Mexico City Metropolitan Area using a mobile laboratory in chase and fleet average measurement modes during the MCMA-2003 field campaign: Atmospheric Chemistry and Physics, **6,** 5129-5142.